AD NUMBER

AD913719

LIMITATION CHANGES

TO:

Approved for public release; distribution is unlimited.

FROM:

Distribution authorized to U.S. Gov't. agencies only; Test and Evaluation; SEP 1973. Other requests shall be referred to Air Force Avionics Lab., Wright-Patterson AFB, OH 45433.

AUTHORITY

AFAL ltr 12 Jan 1976

AFAL-TR-73-312

DEVELOPMENT OF UNCONVENTIONAL GYRO (NUTATRON TECHNIQUE) FOR TACTICAL AIRCRAFT INERTIAL SYSTEMS

Giles M. Hofmeyer
Ernest H. Metzger
Bell Aerospace Division of Textron

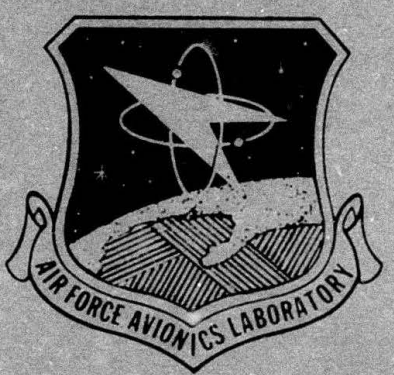

TECHNICAL REPORT AFAL-TR-73-312

September 1973

Air Force Avionics Laboratory
Air Force Systems Command
Wright-Patterson Air Force Base, Ohio

NOTICE

When Government drawings, specifications, or other data are used for any purpose other than in connection with a definitely related Government procurement operation, the United States Government thereby incurs no responsibility nor any obligation whatsoever; and the fact that the Government may have formulated, furnished, or in any way supplied the said drawings, specifications, or other data, is not to be regarded by implication or otherwise as in any manner licensing the holder or any other person or corporation, or conveying any rights or permission to manufacture, use, or sell any patented invention that may in any way be related thereto.

Copies of this report should not be returned unless return is required by security considerations, contractual obligations, or notice on a specific document.

AFAL-TR-73-312

DEVELOPMENT OF UNCONVENTIONAL GYRO (NUTATRON TECHNIQUE) FOR TACTICAL AIRCRAFT INERTIAL SYSTEMS

Giles M. Hofmeyer
Ernest H. Metzger

FOREWORD

This final technical report covers the work performed under Contracts F33615-71-C-1092 and F33615-72-C-1137, Project No. 6095, Task 02, from October, 1970 to March, 1973 by Bell Aerospace Company, P. O. Box 1, Buffalo, New York 14240.

The Air Force Project Engineer was R. McAdory, AFAL/NVN, Air Force Avionics Laboratory, Wright-Patterson Air Force Base, Ohio 45433.

The program was carried out in the Inertial Instrument Section of Bell Aerospace under the direction of Ernest H. Metzger, Manager, Advanced Inertial Instrument and Systems. William E. Bascomb was Program Manager, and Giles M. Hofmeyer was Technical Director. Others who contributed to the program were Dr. Donald R. Allen, Analysis; Robert R. Martin, Mechanical Design; and Lou L. Pfohl, Mechanical Design.

This report was submitted by the authors in June 1973.

This Technical Report has been reviewed and is approved for publication.

WILLIAM J. DELANEY, Colonel, USAF
Chief, Navigation and
Weapon Delivery Division

ABSTRACT

This report covers the latest phase of the Nutatron angular rate sensor development effort, culminating in the delivery of two prototype sensor and an electronic test set to the U. S. Air Force CIGTF at Holloman AFB. The objectives of the Nutatron program is to lead to an angular rate sensor for tactical fighter navigation systems, offering fast reaction from a cold start, low temperature coefficients and good long term stability. The Nutatron concept features an automatic drift compensation technique, eliminating the requirement for high tolerance, highly stable parts and materials. The report tabulates the attained performance parameters, discusses the results and underlying remaining error mechanisms and concludes in recommendations to further improve performance. The electromechanical and electronic modifications made under this phase are discussed and their impact on performance described.

Reports AFAL-TR-65-170, AFAL-TR-67-54, and AFAL-TR-69-76, give the results of the previous efforts of this unconventional angular rate sensor development program.

CONTENTS

CONTENTS (CONT)

ILLUSTRATIONS

ILLUSTRATIONS (CONT)

TABLES

I. SUMMARY

A. PERFORMANCE SUMMARY

Two Nutatron angular rate sensors were fabricated and tested with the deliverable electronics test set. Except for a difference in the spin bearing geometry, the two instruments are identical. The performance evaluation was conducted with the instruments mounted on precision indexing heads operating in the rate capture mode. This setup permitted orienting the Nutatrons at various attitudes with respect to the earth rotation and the g vector and hence the determination of a number of performance parameters including g and g^2 sensitive drift. The results are listed on Table I and discussed in more detail in Section VI.

TABLE I. SUMM' .Y OF NUTATRON TEST RESULTS

	Nutatron SN-1		Nutatron SN-2	
	x Axis	y Axis	x Axis	y Axis
1. Drift (Spin Axis Vert)				
a. Mean Value	0.16°/hr	0.15°/hr	0.05°/hr	0.05°/hr
b. Repeatability from Cold start (1 sigma)	0.039°/hr	0.035°/hr	0.0045°/hr	0.0074°/hr
c. Randomness - (1 sigma)	^029°/hr	0.031°/hr	0.038°/hr	0.032°/hr
d. Trend (16 hr run)	∪. `26°/hr²	0.0031°/hr²	0.0022°/hr²	0.0014°/hr²
e. Temperature Coefficient - Drift (73-100°F)	0.001°/hr/°F	0.001°/hr/°F	0.001°/hr/°F	0.003°/hr/°F
f. Temp. Coefficient - Scale Factor	0.0010 pp/°F	0.0010 pp/°F	0.0009 pp/°F	0.0009 pp/°F
g. Magnetic Drift Sensitivity (All Axes - 20 gauss)	None Measurable (< 0.001 0/hr/gauss)			
h. Magnetic Scale Factor Sensitivity (All Axes - 20 gauss)	None Measurable (< 0.0001 pp/gauss)			
2. Drift (Spin Axis at Polar Angle)				
a. Repeatability from Cold Start (1 sigma)	0.034°/hr	0.054°/hr	0.0097°/hr	0.0034°/hr
b. Randomness - 1 sigma	0.048°/hr	0.071°/hr	0.023°/hr	0.018°/hr
c. Trend (16 hour run)	0.0053°/hr²	0.0090°/hr²	0.0057°/hr²	0.0002°/hr²
d. Drift Temp. Coefficient (73-100°F)	0.004°/hr/°F	0.006°/hr/°F	0.016°/hr/°F	0.007°/hr/°F
3. G Sensitive Drift (12 Pt Test)	0.13°/hr/g	0.1°/hr/g	0.15°/hr/g	0.14°/hr/g
4. G^2 Sensitive Drift Coeff (12 Pt Test)	0.86°/hr/g²	0.16°/hr/g²	0.26°/hr/g²	0.22°/hr/g²

The outstanding characteristics of the Nutatron are the excellent performance stability with time, the low temperature and magnetic sensitivities and good drift repeatability in a very short reaction time of under seven minutes. The trend (change of drift with time) listed on Table I is most certainly pessimistic and is influenced by the randomness over a relatively short drift run of 16 hrs. Longer drift runs (36 hrs) have been conducted during the development cycle with trend figures of under 0.0005 deg/hr/hr.

Somewhat disappointing is the short term randomness in the order of 0.03 deg/hr. On closer examination the randomness consists of discrete periodic components which have the characteristic of a beat between the spin and housing rotation frequency. This is discussed in Section VI and illustrated by a typical strip chart drift recording, Figure 53. The drift periodicity will have little impact on navigation performance as its frequency content is considerably above the Schuler frequency. However, it prevents fast and accurate azimuth alignment of the IRU by gyrocompassing. The mechanism for this periodic drift has been identified and methods to eliminate it are discussed in Section VI of this report.

The g^2 sensitive drift turned out somewhat higher than expected, with Nutatron SN-2 exhibiting approximately 1/3 the value of SN-1. The spin bearings of SN-2 have a much lower outer race curvature and anlysis seems to confirm that the curvature is associated with this error source. Further development efforts to reduce the g^2 sensitive drift are outlined in this report and recommended.

B. SUMMARY OF NUTATRON SENSOR MODIFICATIONS

Except for a few simplifications and minor but important modifications, the Nutatron Sensors delivered to CIGTF are in the original configuration as developed under second and third phase of the program. The anisometric rotor, the capacitive pickoff, the capacitive phase detector, the suspension spring compensators, and the rotating housing electromagnetic torquers, remain essentially as described in Technical Reports AFAL-TR-67-54 and AFAL-TR-69-76, and again in Section III of this report. The simplification and modifications made from the original configuration and the underlying reason are briefly summarized here and discussed in greater detail in Sections III, VI, and Appendix II.

1. Simplifications

The original Nutatron stressed symmetric design which is sound practice for conventional inertial instruments (see cross-sectional sketch, Figure 9). Capacitance pickoffs spring compensators and torquing systems were mounted symmetrically on either end of the Nutatron rotor. After it became apparent that conventional gyroscopic design considerations do not apply with the Nutatron, the pickoff spring compensation and torquing system located on the free end of the suspended element were removed (cross-sectional sketch Figure 10). In addition to simplifying the electromechanical design and wiring of the instrument, the modulation factor M was increased by 30% from about 1.5 to 2.0. The modulation factor is defined in Section III of this report. It also greatly facilitated experimenting with preloads and alignment of the bearings without disassembling the instrument.

2. Electromechanical Modifications

Under this phase of the development program four electromechanical modifications were made to the Nutatron. These are briefly summarized below and discussed in more detail in Appendix II, and Section VI of the report.

a. Revised Suspension Pivot

The simple necked down suspension pivot was replaced with a compound circular pivot (shown on Figure II-3) to provide much higher stiffness about the spin axis. With the original pivot the suspended element of the Nutatron would occasionally oscillate from stop to stop about the spin axis and disrupt measurements. The compound circular and simple necked down pivot have the same compliance about the two sensitive axes and the identical mechanical interface, permitting a simple one for one replacement. The stiffness about the spin axis was increased by a factor of 800 and the lateral stiffness by a factor of fifty. The oscillations about the spin axis have been reduced to an insignificant level. A side benefit of the compound circular pivot stems from a slight axial displacement of the two orthogonal centers of suspension. As a result a signal at twice housing rotation frequency develops proportional to cross axes accelerations. This signal is used effectively to compensate for acceleration sensitive Nutatron drift.

b. Higher Stiffness Flex Leads

The stiffness of the flex leads was increased by a factor of three without any impact on performance. The flex leads have been eliminated as a source of noise.

c. Air Core Torquers for Nutatron Signal

The eight torquer coils in the original torquer block had soft iron cores to provide sufficient capturing capability. One of the torquer coils is used to torque rebalance the suspended element at the Nutatron frequency and provide the precession output signal, while the rest provide the normal torque rebalance function. The soft iron core was removed from the Nutatron signal torquer coil with a 60% reduction of the output signal scale factor temperature coefficient.

d. Ball Spin Bearings

The ball spin bearings have been identified as the major source of acceleration sensitive Nutatron drift. Unequal orthogonal radial compliances of the bearings are the mechanism for this and as derived in Section VI can be caused by elliptic run out of the outer bearing races or nonparallel installation of the two bearings (tilt about a radial axis with respect to each other). Various mechanisms were experimented with to minimize the tilt between the bearings, including wedge shaped preload shims and variable preload mechanisms. The adjustments were found to be very delicate or not stable with time.

A computer bearing analysis discussed in Section VI indicated that the outer race curvature is the prime contributor to the tilt sensitivity. Normal gyro bearings have very closely conforming outer races with curvature ratios near 0.55 and their tilt sensitivity is very high as shown on curve, Figure 71. Bearings with angular outer race curvature above 0.7 should theoretically have a very low tilt sensitivity. Special bearings with outer curvature of 0.8 and 2.0 were procured and installed in the Nutatrons with excellent results. The tilt sensitivity was very much reduced and the g sensitive Nutatron drift is repeatable, stable and exhibits low temperature coefficients (Table I). The need for tilt adjustment has been eliminated.

The magnitude of the acceleration squared sensitive drift also seems to be a function of the outer race curvature. Reduction by a factor of about 3 was demonstrated by reducing the outer race curvature from 2.0 to 0.8. Further analysis and test is recommended for reducing this type of drift and the determination of optimum outer race curvature for both g and g^2 sensitive drift.

3. Electronic System Modification

The development of the Nutatron was carried out with electronic circuits and test equipment contained in three full size racks. These have been replaced by one small test console with the electronic circuits mounted on vector boards. Particular emphasis has been placed on simplicity of operation. Three switches control the operation of the Nutatron to activate the power supplies, turn on the spin motor and energize the control loops respectively. Two output terminals suffice to record the performance of the Nutatron. Additional terminals and control points are provided for troubleshooting.

As discussed in Section IV a number of improvements were incorporated in the electronic circuits including: (a) standardized transformerless modulators and demodulators have reduced the frequency sensitivity of the electronics, (b) current feedback rather than voltage amplifiers to drive the sping compensators minimized the effect of resistance variations of the slip rings at the housing rotation frequency, and (c) the generation of the Nutatron reference frequency is now accomplished electronically by multiplexing through the pickoff resolver thereby eliminating the frequency reference resolver.

Two operational changes have been incorporated in the electronics for improving the precession readout.

(a) Originally the Nutatron precession signal was read out at the pickoff and the measured performance depended on the electronic gain and phase stabilities of the pickoff systems. Overnight runs exhibited slowly changing drift levels of 0.4°/hr. To eliminate the dependence on electronic stabilities, the motions at the Nutatron frequency are torque rebalanced by high gain narrow bandwidth loops, and the torque at the Nutatron frequency rather than the motion becomes the indicated precession rate. The long term stability of the Nutatron drift improved by a factor of 10 as shown on Table I by this revised readout method.

(b) The compound circular suspension pivots had small axial displacement of the two orthogonal centers of suspension and hence torques at twice housing rotation frequency in response to the radial g developed. The normal capture loops were augmented with narrow bandwidth high gain torque reblance loops at t[illegible]quency to prevent saturation of the electronics. In effect these loops measure t[illegible]va-tions along the two input axes and form the basis for a multisensor. These [illegible]a-tion signals were used effectively to trim the g sensitive Nutatron drift.

II. INTRODUCTION

This document is the final report on the latest two phases of the exploratory development program of the Nutatron angular rate sensor. It covers the activity from 15 October 1970 to 15 March 1973 carried out under Contracts F33615-71-1092 and F33615-72-1137 from the U.S. Air Force Avionics Laboratory. The two contracts were interdependent in that the first was for the development, test, and evaluation of the Nutatron angular rate sensor and the second for the design, fabrication, and test of the specialized electronics required to operate and test instruments. The Nutatron and its test electronics are now ready for independent evaluation and have been shipped to Central Inertial Guidance Test Facility (CIGTF) at Holloman AFB for that purpose.

The objective of the Nutatron development effort was to establish the feasibility of an unconventional technique which continuously detects drift and automatically corrects it using a feedback approach. The requirements for precision mechanics, tight tolerances, excellent dimensional and material stabilities and accurate temperature control are substantially reduced or eliminated. The automatic drift compensation technique of the Nutatron therefore leads to a low-cost reliable angular rate sensor with very short reaction time from a cold start. Performance suitable for tactical aircraft navigation systems was set as a goal.

The Nutatron features an anisometric rotor with unequal radial moments of inertia. In other words, the rotor has a configuration somewhat similar to a dumbbell rather than a cylinder or sphere of a conventional gyro. In response to precession rates it exhibits minute oscillations at twice rotor frequency. These oscillations are detected by synchronous demodulation techniques and used to generate a counter torque to stop the drift.

In the strap down mode of operation the amplitude of the oscillation is a direct measure of base precession rate. The Nutatron has been tested in this mode for the development effort with components of earth rate as the input.

After verifying the Nutatron principle on a modified conventional gyro (Technical Report AFAL-TR-65-170), an instrument specifically designed for Nutatron action was fabricated and tested (Technical Report AFAL-TR-67-54). Since then the effort has been directed to identify and subsequently reduce various noise sources at or near the Nutatron frequency by system techniques or modifications to the instrument (Technical Report AFAL-TR-69-76 and as discussed in this report).

As can be expected in an advanced inertial instrument development effort of this kind, error sources and possible improvements have come to light which could not be implemented because of funding and schedule limitations. These are discussed in the report, and recommendations for future developments are made. However, the principal objectives, excellent long term stability, repeatability and low temperature coefficients, have been established by many tests and should be verified by the test program at CIGTF at Holloman AFB. The data and findings indicate that the Nutatron concept has substantial growth potential for a family of precision angular rate sensors for a wide range of applications.

III. DESCRIPTION OF NUTATRON ANGULAR RATE SENSOR

The Nutatron angular rate sensors which have been delivered to the Air Force for independent evaluation are in the basic configuration described in previous reports. Modifications were introduced where tests and analysis indicated a specific need but within the limitation of not requiring a fundamental redesign of the existing hardware. The rotor, spin motor, capacitive pickoff, suspension spring compensation, flex leads and rotating case mechanism remain unaltered. Changes were made in the spin bearings, suspension system, and torquer coils but with the constraint that a one to one replacement could take place. A substantial simplification was introduced by discovering that symmetry adds very little to the Nutatron performance, and the pickoff, torquing and spring compensation system were removed from one end.

The Nutatron instrument is described in this summary with its latest modifications. A brief summary of the Nutatron principle is repeated first for clarity.

A. SUMMARY OF NUTATRON PRINCIPLE

This discussion is simplified to highlight the approach and does not include the dynamics of resonant operation. This is covered in Appendix I.

A conventional gyro with a symmetric rotor (cylindrical or spherical) responds to torques by exhibiting a steady state drift (Figure 1.a). This drift is expressed by the normal gyro equations.

$$\omega_{xdc} = -\frac{T_y}{\nu C}$$

$$\omega_{ydc} = \frac{T_x}{\nu C}$$

where:

$\omega_{xdc}, \omega_{ydc}$ = drift rate about x and y axes

T_x, T_y = drift torques about x and y axes

ν = rotor angular velocity

C = spin axis moment of inertia

If the gyro rotor is made so that it has different principal moments of inertia in the plane of rotation (anisometric), it responds to torques by drifting as shown in Figure 1.b. The steady state drift now has minute oscillations superimposed on it at twice the rotor spin frequency. The amplitude of these oscillations is proportional to the drift rate.

In a gyro with an anisometric rotor, the drift equations become (neglecting the suspension spring restraint)

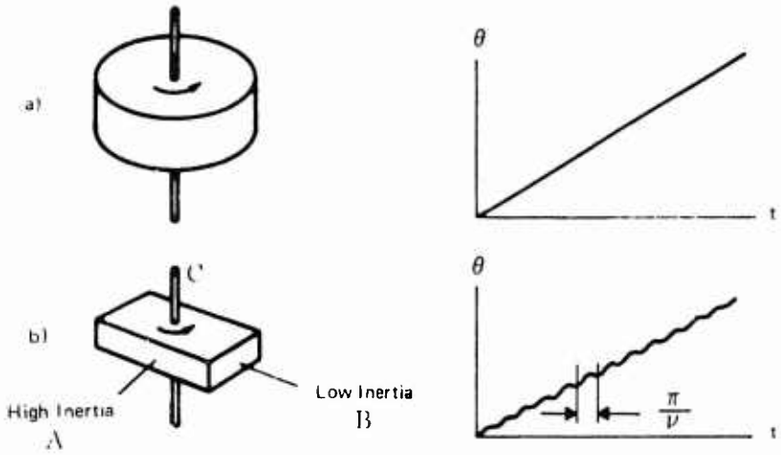

Figure 1. Gyro Drift Characteristics

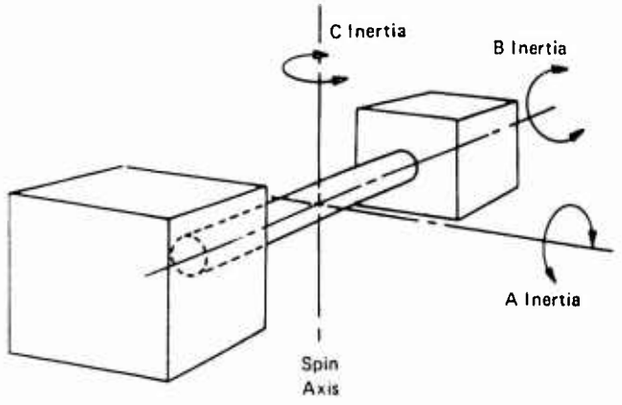

Figure 2. Presentation of an Anisometric Rotor

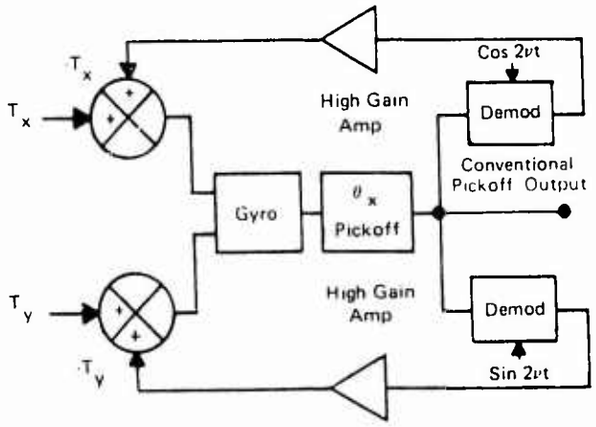

Figure 3. Block Diagram of Nutatron
Servo Loops for Nulling Torques

$$\omega_{xT} = -\frac{T_y}{\nu C}(1 - M\cos 2\nu t) - \frac{T_x}{\nu C} M \sin 2\nu t$$

$$\omega_{yT} = \frac{T_x}{\nu C}(1 + M\cos 2\nu t) + \frac{T_y}{\nu C} M \sin 2\nu t$$

where:

$$M = \frac{A - B}{A + B - C + 2I} \text{ (modulation factor)}$$

A, B = the principle moments of inertia of the rotor about the x and y axes (Figure 2)

I = the symmetric nonrotating inertia of the gyroscopic element

t = time

When the equations are expressed in terms of conventional gyro drift and are integrated, the detected pickoff angles are given.

$$\theta_x = \int_0^t \omega_{xT} dt = \omega_{xdc}\left(t - \frac{M}{2\nu}\sin 2\nu t\right) + \omega_{ydc}\frac{M}{2\nu}\cos 2\nu t$$

$$\theta_y = \int_0^t \omega_{yT} dt = \omega_{ydc}\left(t + \frac{M}{2\nu}\sin 2\nu t\right) + \omega_{xdc}\frac{M}{2\nu}\cos 2\nu t$$

These equations show that the oscillating signals in either pickoff are directly related to the total gyro drift occurring in both axes. Therefore, the signals occurring at the 2ν frequency can be used to compensate for the disturbing (drift producing) torques by a feedback system as illustrated in the block diagram of Figure 3. In this figure, the output of the x-axis pickoff is demodulated at the sine and cosine phases of the 2ν frequency. The demodulator outputs are used in a closed loop through the torquer to produce compensation torques to reduce the gyro drift to zero.

When such a self-compensating technique is used, the gyro performance is no longer affected by small changes in the dimensions of the instrument parts or by changes in the parameters of the materials used. If these changes produce disturbing torques on the gyro, the self-compensating loop automatically detects the torques by means of the Nutatron oscillations produced, and corrects for them.

The Nutatron concept combines the operation of a conventional gyro with an unconventional drift compensation scheme. The pickoff signals of a two-degree-of-freedom gyro are used for angular rate sensing for short term attitude information while the Nutatron signal at twice the rotor frequency is used for longer term drift compensation. This concept permits rapid system preparation since the automatic drift compensation can take place after the system is in operation and airborne.

1. Effect of Noise at the Nutatron Frequency

In the ideal situation without noise, there is a direct relationship between oscillating pickoff signals at twice the rotor frequency (2ν) and gyro drift, and gyro drift can be effectively eliminated by nulling all of the 2ν oscillations in the pickoff. In the actual instrument, however, there are several potential sources of 2ν oscillations that are not caused by gyroscopic torques. These erroneous oscillations are considered noise and constitute the only potential drift error source in the Nutatron instrument. Gyroscopic torques, which are the limiting factors in performance and reaction time of conventional gyros, are of no concern here.

Including the noise signal at an arbitrary phase, ϕ, in the expression for the pickoff angle and ignoring the steady state term, the pickoff signal is

$$\theta_{x2\nu} = -\omega_{xdc}\frac{M}{2\nu}\sin 2\nu t + \omega_{ydc}\frac{M}{2\nu}\cos 2\nu t + \theta_N \sin(2\nu t + \phi)$$

$$= \frac{M}{2\nu}(\omega_{ydc}\cos 2\nu t - \omega_{xdc}\sin 2\nu t) + \theta_N \cos\phi \sin 2\nu t$$

$$+ \theta_N \sin\phi \cos 2\nu t$$

Hence, the remaining drift with drift correction loops closed is

$$\omega_{ydc} = \frac{-2\nu}{M}\theta_N \sin\phi$$

$$\omega_{xdc} = \frac{2\nu}{M}\theta_N \cos\phi$$

From these expressions it can be seen that the residual drift of a Nutatron gyro can be minimized by three considerations:

Maximizing the M ratio

Minimizing the noise amplitude θ_N

Minimizing the rotor speed ν

B. DESCRIPTION OF NUTATRON

The Nutatron was designed to meet the following basic goals:

1. Obtain as high an M as possible.

2. Minimize potential sources of noise at the Nutatron frequency.

3 Achieve an unfloated configuration that eliminates the problems of filling, sealing, gas bubbles, etc.

4. Design an instrument that is simple to assemble and disassemble so that development type changes can be made with relative ease.

5. Obtain a low running speed.

6. Eliminate hard magnetic materials from the gyro rotor to avoid magnetic noise sources.

7. Achieve all of the above with a design that will eventually lend itself to mass production at a reasonable cost.

It consists of the following eight subsystems.

1. Gyroscopic Element

This gyroscopic element shown in Figure 4 contains:

(a.) The anisometric rotor structure including the spin motor and bearings.

(b.) A single common pickoff plate that is used by the pickoff system to detect the rotational position of the gyroscopic element.

(c.) A permanent magnet required for excitation of the torquing system.

2. Nutatron Rotor (Figure 5)

The rotor assembly of the Nutatron consists of the anisometric inertia ring and supporting structure, the spin motor, and the spin bearings. The inertia ring is screwed to an aluminum housing which couples it to the rest of the rotor structure. The rotor housing end caps contain the ball bearings. The spin motor is mounted inside the rotor housing.

The inertia ring provides different moments of inertia about two orthogonal axes in the equatorial plane, and establishes the proper ratio of inertias so that stable operation can be achieved. It consists of two large diametrically opposite masses connected by a slender ring. The two masses provide a large moment of inertia about any axis perpendicular to the diameter connecting them (hence, large A and C inertias), but a small moment of inertia about the connecting diameter, B. The addition of the slender ring makes the C inertia larger than the A and B inertias so that stable rotational operation is achieved.

An eddy current motor is used to provide the torque required to drive the rotor. This type of motor was selected because it:

(a.) Operates well at low speed.

(b.) Has nonsynchronous driving torques and, therefore, low noise at 2ν.

(c.) Has a nearly linear speed torque characteristic which aids in implementing speed control.

(d.) Requires no hard magnetic materials on the rotor.

Ball bearings are used because they have the following characteristics:

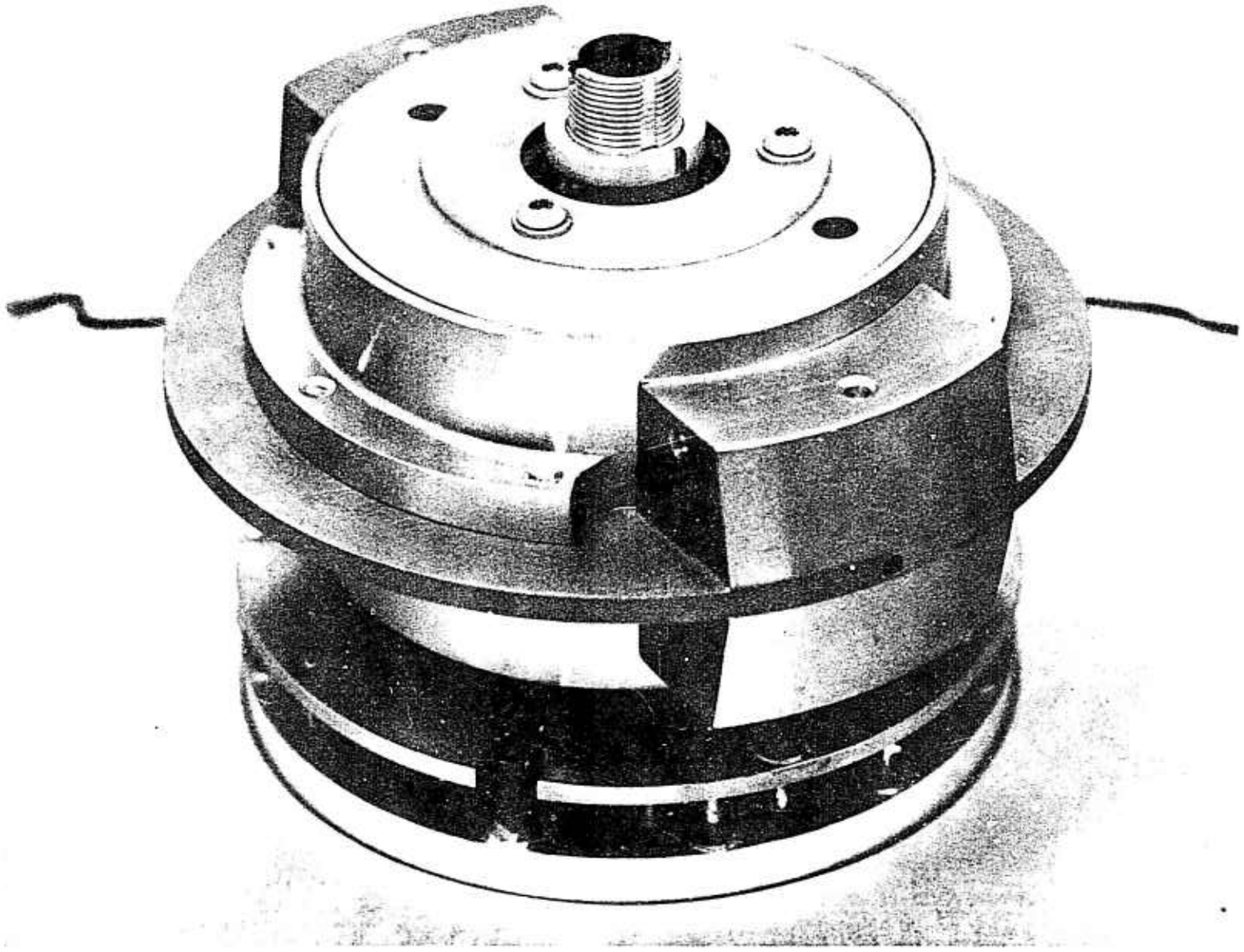

Figure 4. Gyroscopic Element

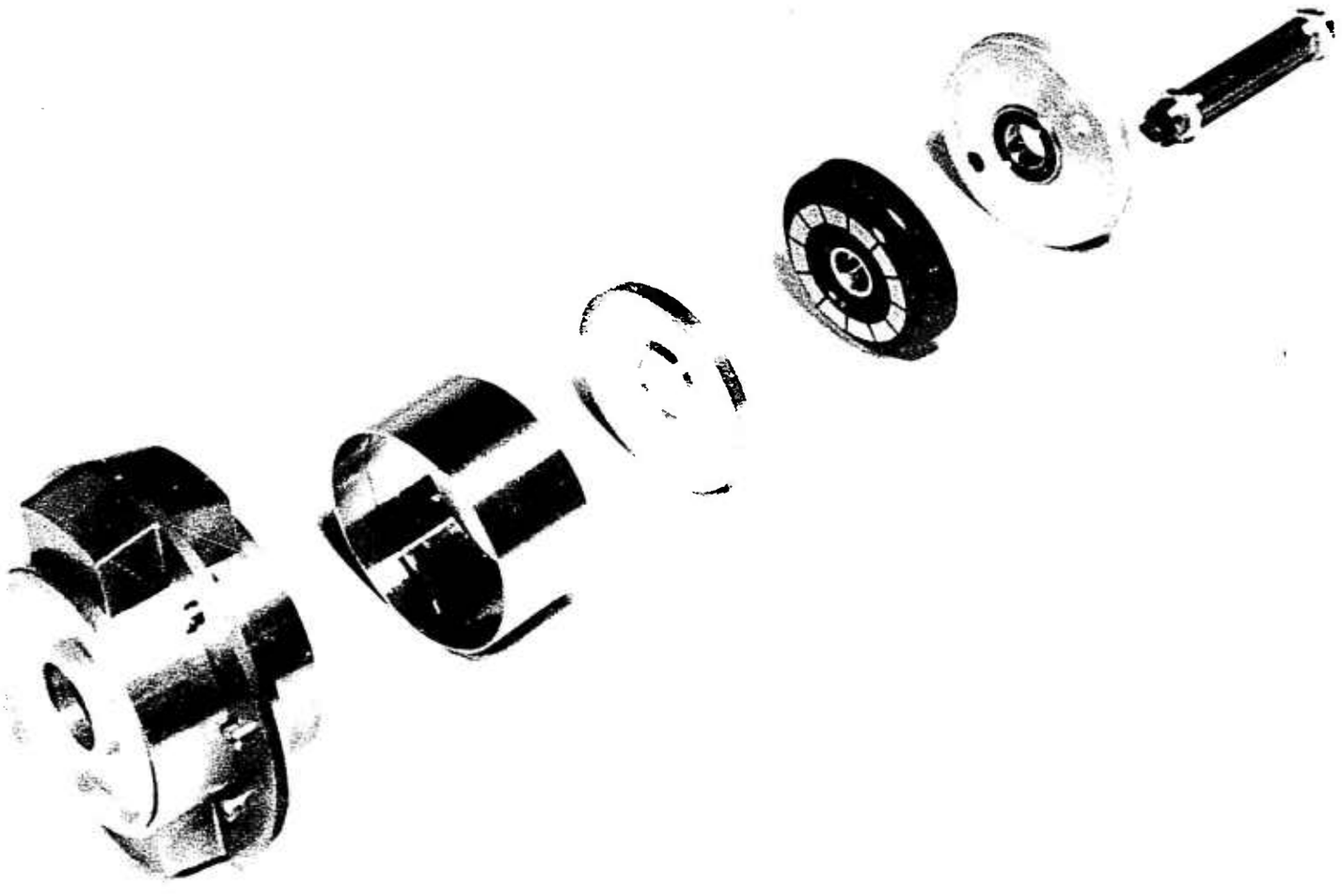

Figure 5. Nutatron Rotor

(a.) Capability of running at low speeds.

(b.) Low noise at twice the rotor speed.

(c.) Minimum inertia about an input axis.

(d.) Low running torques

3. Suspension System

The Nutatron uses a compound circular flexure type of suspension system. The flexure is supplemented by an electromagnetic spring rate compensator shown in Figure 6. The electromagnetic spring rate compensator is used to produce a negative spring rate that cancels the positive spring rate of the pivot. In addition to this function, the compensator is used for torquing in the rotating system. Spin motor power is supplied through flex leads shown in the lower portion of Figure 6. The pivot is held in place by a pivot holder shown in the middle of the figure. The holder is required to provide a magnetic "window" for the torquing system.

The flexure suspension system:

(a.) Permits two degrees of freedom of motion.

(b.) Presents a minimum moment of inertia about the input axes.

(c.) Has low rotational restraint about the input axes.

(d.) Has the ability to support the suspended element in an acceleration field of several g's without the aid of flotation fluid.

(e.) Has a high transverse ridigity to limit lateral deflections and eliminate the possibility of translational resonance near the Nutatron signal frequency.

(f.) Has high torsional stiffness to prevent motions about the spin axis.

The analysis of the compound annular flexure is presented in Appendix II.

4. Pickoff System

A capacitive pickoff system is used in the Nutatron because:

(a.) The configuration of a capacitive system is simple and inexpensive to build.

(b.) It adds very little to the nonworking (symmetric) inertia of the gyroscopic element.

(c.) The sensitivity in volts per radian is very high.

(d.) The power required to excite and operate a capacitive pickoff is very low.

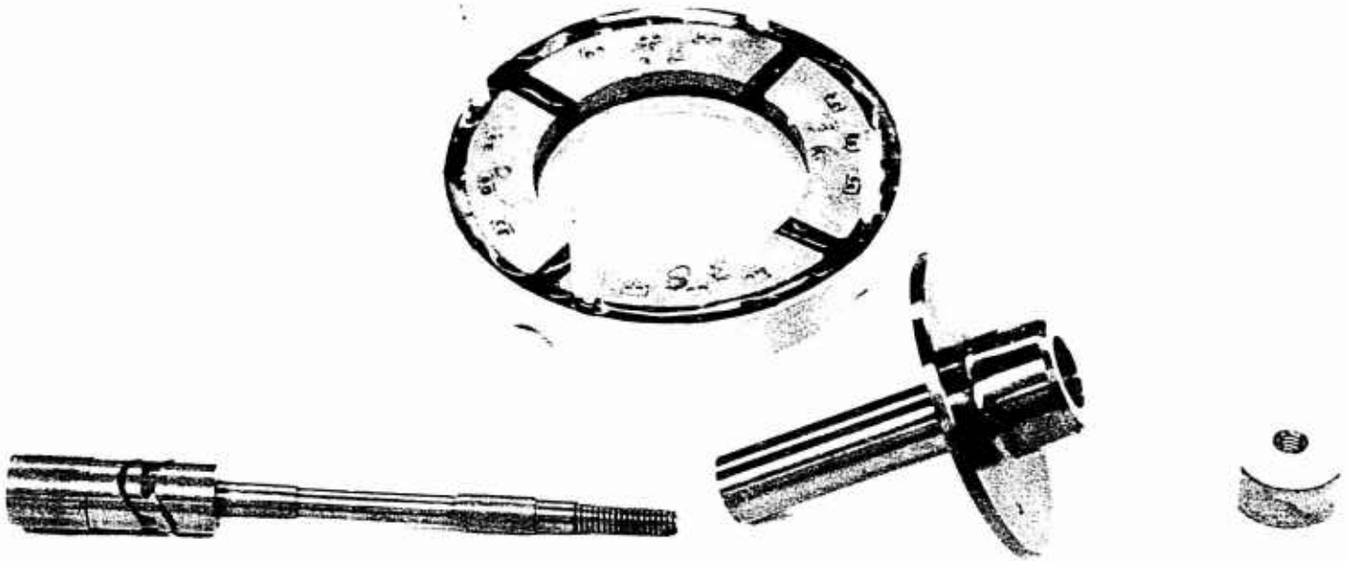

Figure 6. Suspension System

The present capacitive pickoff consists of two conductive plates: one mounted on the gyroscopic element and the other fixed to the gyro housing (Figure 7). These plates are flat, annular rings that are mounted so that a small gap exists between them. The plate mounted to the housing (fixed plate) is segmented into quadrants to provide two quadrants for each axis. Hence, four capacitors are formed between the quadrants of the fixed plate and the common plate on the gyroscopic element (moveable plate). These capacitors for each axis are connected in a Wheatstone type bridge, so that a signal is produced that is proportional to the angle of rotation of the gyroscopic element.

5. Torquing System

The Nutatron uses an electromagnetic torquing system to produce rebalance torques on the gyroscopic element and to precess the gyro on command. The torquing system (Figure 8) uses a cylindrical permanent magnet that is mounted on the gyroscopic element. The field of this permanent magnet is shaped by a soft iron cup. Eight small coils are mounted on the outside case of the gyro and extend into the field of the permanent magnet. When a current is passed through these coils, a torque is generated. Six of the coils are wound on soft iron cores, and are used for dc torque rebalancing and precession. The remaining two coils are wound on nonmagnetic cores, and are used for ac torque rebalancing.

6. Rotor Speed and Phase Detector

To synchronously demodulate the Nutatron signals, it is necessary to know the exact frequency and phase of the rotor rotation. To accomplish this, a capacitance plate is mounted to the gyro rotating housing and placed so that, each time one of the anisometric masses passes the plate, a change in the capacity of the plate to ground occurs. The capacitance is connected in a Wheatstone type bridge so that a voltage impulse is generated each time an anisometric mass passes. The output pulse is used for speed control and to generate a reference for the Nutatron signal demodulators.

7. Housing Rotation System

Housing rotation is accomplished by the addition of four major parts to the basic instrument. These parts are:

(a.) A housing rotation drive motor.

(b.) The bearings on which the housing rides.

(c.) A set of slip rings to provide electrical connection to parts inside the rotation housing.

(d.) A resolver to resolve the rotating pickoff signals into the fixed coordinate system.

8. Nutatron Electronics

The electronics required for the Nutatron consist of ten subsystems which are discussed in Section IV.C.

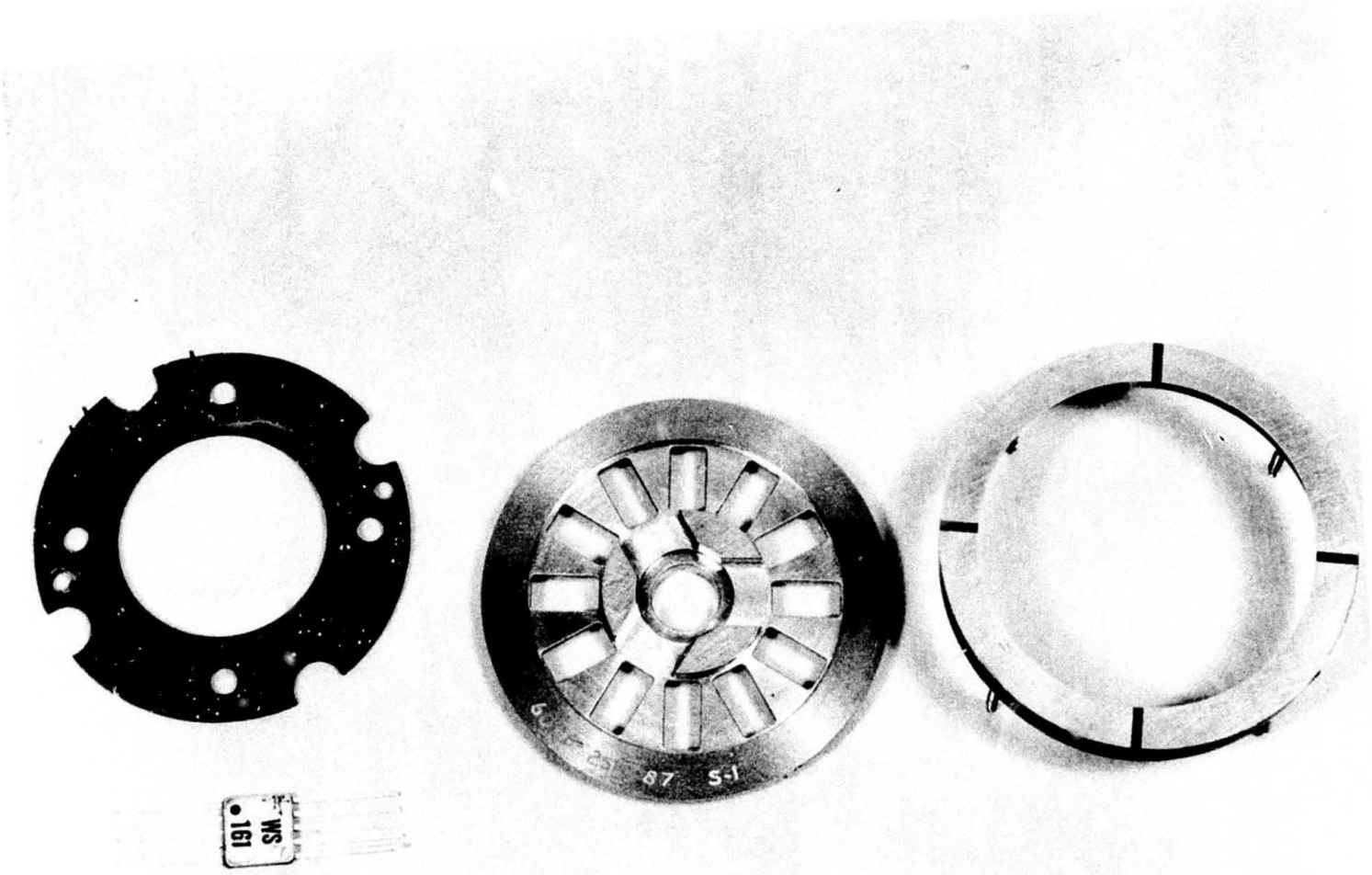

Figure 7. Pickoff System

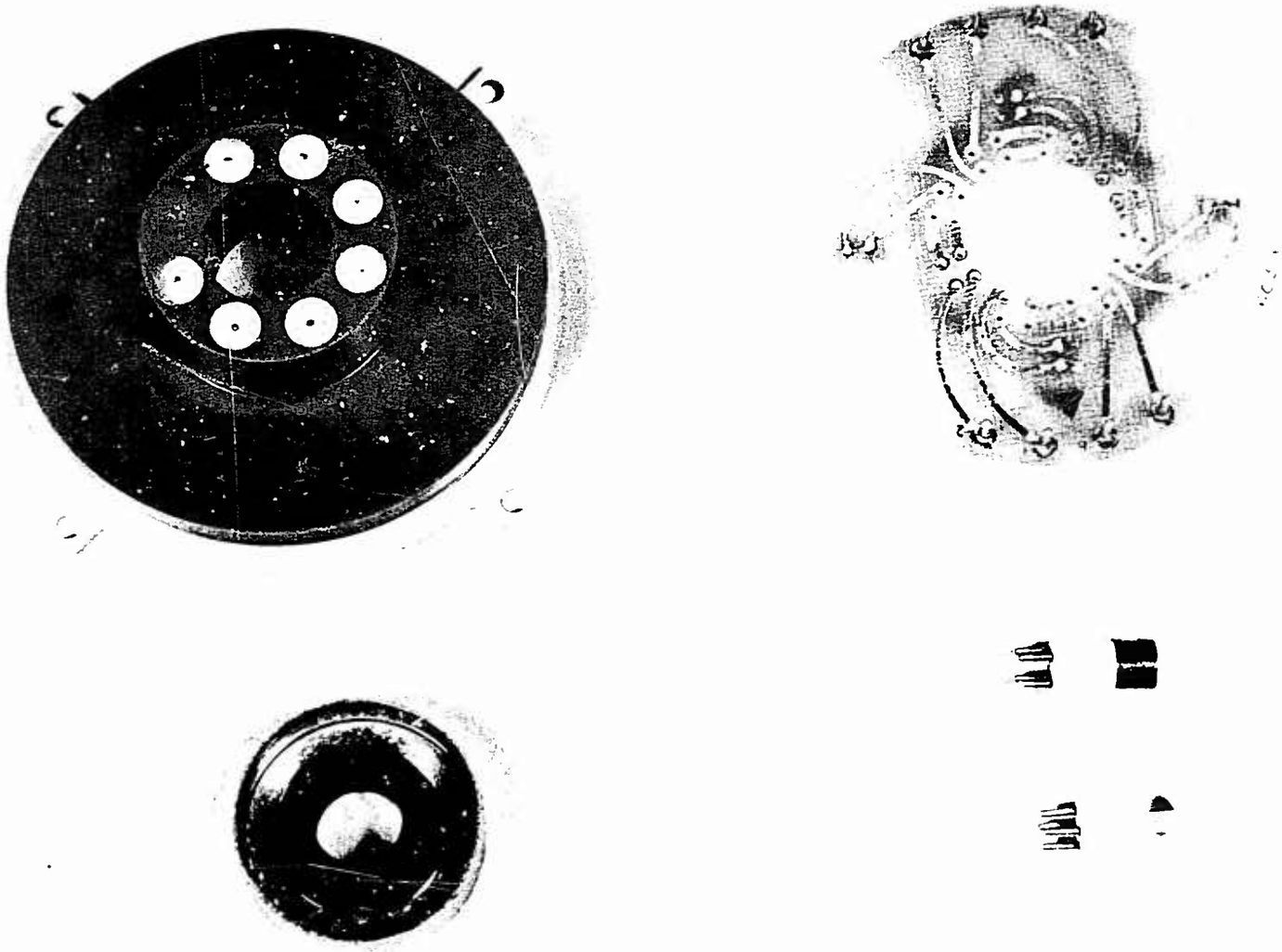

Figure 8. Torquing System

The Nutatron, in its present configuration and prior to modification, is illustrated with cross-sectional diagrams in Figures 10 and 9. The simplifications are evident on the lefthand side of the cross-section with the removal of one capacitive pickoff and spring compensation system from the rotating housing structure and the suspended element. The torquing system (torquer block on fixed housing and permanent magnet on suspended element) has also been taken off. The clear accessibility to the lefthand spin bearing is apparent which made it possible to change preload and shim adjustments while the Nutatron was on the test stand and without disassembly.

The one for one replacement of the pivot suspension by the compound circular flexure is seen in the center of the diagrams.

The major subsystems have been described in previous reports and are not covered here. The capacitive pickoff system, the rotor design, the eddy current spin motor, and the case rotation are covered in report No. AFAL-TR-67-54. The spring compensators and rotor speed control pickoff are discussed in Report No. AFAL TR-69-76.

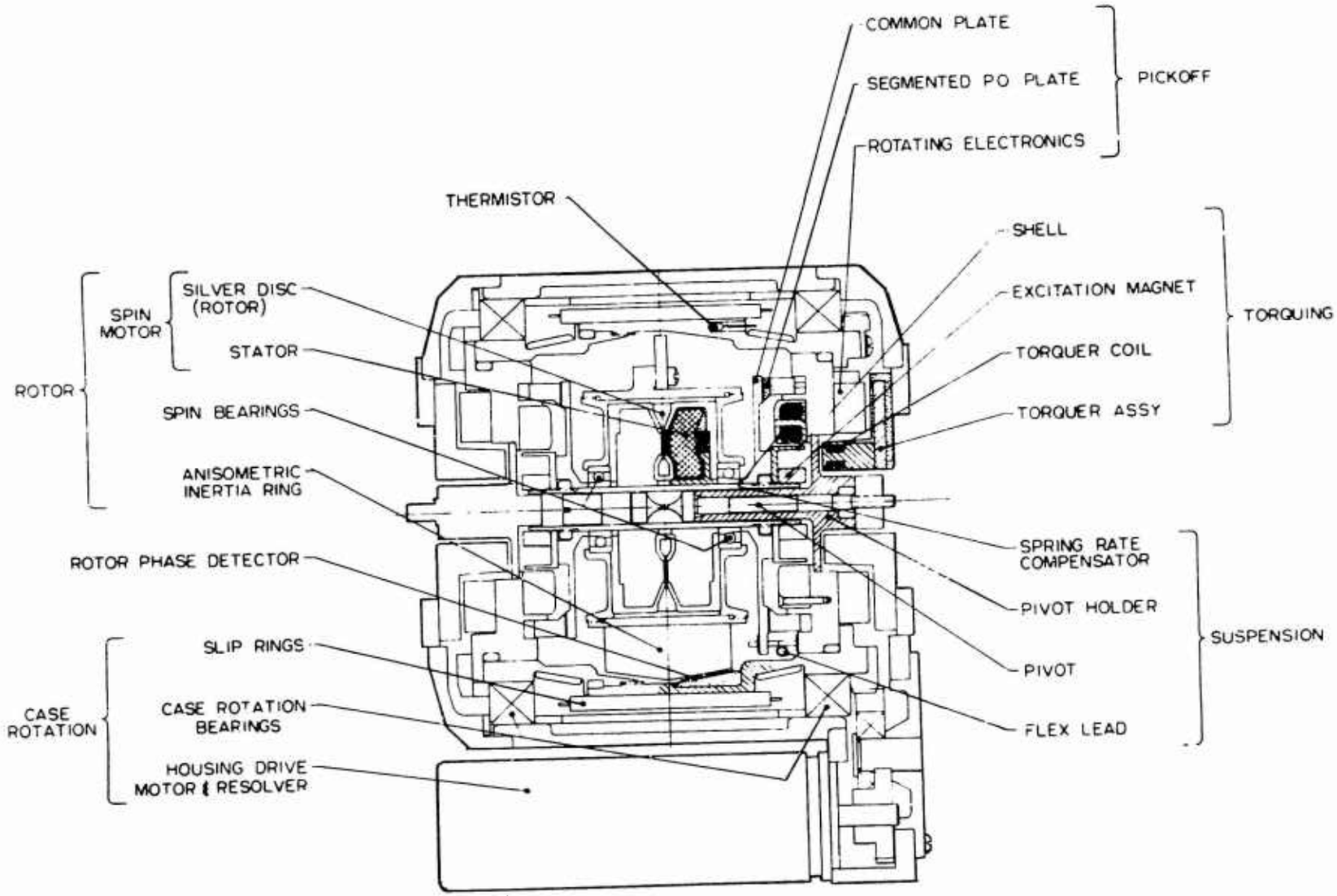

Figure 9. Simplified Cross-Section – Original Nutatron

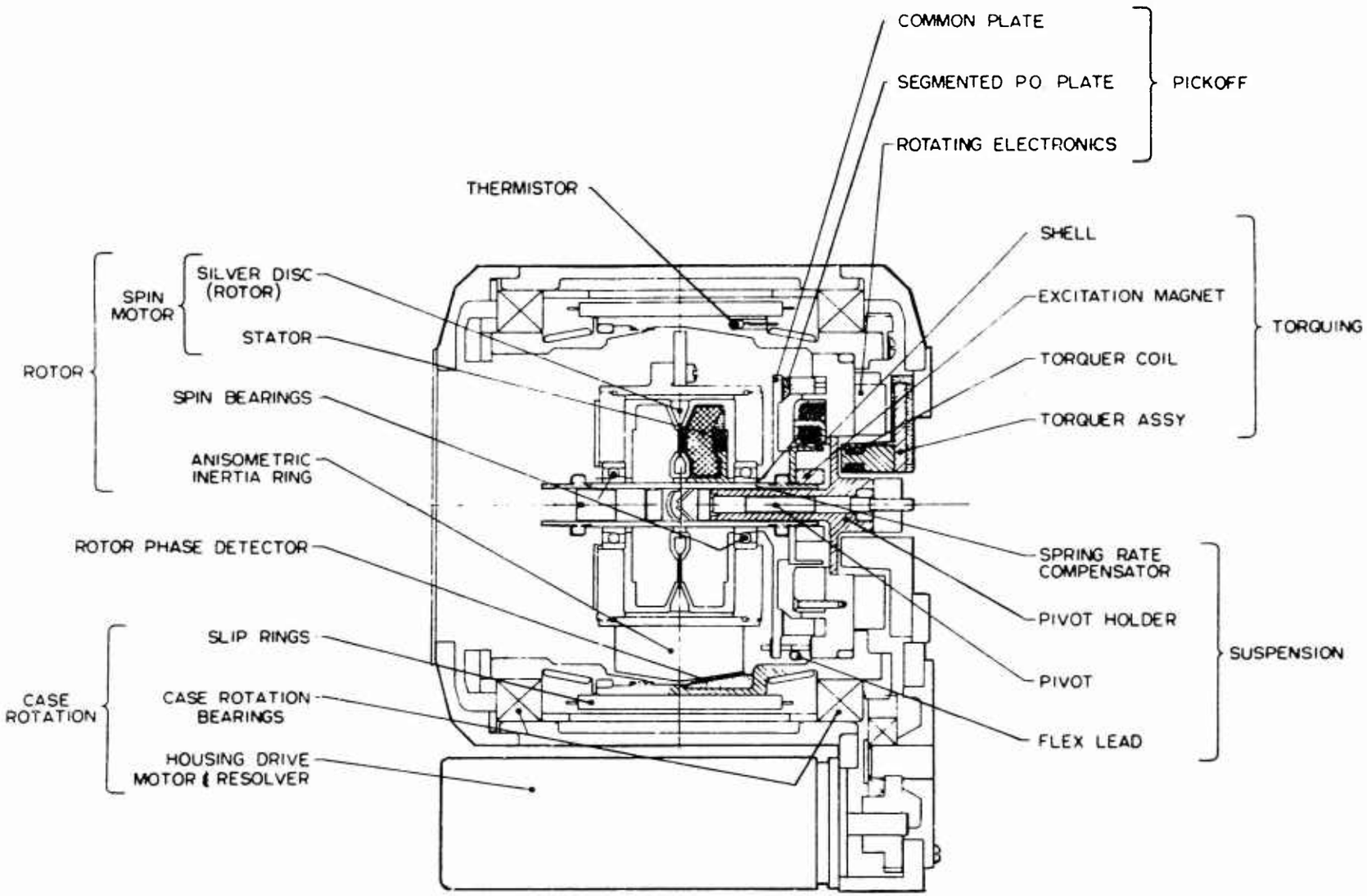

Figure 10. Simplified Cross-Section Present Nutatron

IV. NUTATRON TEST SET

The electronic test set in combination with the Nutatron is a self-contained system to measure angular input rates (components of earth rotation). It provides the special drive voltages to operate the instruments. It also furnishes a number of feedback functions unique to the Nutatron and the readout electronics for performance evaluation. For the engineer who is primarily interested in the overall operation of the Nutatron test system, the subsystems of the test set are described in block diagram form with a short description. This is followed by a discussion of the test console with its switching provisions and availability of terminals. The section concludes with a detailed description of the test set electronic circuits.

A. SUBSYSTEM DESCRIPTION

The electronic test set contains ten subsystems which can be grouped by three major functions:

1. Power Supplies and Reference Signal Generators

2. Nutatron Torque Rebalance Loops

3. Operating Condition Feedback Loops

Except for the zener diode to control the rotor speed, the Nutatron electronic test set contains no precision electronics. While the overall block diagram (Figure 11) may appear complex, the same functions are duplicated many times, namely demodulation, multiplication and integration. The system uses 13 standard demodulators, 16 commercially available multipliers, and 12 operational amplifiers rigged as integrators. It now appears that more than half the electronics can be eliminated in the future. It is likely that the resonance control loops, the axis alignment loops and dc capture loops can be dropped and the rest of the electronics simplified. The prime purpose of the electronic test set was the verification of the Nutatron principle. Flexibility of operation for investigative tests was the principal objective for the electronic test set rather than low cost and simplicity.

1. Power Supplies and Reference Signal Generators.

The voltages and frequencies required for the operation of the Nutatron are generated in three subsystems as follows.

a. Power Supplies (Block Diagram Figure 11, Section G)

The power supplies consist of the dc supplies required by the individual electronic circuits and the ac supply required to operate the case rotation motor. In addition a frequency reference unit, consisting of a crystal oscillator and a frequency divider, supplies the various frequencies required by the pickoff excitation, the rotor speed detector, the spin motor, the housing drive motor, etc. These signals are harmonically related to prevent low frequency beats due to interaction of the various circuits

b. 2ν and $2\nu+2\Omega$ Reference Signal Generation Electronics (Figure 11, Section F)

Various signals related to the rotor and case rotation frequencies are required by the electronics discussed above. These signals are generated by electronics which make use of the

rotor speed (and phase) detector to sense the rotor frequency, and the pickoff resolver to obtain the case rotation frequency.

These frequencies are processed by multipliers and amplifiers to derive

(1) sine and cosine phases of $2\nu+2\Omega$ for Nutatron signal detection demodulators and for the resonance control loop

(2) sine and cosine of 2ν for the axis alignment loops

(3) 2Ω Reference Generator (Figure 11, Section H)

This circuitry provides the reference signals required for the synchronous demodulators and modulators in the 2Ω nulling loop.

2. Torque Rebalance Loops

The Nutatron suspended element is torque rebalanced to its case with narrow bandwidth around three discrete frequencies, dc, $2\nu+2\Omega$ and 2Ω. The torque rebalance at these frequencies has very high gain supplied by integration in the loops. The dc torque rebalance loops only serve the function of slaving the Nutatron suspended element to the case. The dc rebalance torques are not normally measured or recorded in contrast to conventional gyros where they yield the performance. The rebalance torque at the Nutatron frequency stops the oscillations of the suspended element at $2\nu+2\Omega$ and serves as the indicated precession rate. The rebalance torque at 2Ω is direct measure of the acceleration inputs perpendicular to the spin axis and is used for correcting the standing level of acceleration sensitive Nutatron drift.

a. dc Constrainment Electronics (Figure 11, Section A)

These loops constrain the gyroscopic element by sensing its position relative to the case in two axes (x and y) and generating signals to the dc torquer. Because the Nutatron uses case rotation, the constrainment loops consist of rotating system pickoff electronics and fixed system torquing electronics. Resolution of the pickoff signals in the rotating system to the fixed torquing system is accomplished by an electromechanical resolver driven with the rotating case (Figure 12) by the housing drive motor.

b. Nutatron Frequency Torque Rebalance Electronics (Figure 11, Section B)

The Nutatron oscillations are sensed at and processed by the gyro pickoff electronics. The response of the gyro constrainment loop, however, is shaped to prevent these oscillations from reaching the dc torquers. The output of the pickoff electronics is fed to the Nutatron signal detection electronics, which consists of bandpass amplifiers and synchronous demodulators. The Nutatron oscillations are thus amplified and converted to dc signals. They are then integrated, remodulated at the Nutatron frequency, and fed back to a special air-core torquer, which nulls the Nutatron motions. The integrator outputs (after filtering) are the analog output signals representing the precession input and drift rates about the two sensitive axes.

c. 2Ω Torque Rebalance Electronics (Figure 11, Section J)

Because the two suspension axes of the compound circular flexure do not lie

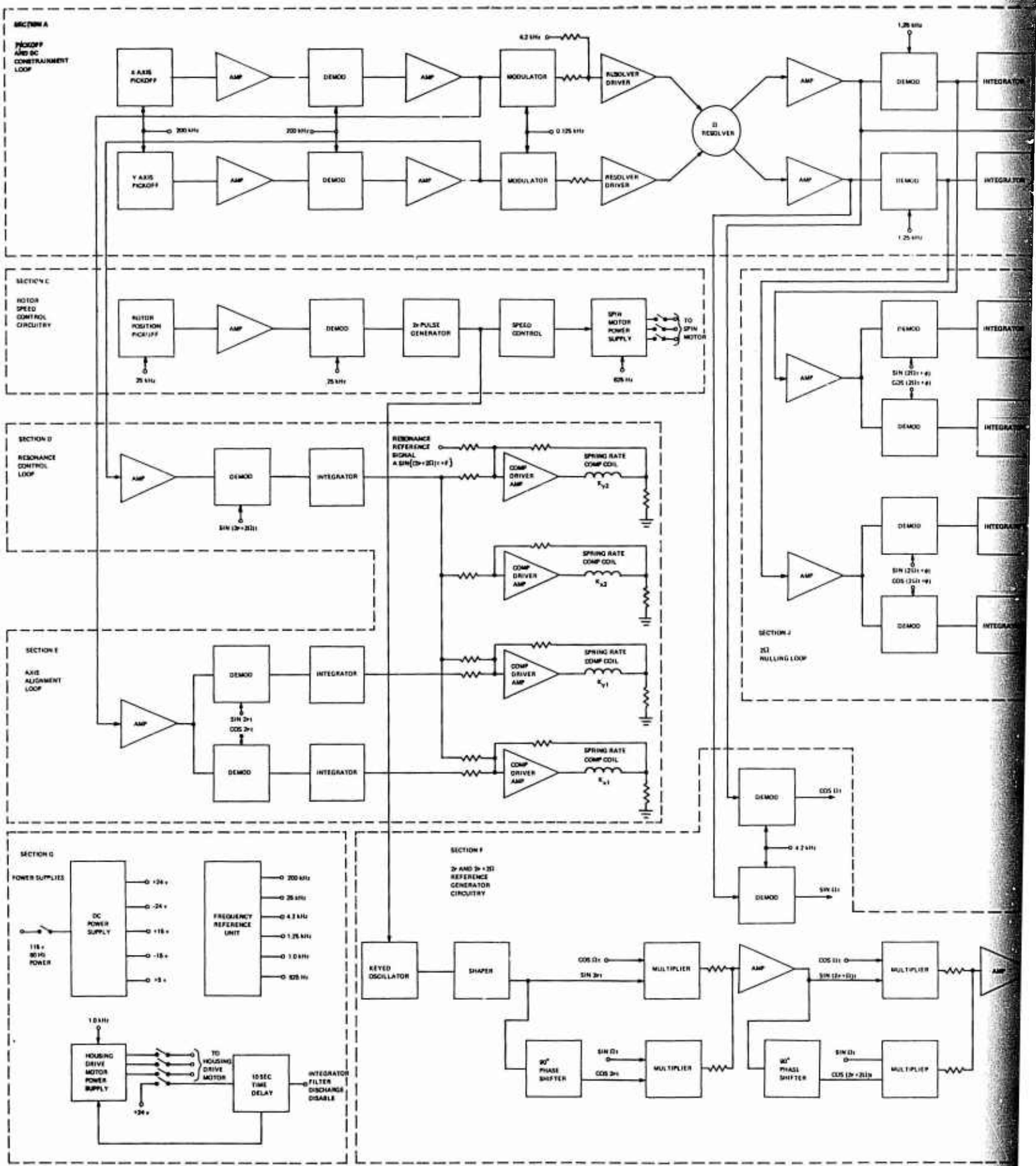
SECTION A
PICKOFF AND DC CONSTRAINMENT LOOP
X AXIS PICKOFF
Y AXIS PICKOFF
AMP
DEMOD
MODULATOR
RESOLVER DRIVER
RESOLVER
INTEGRATOR
SECTION C
ROTOR SPEED CONTROL CIRCUITRY
ROTOR POSITION PICKOFF
2r PULSE GENERATOR
SPEED CONTROL
SPIN MOTOR POWER SUPPLY
TO SPIN MOTOR
SECTION D
RESONANCE CONTROL LOOP
RESONANCE REFERENCE SIGNAL
COMP DRIVER AMP
SPRING RATE COMP COIL
SECTION E
AXIS ALIGNMENT LOOP
SECTION J
2Ω NULLING LOOP
SECTION G
POWER SUPPLIES
DC POWER SUPPLY
FREQUENCY REFERENCE UNIT
HOUSING DRIVE MOTOR POWER SUPPLY
TO HOUSING DRIVE MOTOR
10 SEC TIME DELAY
INTEGRATOR FILTER DISCHARGE DISABLE
SECTION F
2r AND 2r ± 2Ω REFERENCE GENERATOR CIRCUITRY
KEYED OSCILLATOR
SHAPER
MULTIPLIER
90° PHASE SHIFTER

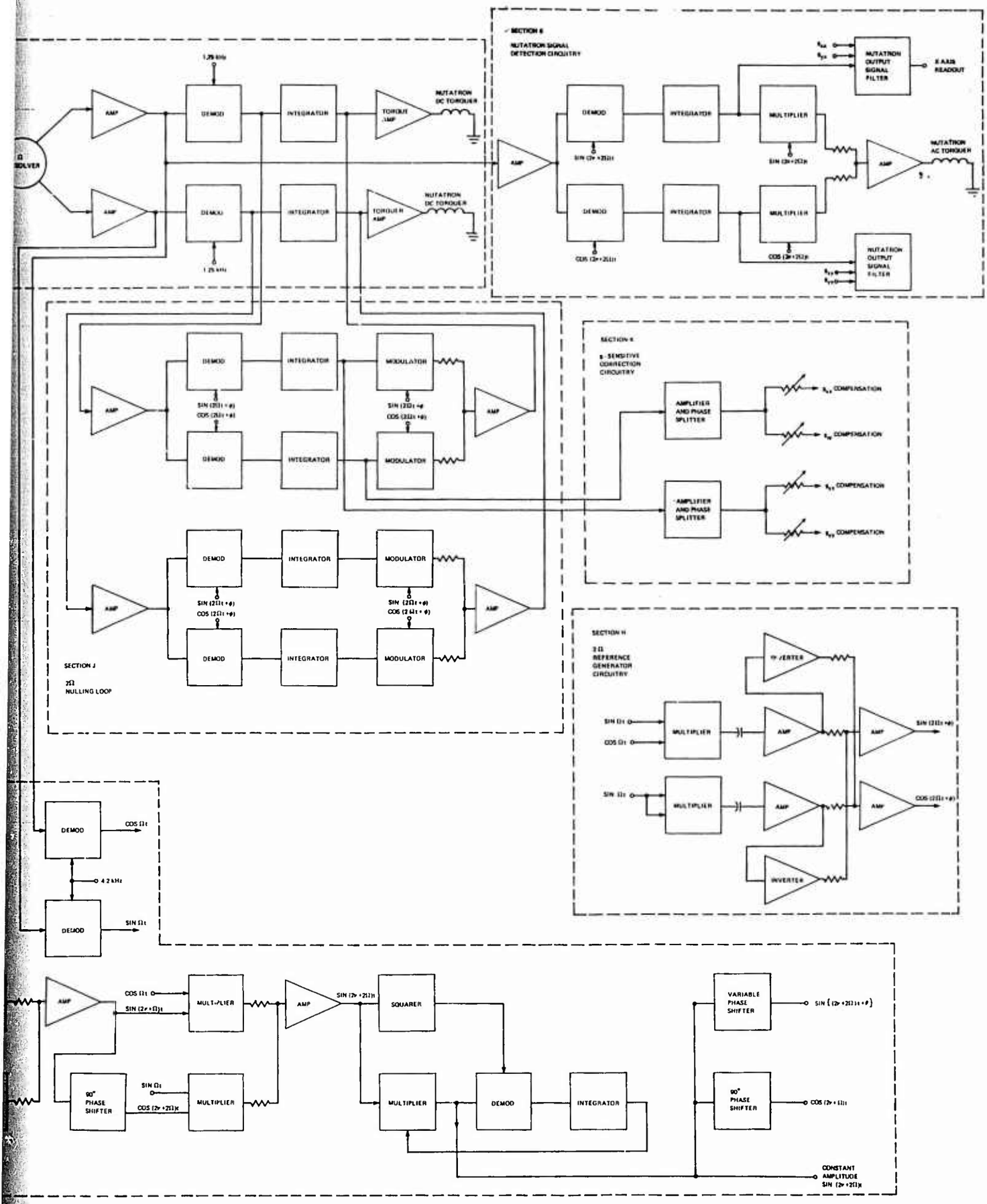

Figure 11. Overall Block Diagram

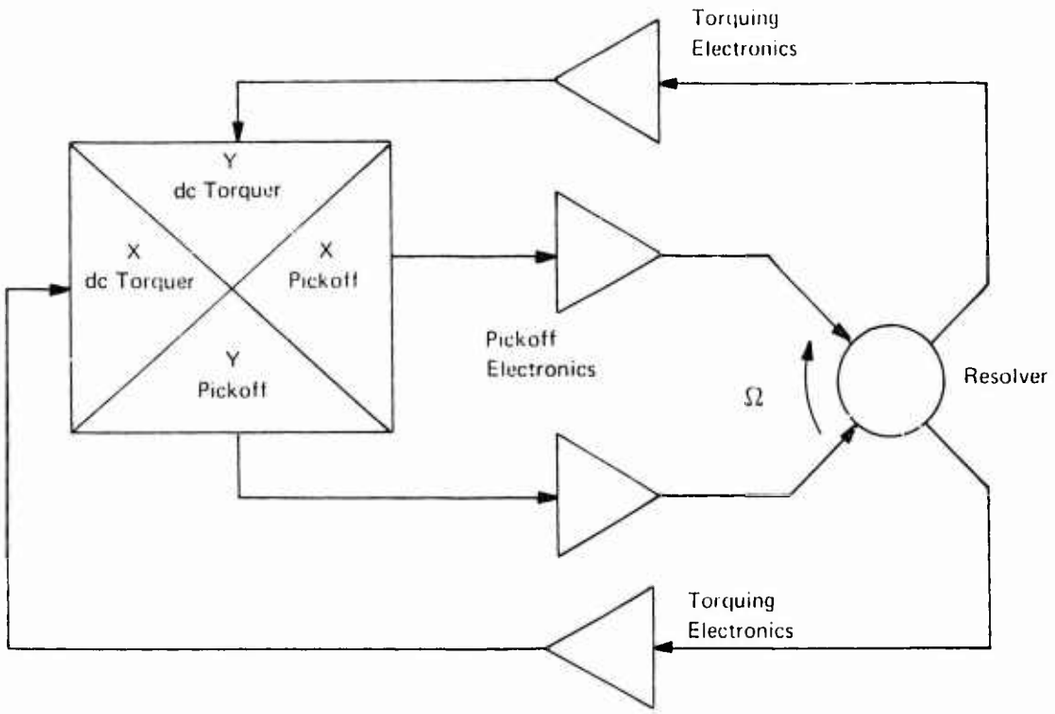

Figure 12. Gyro Constrainment Loops

exactly in the same plane perpendicular to the spin axis, a torque is generated at twice the case rotation frequency (2Ω) in response to accelerations (or g-forces) perpendicular to the spin axis. The normal gyro constrainment loop rolls off at a frequency much lower than 2Ω; therefore, a special 2Ω nulling loop is required to constrain the 2Ω motions.

The output of the pickoff electronics is amplified and synchronously demodulated at 2Ω. The resulting dc signals are integrated, remodulated, and fed into the dc torquers to null the 2Ω motions. This loop provides very high loop gain in a very narrow band about 2Ω.

The integrator outputs of the 2Ω nulling loop above generate dc signals proportional to the acceleration (or g-forces) along the two sensitive axes of the Nutatron. These outputs are appropriately phased and scaled to provide signals to compensate for acceleration sensitive errors in the Nutatron. They are summed along with the Nutatron signal in such a way as to minimize these acceleration sensitive errors.

3. Operating Condition Feedback Loops

For proper operation the Nutatron rotor speed has to be controlled, the rotor and case rotation axes have to be maintained in approximate alignment, and the suspension spring constant maintained to resonate the Nutatron signal $2\nu+2\Omega$. Achieving the latter two conditions by feedback techniques greatly eases the precision requirements of the mechanical parts and assembly techniques.

a. Rotor Speed Control Loop (Figure 11, Section C)

The Nutatron uses an eddy current motor to spin the rotor. A speed control loop is used to hold the rotor spin speed constant. The loop (Figure 12) consists of a rotor speed detector, electronics to adjust the output of the motor supply, and the 3-phase motor supply.

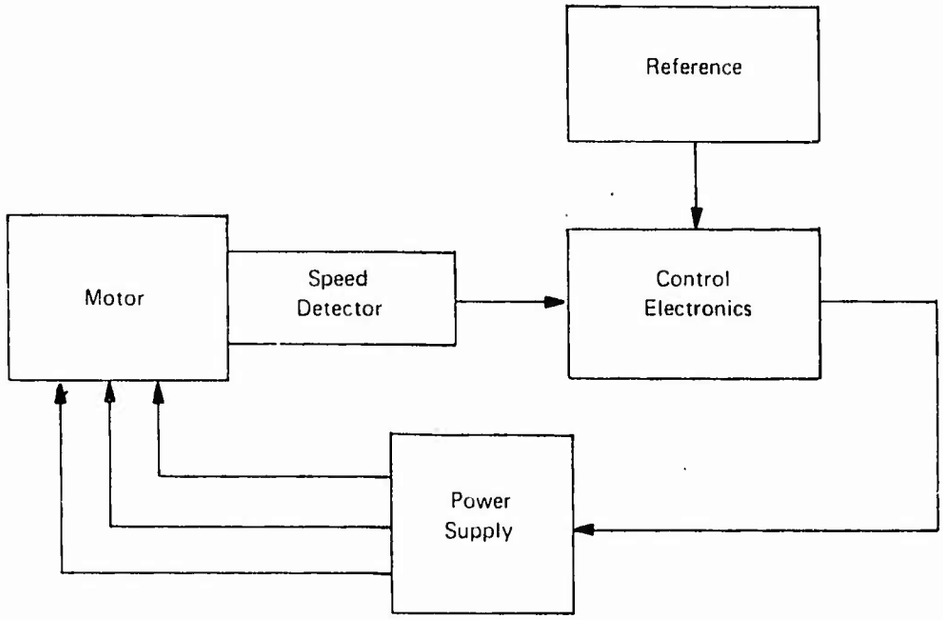

Figure 13. Rotor Speed Control

b. Resonance Control Loop (Figure 11, Section D)

The minute signal oscillations of the Nutatron are enhanced by resonating the suspension system at the Nutatron signal frequency. The internal damping of the Nutatron is very low due to the unfloated configuration, and, as a result, the resonance Q is quite high (≈ 40). To avoid shifts of the resonance peak with time, temperature, etc. a servo loop controls the resonance. This loop (shown in Figure 14) uses a signal derived from the actual rotor speed to sense the resonance condition. The phase of this signal is measured as it passes through the resonant suspension system. Deviations from the desired phase are measured and the current in the spring rate compensators is adjusted to vary the suspension system spring rate. Therefore, the resonant frequency of the suspension system is constant with respect to the rotor speed.

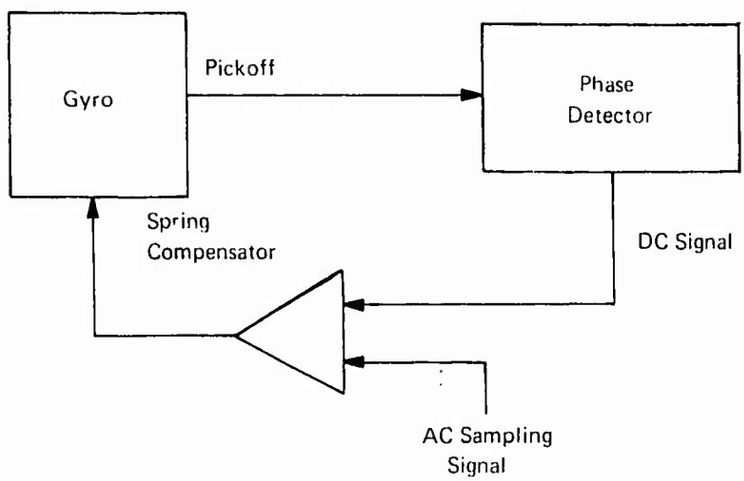

Figure 14. Resonance Control Loop

c. Axis Alignment Loops (Figure 11, Section E)

As stated above, the Nutatron uses case rotation to improve its performance. A misalignment between the spin axis and the case rotation axis introduces a component of the case rotation rate into the gyro. The amplitude of this rate is proportional to the misalignment angle (for small angles). This signal has an effect on the Nutatron performance if it gets too large. Automatic axis alignment loops (Figure 15) are used to align the spin axis to the case rotation axis. These two loops (one for the x axis, one for the y) sense the misalignment of the two axes by detecting the Nutatron signal generated by the misalignment and adjust the position of the spin axis. The electromagnetic spring rate compensators are used as torquers to position the spin axis.

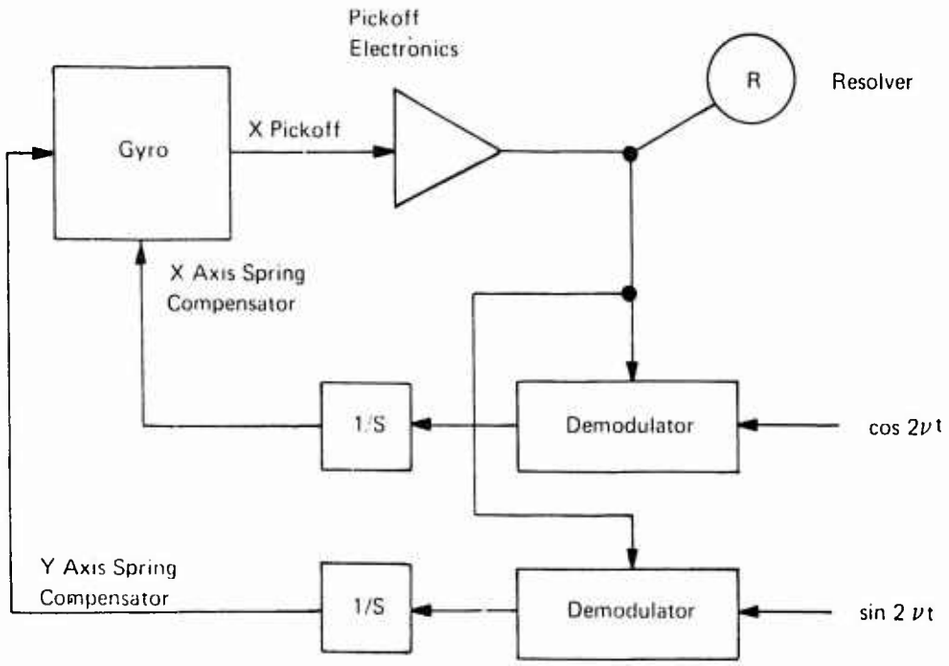

Figure 15. Axis Alignment Loops

B. NUTATRON TEST ELECTRONICS CONSOLE (FIGURE 16)

The Nutatron Test Electronics circuits are enclosed in a standard relay rack (42 in. high x 22 in. wide x 22 in. deep. The dc power supplies are located on a chassis at the bottom of the rack, and the remainder of the electronic circuits are constructed on 4-1/2 inch x 6-1/2 inch plug-in vector boards. There are 26 of these boards mounted in three vector board cages stacked one above the other, with the connectors and interconnecting wiring at the front of the rack. The front of the rack is made up of four panels which provide all the switching, monitoring, and control functions for the operation of the Nutatron. The locations and descriptions of these functions are summarized in Table II.

The performance monitoring signals are Nutatron Signals No. 1 and No. 2 in the form of analog voltages proportional to the input angular rates about the sensitive axes. All of the other

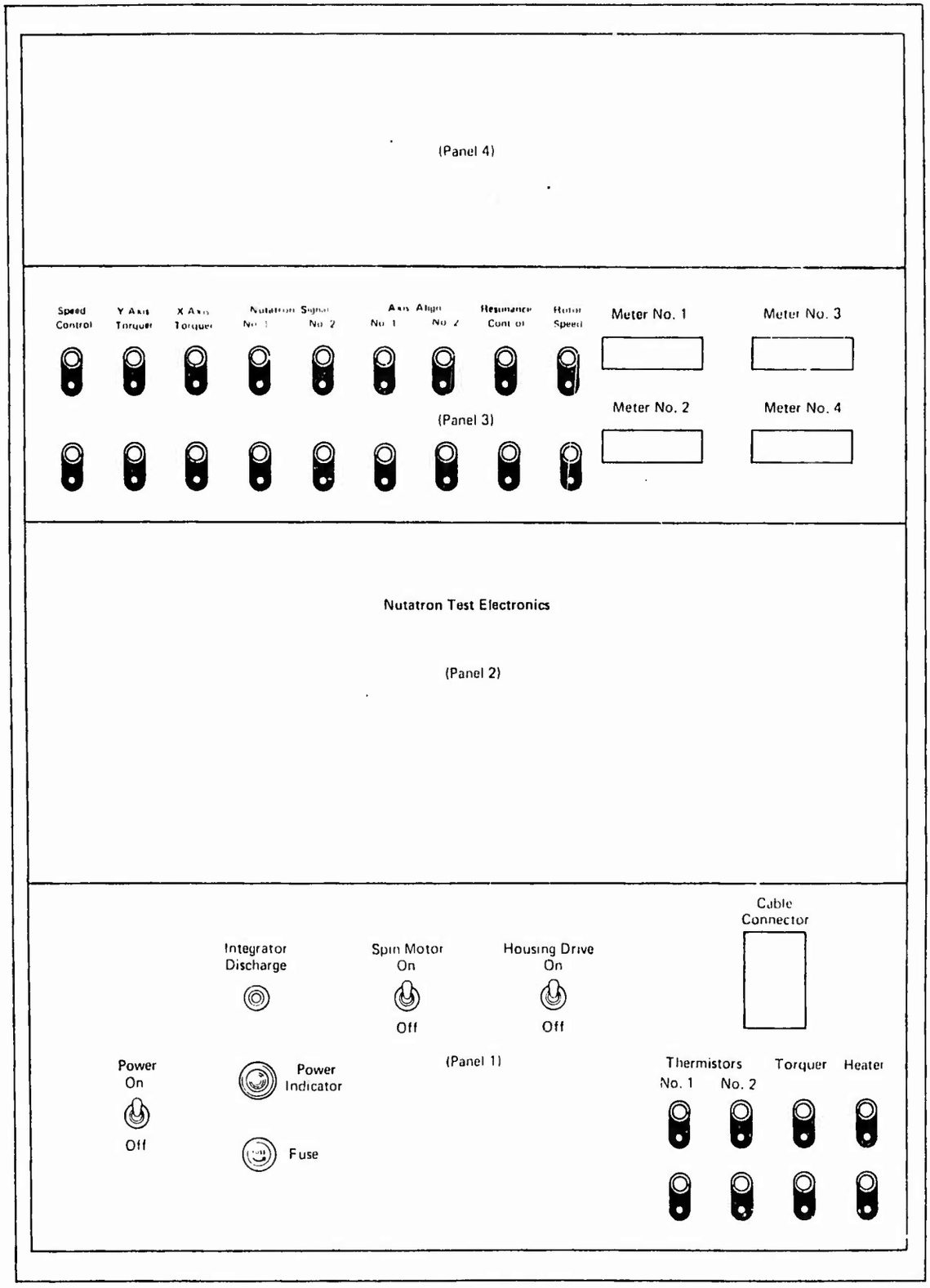

Figure 16. Nutatron Test Electronics

TABLE II. SUMMARY OF FRONT PANEL MONITORING AND CONTROL FUNCTIONS

Front Panel Number	Title	Function
1	Power Switch	Activates the dc power supplies and cooling fan.
1	Integrator Discharge Switch	Nulls the outputs of all the integrators in the system. This is a spring loaded pushbutton switch. It is used only for troubleshooting.
1	Spin Motor Switch	Applies power to the spin motor.
1	Housing Drive Switch	Applies power to the housing drive motor and activates all of the Nutatron Electronic loops.
1	Thermistor No. 1	Test points across Thermistor Number 1 inside the Nutatron.
1	Thermistor No. 2	Test points across Thermistor Number 2 inside the Nutatron.
1	Torquer	Test points across the ac torquer.
1	Heater	Test points across the Nutatron heating element.
3	Speed Control	Test points across speed control circuit output.
3	Y Axis Torquer	Test points across Y axis dc torquer coils.
3	X Axis Torquer	Test points across X axis dc torquer coils.
3	Nutatron Signal No. 1	X Axis Nutatron readout signal.
3	Nutatron Signal No. 2	Y Axis Nutatron readout signal.
3	Axis Align No. 1	Test points across input of axis alignment integrator Number 1.
3	Axis Align No. 2	Test points across input of axis alignment integrator Number 2.
3	Resonance Control	Test points across input of resonance control integrator.
3	Rotor Speed	Test points across 2ν pulse generator output.
3	Meter No. 1	Measures output voltage of X axis compensator driver Number 1.
3	Meter No. 2	Measures output voltage of X axis compensator driver Number 2.
3	Meter No. 3	Measures output voltage of Y axis compensator driver Number 1.
3	Meter No. 4	Measures output voltage of Y axis compensator driver Number 2.

monitoring functions are provided to check on the proper operation of the Nutatron and Test Electronics or to provide indications of any system malfunction.

C. DETAIL DESCRIPTION OF NUTATRON TEST ELECTRONICS

The Nutatron test electronics was designed for the specific purpose of operating and evaluating the instrument in the laboratory. Maximum flexibility, ease of packaging and troubleshooting at minimum cost were the principal objectives for this exploratory development effort. The following design approach and guidelines were used in the design and fabrication of the Nutatron test electronic circuits to achieve these goals.

1. Design Approach and Guidelines

   a. The electronic circuits are packaged and arranged to allow ready access to all components for ease of maintenance.

   b. Access is provided to all of the circuit board connectors for monitoring. Each connector has 16 pins available for monitoring inputs, outputs, and supply voltages.

   c. No special attempt was made to minimize the size of the electronics package. The circuits are reasonably compact without being overcrowded.

d. The circuits are rugged enough to withstand shipping and handling but are not to be subjected to shock or vibration tests.

e. The circuits are designed to operate in a moderately clean, temperature controlled laboratory environment, and are not to be subjected to extended temperature testing.

f. Standard designs and components are used wherever possible to simplify overall design and maintenance. For example, a standard transformerless demodulation design is used throughout, and the LM 201A is used as the standard operational amplifier in all circuits requiring a general purpose operational amplifier.

g. Commercial grade components are used throughout.

2. Nutatron Test Electronics Circuit Description

The electronic circuits are described in this section to explain their function and to highlight the special techniques to minimize error mechanisms at the Nutatron frequency ($2\nu + 2\Omega$). As a result of the extensive investigative analysis and test effort, the performance degradation contributed by the electronics has been held to a negligible level. The circuits are illustrated in detail in Appendix III.

a. Constrainment Loop

The Nutatron is operated in a rate constrained mode. Deflections about the x and y axes are sensed by capacitance pickoffs. The resulting signals are processed by the pickoff electronics and supplied to the dc torquers to make the gyroscopic element follow the case. The response of the loops is set to provide high gain at dc. The response falls off quickly so the loop is open at the Nutatron signal frequency (20 Hz) to allow the Nutatron oscillation to exist. The circuit blocks that constitute the constrainment loops are shown in Section A of Figure 11.

(1) Pickoff Circuit (Figure 17)

The Nutatron utilizes a capacitance pickoff system to detect relative motion between the case and the gyroscopic element. The pickoff capacitors are connected in a Wheatstone type bridge which is excited by 200 kHz. Motions of the case produce a 200 kHz bridge unbalance signal which is proportional to the deflection of the case with respect to the gyro element.

An IC differential amplifier amplifies the pickoff signal and isolates the bridge from loading. The amplifiers for the x and y axes are mounted inside the gyro rotating housing. Their outputs are passed through slippings before exiting from the gyro. The gyro pickoff signal is fed to a 200 kHz demodulator.

(2) 200 kHz Demodulator (Figure 18)

The pickoff signal is demodulated at 200 kHz to remove the carrier signal and provide a steady-state signal proportional to the relative position of the gyroscopic element in the rotating case. The demodulation is accomplished by synchronously switching a field effect transistor. A 0V to -10V, 200 kHz reference signal is applied to the gate of the demodulator switch-

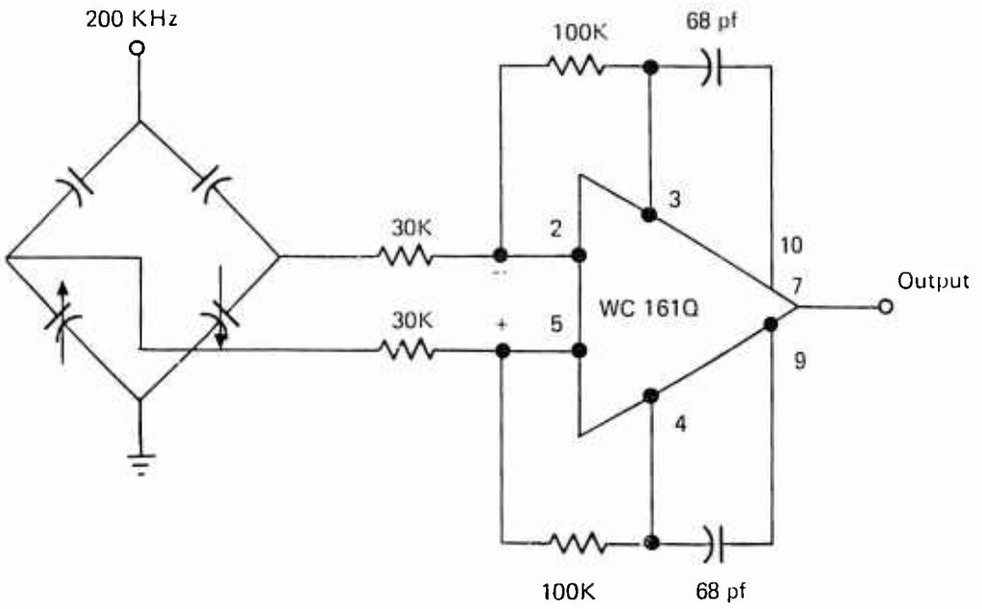

Figure 17. Pickoff Circuit

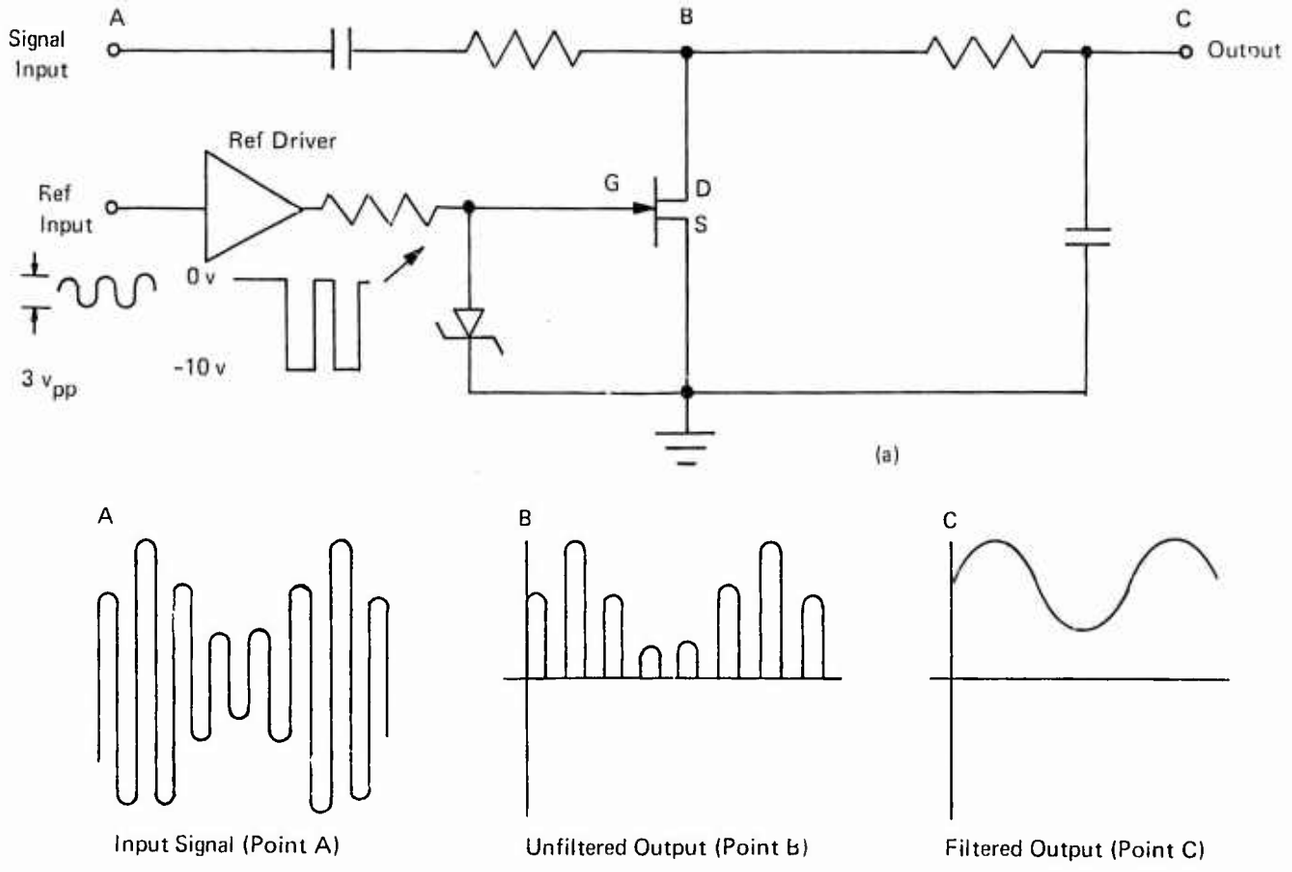

Figure 18. 200 kHz Demodulator

ing transistor. This transistor has a very low saturation resistance when the gate voltage is above -8 volts, and switches to very high resistance for voltages below -8 volts. Therefore, it becomes a shunt switch to ground every half cycle of the 200 kHz. The resultant output is a half-wave rectified 200 kHz output whenever a 200 kHz signal is present at the input. This output is subsequently filtered to remove the 200 kHz carrier. Figure 18 is a representation of the waveforms seen at points A, B and C of the demodulator circuit. The 200 kHz demodulators are located on the Nutatron Holding Fixture. Figures III-1 and III-2 of Appendix III give the details of the circuit and its layout.

(3) Pickoff Amplifiers (Rotating System dc Amp) (Figure 19)

In addition to providing gain in the constrainment loop, the pickoff amplifiers are also used to block dc signals in the rotating system. These signals represent the position of the gyroscopic element with respect to the rotating case and become Ω signals upon resolution into the fixed (nonrotating) system. Feeding these signals back through the torquer tightly constrains the gyroscopic element to the rotating case. This conflicts with the operation of the axis alignment loops which are described below. In the overall loop response, the blocking action of the dc amplifier introduces a notch at Ω. Otherwise the loop response is unaffected. These amplifiers also incorporate a notch at the rotor frequency, ν (which results from dynamic unbalance of the rotor). The 1ν frequency signal component is blocked before it is passed through the pickoff resolver (see below), which would convert it to a signal at $(\nu + \Omega)$. Subsequent second harmonic electronic distortion would generate an error signal at the Nutatron signal frequency $(2\nu + 2\Omega)$.

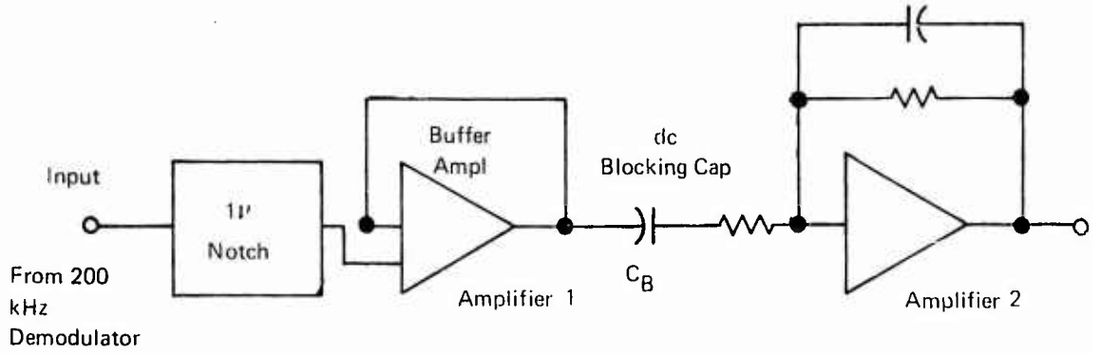

Figure 19. Pickoff Amplifier

As shown in Figure 19, 1ν frequency components in the signal are greatly attenuated by the 1ν notch (Twin T) filter. The buffer amplifier provides the required high output impedance for the notch filter. The dc component in the output signal of the buffer amplifier is blocked by the capacitor C_B. Amplifier 2 provides further gain and high frequency roll-off. The complete schematic and layout of the circuit are Figures III-31 and III-32, Appendix III. The pickoff amplifiers are located on circuit board number 15.

(4) Rotating to Fixed Coordinate Axis Resolution

Resolution of the output of the pickoffs, which are attached to the rotating case, into the fixed (nonrotating) system is carried out by an electromechanical resolver driven at Ω by the rotating case. Passage of the low frequency signals of the pickoff system through the

resolver requires that the signals be modulated by a higher frequency carrier (1.25 kHz) and demodulated afterwards. The circuitry shown in Figure 20 accomplishes this. The circuitry consists of a modulator, a driver amplifier to drive the low impedance of the resolver winding, a fixed system amplifier and a demodulator for each axis (see Figure 20).

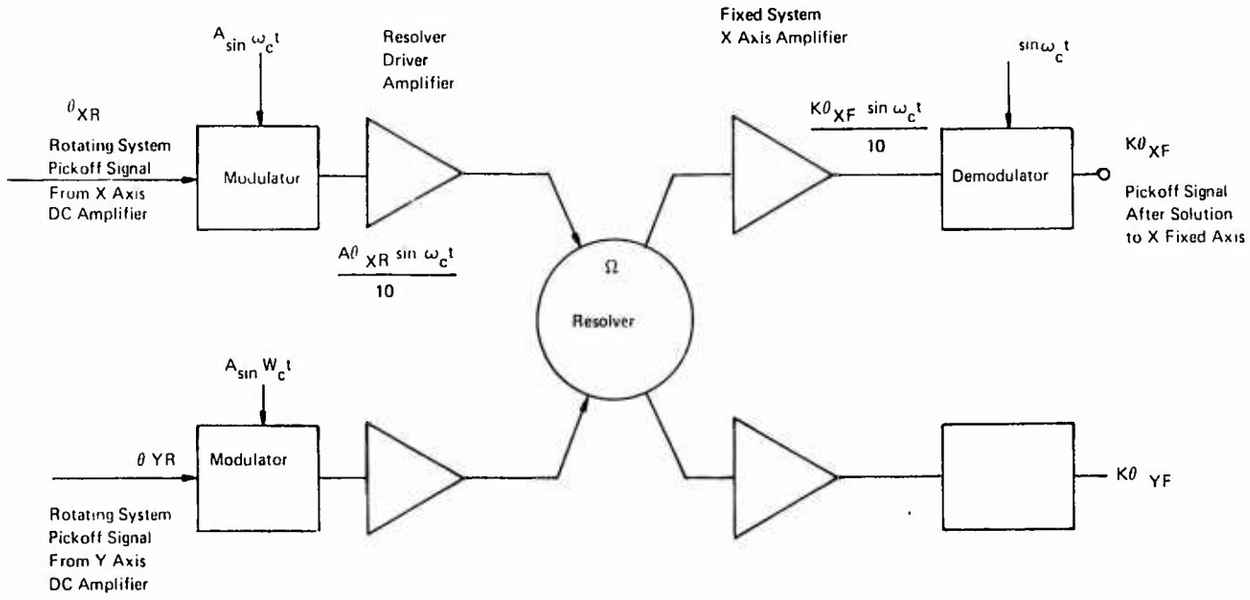

Figure 20. Rotating System to Fixed System Coordinate Resolution

(a) Modulator

The modulator is an integrated circuit multiplier (AD 530), whose output is proportional to the product of the two inputs. In Figure 20,

θ_{XR} represents the rotating system x axis pickoff signal.

A sin $\omega_c t$ is the 1.25 kHz carrier signal. The output of the multiplier is the product of the two signals divided by 10.

$$V_{out} = \theta_{XR} \times A \sin \omega_c t / 10.$$

(b) Driver Amplifier

The resolver driver amplifier is an integrated circuit operational amplifier (LM 201A), whose gain is 1V/V at 1.25 kHz.

(c) Fixed System Amplifier

The fixed system amplifier provides gain and phase splitting. It consists of an operational amplifier (LM 201A) whose gain is 3.3 V/V, followed by a unity gain inverter (see Figure 21).

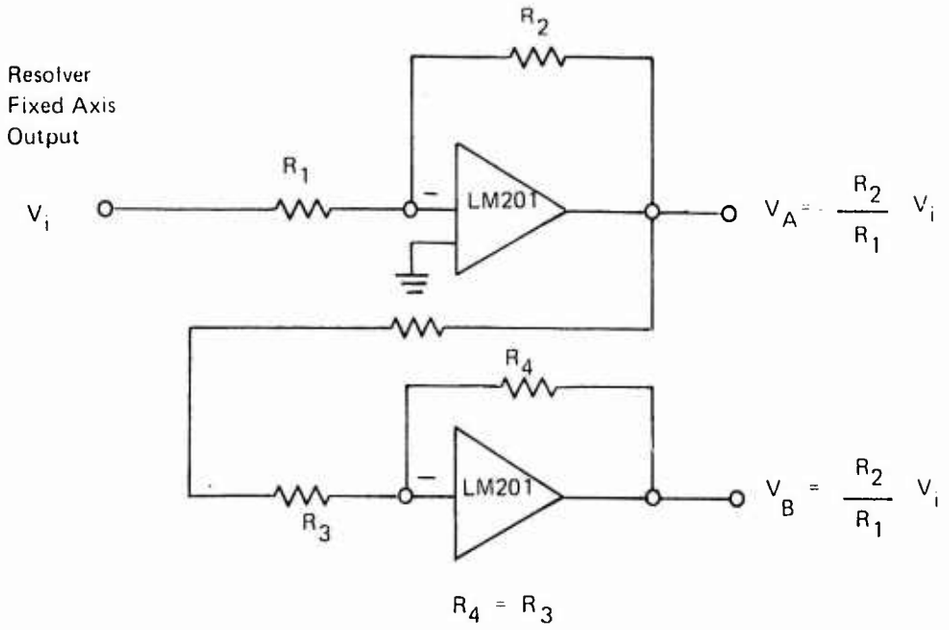

Figure 21. Fixed-Axis Amplifier

(d) Demodulator (Figures 22a and 22b)

The demodulator is required to remove the 1.25 kHz carrier and provide an analog signal proportional to the position of the gyroscopic element relative to the fixed housing coordinate system. It consists of an integrated circuit, DPST, J-FET switch and driver, followed by an operational amplifier.

The outputs of the fixed axis amplifier (V_A and V_B) are applied to inputs A and B respectively (Figure 22a). The solid-state switch alternately connects A to C then B to D, each for one-half cycle. The resultant waveforms (V_C and V_D) are seen in Figure 22b. These voltages are applied to the input resistors of the operational amplifier, which adds the demodulated signals, supplies gain, and attenuates the carrier frequency (1.25 kHz) with a high frequency roll-off filter.

(5) Integrator (Figure 23)

The torquing integrator provides a high constrainment loop gain at dc. The gain falls off at 6 dB/octave up to 2 rad/sec and levels off at that point. The integrator consists of an operational amplifier (LM 201A) with the input and feedback components arranged as shown in Figure 23. The high loop gain preceding the integrator provides an input sensitivity of 3 mv/sec. The important consideration in the design of this integrator stage is to ensure that its input noise voltage and low frequency drift do not cause significant precession rates in the 0 to 0.1 rad/sec range. The LM 201A input noise spectral density below 10 Hz is primarily of the form:

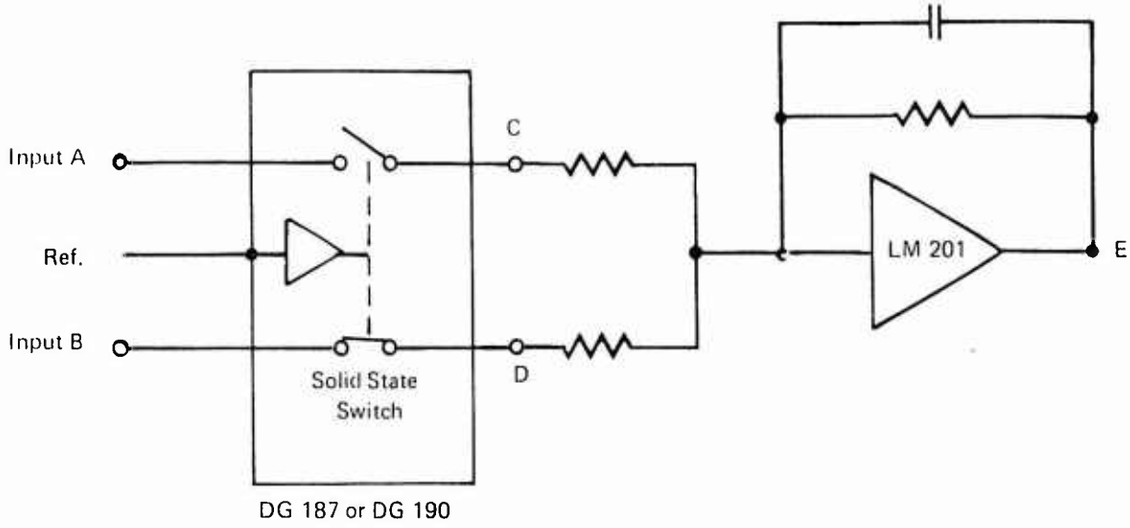

(a) Demodulation

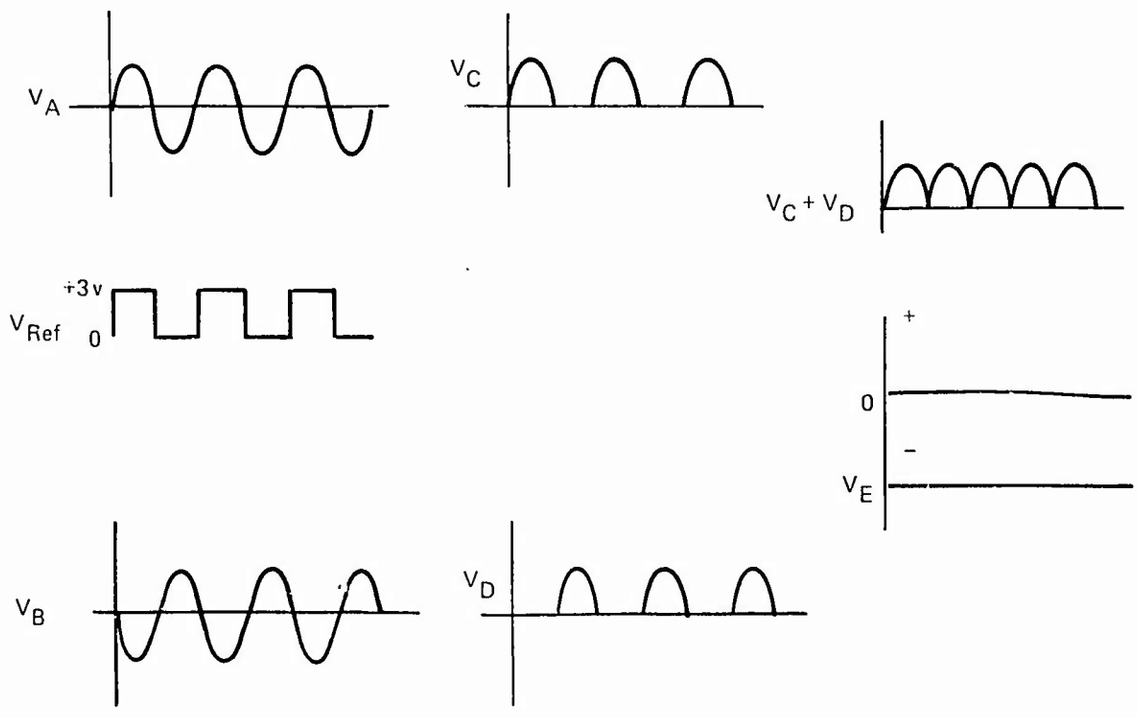

(b) Typical Demodulator Waveforms

Figure 22. Standard Demodulator

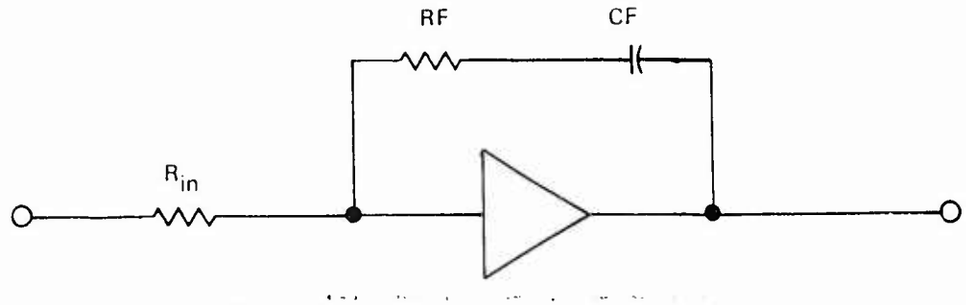

Figure 23. Constrainment Loop Integrator

$$e_n = K\sqrt{\frac{1}{f}} \quad .$$

where

$$K = 3 \times 10^{-8} \quad \frac{V}{\sqrt{Hz}} \quad .$$

Therefore, the RMS noise,

$$E_n = K\sqrt{\ln\left(\frac{f_2}{f_1}\right)} = 4.5 \times 10^{-8} \quad \frac{V}{\text{decade}} \quad .$$

In equivalent displacement of the Nutatron suspended element becomes:

$$\theta_n = \frac{1\ \widehat{sec}}{3 \times 10^{-3}\ V} \times 4.5 \times 10^{-8}\ V = 1.5 \times 10^{-5}\ \widehat{sec}\ \frac{RMS}{\text{decade}}$$

The maximum rate is $\dot{\theta}_n \omega$ (max)

$$= 1.5 \times 10^{-5}\ \widehat{sec} \times 0.1 \frac{rad}{sec} = 1.5 \times 10^{6} \frac{\widehat{sec}}{sec} = 1.5 \times 10^{-6}\ deg/hr.$$

Thus, it is seen that a standard LM 201A operational amplifier is suitable for this application.

(6) Torquer Amplifier (Figure 24)

The torquer amplifier converts the voltage output of the integrator to a current and passes this current through the torquer coil. The only specifications for the amplifier

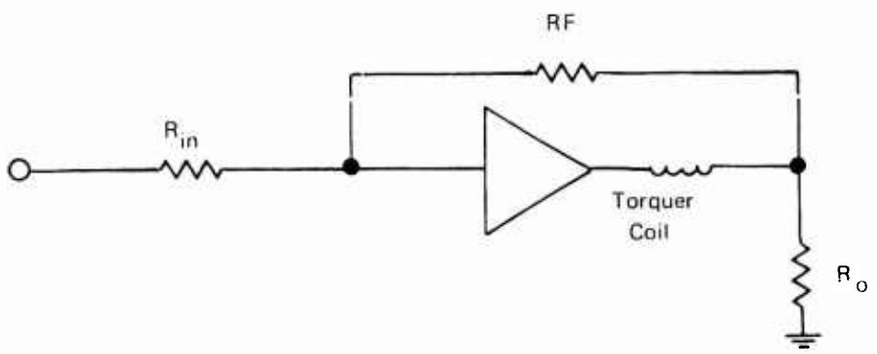

Figure 24. Torquer Amplifier

that are important are the output capabilities of ±100 ma at ±10 volts. A high current operational amplifier (Burr-Brown 3043/15) is used for this application and is connected as shown in Figure 24. This amplifier is identical to the amplifiers used to drive the spring rate compensator coils.

The layouts and schematics of the constrainment loop circuits which are discussed in this section are shown in the following figures of Appendix III.

(a) Pickoff Amplifiers - Board No. 15
- Schematic - Figure III-31
- Board Layout - Figure III-32

(b) Modulators, Resolver Drivers, Fixed Axis Amplifiers - Board No. 16
- Schematic - Figure III-33
- Board Layout - Figure III-34

(c) Demodulators, Integrators, Torquer Amplifiers - Board No. 17
- Schematic - Figure III-35
- Board Layout - Figure III-36

b. Nutatron Signal Detection Electronics (Figure 11, Section B)

The Nutatron responds to imposed precession rates with minute oscillations at the Nutatron frequency ($2\nu + 2\Omega$). The amplitude of these oscillations is proportional to the precession rate and constitutes the output information in the rate capture mode of operation. (Appendix I of the report gives a theoretical relationship for the Nutatron signal.) Originally, the amplitudes of the oscillations at the sine and cosine phase were detected open loop with synchronous demodulators and their outputs constituted the indicated Nutatron precession rates.

To eliminate the effect of long-term gain and phase variations of the pickoff electronics, the outputs of the demodulators are now further integrated with operational amplifiers and remodulated to produce a torquing current which is introduced into the aircore torquing coil. In the steady state, the Nutatron frequency torque rebalance loops stop the oscillations at the Nutatron frequency, and the integrator output voltages represent the indicated precession rate. The following circuits make up the Nutatron signal detection electronics.

(1) Nutatron Signal Amplifier (Figure 25)

The Nutatron signal amplifier is a three-stage amplifier providing gain of 30 V/V in the frequency band between 2 Hz and 80 Hz. The response rolls off at 6 dB/octave below 2 Hz and 12 dB/octave above 80 Hz. In Figure 25, amplifiers 1 and 2 provide the bandpass amplification, and amplifier 3 is a unity gain inverter. Standard operational amplifiers (LM 201) are used for amplifiers 1 and 2. Amplifier 3 is a chopper stabilized operational amplifier (AD 233). This amplifier has a very low and very stable dc offset, and therefore contributes no significant error. A dc offset of amplifier 2 is inverted by amplifier 3, and since the outputs of both amplifiers are fed to the full wave demodulator, the offset of amplifier 2 is cancelled.

(2) Nutatron Signal Demodulators and Integrators (Figure 26)

The outputs of the Signal Amplifier are demodulated simultaneously at $\sin(2\nu + 2\Omega)t$ and $\cos(2\nu + 2\Omega)t$ and applied to the integrator inputs. In the closed loop torque

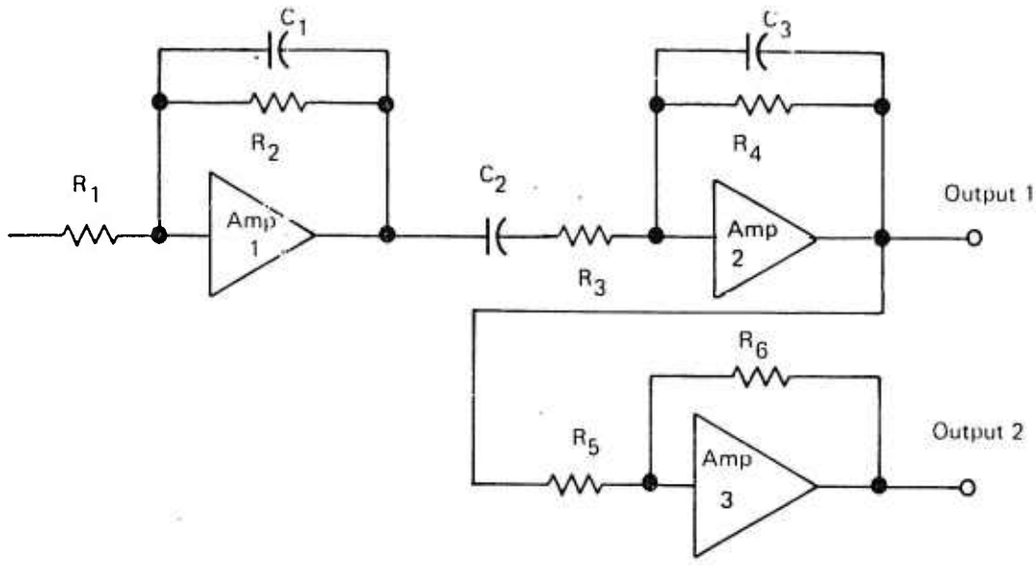

Figure 25. Nutatron Signal Amplifier

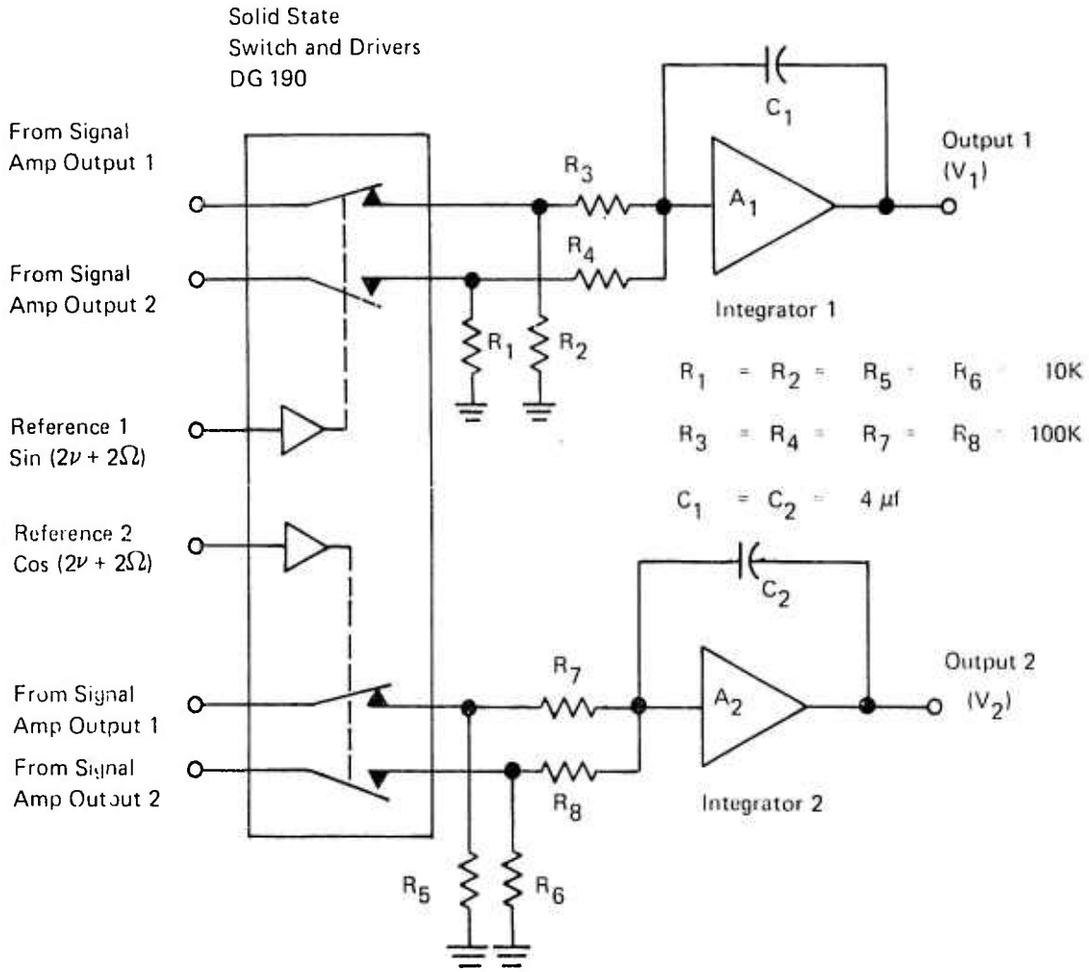

Figure 26. Nutatron Signal Demodulators and Integrators

rebalance mode of operation, the outputs of these two integrators (after filtering) yield the Nutatron precession rate signals. Output 1 represents the angular rate about one of the sensitive axes; output 2 represents the angular rate about the other (orthogonal) sensitive axis. The Nutatron signal level at the integrator inputs is approximately 10 mv ($2\nu + 2\Omega$ at resonance) per deg/hr. In order to keep the error contributed by the electronics well below that of the sensor, it is necessary to keep the input offset voltage from all sources to a level below the equivalent of 0.01 deg/hr (100 μV). There are three electronic sources contributing to the integrator input offset error:

(a) Nutatron Signal Amplifier offset
(b) Demodulator switch offset
(c) Integrator input voltage and current offset.

The effect of offsets in the Signal Amplifier are minimized by using a chopper stabilized operational amplifier (AD 233) for the unity gain inverter (A3, Figure 25). This inverter generates a voltage opposite in polarity to a dc offset at Output 1. Outputs 1 and 2 are passed through the demodulator switch (Figure 26), and appear at the integrator input summing resistors. Since the two are equal in magnitude and of opposite polarity, the net effect of an offset at Output 1 is near zero. The only uncompensated offset voltage from the Signal Amplifier is that from A3, which is less than 25 μV, with a temperature coefficient of $\leq 0.5\ \mu V/°C$.

The demodulator switch offset voltage is caused by leakage current from the switch driver into the switch ($\simeq 0.5 \times 10^{-9}$ amp) and from a switching transient caused by switch turnoff. This switching transient causes an equivalent average current of approximately 1×10^{-9} amp. The maximum total current thus equals 1.5×10^{-9} amp. This results in a voltage equal to $2 \times 1.5 \times 10^{-9} \times \left(\frac{R1R4}{R1 + R4}\right)$, see Figure 26, or, $3 \times 10^{-9} \times 10^{4} = 30\ \mu V$. This offset voltage has a temperature coefficient of approximately 1 μV per °C.

The remaining integrator offset is caused by the input offset voltage of the integrators ($\leq 50\ \mu V$) and the product of the offset current times the input resistance: $50 \times 10^{-12} \times 5 \times 10^{4} = 2.5\ \mu V$. Therefore, the maximum untrimmed integrator offset is seen to be approximately 100 μV (0.01 deg/hr) with a maximum temperature coefficient of approximately 2.5 μV per °C (0.00025 deg/hr/°C).

(3) Nutatron Signal Modulators and ac Torquer Driver (Figure 27)

The Nutatron Signal Modulators convert the integrator output signals to torque rebalance signals at the Nutatron frequency, ($2\nu + 2\Omega$). Each modulator generates a signal at $2\nu + 2\Omega$ whose amplitude is proportional to the dc at the integrator output (assuming a constant amplitude reference input at $2\nu + 2\Omega$). The modulators are Analog Devices Model 426A multipliers whose outputs are the product of their two inputs divided by ten.

The output of Multiplier 1 is

$\frac{V_1}{10}$ A sin $(2\nu + 2\Omega)t$, and that of Multiplier 2 is

$\frac{V_2}{10}$ A cos $(2\nu + 2\Omega)t$.

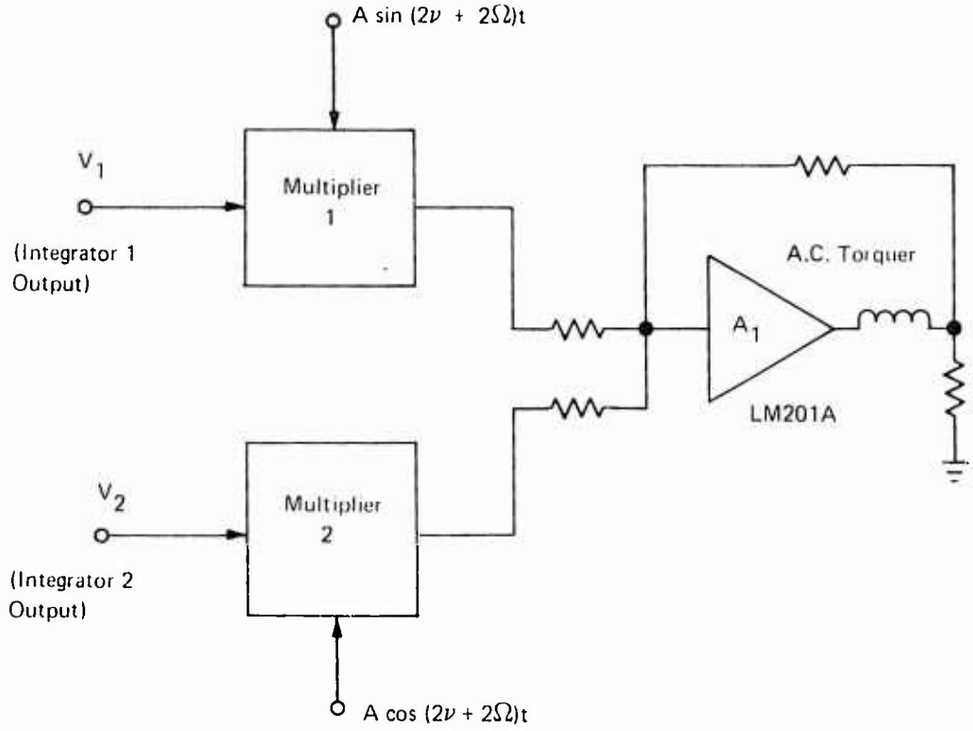

Figure 27. Nutatron Signal Modulator and ac Torquer Driver

These signals are summed, amplified, and converted to a current through the ac torquer equal to

$$I_T = \frac{AK}{10}\left[V_1 \sin(2\nu + 2\Omega)t + V_2 \cos(2\nu + 2\Omega)\right]$$

where

I_T is the total ac torquer current,

A is the amplitude of the $(2\nu + 2\Omega)$ modulator reference signals,

K is the ac torquer driver amplifier gain.

In closed loop operation this is the torquing current required to stop the oscillations at the Nutatron frequency and thus null the integrator inputs (within the electronic offsets).

Since the integrator outputs (after filtering) are the angular rate readout signals, errors in the Modulators, ac Torquer Driver Amplifier, and Torquer result directly in readout errors. These error sources must, therefore, be kept low so that their effect is insignificant compared to the total instrument error. The Nutatron is usually tested in orientations such that the rate input to one of the input axes is nulled and the other measures a component of earth rate (both inputs are nulled at the polar axis orientation). The following is a discussion of the Nutatron detection electronics error sources and an estimate of their maximum effect on indicated performance.

(a) Changes in Amplitude of the $(2\nu + 2\Omega)t$ Modulator Reference Signals

Any change in reference amplitude causes a corresponding change in integrator output amplitude so that product of the two remains constant. This problem is minimized by controlling the amplitude of the $(2\nu + 2\Omega)t$ reference signal to 0.01% of normal. The maximum error caused by this source is therefore in the order of 0.01% of the input precession rate or 0.0015 deg/hr with the Nutatron oriented to measure the whole earth rotation vector. In the absence of an input rate (polar angle orientation) this error source constitutes no readout error.

(b) Phase Stability of the Nutatron Frequency $(2\nu + 2\Omega)$ Reference Signals for Modulators

The phase of the demodulator reference signals, $A \cos (2\nu + 2\Omega)t$ and $A \sin (2\nu + 2\Omega)t$ (Figure 27) determines the orientation of the two measurement axes with respect to the input rate. It is desirable to have the two phases as orthogonal as possible and their phase relation constant. The reference generation circuitry described in Section IV.C.2.f.(8) maintains the phase stability to better than one minute of arc with a temperature coefficient 0.3 minute of arc per °C. The maximum error from this source is therefore:

$$15 \text{ deg/hr} \times 0.0003 = 0.0045 \text{ deg/hr} \quad .$$

(c) Multiplier Scale Factor Variations

Changes in scale factor of the multipliers cause corresponding changes in the integrator outputs, and thus result directly in readout scale factor errors. The Model 426A multiplier has a scale factor temperature coefficient of 0.03%/°C. With an angular input rate of 15 deg/hr (earth rate), the readout temperature sensitivity caused by this effect is less than 0.0045 $\widehat{\text{deg}}$/hr/°C.

(d) Multiplier Nonlinearity

Multiplier nonlinearity results in readout errors that are dependent on signal level. The 426A multiplier has a specified maximum nonlinearity of 0.3% of full scale. This would result in an error of 0.045 deg/hr at 15 deg/hr. Nonlinearity does not affect repeatability or stability data. It does enter into a g and g^2 sensitive drift determination. With the recommended sensor performance improvements better multipliers will have to be used.

(e) Multiplier Feedthrough

The feedthrough of $(2\nu + 2\Omega)t$ reference signals to the output of the multipliers will result in a proportional readout error. In the torque rebalance mode, this feedthrough signal causes an integrator output offset. The Model 426A Multiplier has a maximum feedthrough of 5 mv pp $(2\nu + 2\Omega)$. The multiplier output scale factor is 0.7 $V_{pp}/\widehat{\text{deg}}$/hr; therefore, this feedthrough error is equivalent to

$$\frac{1 \text{ deg/hr}}{0.7\text{V}} \times 5 \times 10^{-3} \text{ V} = 0.007 \text{ deg/hr}.$$

The temperature sensitivity is 1 mv pp/°C, or 0.0014 deg/hr/°C (maximum).

(f) Torquer Driver Gain Changes

The Torquer Driver Amplifier (LM 201A) is a feedback operational amplifier, whose current gain is determined primarily by the input, sampling, and feedback resistors. Standard 1% 100 ppm/°C metal film resistors are used for this application; therefore, the maximum error contributed by the Torquer Driver is 0.0015 deg/hr/°C for an input rate of 15 deg/hr.

(g) ac Torquer Scale Factor Changes

The ac Torquer consists of an air core coil mounted on the fixed housing of the Nutatron, and a permanent magnet located on the suspended Nutatron element. Current through the coil generates a magnetic field which interacts with the permanent magnet causing a torque on the suspended element. The current through the coil is determined by the Torquer Driver Amplifier gain and input voltage and is independent of the coil resistance. Therefore, the principal source of torquer error is the temperature sensitivity and aging of the permanent magnet. Tests performed with the Nutatron have shown this sensitivity to be 0.18%/°C; that is, the readout scale factor changes 0.18%/°C when the Nutatron internal temperature is changed by supplying current to the Nutatron heaters.

Table III is a summary of the errors discussed in this section. Comparison of these error magnitudes with actual test results (Section V) indicates that their contribution to the total error is insignificant except for the ac Torquer scale factor temperature sensitivity. The test results also show that there is no measurable difference in performance of the nulled axis and the axis measuring earth rate.

TABLE III. SUMMARY OF ERROR SOURCES IN NUTATRON SIGNAL MODULATORS, TORQUER DRIVERS, AND AC TORQUERS

Error Source	Readout Error	Error Magnitude (Maximum)	Axis Affected
$(2\nu + 2\Omega)$ t Reference Amplitude Instability	Scale Factor Change	0.0015 deg/hr pp random ness at 15°/hr input	Full Earth Rate Axis
$(2\nu + 2\Omega)$ t Reference Phase Instability	Sensitive Axis Orientation Shift	0.0013 deg/hr/°C at 15°/hr input	Null Axis
Multiplier Scale Factor	Scale Factor Change	0.0045 deg/hr/°C at 15°/hr input	Full Earth Rate Axis
Multiplier Feedthrough	Systematic Drift	0.007 deg/hr 0.0014 deg/hr/°C	Both Axes
Multiplier Non-Linearity	Readout Non-Linearity	0.3% of reading 0.045 deg/hr at 15 deg/hr	Earth Rate Axis
Torquer Driver Gain Instability	Scale Factor Change	0.0015 deg/hr at 15 deg/hr	Earth Rate Axis
AC Torquer Scale Factor Change	Scale Factor Change	0.027 deg/hr/°C at 15 deg/hr	Earth Rate Axis

The layouts and schematics of the Nutatron Signal Detection and Torque Rebalance Electronics are shown on the following figures of Appendix III:

(1) Nutatron Signal Amplifier, Demodulators, and Integrators:

Board Number 18
Schematic: Figure III-37
Board Layout: Figure III-38

(2) Nutatron Signal Modulators and ac Torquer Driver:

Board No. 21
Schematic: Figure III-43
Board Layout: Figure III-44

(3) Nutatron Output Signal Filter

Single pole, active filters using chopper stabilized operational amplifiers (Analog Devices Model 233) are used to provide a 1 rad/min rolloff for the precession output signals. The 1-minute time constant is short enough to permit demonstrating the fast reaction capability of the Nutatron from a cold start, and yet eliminates much of the higher frequency noise from the drift recordings. The filters (Figure 28) have provisions for nulling the systematic drift offsets discussed in previous sections. They also provide summing points for the acceleration sensitive drift compensation signals discussed in Section IV.C.2.h. The layouts and schematics of the Nutatron Signal Filters are shown on the following figures of Appendix III:

Board No. 19
Schematic: Figure III-39
Board Layout: Figure III-40

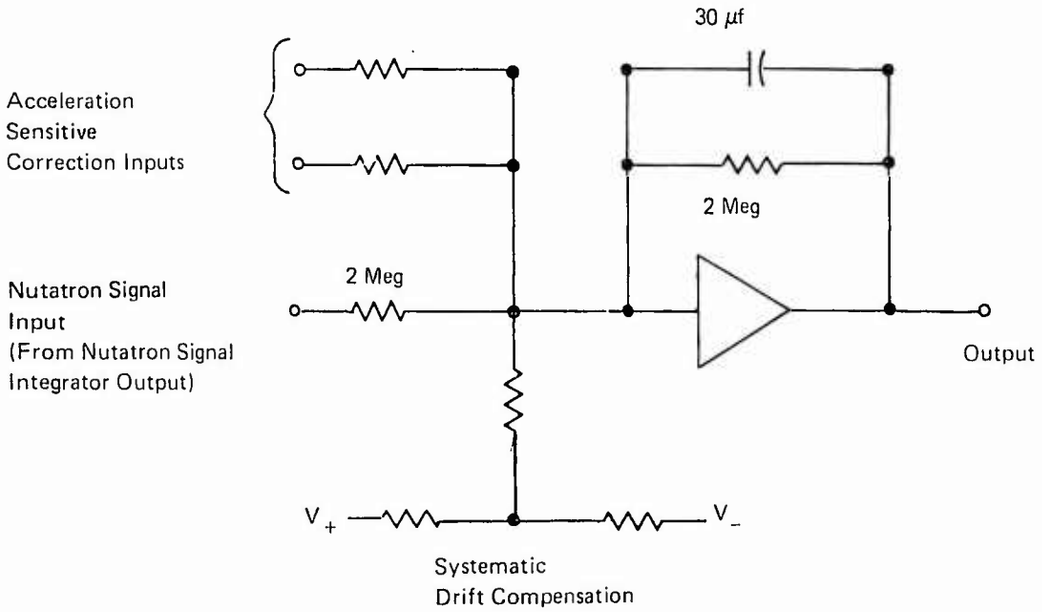

Figure 28. Nutatron Signal Filter

c. Rotor Speed Control Loop

An eddy current motor drives the Nutatron rotor. This type of motor was selected in preference to a synchronous motor for noise considerations. The tradeoffs for low noise were a high slip and large changes in speed for slight changes in load torque. To prevent these speed changes a servo loop (Section C, Figure 11) controls the rotor speed to 0.01%.

The speed control loop consists of a capacitance speed detector, a constant area pulse generator, a comparator and integrator and a three-phase spin motor power supply. The loop operates by converting the detected speed to constant area pulses at twice the spin speed (2ν), comparing the net area of these pulses to a zener reference and adjusting the amplitude of the spin motor excitation voltage .

(1) Rotor Speed Pickoff

The speed of the rotor is detected by measuring the capacitance between a plate mounted on the inner wall of the housing and the rotor. This capacitance changes at twice per revolution by increasing each time one of the inertia masses of the rotor passes by the plate. The pickoff plate is connected as one arm of a capacitance bridge so that the bridge is unbalanced twice during each revolution of the rotor. The bridge is excited by 25 kHz and the bridge output signal is amplified by the circuit shown in Figure 29a. The preamplifier output is an amplitude modulated 25 kHz signal (Figure 29b) which is near null for the most of the rotor cycle and increases sharply in amplitude as an inertia mass passes the pickoff plate. The 25 kHz parallel tuned circuit across the bridge provides some tuning of the bridge at 25 kHz. This reduces the effect of noise pickup on the lead which connects the Rotor Position Pickoff Plate inside the Nutatron to the remainder of the bridge, which is located on the Nutatron Holding Fixture.

(2) 25 kHz Amplifier-Demodulator (Figure 30a)

The 25 kHz amplifier is a tuned 25 kHz amplifier, which provides 15 V/V at 25 kHz. The 25 kHz demodulator is composed of the demodulator switch (DG 187) and the difference amplifier, A_2 (LM 201A). The low-frequency drift of this demodulator is not critical; therefore, the standard demodulator design was simplified to provide synchronous full-wave rectification of the 25 kHz amplifier output signal by alternately switching to the inverting and noninverting inputs of A_2. During the positive half cycle, S_2 is closed, and an amplified version of the signal appears at the output of A_2. During the negative half cycle, S_1 is closed, and an inverted, amplified version of the output of A_1 appears at the output of A_2. In this manner, the full wave rectification is accomplished. The output of A_2 is then filtered to remove the 25 kHz carrier, and what remains is a small pulse each time a rotor inertia mass passes the rotor position pickoff plate.

(3) 2ν Pulse Generator (Figure 30b)

The rotor position pulses are amplified by A_3 and A_4 and converted to a sharp rectangular positive pulse of 4V peak. The combination of A_3 and A_4 provide gain in the band between 5 kHz and 60 Hz, with 12 dB/octave rolloff below 5 Hz and 18 dB/octave rolloff above 60 Hz. The inverting input of the comparator (LM 211) is biased so that the output is nominally zero until the most positive portion of the rotor pulse is present. At that time the signal from A_4 becomes greater than the reference voltage and the output of A_5 goes to +4V and remains at that level until the output of A_4 once again becomes less than the reference.

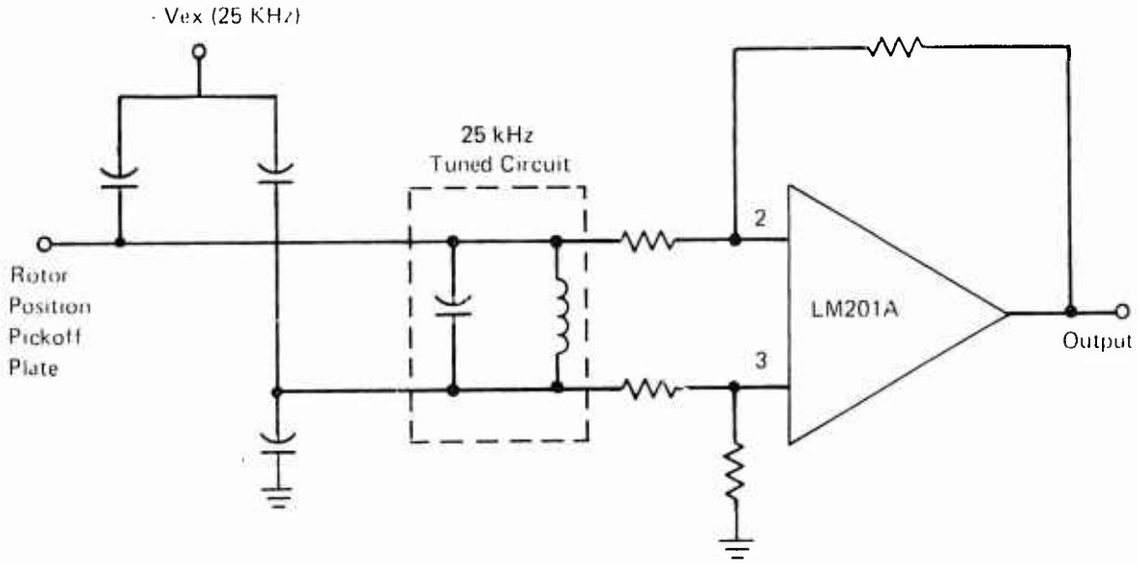

a) Bridge and Preamplifier Circuit

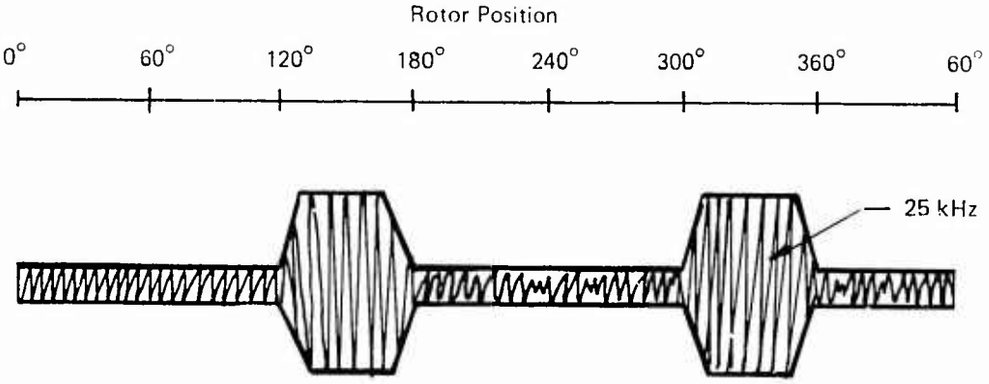

b) Output Waveform

Figure 29. Rotor Speed Pickoff

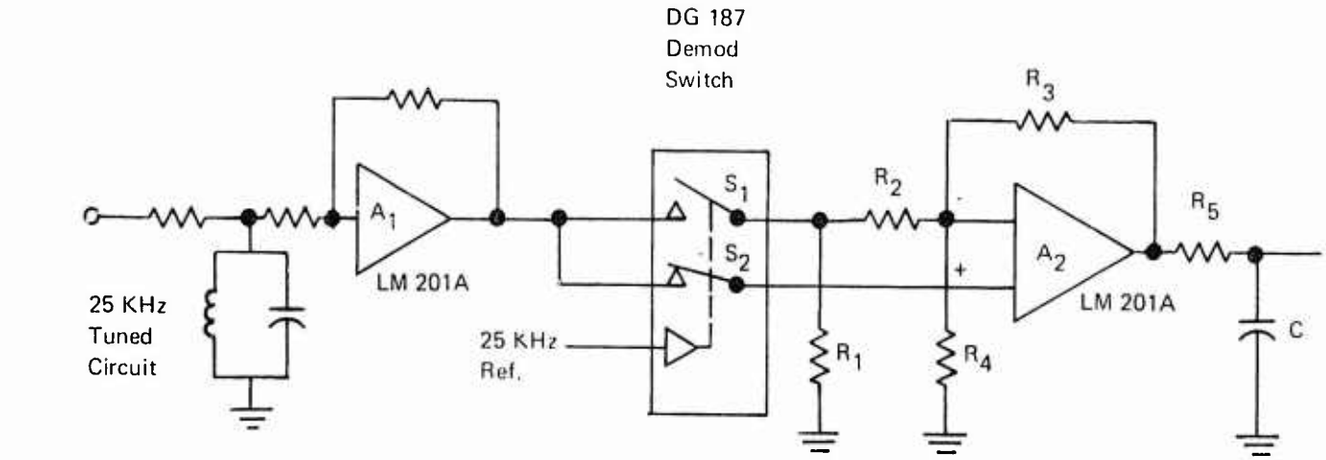

a) 25 KHz Amp - Demod

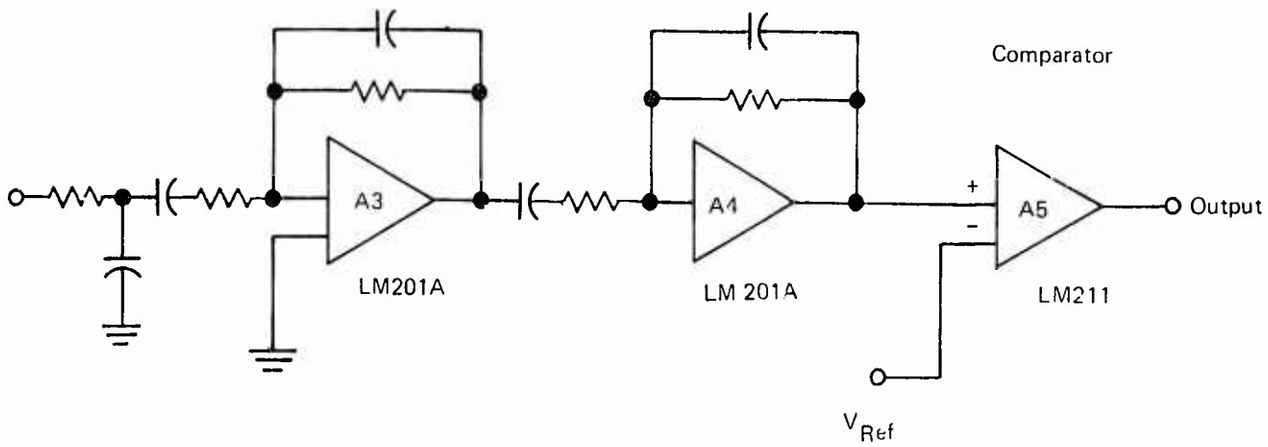

b) 2ν Pulse Generator

Figure 30. 25 kHz Amplifier-Demodulator and 2ν Pulse Generator

The 25 kHz Amplifier-Demodulator, and the 2ν Pulse Generator are located on circuit board number 8; Schematic: Figure III-17, Appendix III; Board Layout: Figure III-18.

(4) Speed Control Circuitry (Figure 31)

The Constant Area Pulse Generator, converts the 2ν pulses from the speed detection circuitry into constant area pulses. The pulses are generated by triggering a stabilized, one shot multivibrator which in turn switches a precision voltage into the summing amplifier. Two pulses are generated for each revolution of the rotor. The 2ν notch filter removes the 2ν component of the constant area pulses to prevent cross-coupling of the 2ν torques into the sensitive axes.

The summing amplifier generates an error voltage proportional to the difference between the reference voltage (speed adjustment) and the average value of the volt times time integral of the constant area pulses. The integrating amplifier provides the proper gain and

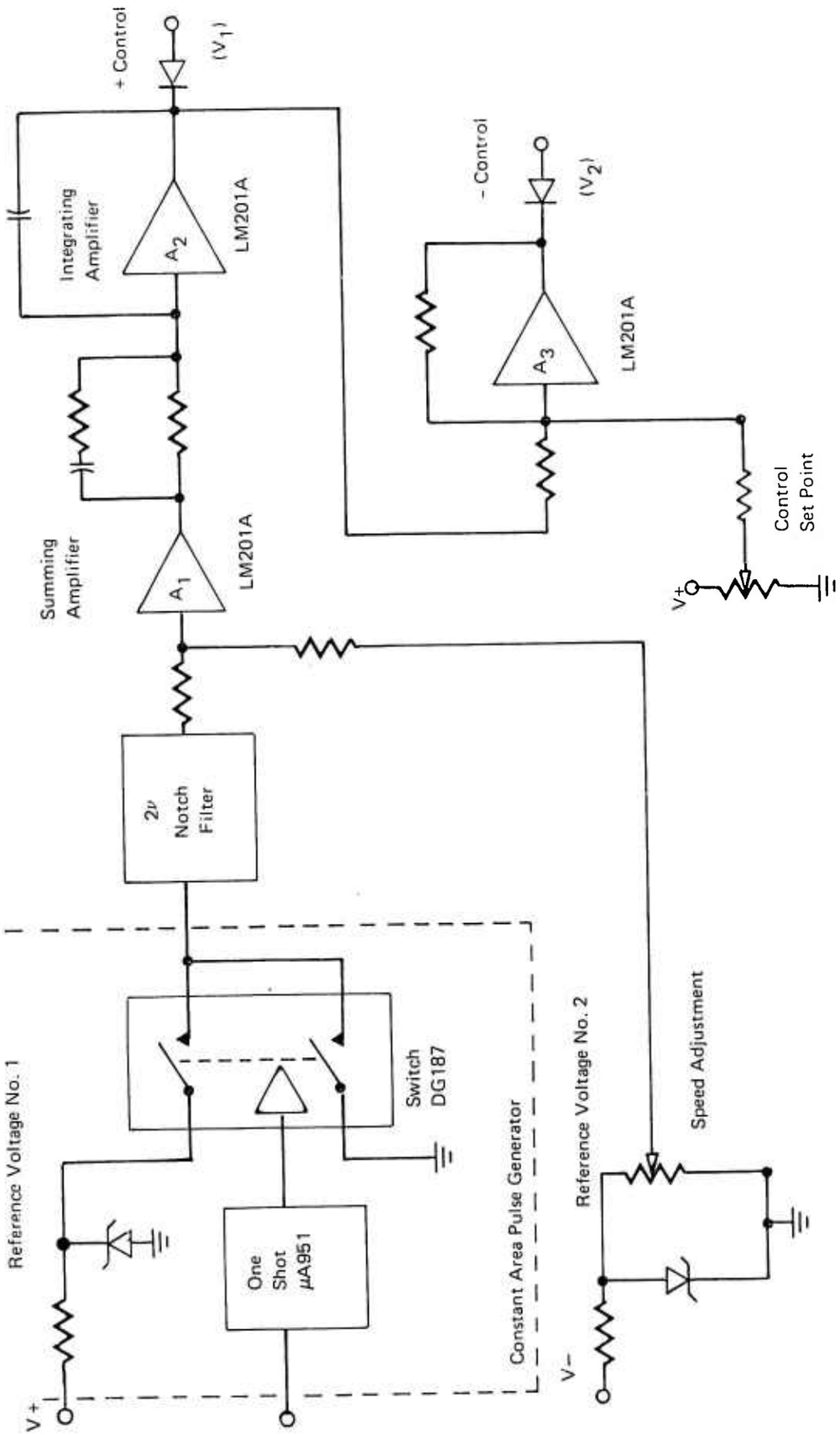

Figure 31. Speed Control Circuitry

response for speed control loop stability. Two control signals are generated by the speed control circuitry: the + control (V_1) signal causes clockwise torque on the rotor; the - control (V_2) causes a counterclockwise torque on the rotor. This type of control is required because the disc eddy current motor has no inherent self braking (see Technical Report AFAL-TR-69-76).

When power is initially applied, no pulses are being generated by the rotor, and consequently the output of A_1 (Figure 31) assumes a positive output. This causes a negative 14V to appear at the output of A_2. This control signal produces the appropriate output from the Spin Motor Power Supply (see Figure 33) to cause the rotor to spin clockwise. The rotor speed increases until the $2r$ pulse rate is such that the volt times time integral of the $2r$ pulse equals the speed reference voltage. The error voltage goes to zero, and the loop continues to control about this point.

Figure 32 is a plot of rotor speed versus time from turn-on. As is seen from the plot, the rotor settles to the operating speed in approximately six seconds.

The rotor speed control circuit is located on Board number 7. Figure III-15, Appendix III is the complete schematic. Figure III-16 is the board layout.

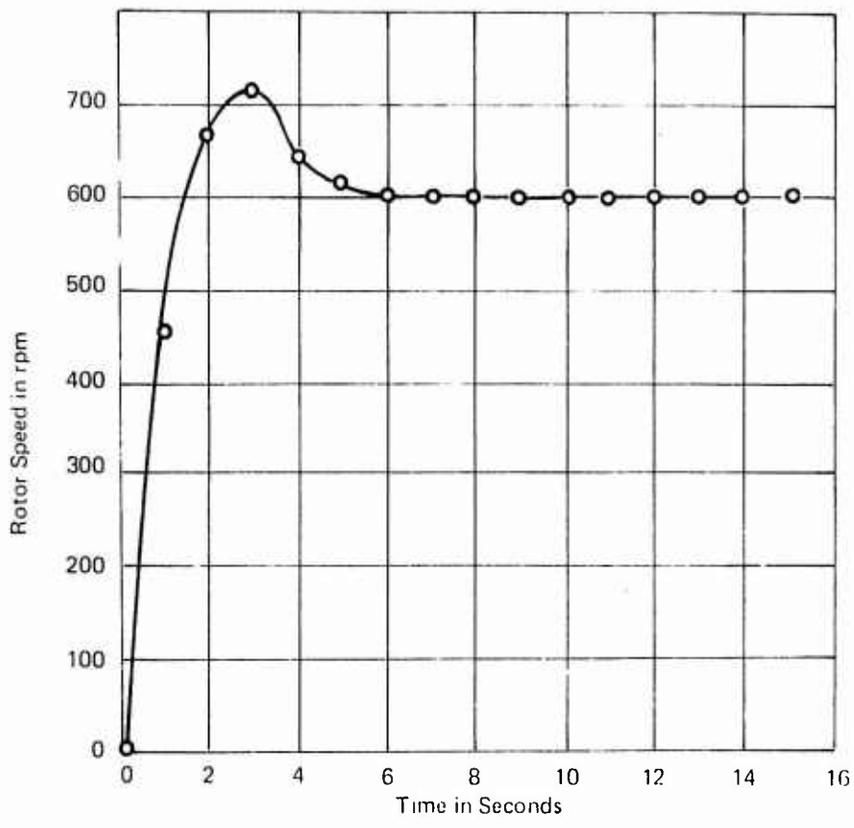

Figure 32. Rotor Speed versus Time from Turn-on

(5) Spin Motor Power Supply (Figure 33)

The outputs of the Speed Control Circuitry (V_1 and V_2, Figure 31) are converted to 625 Hz sine wave signals by Multiplier 1 and Multiplier 2 (see Figure 33). The output of Multiplier 1 is split up into 0 deg phase and -60 deg phase signals. These signals are power amplified to supply the proper current drive to the spin motor. The required three-phase excitation is obtained by the 0 deg phase (Phase A), inversion of the -60 deg phase to +120 deg (Phase B), and connection of the third Y winding to ground (Phase C). This provides the proper phase rotation to cause clockwise torque on the rotor. Counterclockwise torque is provided by interchanging the 0 deg phase and -60 deg phase outputs from Multiplier 2: the 0 deg phase signal is fed into Power Amplifier 2, and the -60 deg phase signal into Power Amplifier 1. Control of the motor speed is obtained because changes in the dc control signals at the inputs to the multipliers cause corresponding changes in the amplitude of the 625 Hz torque producing currents.

The Spin Motor Power Supply circuitry is located on Board 1. Figure III-3, Appendix III, is the schematic, and Figure III-4, is the board layout.

d. Resonance Control Loop

The Nutatron is operated at resonance to enhance the signal to noise ratio. Because of the high Q of the Nutatron, control of the resonance operation is necessary to avoid changes due to temperature, etc. This control is achieved by introducing a signal at a frequency ($2\nu + 2\Omega$) very near the Nutatron frequency ($2\nu + \Omega$ in the rotating case system) into the gyro transfer function. The response of the gyro is measured by detecting the phase of the x axis pickoff signal at this sampling frequency. The high Q of the Nutatron makes the phase of the sampling frequency very sensitive to slight changes in the resonant frequency. Adjustment of the resonant frequency is obtained by varying the current in the electromagnetic spring rate compensators. This produces a change in the net spring rate (downward for increasing current and vice versa) and in turn a change in the resonant frequency.

The resonance control loop consists of an amplifier, a synchronous demodulator to detect the phase of the sampling frequency, an integrator to provide the desired loop response and current amplifiers to drive the compensator coils. The major blocks of the loop are shown in Section D of Figure 11.

(1) Amplifier

The Resonance Control Loop amplifier provides 40V/V gain with a low frequency roll-off of 6 dB/octave below 3 Hz. It consists of a standard operational amplifier stage (LM201A) followed by a chopper stabilized unity gain inverter (AD233). It provides 0° phase and 180° phase outputs to the demodulator switch.

(2) Demodulator

The demodulator switch (DG 187) is connected as in Figure 22a. Its operation and typical waveforms are as shown in Figure 22b.

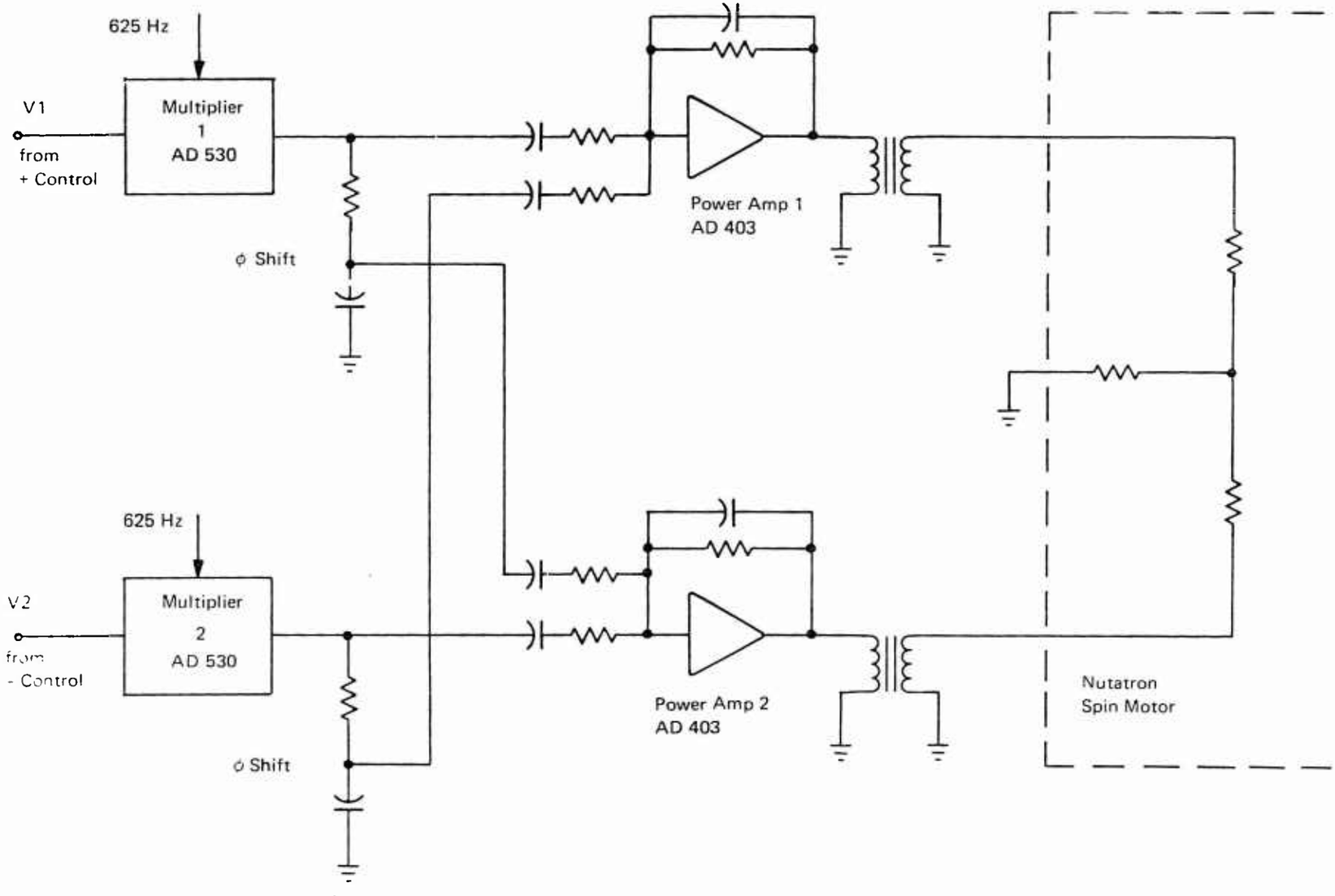

Figure 33. Spin Motor Power Supply

(3) Integrator

The demodulator switch output signals are summed into two input resistors of a chopper stabilized operational amplifier (AD 233). The integrator time constant is set at 1.5 seconds.

(4) Compensator Driver Amplifiers

The integrator output is fed simultaneously into four Compensator Driver Amplifiers. These amplifiers provide the correct current to the Spring Rate Compensator coils to maintain resonant operation.

The coils are connected to the amplifers such that there are two amplifiers for each input axis and of these two, one amplifier supplies the current to the coils to produce a clockwise torque and the other a counterclockwise torque. (When the currents are equal, the net torque is zero). The magnitude of the total current determines the net spring constant.

The amplifiers each have a maximum output of 100 ma dc and have a gain of 1 ma/V for the resonance signal input. The nominal output current of each amplifier is set by means of a dc reference voltage fed into a separate set of input resistors. The resonance control loop has a range of ± 10 ma dc about the nominal operating current of approximately 40 ma dc.Burr-Brown Model 3043/15 operational amplifiers are used for the Compensator Driver Amplifiers.

The Resonance Control Loop Amplifier, Demodulator, and Integrator are located on Circuit Board number 14. The Compensator Driver Amplifiers are located on Circuit Board number 12. Figure III-29 and III-30, Appendix III are the schematic and layout of Circuit Board number 14. Figures III-25 and III-26 are the schematic and layout of Circuit Board number 12.

e. Axis Alignment Loops

As described briefly in Section IV.A-3, the rotor spin axis and the housing rotation axis are aligned by servo loops. These loops make use of the Nutatron action in the housing rotation system to detect the misalignment and torque the rotor until alignment is achieved. The torque is provided by the spring rate compensators.

The gyro pickoff signal in the x axis of the rotating system is amplified and demodulated at sine and cosine phase of 2ν to determine the misalignment about the x and y axes respectively. The demodulator outputs ar ' integrated and used to bias the spring compensator currents to produce the torque necessary for alignment. The block diagram of these loops is shown in Section E, Figure 11.

(1) Amplifier

The Axis Alignment Loop amplifier provides 10 V/V gain with a low frequency rolloff of 6 dB/octave below 3 Hz. It consists of a standard operational amplifier stage (LM 201A) followed by a unity gain inverter (LM 201A). It provides 0 deg phase and 180 deg phase outputs to the demodulator switches.

(2) Demodulators

Two demodulators are required for axis alignment: one has a sine $2\nu t$ reference, and the other a cosine $2\nu t$ reference. These demodulator circuits are identical to the resonance loop demodulator. Both demodulators are encased in the same dual in-line integrated circuit package (DG 190 BP).

(3) Integrators

With the exception of the input and feedback components (i.e., time constant) the integrators used in this loop are identical to the resonance control loop integrator. The integrator outputs are supplied to the appropriate compensation coil driver amplifier inputs.

The Axis Alignment Loop Amplifier, Demodulators, and Integrators are located on Circuit Board number 2. Figures III-5 and III-6, Appendix III are the schematic and board layout.

f. Reference Signal Generators

The detection of the Nutatron signal and the operation of the resonance control and axis alignment loops require reference signals related to the rotor and housing rotation speeds. These signals are:

$\sin \quad 2\nu t$

$\cos \quad 2\nu t$

$\sin \quad (2\nu + 2\Omega)t$

$\cos \quad (2\nu + 2\Omega)t$

$\sin \quad \{(2\nu + 2\Omega)t + \phi\}$

Special electronics are incorporated in the test set to derive these signals. The technique, which makes use of analog multipliers, is described below. The block diagram for this technique is shown in Section F of Figure 11.

The 2ν pulses provided by the rotor speed detection circuitry are fed to a synchronized oscillator. The 2ν square wave out of the oscillator is filtered to produce a sine wave which is phase shifted by 90 deg to provide both sine $2\nu t$ and cosine $2\nu t$.

Sine Ωt and cosine Ωt are developed by introducing a steady state signal at 4.2 kHz into one of the rotating system inputs of the pickoff resolver. This produces a sin Ωt modulation of 4.2 kHz at one fixed system output of the resolver and a cos Ωt modulation of 4.2 kHz at the other. These signals are demodulated at 4.2 kHz to obtain sin Ωt and cos Ωt.

(1) Synchronized Oscillator

The 2ν synchronized oscillator is a free-running multivibrator which is locked to the incoming frequency when the signal from the 2ν pulse generator is present. If the 2ν pulses are not present, it runs at its natural frequency near 2ν. This feature permits adjustments and evaluation of many of the electronics without the necessity of running the rotor.

(2) Shaping Circuit

The output of the synchronized oscillator is a square wave which is synchronized with the rotor position pulses. The shaper (Figure 34) converts this to a sine wave by removing the odd harmonics from the square wave. Filter 1 (Figure 34) provides gain of 1 V/V at 2ν, and attenuation of higher harmonics in proportion to the order of the harmonic. The 6ν, and 10ν notches remove the remaining components at these frequencies. The RC filters in combination with Filter 1 produce 18 dB/octave roll-off for all harmonics above 10ν. This method produces a clean sine wave of excellent phase stability with respect to the rotor pulses, which are the primary reference for the Nutatron System.

The Synchronized Oscillator and Shaping Circuit are located on Circuit Board number 6. Figures III-13 and III-14, Appendix III are the schematic and layout of the circuits.

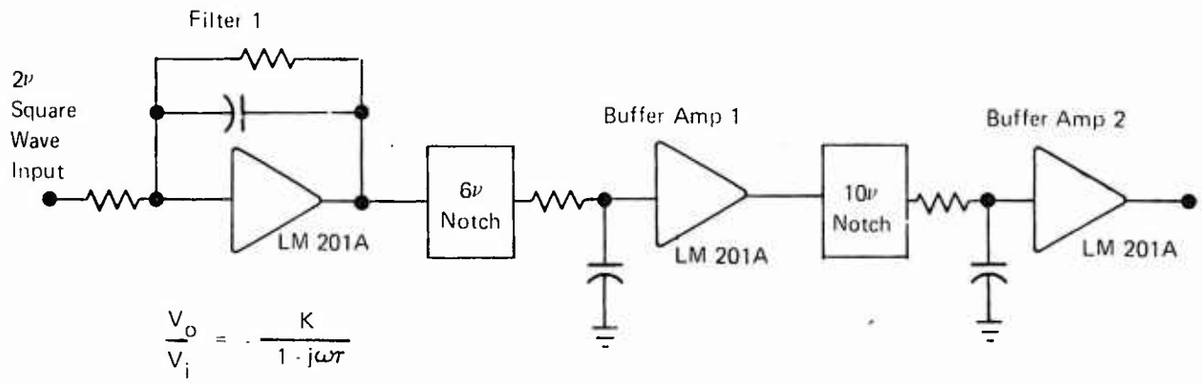

Figure 34. Shaping Circuit

(3) 2ν Reference Generator (Figure 35)

The 2ν Reference Generator provides the switching signals for the 2ν demodulators in the Axis Alignment loop. In order to provide the proper switching of the solid state demodulators, these signals must be of the form:

0 to -0.5 vdc for one half cycle, and
+ 3 to + 5 vdc for the other half cycle.

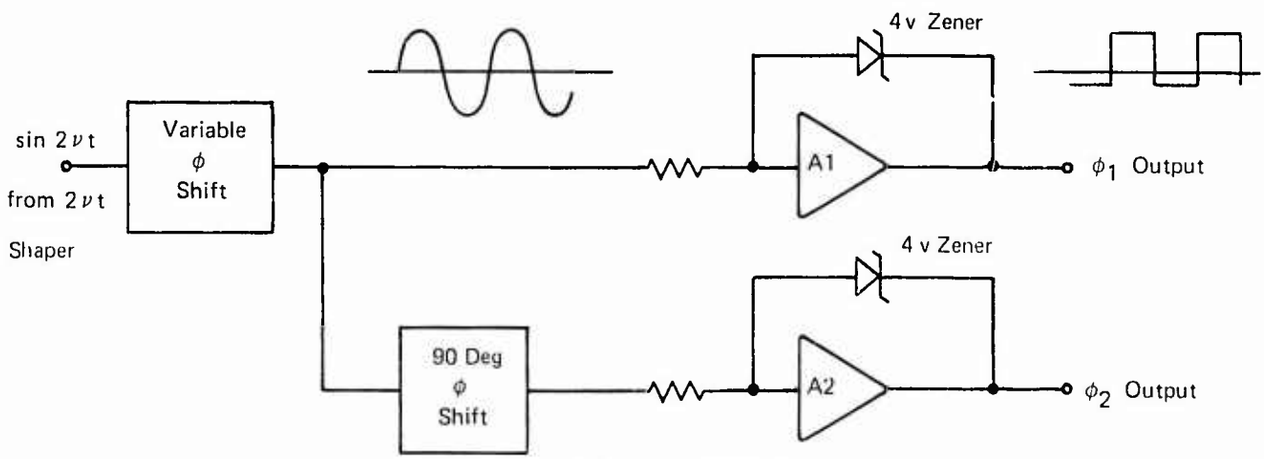

Figure 35. 2ν Reference Generator

The 2ν signal from the 2ν Shaping Circuit is phase shifted so that one of the 2ν demodulator outputs in the Axis Alignment loop is proportional to the misalignment angle in the rotating system x axis. This signal is then shifted an additional 90 deg so that the other Axis Alignment demodulator output is proportional to the misalignment angle in the rotating system y axis. The sine waves are converted to the demodulator switching signals by A_1 and A_2 (see Figure 35). Use of the 4 volt zener diode for the feedback element in the operational amplifier circuit provides very high gain when the diode is not conducting, clamping of the output to +4 volts when the diode is conducting in the reverse direction, and -0.5 v when the diode is conducting in the forward direction. This results in an almost instantaneous transition between to two output levels as the input sine wave goes through the zero crossings.

The 2ν Reference Generator circuitry is located on Circuit Board number 5. Figures III-11 and III-12, Appendix III are the schematic and layout.

(4) Ω Reference Generator (Figure 36)

Sine Ωt and cosine Ωt signals are developed by feeding a low level steady state 4.2 kHz signal into the x input of the pickoff resolver (see Figure 36). The input signal (A sin ωt) becomes in the fixed system:

$$X = A \sin \omega t \cos \Omega t$$
$$Y = A \sin \omega t \sin \Omega t$$

These signals are amplified by the fixed system amplifiers and demodulated by 4.2 kHz demodulators. The output of these demodulators are:

$$X = B \sin \omega t \cos \Omega t \sin \omega t$$
$$= \frac{B}{2} \cos \Omega t (1 - \cos 2\omega t), \text{ and}$$
$$Y = \frac{B}{2} \sin \Omega t (1 - \cos 2\omega t).$$

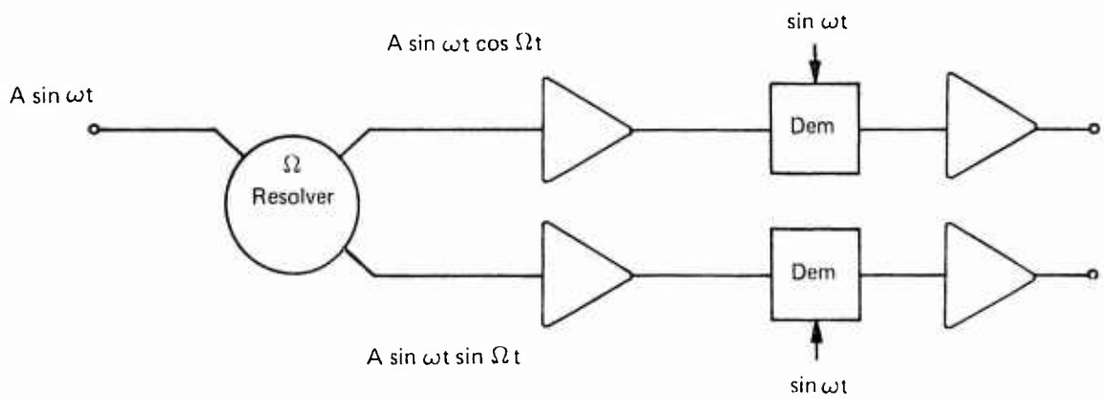

Figure 31. Ω Reference Generator

The high frequency terms are filtered out leaving the desired signals:

$$X = \frac{B}{2} \cos \Omega t$$

$$Y = \frac{B}{2} \sin \Omega t \ .$$

where B is the amplitude of the 4.2 kHz signal before demodulation. Each of these signals is then amplified to the level of 6V pp.

The Ω Reference Generator is located on Circuit Board number 5. Figures III-11 and III-12, Appendix III are the schematic and layout.

(5) Multipliers

Addition of the 2ν and Ω frequenceis is accomplished by the multipliers as shown in Figure 37. The sine and cosine phases of $2\nu t$ are supplied to the inputs of two multipliers. The two phases of Ωt are applied to the second set of multiplier inputs. As a result the output of one multiplier is sin $2\nu t$ cos Ωt which is identical to

$$\frac{1}{2} [\sin (2\nu+\Omega) t + \sin (2\nu - \Omega) t].$$

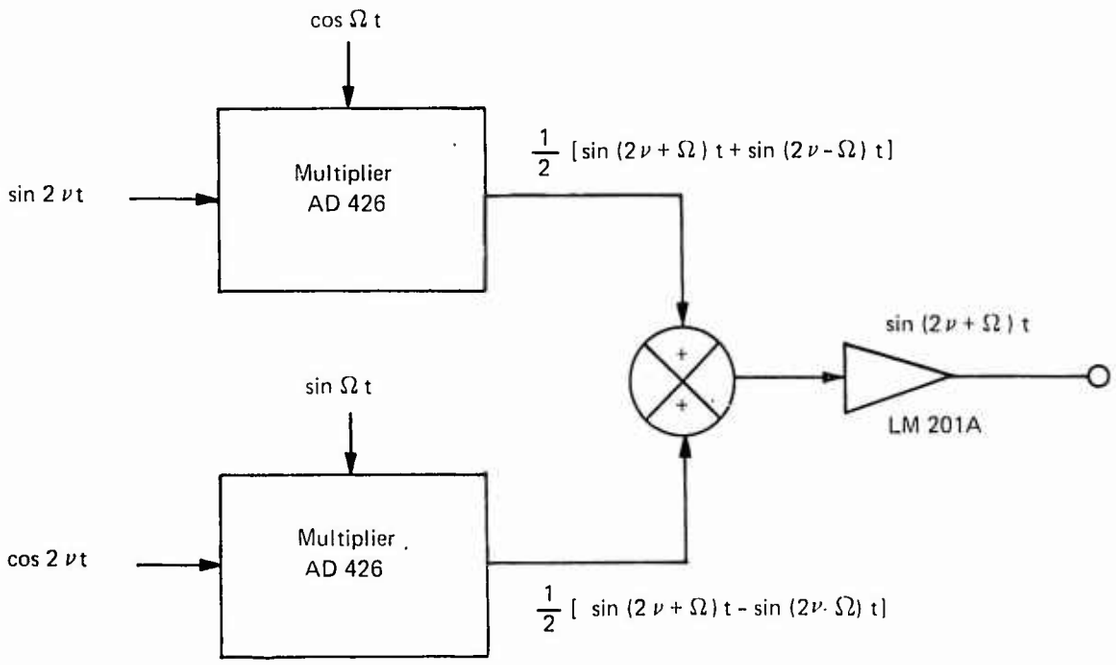

Figure 37. Frequency Addition Technique

The second multiplier output is

$$\cos 2\nu t \sin \Omega t \ .$$

which is

$$\frac{1}{2}[\sin (2\nu+\Omega) t \ - \ \sin (2\nu - \Omega) t] \ .$$

These outputs are added by a summing amplifier to produce a signal at

$$\sin (2\nu+\Omega) t.$$

This signal is passed through a 90 deg phase shift to obtain $\cos (2\nu+\Omega) t$. The $2\nu+\Omega$ Generator is located on Circuit Board number 4. Figures III-9 and III-10, Appendix III are the schematic and layout. The $2\nu+ 2\Omega$ Generator is located on Circuit Board number 3. Figures III-7 and III-8 of Appendix III are the schematic and layout.

(6) $2+ 2\Omega$ Amplitude Control

Section IV.C.2 discussed the need for controlling the amplitude of the $2\nu+ 2\Omega$ reference signals for the Nutatron Signal Modulators. Figure 38 is a block diagram of the control loop. The output of the $2\nu + 2\Omega$ Generator is fed into one input of the multiplier. The

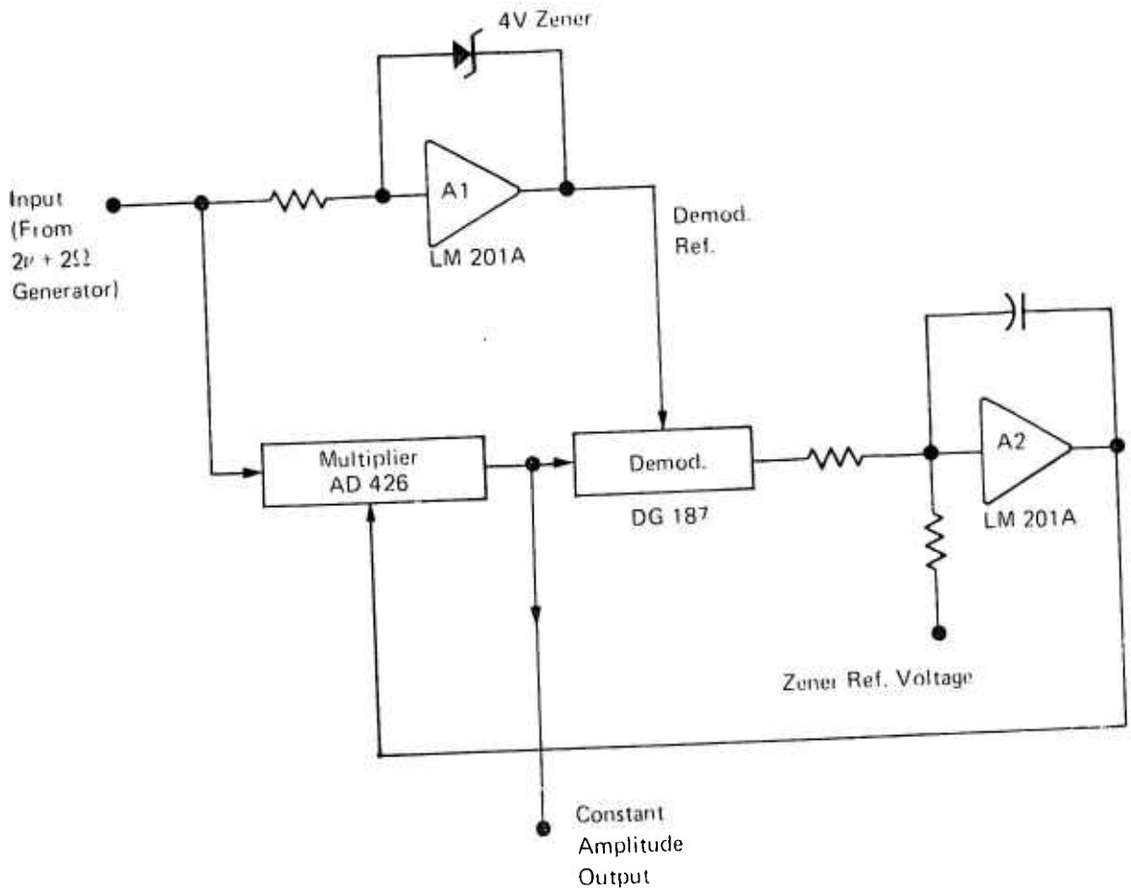

Figure $2\nu + 2\Omega$ Amplitude Control

other input to the multiplier is the automatic gain control signal developed by the integrator (A_2). The gain control signal is developed by comparing the output of the demodulator (which performs full wave rectification to the $2\nu+2\Omega$ signal appearing the multiplier output) to a reference voltage applied to the other input resistor of the integrator (A_2). If the net current into the integrator input is non-zero, the integrator output is driven in a direction which causes the multiplier output to reduce this net input current to zero. Thus, the average value of the rectified $2\nu+2\Omega$ signal is made to be equal to the reference voltage.

(7) Phase Shifter

Sin $(2\nu+2\Omega)$ t and cos $(2\nu+2\Omega)$ t reference signals are required for the Nutatron Signal Modulators; therefore, a means must be provided for shifting the constant amplitude $(2\nu+2\Omega)$ signal by 90 deg without introducing amplitude or phase instability. Figure 39 is the circuit used for this application. If $R_1 = R_2$ the gain of the circuit is 1 V/V, independent of the values of C and R_3. The phase shift is dependent only on the values of C and R_3. Figure 40 is a plot of phase shift versus R_3 with constant C. From the plot it can be seen that at R_3 = 10K the slope is equal to 0.005 deg/ohm. Metal film resistors with a maximum temperature coefficient of 0.01%/deg C are used for R_1, R_2 and R_3. The capacitor (C) is a metallized polycarbonate film capacitor which has a temperature coefficient of less than 0.01%/deg C at room temperature. This results in an amplitude stability of at least 100 ppm/deg C and a phase stability of at least 0.005 deg/C. This is used as the standard design for all the low frequency phase shifters in the Nutatron System.

The $2\nu+2\Omega$ Amplitude Control and phase Shifter are located on Circuit Board number 21. Figures III-43 and III-44, Appendix III, are the schematic and layout of this circuit board.

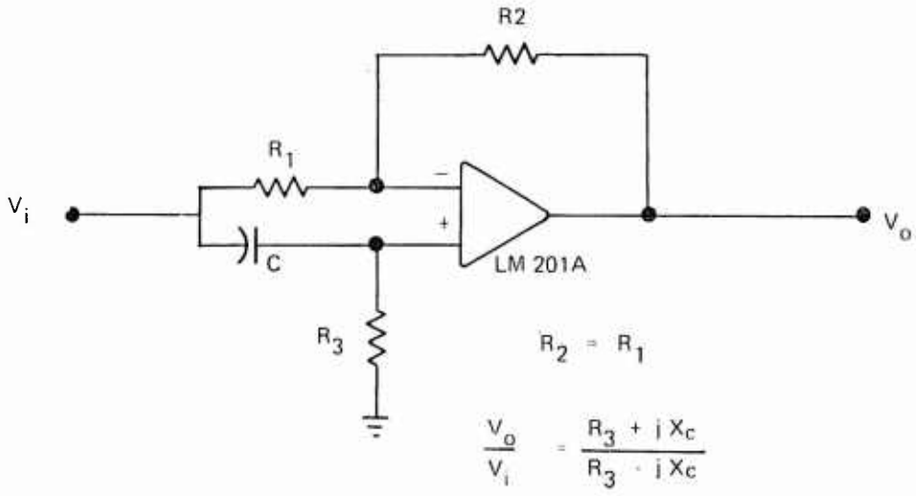

Figure 39. Constant Amplitude Phase Shifter

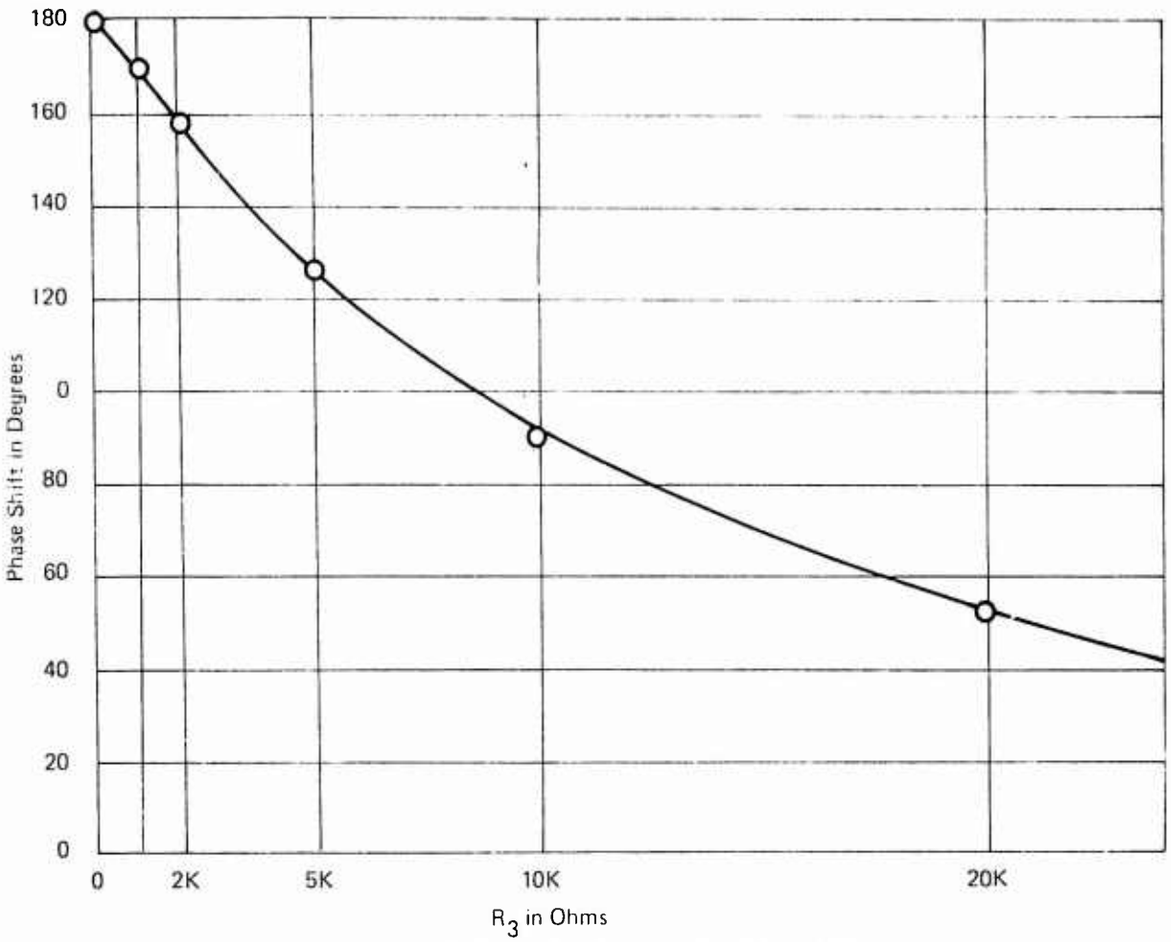

Figure 40. Phase Shift versus R_3 (X_c = 10K)

g. 2Ω Nulling Loop (Figure 45)

This circuitry detects motion of the suspended element at twice the housing speed (2Ω) and generates the required torque rebalance signals to reduce the motion to zero. This motion at 2Ω is caused by acceleration (g - loading) perpendicular to the spin axis (see Appendix II). Open loop, it is of the form:

$$\theta_x = k\ a_y \cos(2\Omega t + \phi) + k\ a_x \sin(2\Omega t + \phi)$$

$$\theta_y = k\ a_x \cos(2\Omega t + \phi) + k\ a_y \sin(2\Omega t + \phi),$$

where θ_x and θ_y are the displacements of the suspended element with respect to the fixed system x and y axes respectively; k is a constant; a_x and a_y are the accelerations along the fixed system x and y axes respectively.

Figure 41 is a block diagram of the 2Ω nulling loop. When the loop is closed, the output of Integrator 1 is driven to a level proportional to a_x. Modulator 1 converts this to a signal proportional to $a_x \cos(2\Omega t + \phi)$. In a like manner the output of Integrator 2 is proportional to a_y, and the out-

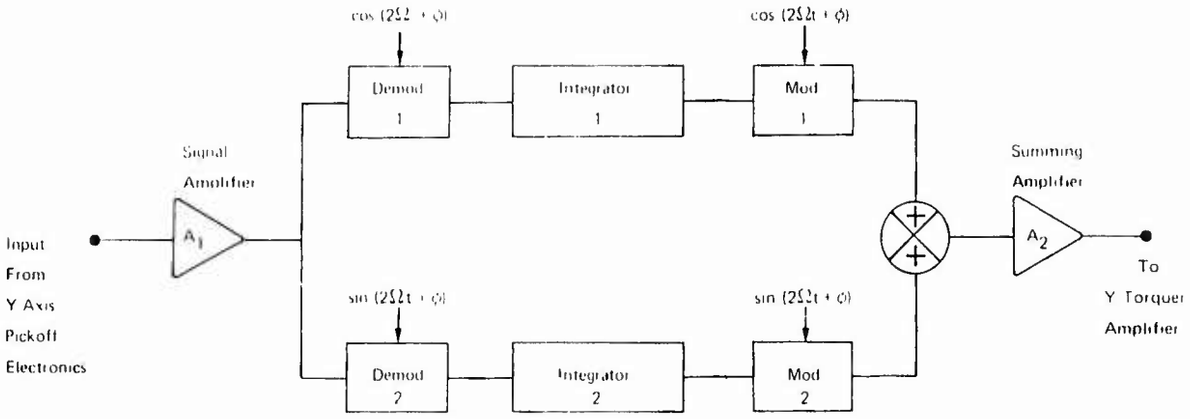

Figure 41. 2Ω Nulling Loop (Y Axis)

put of Modulator 2 is proportional to $a_y \sin(2\Omega t + \phi)$. These are summed in A_2 to produce a signal proportional to

$$a_x \cos(2\Omega t + \phi) + a_y \sin(2\Omega t + \phi) .$$

This signal is fed to the y axis Torquer Amplifier which converts it to a torquing current to null the 2Ω motion of the suspended element.

(1) Signal Amplifier

The signal amplifier provides 25 V/V gain with a high frequency roll-off of 6 dB/octave above 30 Hz. It consists of a standard operational amplifier stage (LM201A) followed by a unity gain inverter stage (LM201A). It provides 0 deg phase and 180 deg phase outputs to the demodulator switch.

(2) Demodulator

Both demodulators are encased in the same dual in-line integrated circuit package (DG 190 BP). These demodulator circuits are identical to those used in the axis alignment loop and in the Resonance Control loop (see Figure 22).

(3) Integrator

Chopper stabilized amplifiers (AD 233) are used for the integrators. The integrator time constant is 6 seconds.

(4) Summing Amplifier

The Summing amplifier is a standard operational amplifier (LM201A).

The circuitry for the x axis of the 2Ω Nulling loop is located on Circuit Board number 24; the y axis circuitry is on Circuit Board number 25. Figures III-48 and III-49, Appendix III are the schematic and layout of these boards.

h. G-Sensitive Error Compensation Circuitry (Figure 42)

Because of unequal radial compliance of the rotor bearings along orthogonal axes perpendicular to the spin axis, a spurious $2\nu + 2\Omega$ signal is developed in proportion to g-loading perpendicular to the spin axis (see Section VI.C). The outputs of the integrators in the 2Ω nulling loop are also proportional to the g-loading perpendicular to the spin axis. The phase angle (ϕ) of the demodulator and modulator reference signal (see Figure 43) is chosen so that the output of Integrator 1 is proportional to g_x, and that of Integrator 2 is proportional to g_y. These signals are appropriately scaled and fed into the Nutatron Signal Filters to reduce the readout error caused by the bearing imperfections.

Figure 42 is a block diagram of one axis of the compensation circuit. A_1 amplifies the output of Integrator 1 of the 2Ω Nulling Loop. A_2 is a unity gain inverter. Therefore, two dc correction signals are available: one proportional to $+g_x$ and one proportional to $-g_x$. Resistors R_1, R_2, R_3, R_4 form the scaling network. Output 1 is fed to Nutatron Signal Filter 1; Output 2 is fed to Nutatron Signal Filter 2. The adjustment is made by selecting the polarity ($+g_x$ or $-g_x$) and adjusting the ratios $\frac{R_1}{R_2}$ and $\frac{R_3}{R_4}$ so that the g-sensitive error is minimized.

The g-Sensitivity Correction Circuitry is located on Circuit Board number 26. Figures III-50 and III-51, Appendix III are the schematic and board layout.

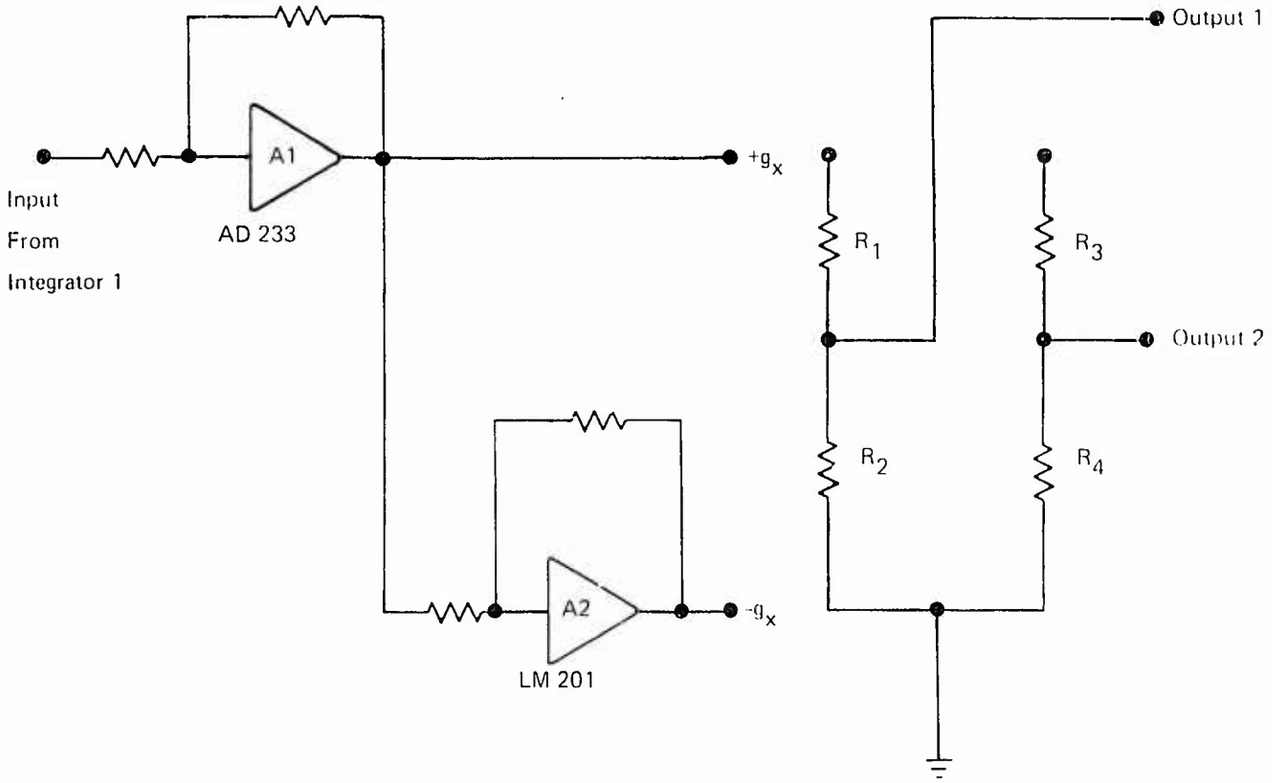

Figure 42. G-Sensitive Correction Circuit (One Axis)

i. 2Ω Reference Generator (Figure 43)

The 2Ω Reference Generator provides the reference signals for the 2Ω Nulling Loop demodulators and modulators. Figure 43 is a block diagram of the circuit. Inputs to multipliers 1 and 2 are provided by the Ω Reference generator. The output of Multiplier 1 is:

$$\frac{1}{10}(\sin \Omega t \cos \Omega t) = \frac{1}{20}(\sin 2\Omega t).$$

This is amplified and inverted by A_2, and inverted once again by A_1. The output of multiplier 2 is:

$$\frac{1}{10}(\sin \Omega t \sin \Omega t) = \frac{1}{20}(1-\cos 2\Omega t).$$

The dc component is blocked by the coupling capacitor in the input of A_3. The 2Ω signal is amplified and inverted by A_3, and inverted once again by A_4. These signals are appropriately scaled and added to produce reference signals of the phase required for the g-Sensitive Correction Circuitry. For example, in Figure 43, the required output of A_5 is

$A \sin (2\Omega t + \phi)$, where

$A = 3V$, and ϕ is the required phase angle.

This output is related to the inputs by the equation:

$$-A \cos 2\Omega t \left(-\frac{R_3}{R_4}\right) - A \sin 2\Omega t \left(-\frac{R_3}{R_4}\right) = A \sin (2\Omega t+\phi),$$

which can be re-written,

$$\left(\frac{R_3}{R_4}\right)\cos 2\Omega t + \left(\frac{R_3}{R_1}\right) \cos 2\Omega t = \sin \phi \cos 2\Omega t + \cos \phi \sin 2\Omega t.$$

Therefore,

$$\sin\varphi = \frac{R_3}{R_4}, \text{ and}$$

$$\cos\phi = \frac{R_3}{R_4}, \text{ which gives the relationship}$$

between R_1, R_2, and R_3:

$$R_1^2 + R_2^2 = R_3^2, \text{ and}$$

$$\frac{R_1}{R_2} = \tan\phi.$$

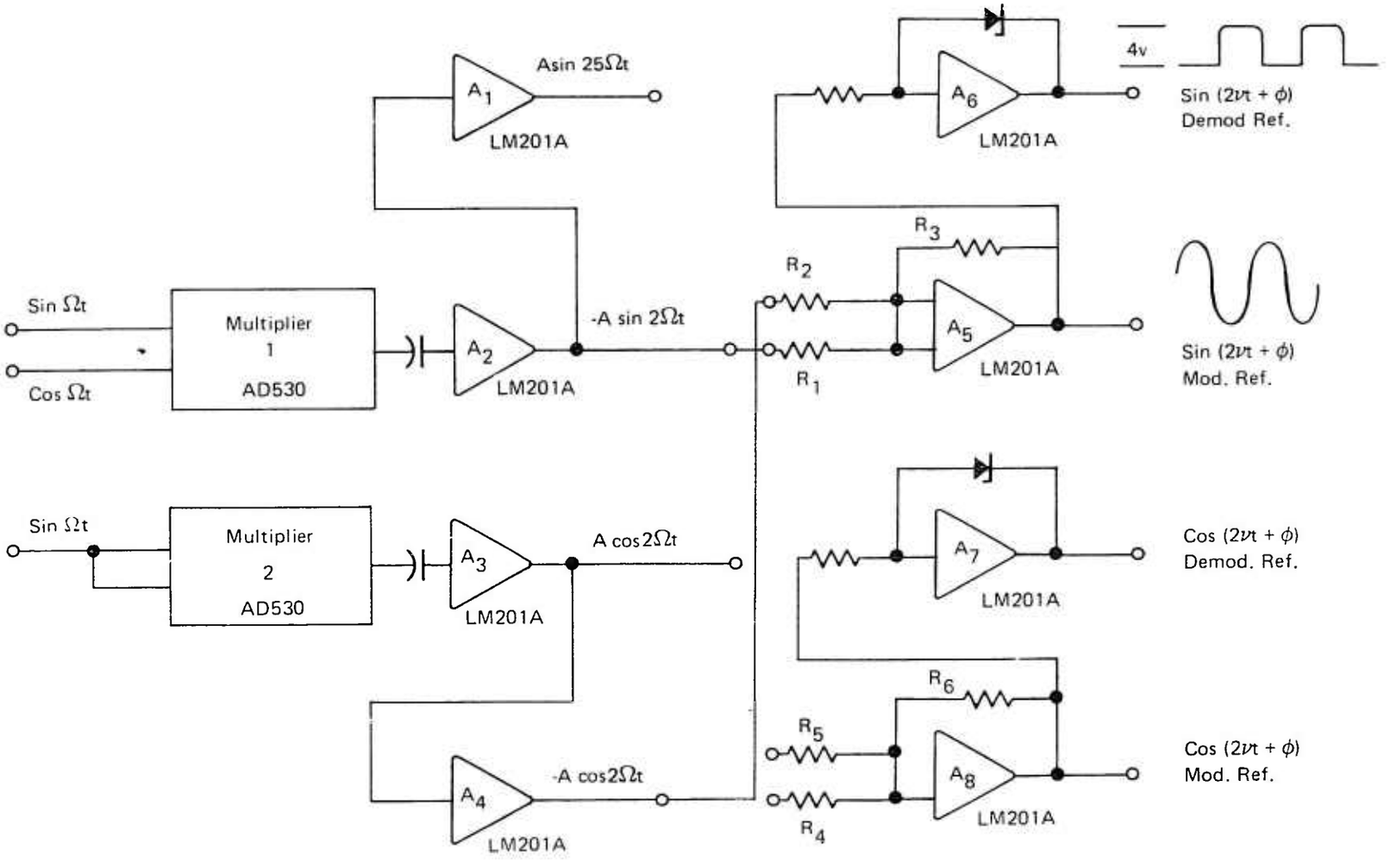

Figure 43. 2Ω Reference Generator

Figure 44 is a plot of the value of R_1 and R_2 (with R_3 = 10K) for any desired phase from 0 deg to 90 deg. Similarly, the output of A_8 is set to a cos ($2\Omega t+\phi$). The outputs of A_6 and A_7 provide -0.5 to +4V switching signals to the 2Ω demodulators.

The 2Ω Reference Generator is located on Circuit Board number 23. Figures III-46 and III-47, Appendix III are the schematic and layout of this circuit.

j. Power Supplies

(1) Frequency Reference Unit (Figure 45)

The Frequency Reference Unit provides all of the excitation signals necessary for operation of the Nutatron system. The 200 kHz crystal oscillator provides the basic stable reference from which all other frequencies are derived. It is also used directly for excitation of the gyro axis capacitive pickoff system. Provisions are made for shifting the demodulator reference with respect to the pickoff excitation because the output of the capacitive pickoff bridge is in quadrature with the bridge excitation.

Integrated circuit frequency dividers (Fairchild 9390, 9392, 9393) are used to provide the desired frequencies (see Figure 45). The outputs of the dividers are 0V to +4V square wave signals, which are used directly as demodulator switching signals for the 25 kHz, 4.2 kHz, and 1.25 kHz demodulators. However, each of these signals and also the 1.0 kHz and 625 Hz signals must be further processed as follows:

(1) The 25 kHz is used to provide excitation for the capacitive Rotor Position Pickoff bridge; therefore it must be converted to a sine wave and then shifted with respect to the demodulator reference to provide the proper phasing.

(2) The 4.2 kHz signal is used to excite the rotating x axis of the Ω Resolver. It is converted to a sine wave to keep well below the maximum slew rate of the Resolver Driver amplifier and succeeding amplifiers.

(3) The 1.25 kHz is used to provide the reference for the rotating system signal modulators. Sine wave modulators are used to keep well below the maximum slew rate of the Resolver Driver amplifier and succeeding amplifiers.

(4) The 1.0 kHz and 625 Hz signals are used for excitation of the Housing Drive Motor Power Supply and the Spin Motor Power Supply. Each of these signals must be converted to a sine wave for this purpose.

The Frequency Reference Unit consists of two circuit boards. The 200 kHz Oscillator and Divider is located on Circuit Board number 10. The Frequency Reference Shaper is located on Circuit Board number 9. Figures III-21 and III-22, Appendix III are the schematic and layout of Circuit Board number 10. Figures III-19 and III-20 are the schematic and layout of Circuit Board number 9.

(2) Housing Drive Motor Power Supply (Figure 46)

The Housing Drive Motor Power Supply provides three-phase 1.0 kHz power to the Housing Drive Motor. The 1.0 kHz input is split into 0 deg and -60 deg phase signals and

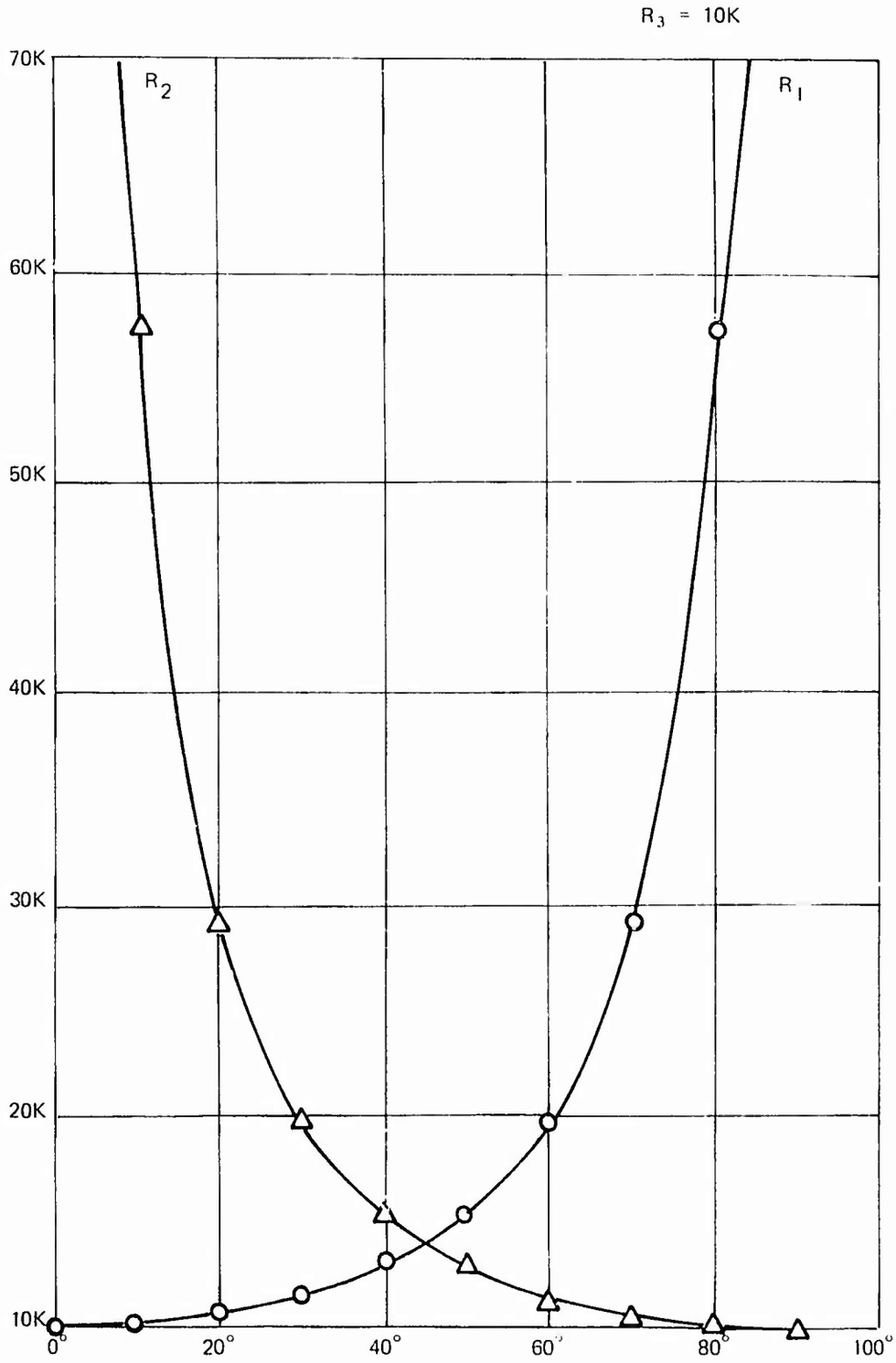

Figure 44. Input Resistor Values versus Phase Shift

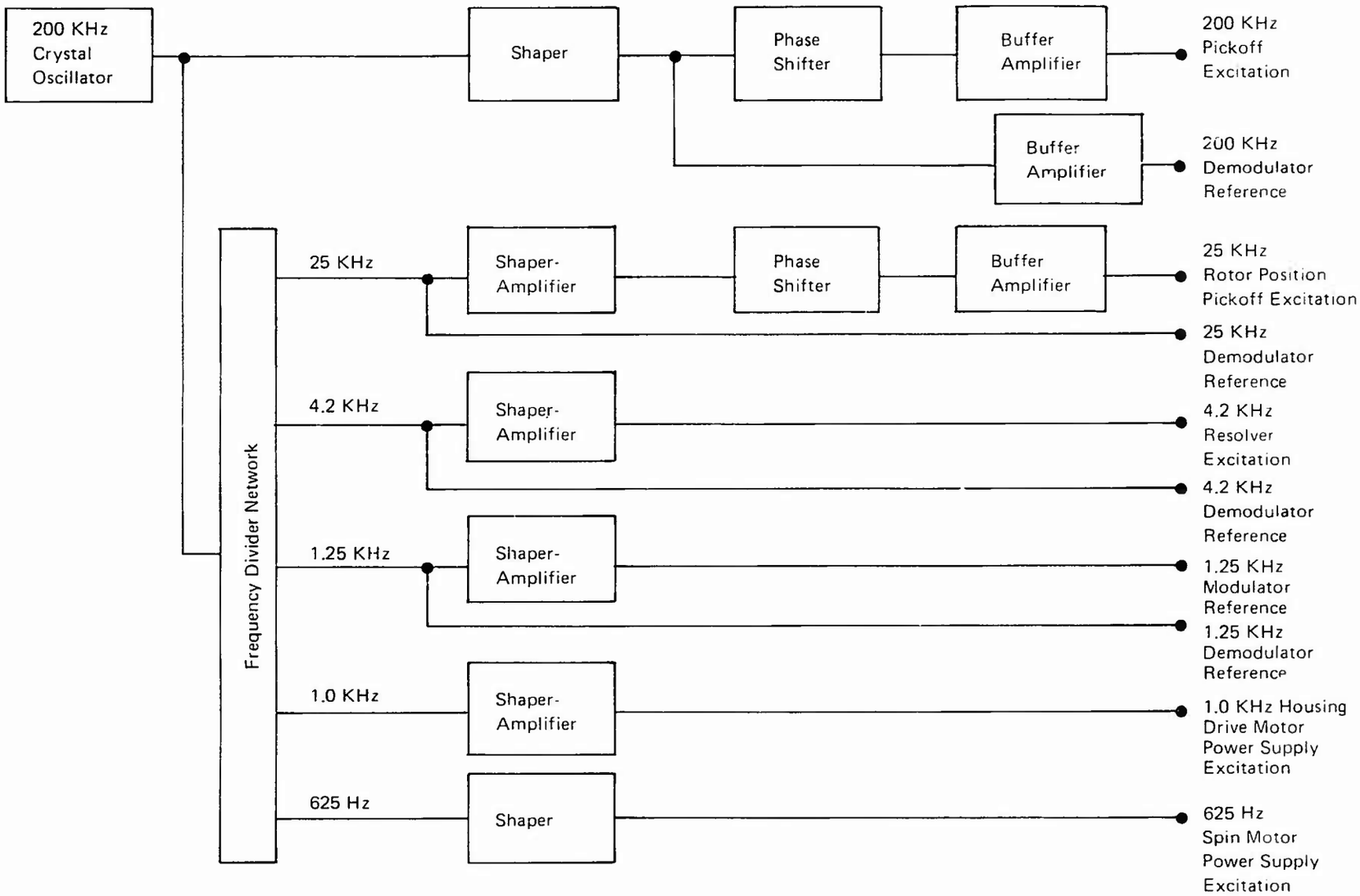

Figure 45. Frequency Reference Unit

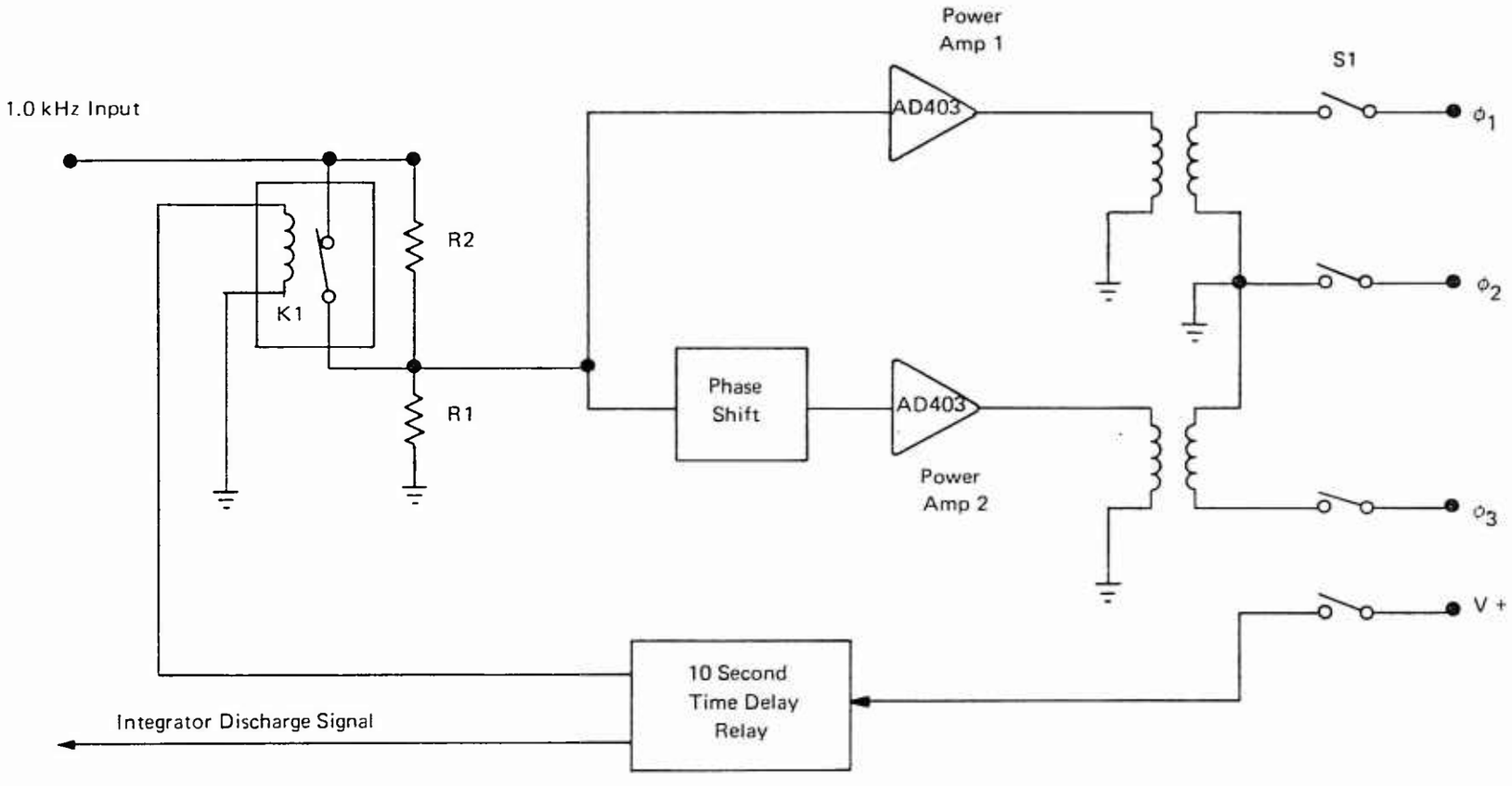

Figure 46. Housing Drive Motor Power Supply Block Diagram

power amplified by Power Amplifiers 1 and 2. Relay K_1 controls the amplitude of the output between two levels. When K_1 is closed the full input is applied to both power amplifiers. When S_1 is closed, full power is applied to the Housing Drive Motor and the ten second time delay relay is activated. After ten seconds, K_1 opens and R_2 is placed in series with R_1. This reduces the output power by about 35%, and is the normal running condition. The ten second time delay relay also controls a signal used to discharge all of the integrators in the Nutatron System. When power is applied to the Nutatron Electronics, each of the integrator capacitors is shunted with a low value resistor. These shunt resistors remain in the circuits until ten seconds after S_1 is closed. At that time, the ten second time delay relay sends out a signal which removes the shunt resistors and the integrators begin their normal operations.

The Housing Drive Motor Power Supply circuitry is located on Circuit Board number 11. Figures III-23 and III-24, Appendix III are the schematic and layout of this board. The ten second time delay relay is located on the Power Supply Chassis (Figure 48).

(3) dc Power Supplies

Commercial modular power supplies and regulators are used to provide the dc operating voltages. Separate modules are used for the various functional circuit groups. This approach reduces the need for decoupling the various functional groups separately and eliminates the problem of ground currents being cross coupled into the various circuits. Figure 47 lists the power supplies and the circuits they power.

Power Supplies 1 thru 8 are located on the dc POWER SUPPLY Chassis (Figure 48). Power Supply 9 is located on Circuit Board number 22. Figure III-45, Appendix III is a layout of this board. Power Supply number 10 is located on Circuit Board number 8. Figures III-17 and III-18 are the schematic and layout of this board.

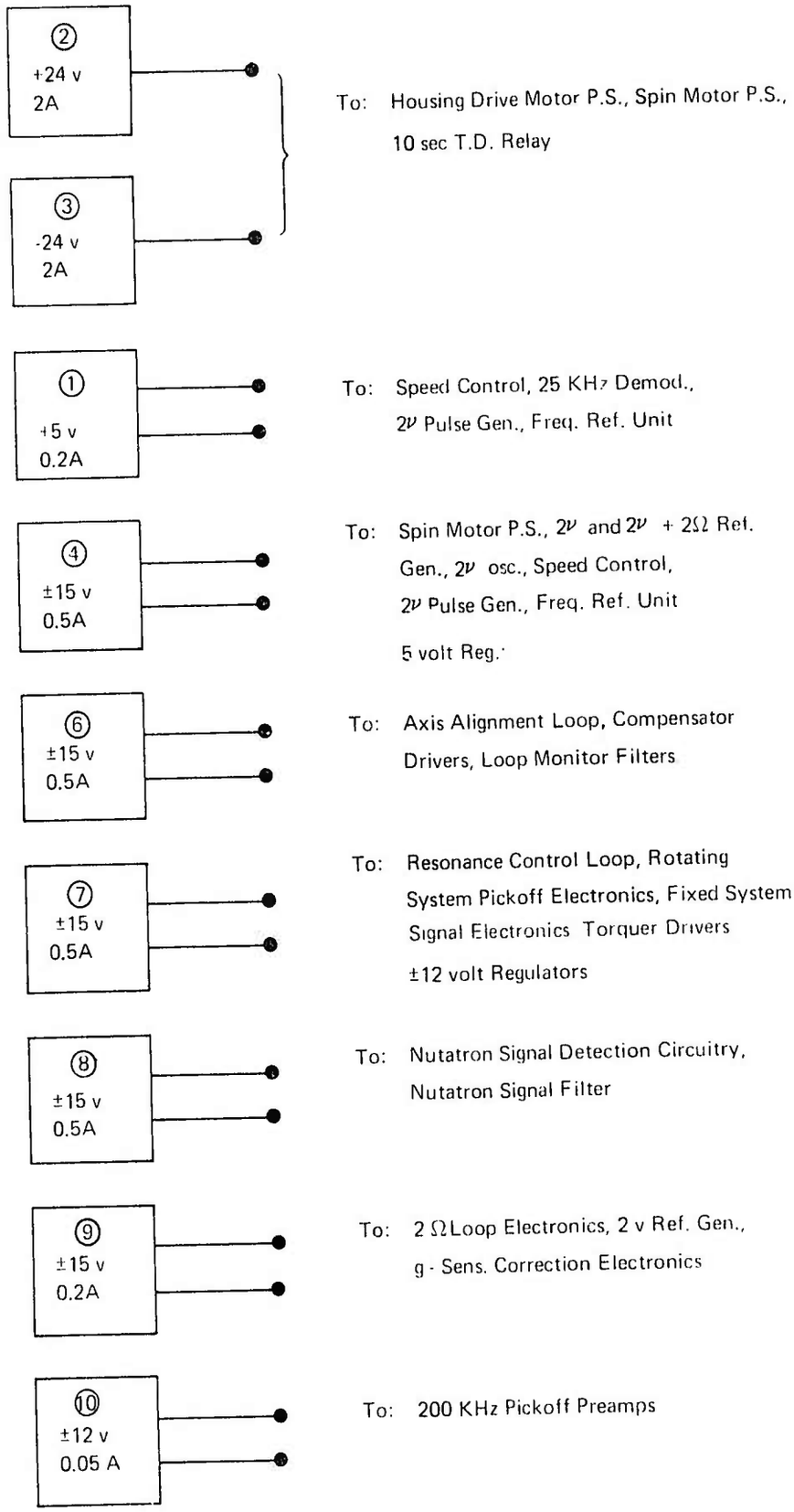

Figure 47. dc Power Supplies

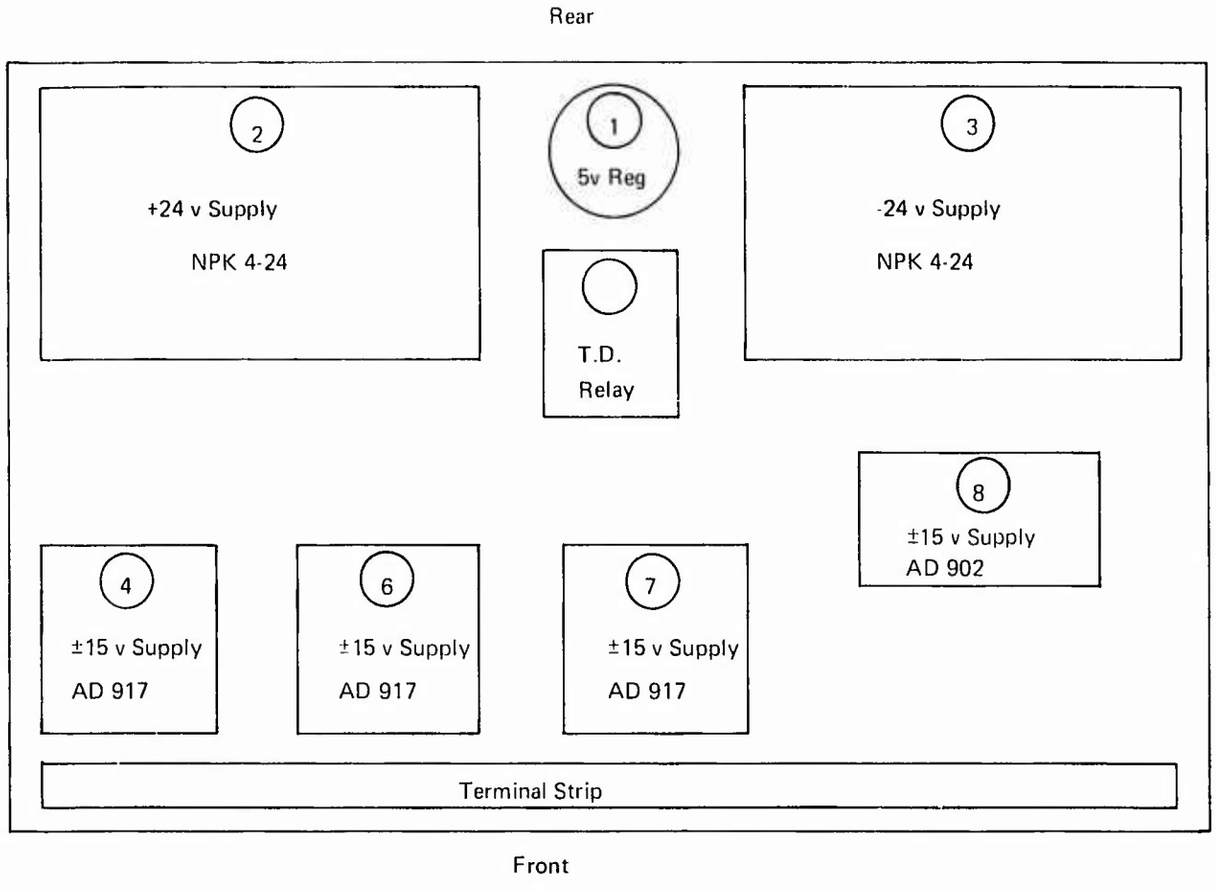

Figure 48. dc Power Supply Chassis Layout -- Top View

V. NUTATRON TEST PROGRAM AND RESULTS

Two Nutatron instruments, SN-1 and SN-2, were tested in the laboratory. Particular emphasis was placed on those performance parameters which were the primary objectives of the Nutatron exploratory development program and which would substantiate the growth potential of this new angular rate sensor concept. The acceleration independent, and the acceleration sensitive drift terms were investigated in depth including the following characteristics.

a. Long and short term stabilities
b. Randomness
c. Repeatability from cold start and reaction time
d. Temperature coefficients (ΔT of 27° F)
e. Magnetic sensitivity
f. Repeatability after exposure to temperature cycles (0° - 150°)

Separate determinations for the bias drift and scale factor errors were made. In addition, the magnitude of the acceleration square sensitive drift was determined. The results are summarized in Table 1, and the test methods are described in this section.

A. TEST METHOD

The Nutatrons were tested in the rate capture mode, with components of earth rotation as the input. The conventional low-frequency torque rebalance loops were augmented by narrow-band, high-grain torque rebalance loops at the nutatron frequency ($2\nu + 2\Omega$) which nulled oscillations at that frequency. These torques are proportional to the input precession rates, and in the absence of noise torque at that frequency, would be a true indication of the component of earth rotation coupled into the input axes by appropriate orientation of the instrument. Noise torques at the Nutatron frequency are equivalent to drift as indicated by the relationships:

$$T_{Xsin} = + \Omega_{EX} \ \nu \ (A\text{-}B) + T_{nxsin}$$

$$T_{Xcos} = - \ \Omega_{EY} \ \nu \ (A\text{-}B) + T_{nxcos}$$

where T_{Xsin} and T_{Xcos} are the indicated torques at sin $(2\nu + 2\Omega)t$ and cos $(2\nu + 2\Omega)t$ by the Nutatron torque rebalance loops.

T_{nxsin}, and T_{nxcos} are the noise torques at sin $(2\nu + 2\Omega)t$ and cos $(2\nu + 2\Omega)t$.

Ω_{EX}, and Ω_{EY} are components of earth rotation about input axes.

ν is the rotor speed
Ω is the housing rotation speed

A and B are the radial moments of inertia of the rotor. The derivation of the Nutatron equation is presented in Appendix I of this report.

The $(2\nu + 2\Omega)$ Nutatron capturing loops, and the method of recording the torques at the Nutatron frequency are illustrated by the double lined portion of block diagram Figure 49.

The relationship between noise torques and drift is

$$\omega_x = -\frac{T_{nx\sin}}{\nu\,(A-B)}$$

$$\omega_y = \frac{T_{nx\cos}}{\nu(A-B)}$$

where ω_x and ω_y are the nutatron drift about the two input axes.

The mounting arrangement of the Nutatron on the Leitz and OMT head is illustrated on Figure 50 and photograph Figure 51.

It allows for precision indexing about all axes to accuracies of 2 arc seconds.

B. TEST RESULTS

A test procedure was written prior to initiating the final evaluation program of two instruments. The tests were conducted in the sequence reported here with the set of test electronics which will be used by the Air Force at Holloman Air Force Base.

1. Test 1. Cardinal Points - Spin Axis Vertical.

a. Purpose

To determine the following eight parameters:

(1) K_x = x axis read out scale factor (V/deg/hr)

(2) K_y = y axis read out scale factor (V/deg/hr)

(3) ω_{XD}= x axis acceleration insensitive drift

(4) ω_{YD}= y axis acceleration insensitive drift

(5) α = angular displacement of y input axis below horizontal plane

(6) β = angular displacement of x input axis above horizontal plane

(7) θ = angular displacement of the y input axis from the Leitz head spindle axis.

(8) ϕ = angular displacement of the x input axis from an axis perpendicular to the Leitz head spindle axis.

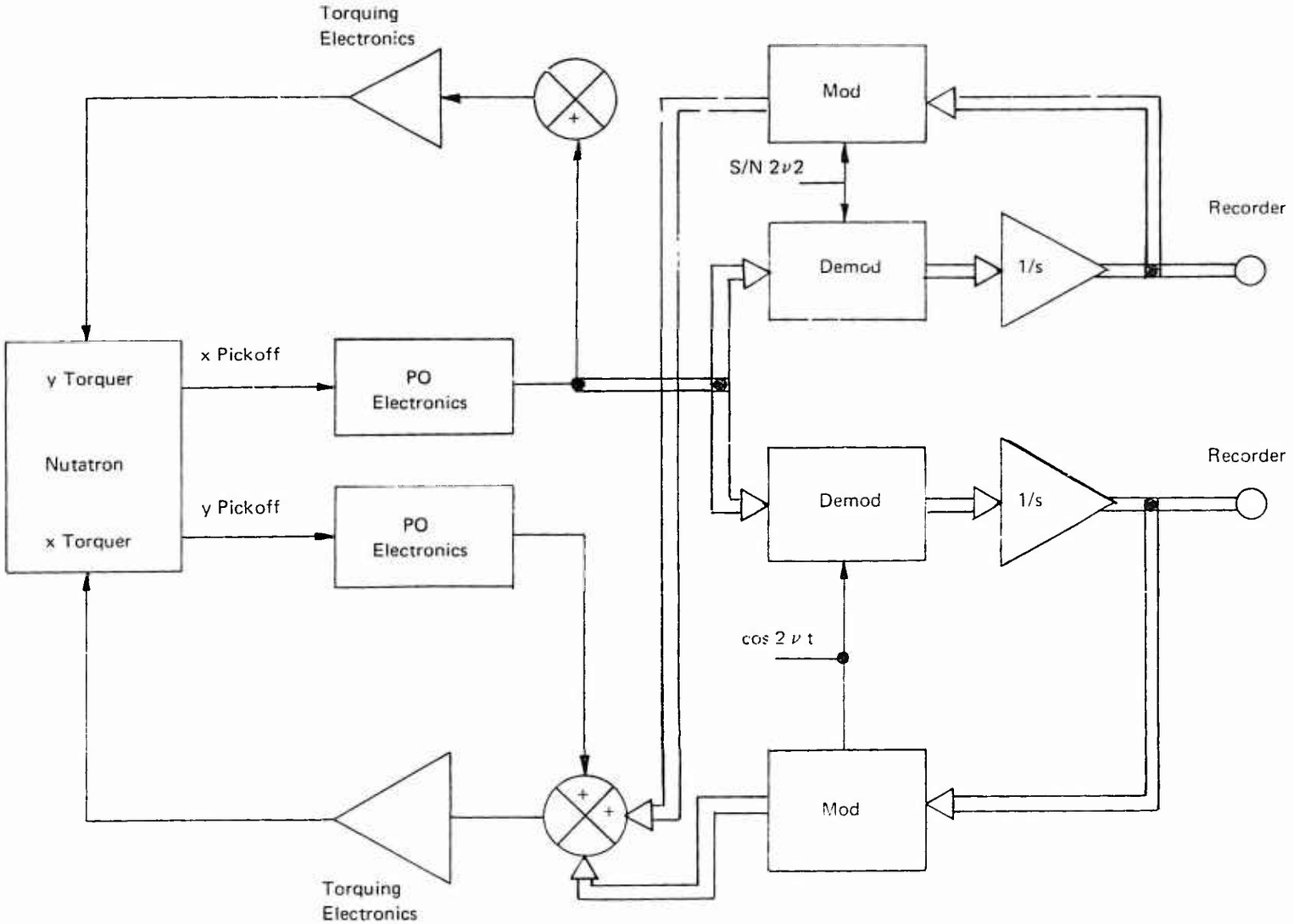

Figure 49. Nutatron Rate Capture Mode

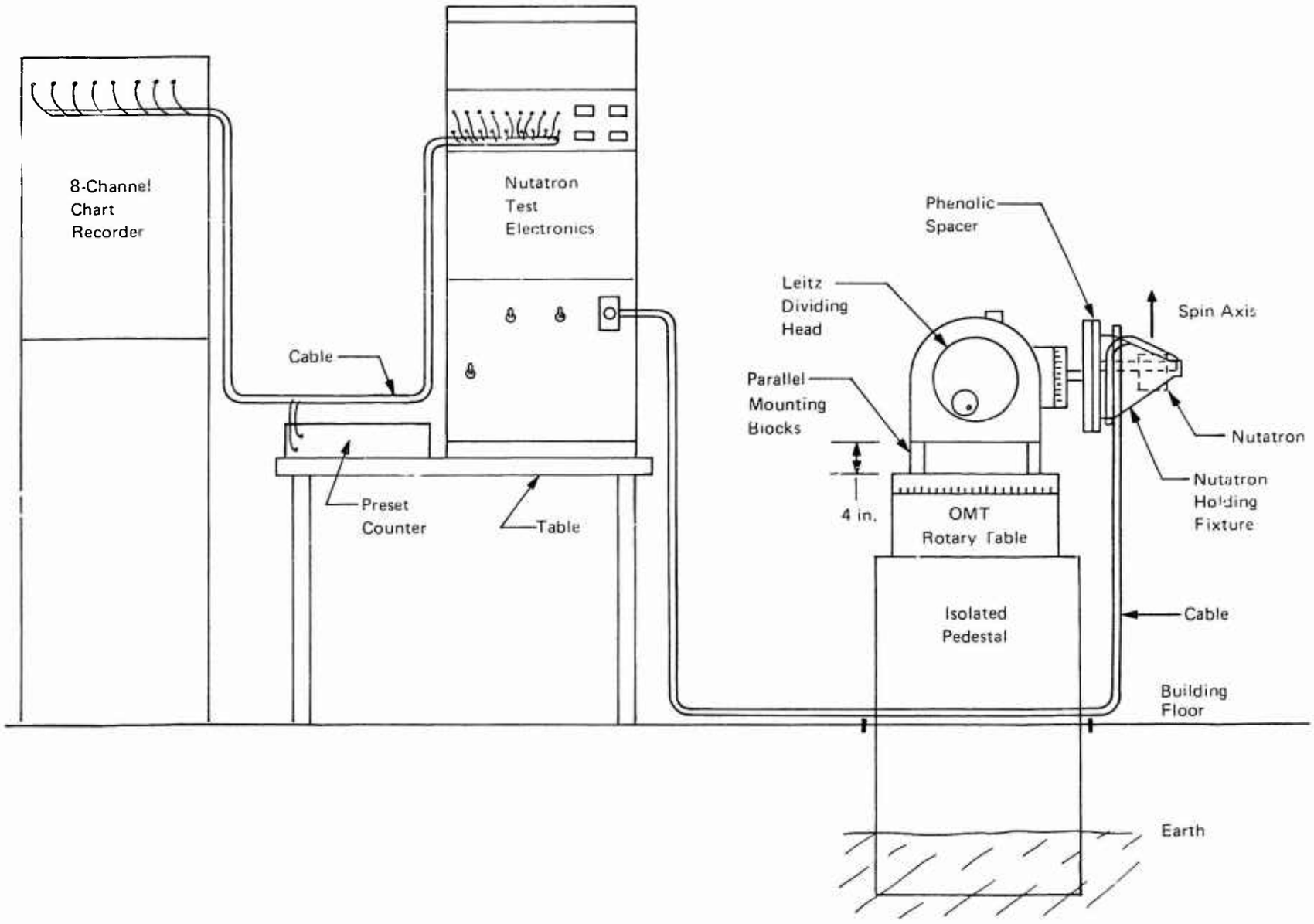

Figure 50. Nutatron Test Station

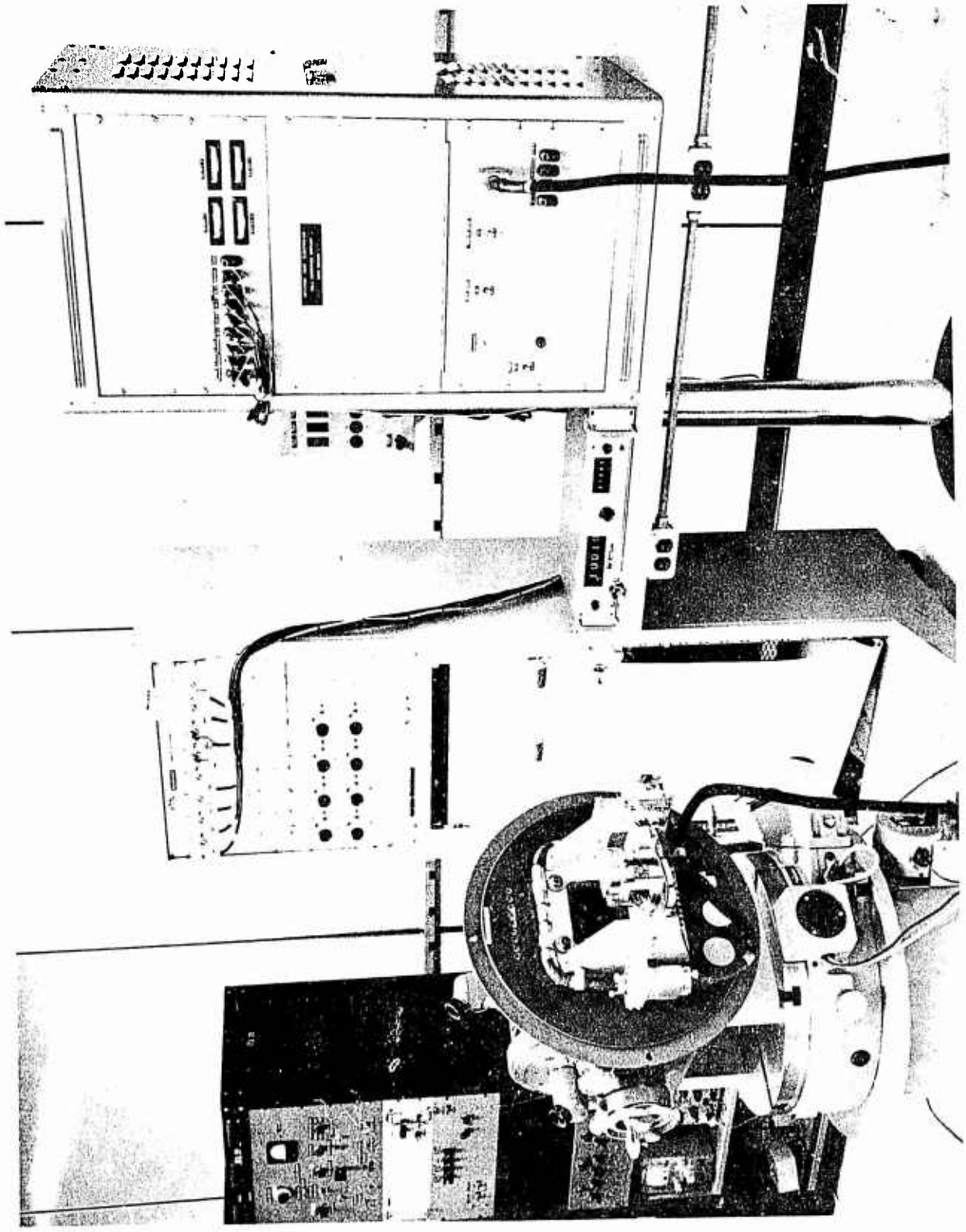

Figure 51. Nutatron Test Station

Figure 52 represents the Y axis North, $\vec{H}$ up test position and defines θ and ϕ. Angles α and β are not shown.

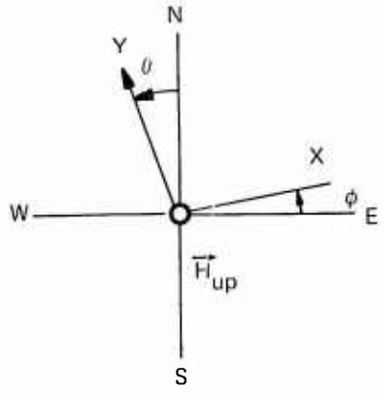

Figure 52. Definition of Axes

b. Test Procedure

The Nutatron is positioned for two hours in each of the eight positions listed in Table IV, and the x and y axis outputs are recorded. The readout voltages averaged over the last 1.5 hours of each run are used for the calculations. Inspection of Table IV yields the following (assuming all angles are small).

(1) Readout Scale Factor Calculations:

$$K_x = \frac{X_1 - X_3}{2\Omega_H}$$

$$= \frac{X_7 - X_5}{2\Omega_H}$$

$$K_y = \frac{Y_2 - Y_4}{2\Omega_H}$$

$$= \frac{Y_6 - Y_8}{2\Omega_H}$$

where $x_1, x_2 \ldots x_n$; $y_1, y_2 \ldots y_n$ are readout voltages in the attitudes listed on Table IV.

(2) Acceleration Insensitive Drift Calculations:

TABLE IV. CARDINAL POINTS - SPIN AXIS VERTICAL

y Axis	x Axis	$\vec{H}$	Attitude Number	X Readout	Y Readout
West	North	Up	1	$X_1 = K_x (\Omega_H \cos\phi + \Omega_v \sin\beta + \omega_{XD})$	$Y_1 = K_y (-\Omega_H \sin\theta - \Omega_v \sin\alpha + \omega_{YD})$
North	East	Up	2	$X_2 = K_x (\Omega_H \sin\phi + \Omega_v \sin\beta + \omega_{XD})$	$Y_2 = K_y (\Omega_H \cos\theta - \Omega_v \sin\alpha + \omega_{YD})$
East	South	Up	3	$X_3 = K_x (-\Omega_H \cos\phi + \Omega_v \sin\beta + \omega_{XD})$	$Y_3 = K_y (\Omega_H \sin\theta - \Omega_v \sin\alpha + \omega_{YD})$
South	West	Up	4	$X_4 = K_x (-\Omega_H \sin\phi + \Omega_v \sin\beta + \omega_{XD})$	$Y_4 = K_y (-\Omega_H \cos\theta - \Omega_v \sin\alpha + \omega_{YD})$
West	South	Down	5	$X_5 = K_x (-\Omega_H \cos\phi - \Omega_v \sin\beta + \omega_{XD})$	$Y_5 = K_y (\Omega_H \sin\theta + \Omega_v \sin\alpha + \omega_{YD})$
North	West	Down	6	$X_6 = K_x (\Omega_H \sin\phi - \Omega_v \sin\beta + \omega_{XD})$	$Y_6 = K_y (\Omega_H \cos\theta + \Omega_v \sin\alpha + \omega_{YD})$
East	North	Down	7	$X_7 = K_x (\Omega_H \cos\phi - \Omega_v \sin\beta + \omega_{XD})$	$Y_7 = K_y (\Omega_H \sin\theta + \Omega_v \sin\alpha + \omega_{YD})$
South	East	Down	8	$X_8 = K_x (\Omega_H \sin\phi - \Omega_v \sin\beta + \omega_{XD})$	$Y_8 = K_y (\Omega_H \cos\theta + \Omega_v \sin\alpha + \omega_{YD})$

$\vec{H}$ = Angular momentum vector

Ω_H = Horizontal component of earth rate (10.98°/hr at Wheatfield, New York)

Ω_v = Vertical component of earth rate (10.28°/hr at Wheatfield, New York)

X_1 through X_8 = X axis readout outputs

Y_1 through Y_8 = Y axis readout outputs

ω_{XD} = X axis acceleration insensitive drift

ω_{YD} = Y axis acceleration insensitive drift

K_x = X axis scale factor

K_y = Y axis scale factor

$$\omega_{XD} = \frac{X_1 + X_5}{2K_X}$$

$$= \frac{X_4 + X_6}{2K_X}$$

$$\omega_{YD} = \frac{Y_1 + Y_5}{2K_y}$$

$$= \frac{Y_2 + Y_8}{2K_y}$$

(3) Spin Axis Tilt Calculations:

$$\beta = \frac{X_1 - X_7}{2K_X\Omega_V}$$

$$= \frac{X_2 - X_6}{2K_X\Omega_V}$$

$$\alpha = \frac{Y_6 - Y_2}{2K_y\Omega_V}$$

$$= \frac{Y_7 - Y_1}{2K_y\Omega_V}$$

(4) Location of Sensitive Axes in the Horizontal Plane:

$$\phi = \frac{X_2 - X_4}{2K_X\Omega_H}$$

$$= \frac{X_6 - X_8}{2K_X\Omega_H}$$

$$\theta = \frac{Y_3 - Y_1}{2K_y\Omega_H}$$

$$= \frac{Y_5 - Y_7}{2K_y\Omega_H}$$

It is seen that each parameter is calculated from two independent sets of data. This method provides a check on the data and the calculations and provides a measure of the uncertainty in the calculated value of each parameter.

c. Test Results

Table V lists the parameters obtained for Nutatrons SN-1 and SN-2. The uncertainty in the readings is ±0.05 deg/hr or ±20 arc minutes. The values listed are the averages obtained from the two calculations for each parameter.

TABLE V. PARAMETERS OBTAINED FROM CARDINAL POINT DATA - SPIN AXIS VERTICAL

Nutatron SN	K_x	K_y	ω_{XD} deg/hr	ω_{YD} deg/hr	β	α	ϕ	θ
1	$\frac{0.58V}{deg/hr}$	$\frac{0.56V}{deg/hr}$	0.16 ± 0.05	0.15 ± 0.05	0 deg ± 20 min	0 deg ± 20 min	0 deg ± 20 min	0 deg ± 20 min
2	$\frac{0.69V}{deg/hr}$	$\frac{0.69V}{deg/hr}$	0 ± 0.05	0 ± 0.05	0 deg ± 20 min	0 deg ± 20 min	0 deg ± 20 min	0 deg ± 20 min

2. Test 2. Sixteen Hour Stability Run - Spin Axis Vertical.

a. Purpose

To obtain a measure of the short-term randomness and trend of the Nutatron output signals.

b. Test Procedure

The Nutatron is oriented in cardinal position 1 of the previous test. The x and y axis readouts are monitored and recorded for 16 hours. In cardinal position 1, the input rate into the Y axis is normally zero, and the rate into the X axis is the full horizontal component of earth rate (10.98 deg/hr at Wheatfield, New York). The trend and randomness in each axis are calculated using 25 minute averages of the recorded data. The Nutatron is not temperature controlled during this test.

c. Test Results

Table VI is a summary of the results obtained from these tests. Figure 53 is a six hour recording of the data obtained from SN-2. It can be seen from the recording that the output signal variations are primarily periodic rather than truly random. This phenomenon is discussed in detail in Section VI. Figures 54 and 55 show the sixteen hour stability runs for SN-1 and SN-2 respectively.

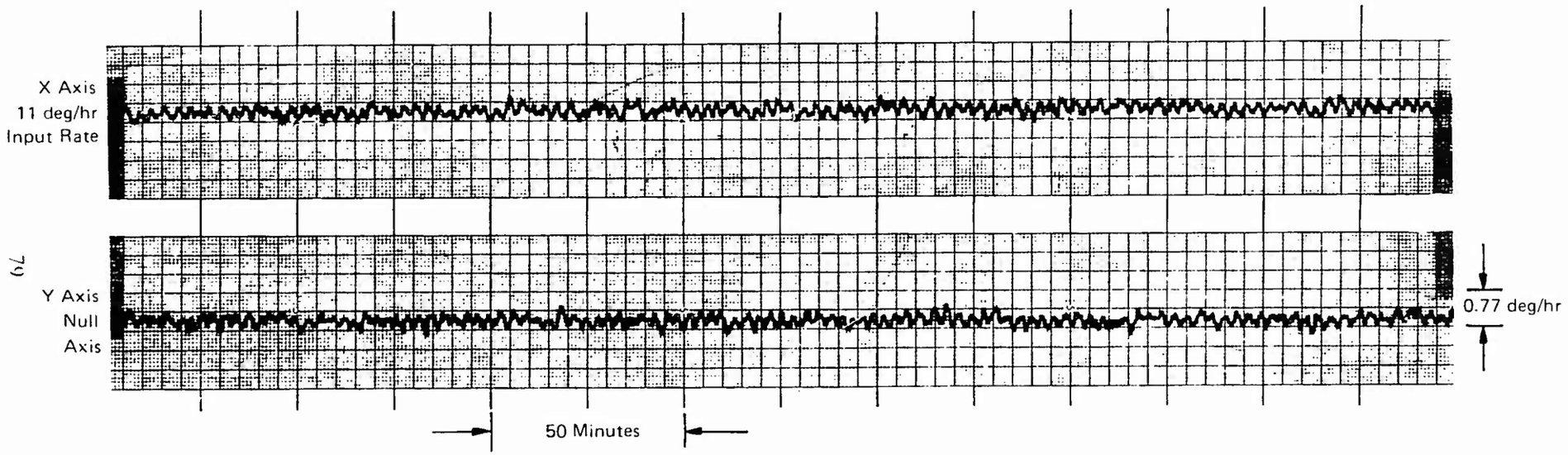

Figure 53. Nutatron Stability Run – Spin Axis Vertical – No Temperature Control

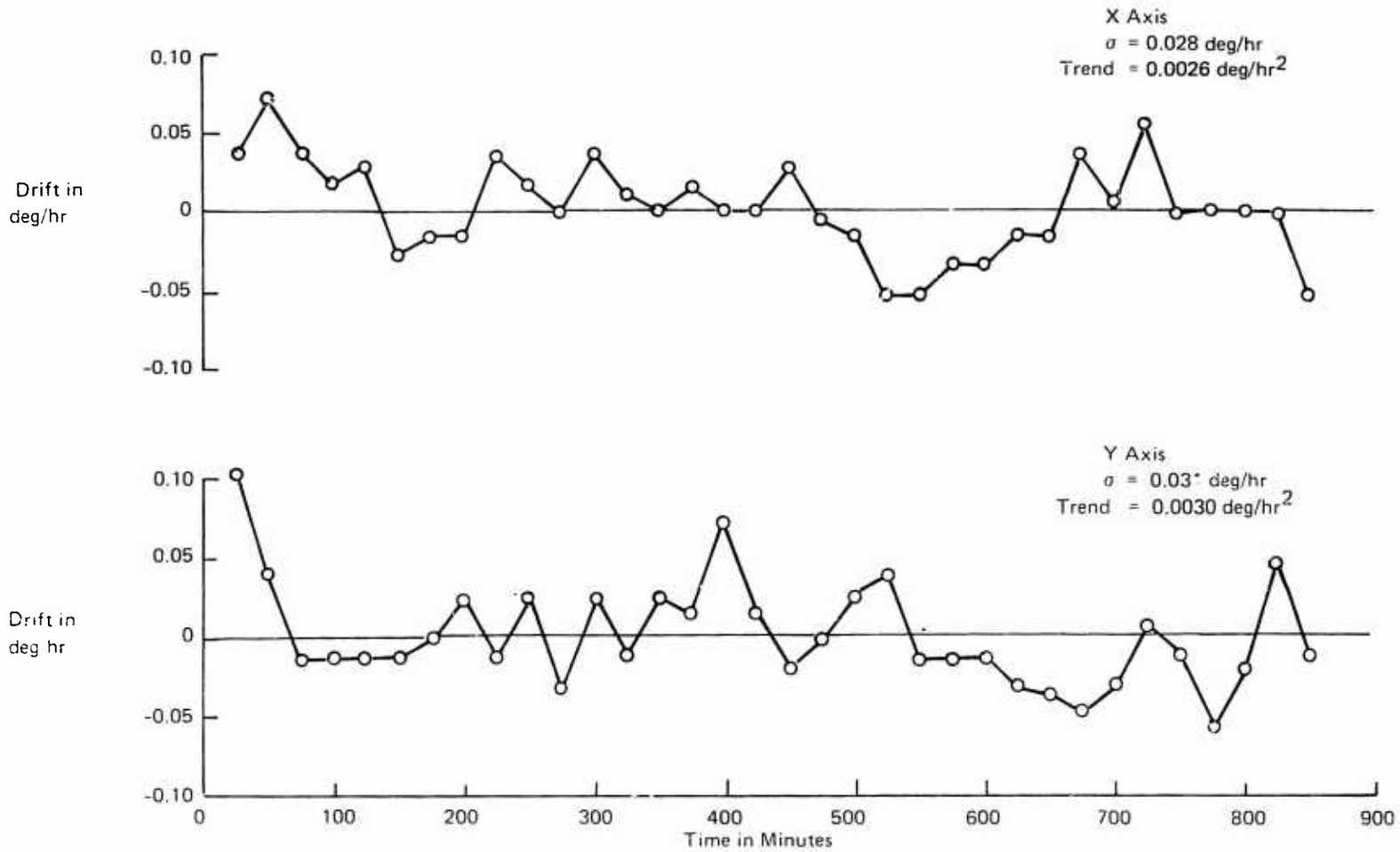

Figure 54. Vertical Spin Axis Drift Data, SN-1, 25-Minute Averages

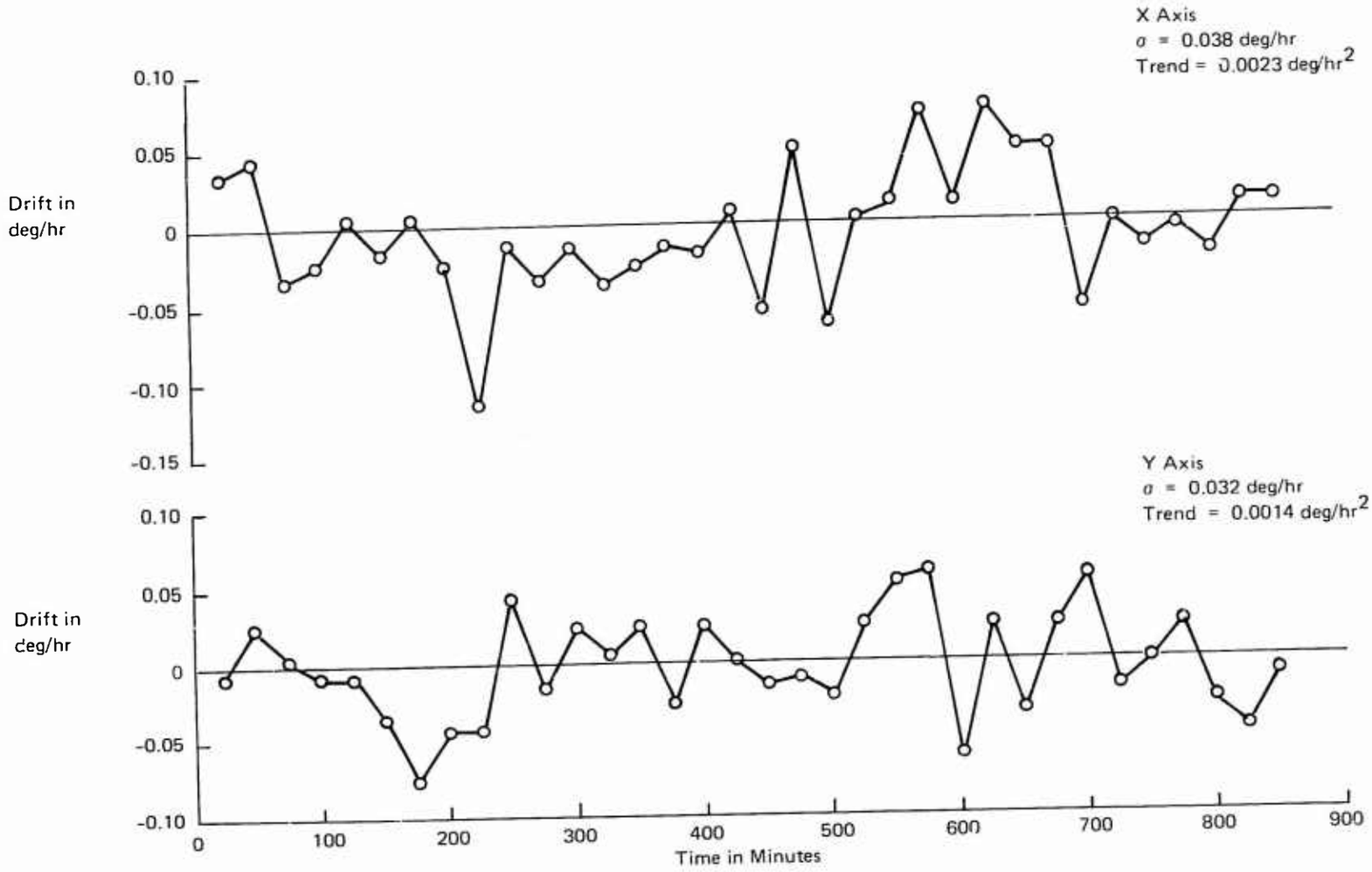

Figure 55. Vertical Spin Axis Drift Data, SN-2, 25-Minute Averages

TABLE VI. RESULTS OBTAINED FROM 16-HOUR STABILITY RUNS - SPIN AXIS VERTICAL

Nutatron SN	y Axis (Null Axis)		x Axis (10.98 deg/hr Axis)	
	Randomness (σ) (deg/hr)	Trend (deg/hr/hr)	Randomness (σ) (deg/hr)	Trend (deg/hr/hr)
1	0.031	0.0031	0.028	0.0026
2	0.023	0.0014	0.038	0.0023

3. Test 3. Temperature Sensitivity - Spin Axis Vertical.

a. Purpose

To measure the temperature sensitivity of the scale factor and the temperature sensitivity of the acceleration insensitive drift in each axis.

b. Test Procedure

The Nutatron is operated at its normal temperature for two hours in each of two cardinal positions (Position 1 and Position 5). Then 0.5 ampere of dc current is fed into the internal heaters of the Nutatron. This causes an internal temperature rise of approximately 15°C. After the temperature has stabilized, the two cardinal position test is repeated, each point being monitored for two hours. The average values for the last 1.5 hours of each run are used to calculate values for acceleration insensitive drift and scale factor for each temperature As in Test 1 above, the values for acceleration insensitive drift are:

$$\omega_{XD} = \frac{X_1 + X_5}{2K_x}$$

$$\omega_{YD} = \frac{Y_1 + Y_5}{2K_y}$$

From Table IV it is seen that

$$X_1 - X_5 = K_x \left| 2\Omega_H + 2\Omega_V \beta \right|$$

However, β was found to be negligible: therefore,

$$K_x = \frac{X_1 - X_5}{2\Omega_H}$$

In the ac feedback mode of operation, both axes feed the same torquer coil. Therefore, both axes have the same scale factor temperature coefficient.

c. Test Results

Table VII is a summary of the results obtained.

TABLE VII. TEMPERATURE SENSITIVITY OF ACCELERATION INSENSITIVE DRIFT AND SCALE FACTOR

Nutatron SN	Scale Factor Temp. Sensitivity	Acceleration Insensitive Drift Temp. Sensitivity	
		x Axis deg/hr/°C	y Axis deg/hr/°C
1	+0.18%/°C	+0.0015	-0.0015
2	+0.17%/°C	+0.0019	+0.0055

4. Test 4. Measurement of g, g^2 and Higher Order g Sensitive Drift Coefficients.

a. Purpose

To determine the drift error coefficients attributable to acceleration along the various axes of the Nutatron.

b. Test Method

Initial tests are performed with the Leitz head spindle axis horizontal and pointing west. The Nutatron is subsequently indexed in 30 degree increments about the y west spindle axis (see Figure 56). From Figure 56 it can be seen that the angular rates along the sensitive axes are:

$$\left.\begin{aligned} \omega_x &= \Omega_E \cos\gamma\cos\phi \\ \omega_y &= \Omega_E \cos\gamma\sin\theta + \Omega_E \cos(\gamma+90^\circ)\sin\alpha \end{aligned}\right\} \quad (1)$$

The values ϕ, θ, α, and β were found in Test 1 (Cardinal Point Tests). The Leitz head is rotated about its spindle axis an angle equal to $-\beta$ away from nominal spin axis vertical setting. This is the true spin axis vertical position (γ_1).

The outputs of the x and y axes are monitored for one hour in each of 12 positions starting with $\gamma = \gamma_1$ and progressing in 30 degree increments to $\gamma = \gamma_1 + 360$ degrees. The output values obtained are converted to equivalent degrees/hr and compared to the known input rates calculated from Equation (1).

After the acceleration insensitive drift error is subtracted out, the remaining error in each axis is calculated for each of the twelve positions. A twelve point Fourier analysis of the errors is used to find the error coefficients.

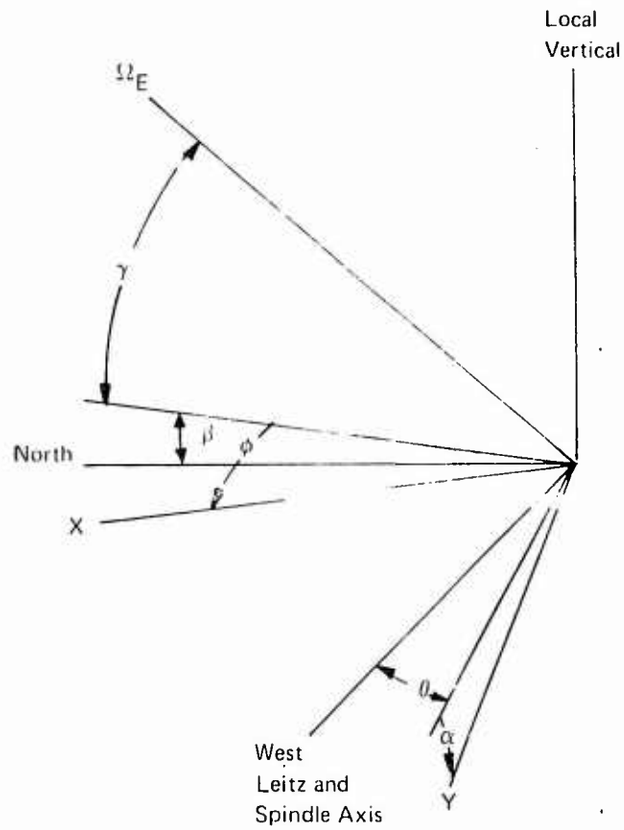

Definition of Terms:

X and Y are Nutatron Sensitive Axes

$\alpha, \beta, \theta, \phi$ are Previously defined in Tests Performed with Spin Axis Vertical

Ω_E is the Earth's Rotation Vector (15.04 deg/hr)

γ is the Angle between the Earth's Rotation Vector and the Nutatron X Axis

Figure 56. Orientation of Axes for g-Sensitivity Tests

c. Test Results

Figure 57 is a plot of the error curves obtained from Nutatron SN-2. Figure 58 is a plot of the error curves from SN-1. Fourier analyses of these curves shows that they can be quite accurately represented by the series:

$$\omega_E = A\sin\Phi + B\sin 2\Phi \qquad (2)$$

where ω_E = the error in deg/hr,

Φ = the angle between the spin axis and local vertical,

A and B are the Fourier coefficients

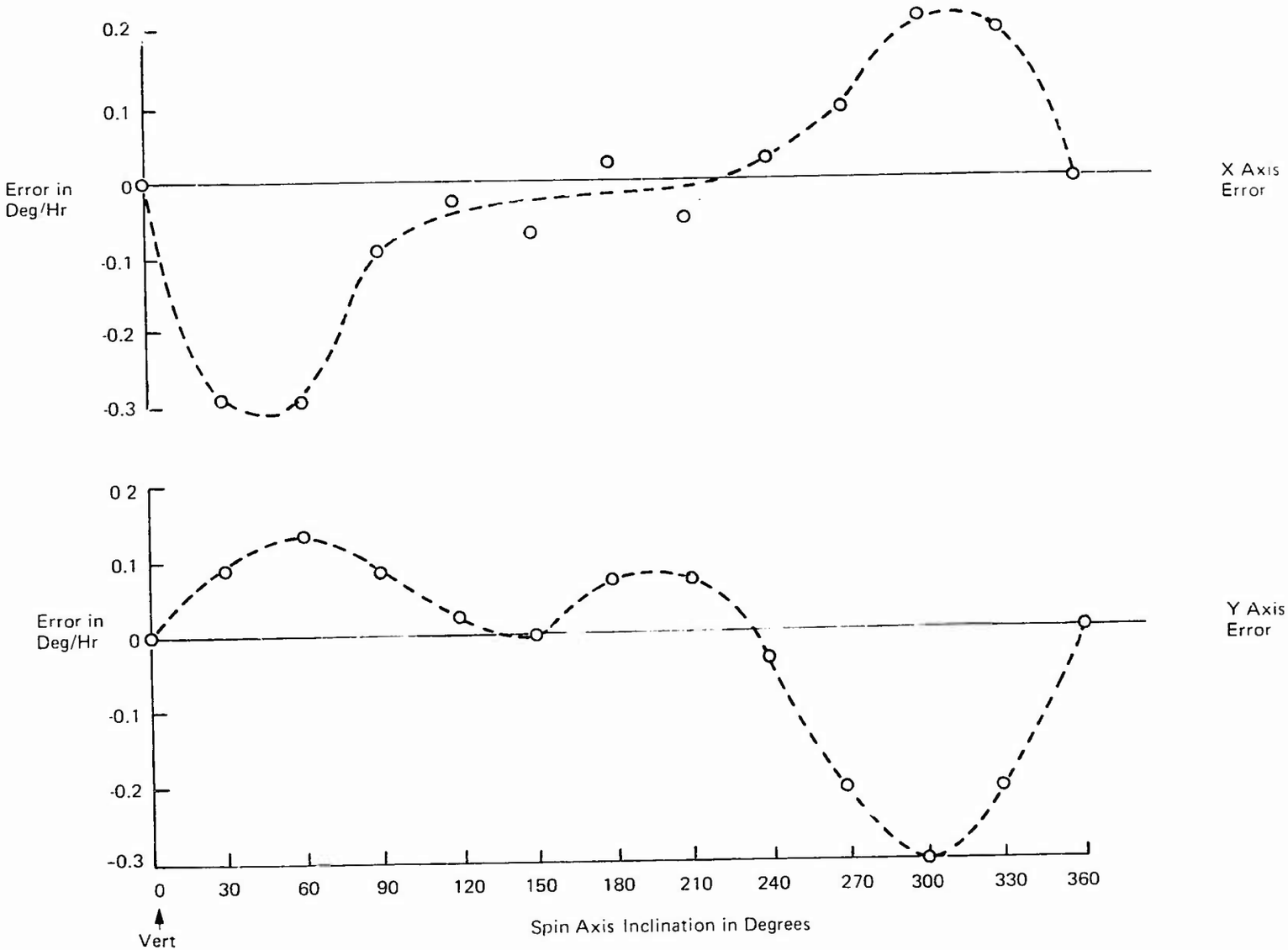

Figure 57. Final Tests, SN-2, Error versus Spin Axis Inclination

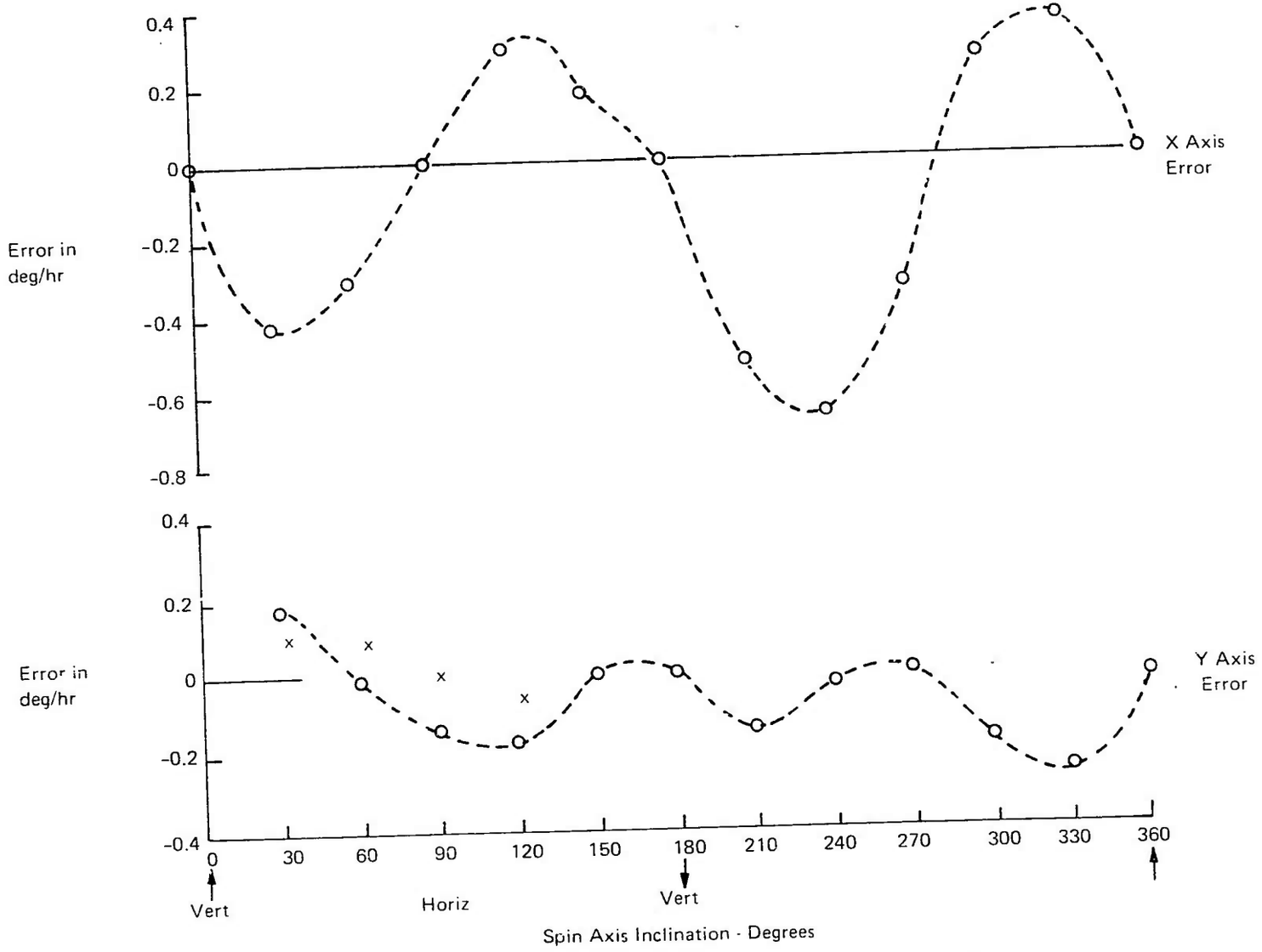

Figure 58. Error versus Spin Axis Inclination for Nutatron SN-1

Equation (2) can be rewritten:

$$\omega_{IS} = A\sin\Phi + 2B\sin\Phi\cos\Phi \quad ,$$

or in terms of g ,

$$\omega_{IS} = ag_r + bg_rg_a \quad , \text{ where}$$

g_r = $g\sin\Phi$ = the component of g perpendicular to the spin axis.

g_a = $g\cos\Phi$ = the component of g along the spin axis.

a and b, the drift coefficients, are seen to be equal to:

$$b = \frac{2B}{g^2}$$

$$a = \frac{A}{g}$$

Table VIII is a summary of the results of the tests on Nutatrons SN-1 and SN-2.

TABLE VIII. G SENSITIVE ERROR FOURIER COEFFICIENTS AND DRIFT COEFFICIENTS

	x Axis				y Axis			
SN	A_x deg/hr	B_x deg/hr	a_x	b_x	A_y deg/hr	B_y deg/hr	a_x	b_x
1	0.10	0.43	$\frac{0.10 \text{ deg/hr}}{g}$	$\frac{0.86 \text{ deg/hr}}{g^2}$	0.02	0.08	$\frac{0.02 \text{ deg/hr}}{g}$	$\frac{0.16 \text{ deg/hr}}{g^2}$
2	0.15	0.13	$\frac{0.15 \text{ deg/hr}}{g}$	$\frac{0.26 \text{ deg/hr}}{g^2}$	0.14	0.11	$\frac{0.14 \text{ deg/hr}}{g}$	$\frac{0.22 \text{ deg/hr}}{g^2}$

5. Test 5. Sixteen Hour Stability Run - Spin Axis Polar

a. Purpose

To obtain a measure of the short term randomness and trend of the Nutatron when its spin axis is aligned with axis of rotation of the earth. In this orientation, the input rate in each of the sensitive axes is normally zero. Both the radial and axial components of the g vector are approximately 0.7g in this orientation (at the Bell Aerospace lab., Wheatfield, New York). The results are to be compared with those obtained with the spin axis vertical. Any significant differences in trend or randomness are assumed to be attributable to instabilities in the g and g^2 sensitive drift coefficients.

b. Test Method

The Leitz head is positioned so that the spin axis is aligned with the polar axis. The x and y axis readouts are monitored and recorded for 16 hours. The trend and randomness in each axis are calculated using 25 minute averages of the recorded data. The Nutatron is not temperature controlled during this test.

c. Test Results

The results of this test are summarized in Table IX and in Figures 59 and 60. Comparison of these results with those obtained vertically shows that randomness and trend of SN-2 are independent of spin axis orientation. The performance of SN-1 is significantly better with the spin axis vertical (by a factor of approximately 2). This is probably due to the relatively higher g^2 drift coefficient of SN-1.

6. Test 6. Temperature Sensitivity - Spin Axis Polar

a. Purpose

To measure the temperature sensitivity of the g-sensitive drift of the Nutatron. As in the above test, the spin axis is aligned with the earth's polar axis. The input rates are normally zero in each sensitive axis, and the input g vectors are 0.7g along the x axis and 0.7g along the spin axis.

b. Test Method

The spin axis is aligned with the earth's polar axis. Both axes are monitored for 1.5 hours. Then 0.5 ampere of dc current is fed into the Nutatron internal heaters. This causes an internal temperature rise of approximately 15°C. After the temperature has stabilized, the outputs are monitored for 1.5 hours. Then the heating current is removed, and the Nutatron is allowed to return to its normal operating temperature. After the temperature has stabilized, the outputs are once again monitored for 1.5 hours. The Nutatron is then turned off for 1/2 hour and allowed to cool to room temperature. It is then turned back on and monitored for 1.5 hours to see how well it repeats the original values. If the drift sensitivities are significantly different from those obtained with the spin axis vertical, the differences are attributed to changes in g-dependent drift parameters.

c. Test Results

Table X lists the drift data obtained for the four operating conditions. In order to interpret and classify the results, it was assumed that the data were points lying on hysteresis type curves. The curves obtained are shown in Figure 61. Three parameters were defined and calculated from these curves:

(1) Temperature Sensitivity - The slope of the curves (expressed in deg/hr°C).

(2) Hysteresis - The difference between the g-sensitive drift at 40°C before and after the +15°C temperature increase.

(3) Repeatability - The difference between the original value of g-dependent drift at 40°C and the final value after allowing the Nutatron to cool to room temperature.

TABLE IX. RESULTS OBTAINED FROM 16 HOUR STABILITY RUNS - SPIN AXIS POLAR

Nutatron SN	y Axis		x Axis	
	Randomness (σ) (deg/hr)	Trend (deg/hr/hr)	Randomness (σ) (deg/hr)	Trend (deg/hr/hr)
1	0.071	0.0090	0.048	0.0053
2	0.018	0.0002	0.023	0.0057

TABLE X. NUTATRON g-DEPENDENT DRIFT AT 40°C AND 55°C (SPIN AXIS POLAR)

Nutatron SN	Nutatron Internal Temp.	x Axis g-Dependent Drift	y Axis g-Dependent Drift
2	40°C	-0.034 deg/hr	-0.068 deg/hr
	55°C	+0.374 deg/hr	+0.136 deg/hr
	40°C	+0.136 deg/hr	+0.204 deg/hr
	40°C after 1/2 hr Shutdown	0.0 deg/hr	0.0 deg/hr
1	40°C	+0.063 deg/hr	-0.063 deg/hr
	55°C	-0.063 deg/hr	-0.250 deg/hr
	40°C	0.0 deg/hr	+0.095 deg/hr
	40°C after 1/2 hr Shutdown	+0.095 deg/hr	-0.205 deg/hr

TABLE XI. G-DEPENDENT DRIFT PARAMETERS DERIVED FROM FIGURE 61 (SPIN AXIS POLAR)

Nutatron SN	Temperature Sensitivity		Hysteresis		Repeatability After Temp. Cycle	
	x Axis deg/hr/°C	y Axis deg/hr/°C	x Axis deg/hr/°C	y Axis deg/hr/°C	x Axis deg/hr/°C	y Axis deg/hr/°C
2	+0.032	+0.014	+0.170	+0.272	+0.034	+0.068
1	-0.008	-0.012	-0.063	+0.158	+0.032	-0.142

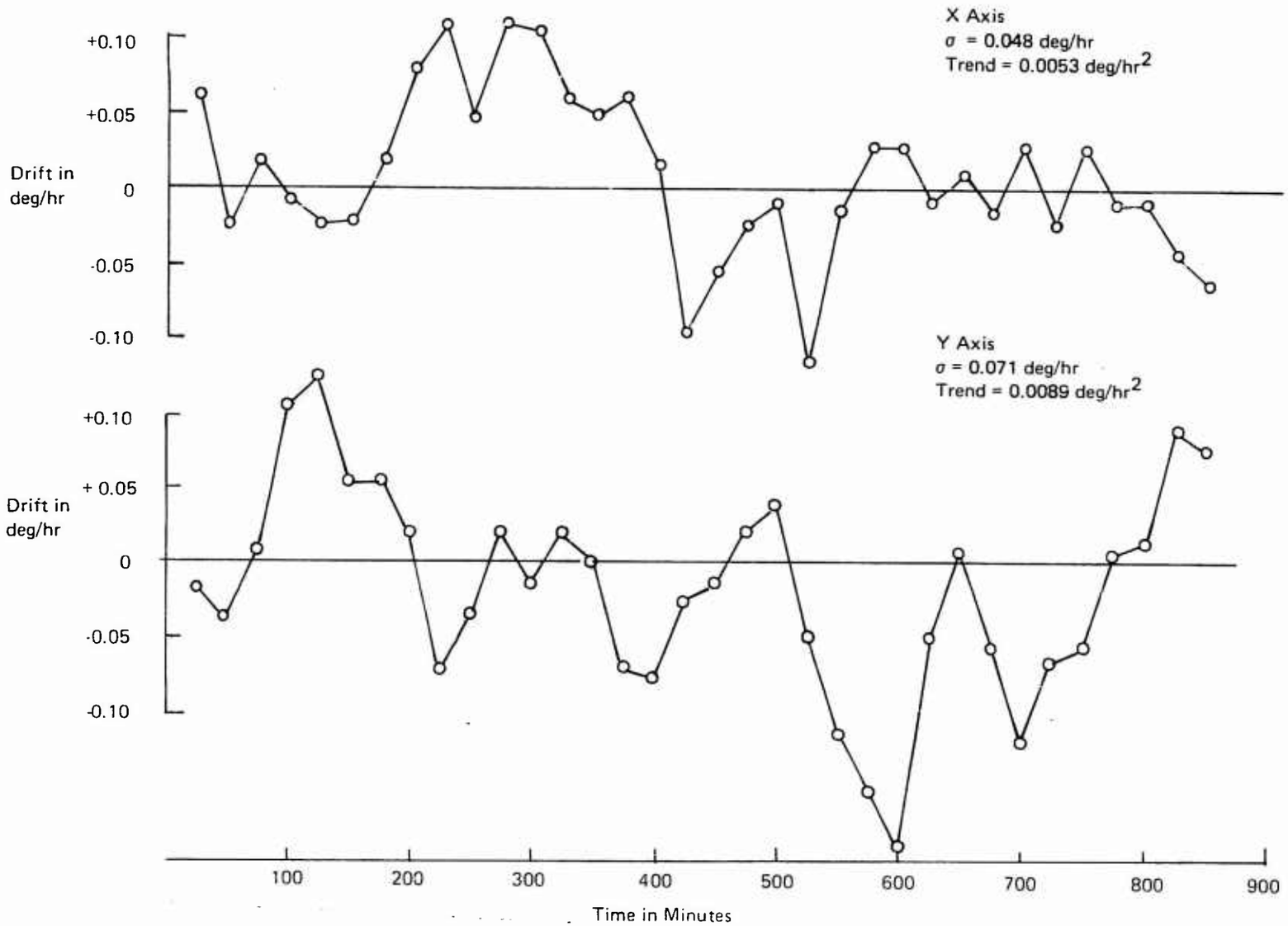

Figure 59. Polar Drift Run, SN-1, No Temperature Control

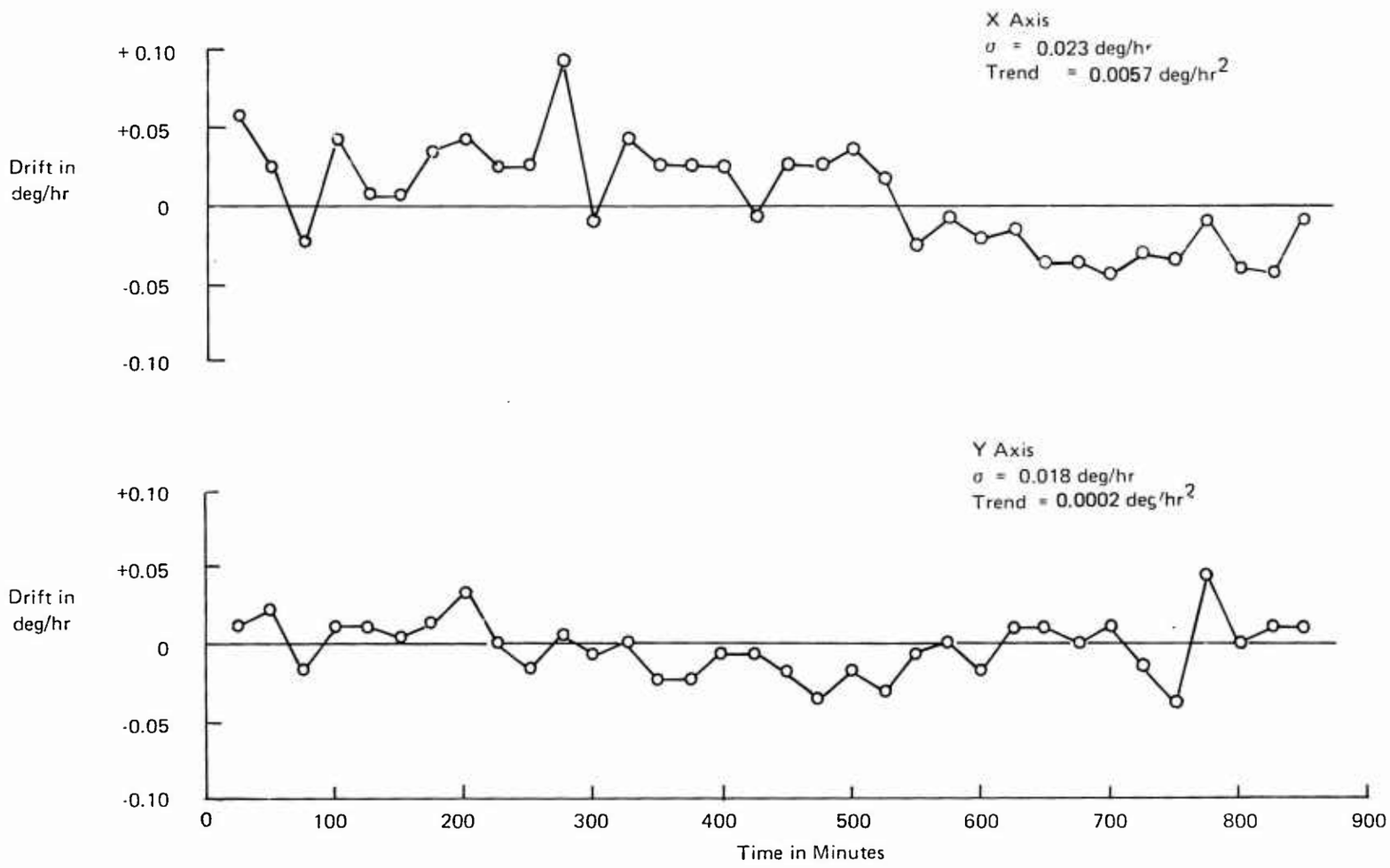

Figure 60. Polar Drift Run, SN-2, No Temperature Control

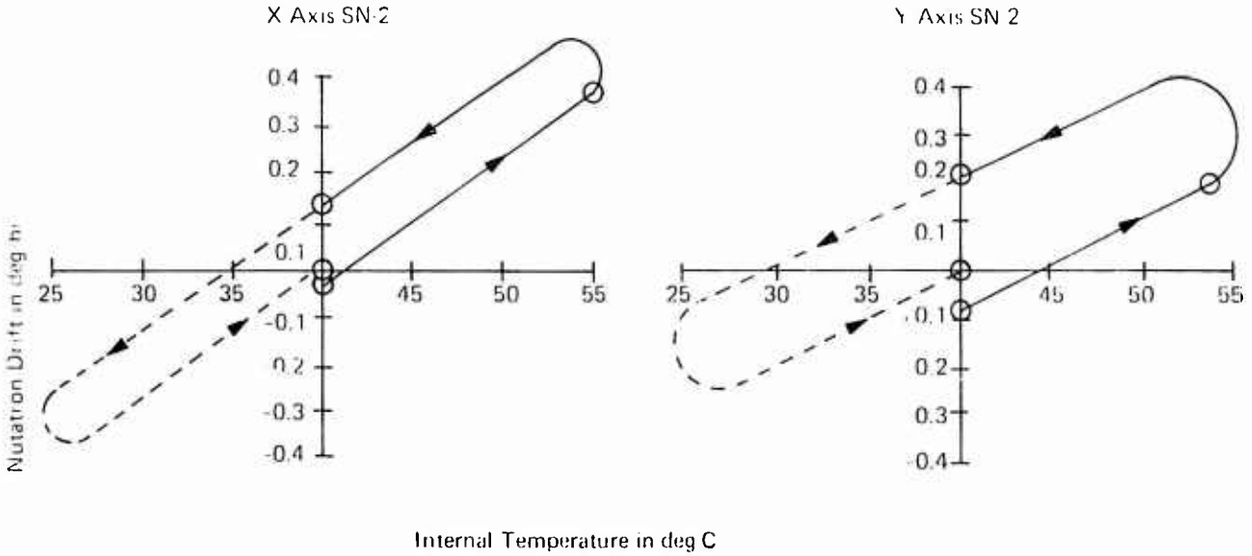

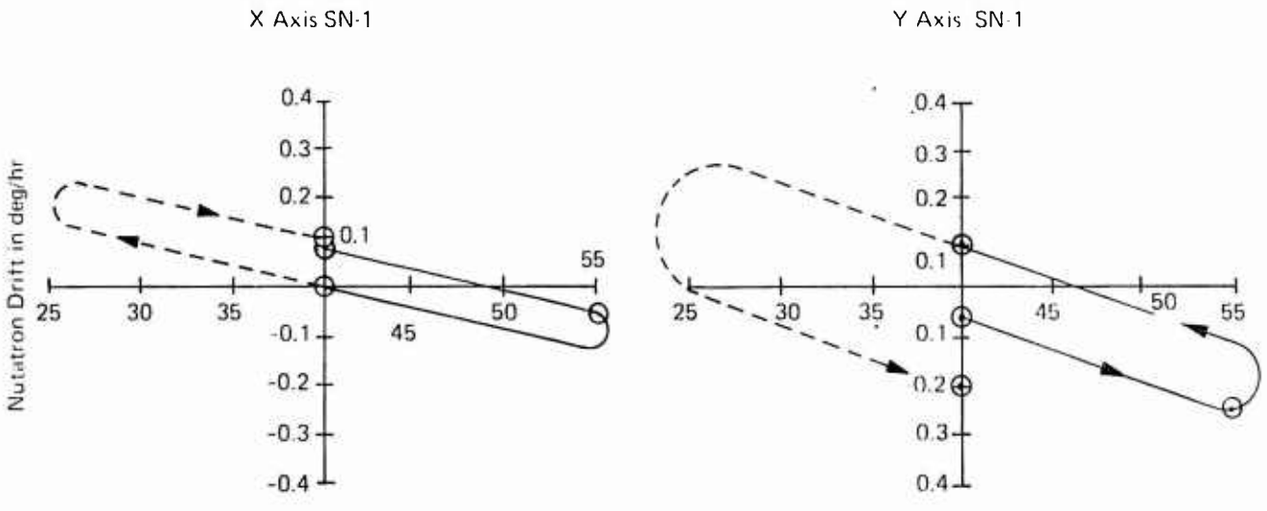

Figure 61. Hysteresis Curves Generated from Data of Table X (Spin Axis Polar)

These values are summarized in Table XI.

7. Test 7. Repeatability - Spin Axis Vertical.

a. Purpose

To obtain a measure of the repeatability of the Nutatron readouts from turn-on-to turn-on with the spin axis vertical. The test includes the repeatability of scale factor and acceleration insensitive drift in each axis. The Nutatron is not temperature controlled during these tests.

b. Test Method

The Nutatron is positioned with its spin axis vertical, y axis west, x axis north. It is turned on and monitored for 1.5 hours. The data from the last 1.0 hour of the run is sampled once each minute, and an average value obtained. Then the Nutatron and the Nutatron Test Electronics are shut down for 30 minutes. Then the test is repeated, and a new average value is obtained. The test is repeated four times and the results are tabulated.

c. Test Results

Table XII and Figure 62 summarize the results of these tests. The results show that the repeatability of SN-2 is better than that of SN-1 by a factor of more than 4.

8. Test 8. Repeatability - Spin Axis Polar.

a. Purpose

To obtain a measure of the turn-on to turn-on repeatability of the Nutatron when the spin axis is aligned with the earth's polar axis. The test includes repeatability of the acceleration insensitive drift and the acceleration sensitive drift of the Nutatron. The temperature of the Nutatron is not controlled during the test.

b. Test Method

The test method is identical to the vertical repeatability test except that the spin axis is aligned to the polar axis.

c. Test Results

Table XIII and Figure 63 summarize the results of these tests. As in the vertical repeatability tests, the results show that the repeatability of SN-2 is better than that of SN-1 by a factor of more than 4. Also, it is seen that within the accuracy of the measurements, the repeatability of both Nutatrons is independent of spin axis orientation.

9. Test 9. Magnetic Sensitivity Test.

a. Purpose

To measure changes in acceleration insensitive drift and scale factor of the Nutatron caused by application of magnetic fields both along and perpendicular to the spin axis.

TABLE XII. VERTICAL REPEATABILITY DATA

Nutatron SN	Run Number	X Axis		Y Axis	
		Deviation From Mean	Total Spread 4 Runs	Deviation From Mean	Total Spread 4 Runs
1	1	- 0.046 Deg/Hr	0.085 Deg/Hr (σ 0.0390)	+ 0.037 Deg/Hr	0.092 Deg/Hr (σ 0.0345)
	2	+ 0.037 Deg/Hr		- 0.002 Deg/Hr	
	3	+ 0.034 Deg/Hr		- 0.055 Deg/Hr	
	4	+ 0.038 Deg/Hr		- 0.018 Deg/Hr	
2	1	+ 0.003 Deg/Hr	0.012 Deg/Hr (σ 0.0045)	- 0.004 Deg/Hr	0.020 Deg/Hr (σ = 0.0074)
	2	- 0.007 Deg/Hr		- 0.009 Deg/Hr	
	3	- 0.000 Deg/Hr		+ 0.002 Deg/Hr	
	4	+ 0.005 Deg/Hr		+ 0.011 Deg/Hr	

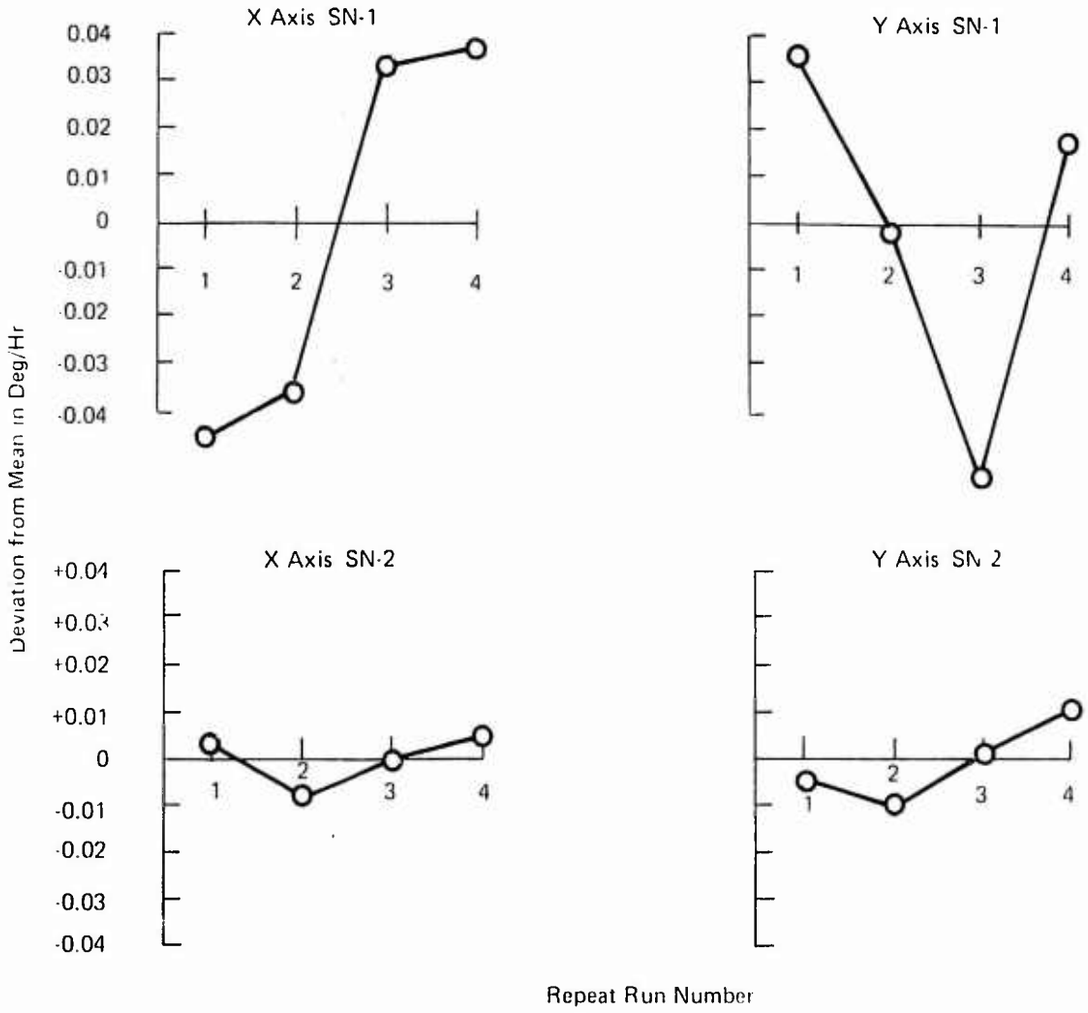

Figure 62. Vertical Repeatability Curves

TABLE XIII. POLAR REPEATABILITY DATA

Nutation SN	Run Number	X Axis		Y Axis	
		Deviation From Mean	Total Spread 4 Runs	Deviation From Mean	Total Spread 4 Runs
1	1	-0.034Deg/Hr		+0.055 Deg/Hr	
	2	-0.024 Deg/Hr	0.087 Deg/Hr	+0.052 Deg/Hr	0.117 Deg/Hr
	3	+0.003 Deg/Hr		-0.046 Deg/Hr	
	4	+0.053 Deg/hr	(σ = 0.0337)	0.062 Deg/Hr	(σ = 0.0540)
2	1	-0.014 Deg/Hr		+0.001 Deg/Hr	
	2	-0.004 Deg/Hr	0.025 Deg/Hr	+0.001 Deg/Hr	0.009 Deg/Hr
	3	+0.011 Deg/Hr		-0.006 Deg/Hr	
	4	+0.007 Deg/Hr	(σ = 0.0097)	+0.003 Deg/Hr	(σ = 0.0034)

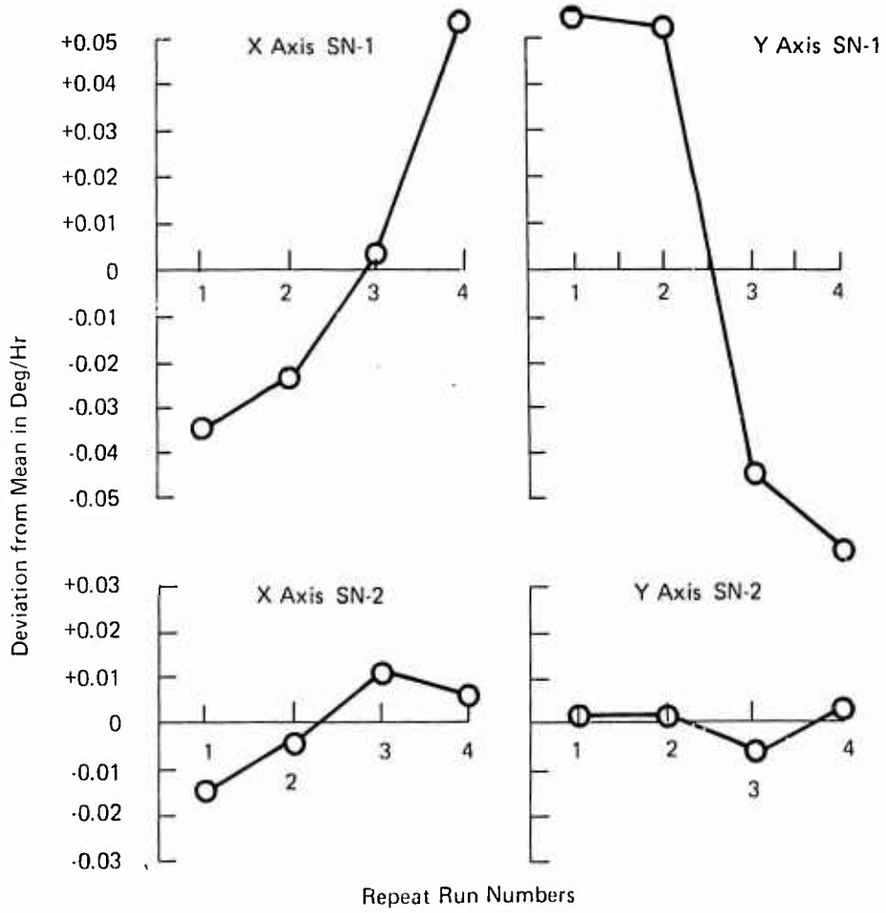

Figure 63. Polar Repeatability Curves

b. Test Method

The Nutatron is run with its spin axis vertical for two hours in each of two cardinal positions (Position 1 and Position 5). This provides a reference data set. Then a set of helmholz coils is mounted on the Nutatron Holding Fixture so that the magnetic field generated by the coils is along the spin axis. dc current is applied to the coils to produce a 15 gauss field measured at the Nutatron. The two-cardinal position test is repeated, each point being monitored for two hours.

After the above test is completed, the helmholz coils are repositioned so that the magnetic field is perpendicular to the spin axis. The test is then repeated, monitoring for two hours in each position with 15 gauss applied.

Values for acceleration insensitive drift and scale factor are calculated for each of the above operating conditions. The method used is identical to that in Test 3.

The tests were run both before and after installation of the external magnetic shield on the instruments.

c. Test Results

The results are summarized in Table XIV. These results show that before installation of the external magnetic shield, the primary sensitivity is a scale factor change resulting from an axial magnetic field. This effect disappears after the shield is installed.

TABLE XIV. RESULTS OF MAGNETIC SENSITIVITY TESTS

Applied Magnetic Field	Nutatron SN	External Magnetic Shield	x Axis Sensitivity		y Axis Sensitivity	
			Scale Factor %/Gauss	Drift Deg./Hr/Gauss	Scale Factor %/Gauss	Drift Deg./Hr/Gauss
15 Gauss Parallel to Spin Axis	1	Off	0.18	0.006	0.18	< 0.003
	1	On	< 0.015	< 0.003	< 0.015	< 0.003
	2	Off	0.12	< 0.003	0.12	0.005
	2	On	< 0.015	< 0.003	< 0.015	< 0.003
15 Gauss Perpendicular to Spin Axis	1	Off	< 0.015	< 0.003	< 0.015	< 0.003
	1	On	< 0.015	< 0.003	< 0.015	< 0.003
	2	Off	0.051	0.006	0.051	0.006
	2	On	< 0.015	< 0.003	< 0.015	< 0.003

10. Test 10. Fast Reaction Test - Spin Axis Vertical.

a. Purpose

To demonstrate the fast reaction capability of the Nutatron.

b. Test Method

The Nutatron is positioned with its spin axis vertical, y input axis east. The turn-on sequence sets the heading and latitude initial conditions to better than one degree, and closes the Nutatron loops only after the power supply transients have settled out. The Nutatron sensitive axes and the internal temperature are monitored and recorded. The test is repeated a number of times to demonstrate the typical reaction time and repeatability.

c. Test Results

Three consecutive repeat runs are shown in Figure 64. The internal temperature rise is shown on top and requires the better part of an hour to rise approximately 14°C. The drift settles out within a matter of four minutes and repeats to better than 0.05 deg/hr.

11. Test 11. Repeatability After Exposure to Temperature Cycles (0°F to 150°F)

a. Purpose

To measure the repeatability of the acceleration insensitive drift, scale factor, and acceleration sensitive drift of the Nutatron after it is exposed to repeated temperature cycles between 0°F and 150°F.

b. Test Method

Prior to final testing, preliminary values for the above parameters are measured. The Nutatron is then removed from the test stand and placed in a temperature chamber. The temperature is cycled between 0°F and 150°F (three hours at each temperature) for eighteen hours. The Nutatron is then placed on the test stand, and the parameters are measured once again.

c. Test Results

No change was observed in the scale factor or acceleration insensitive drift for either Nutatron ($\leq$0.05 deg/hr). The acceleration sensitive drift changed 0.17 deg/hr for SN-2, and 0.15 deg/hr for SN-1.

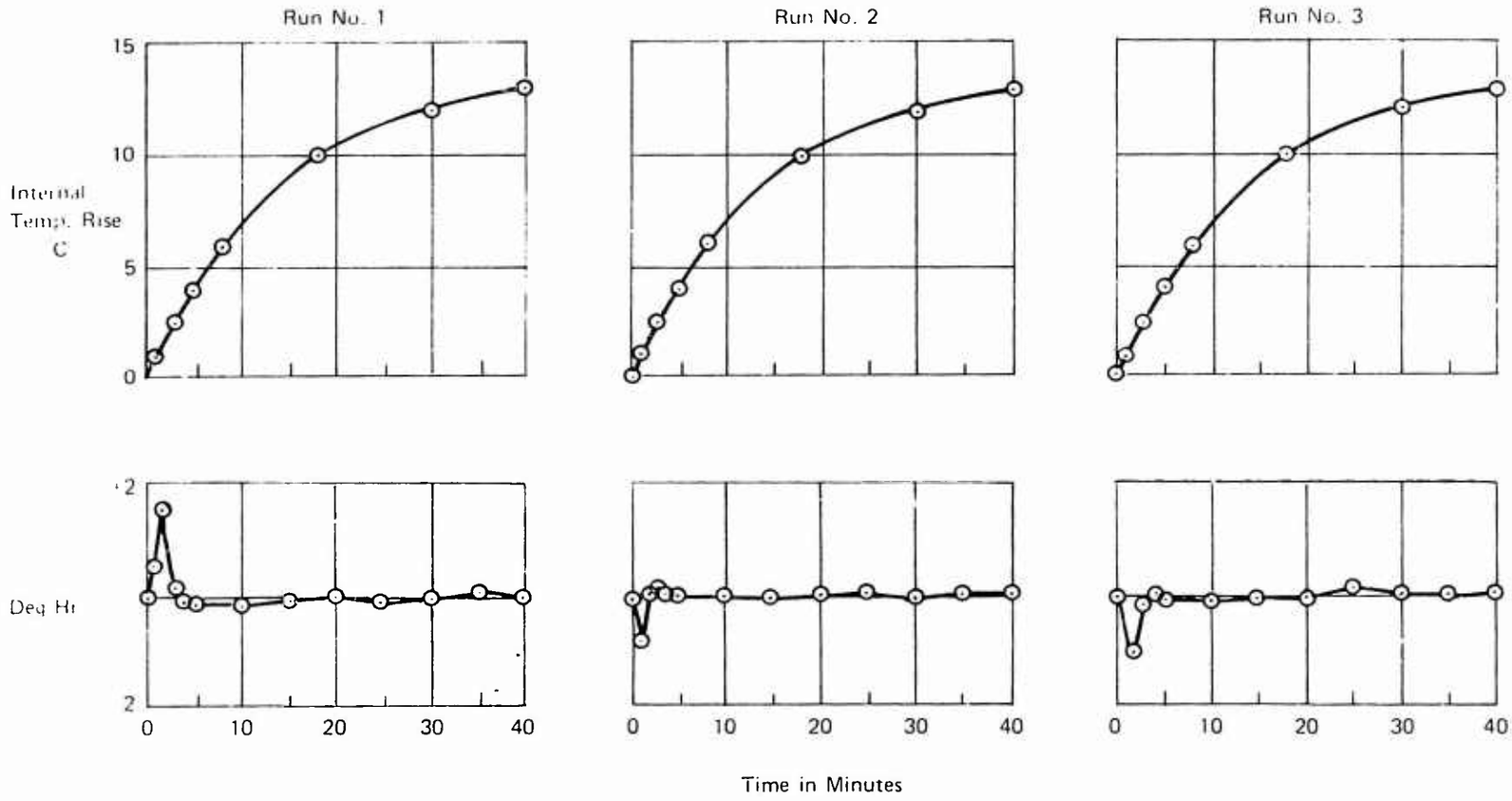

Figure 64. Nutatron Fast Reaction Repeat Cycles (No Temperature Control), SN-2

VI. DISCUSSION OF RESULTS

How can the Nutatron performance be further improved? What are the ultimate performance levels that one can expect to attain with the Nutatron principle? Answers to these questions can only be obtained by an understanding of the error mechanisms and the analysis of potential methods to improve them. It is the realistic assessment of the degree of difficulty or limitation in the potential cures that are indicators of the growth potential of the Nutatron. The development of a new concept is a sequential effort, depending on the reduction or elimination of the larger error sources before the next better performance level can be tackled.

The performance parameters of the Nutatron are discussed in this section to convey some answers to the growth potential of the Nutatron and also to indicate the direction in which further improvement efforts should be directed. As can be seen from the summary of performance parameters of Nutatrons SN-1 and SN-2 (Table I) some are almost identical from unit to unit and others are quite different

Good consistency between the two instruments exists for randomness, long-term stability, temperature coefficients, and magnetic sensitivities. Acceleration, and acceleration square sensitive drift and repeatability from cold start were different, all being significantly better on SN-2. The difference in the latter three parameters can be traced to the difference in the outer race curvature used on the spin bearings, 2.0 and 0.8 respectively.

While a sample of two is far too small to draw firm conclusions, it appears that one of the major goals of the Nutatron principle, namely consistent performance from unit to unit, will be achieved.

The discussion is organized to group together performance parameters which have common error sources as follows:

		Table I Lines
A.	Acceleration Insensitive Drift - Systematic Terms	1 a, b, d, e
B.	Acceleration Insensitive Drift - Randomness	1 c
C.	Acceleration Sensitive Drift - Systematic Term	2 a, c, d & 3
D.	Acceleration Squared Sensitive Drift - Systematic Term	4
E.	Magnetic Sensitivity	1 g, h
F.	Scale Factor Temperature Coefficient	1 f

A. ACCELERATION INSENSITIVE DRIFT - SYSTEMATIC TERMS

The acceleration insensitive drift is the bias drift with the spin axis vertical. It is characterized by mean value, its repeatability from a cold start, stability with time, temperature coefficient and the effect of storage exposure to temperature cycles.

1. Mean Value [Test No. 1 - Table V]

The mean value of the acceleration insensitive drift is in the order of a few tenths of a deg/hr or less for both Nutatrons. Some of this can be attributed to offsets in the readout

demodulators, and some to a small amount of modulation of the case rotation frequency at its 1st harmonic in combination with spin bearing noise at 2ν. Because of its inherent low value and stability it can easily be compensated electronically or in the computer. No specific modifications are recommended to further reduce the mean value, but this would occur as a byproduct of effort to improve the standing level of 2ν bearing noise.

2. Stability (Trend) [Test No. 2 - Table VI - Figures 54 and 55]

The stability with time of the acceleration insensitive drift has been determined by 16 hour runs. (Figures 54 and 55.) The values of 0.0022 deg/hr^2 and 0.0014 deg/hr^2 for SN-2 and 0.0026 deg/hr^2 and 0.0031 deg/hr^2 for SN-1 are pessimistic because the drift randomness masks the stability over a 16 hour period. A 36-hour stability run showed a trend of under 0.0005 deg/hr^2. The high degree of long term stability has been consistently observed during the development phase and highlights the need to improve shorter term randomness. A very long stability run, in the order of many hundreds of hours should be conducted to establish the extent of long term stability. No specific modifications are recommended to improve long term stability (trend) but a reduction in randomness discussed in VI.B will permit a more rapid separation of trend and low frequency randomness.

3. Temperature Coefficient [Test No. 3 - Table VII]

The temperature coefficients over 27°F temperature range have been measured to be between 0.001 and 0.003 deg/hr/°F. This residual temperature coefficient is suspected to be caused by the 2ν spin bearing noise temperature coefficient in combination with case rotation modulation at its first harmonic. The thermal coefficient tests are limited to 27°F to avoid any possibility of destroying the only two prototype Nutatrons prior to their evaluation by the Air Force. While there is no evidence of a nonlinearity in the drift temperature coefficients, wider temperature range tests are recommended in the future to confirm this. An investigation of the raw 2ν bearing noise temperature coefficient is also recommended. Case rotation has been implemented to eliminate this noise source. Levels of 2ν bearing noise between 2 and 50 deg/hr have been measured on various bearings. This wide spread indicates that some specific bearing parameters are the mechanism for it; but because of more pressing development problems and the effectiveness of case rotation, little has been done to explore it. The impact on inner and outer race run outs, outer race curvature, contact angle, preload, etc. on 2ν bearing noise would be the important step in establishing the feasibility of eliminating case rotation and hence a cost reduction in the Nutatron.

4. Repeatability from Cold Start and Fast Reaction

Each Nutatron received four consecutive turn on cycles from a cold start with sufficient time between tests to permit the instrument to return close to room temperatures. Nutatron SN-2 demonstrated better repeatability, a 1 sigma deviation of 0.0045 deg/hr about one and 0.0074 deg/hr about the other axis, than one would expect from its random drift characteristic. One can assume that an improvement in the randomness would indeed lead to extremely good and fast gyrocompassing capability (better than 1 minute of arc). Nutatron SN-1's repeatability is not as good, with 1 sigma repeatability of 0.039 deg/hr and 0.035 deg/hr about the two axes. The suspicion falls on the larger outer race curve spin bearings (ratio of 2.0) than used on SN-2 (ratio of 0.8). A sample of one instrument in each configuration is insufficient to draw conclusions and no analysis has been carried out on the effect of outer race curvature effect on repeatability. It is recommended that an analysis and test effort for optimum tradeoff of outer race curvature between g sensitive drift, g^2 sensitive drift and repeatability be conducted.

The fast reaction is basically limited by the averaging time required to filter drift randomness. The initial drift transient, after turn-on settles out within a few minutes (Figure 64). To achieve fast and high accuracy gyrocompassing capability, efforts to tackle the drift randomness discussed in Section IV.B is recommended.

B. RANDOM DRIFT

Figure 53 illustrates an actual Nutatron drift recorded through a one minute time constant filter. Even a cursory look reveals a predominant periodic function at about 0.3 rpm with an rms amplitude of about 0.10 deg/hr.

A fifteen hour drift run based on 25 minute averages is illustrated on Figures 54 and 55. With the periodic component removed by time averaging, the 1 sigma randomness is in the order of 0.02 deg/hr to 0.03 deg/hr. It has been determined to be white in character by computer analysis and to have a power spectral density of 5×10^{-5} (deg/hr)^2 per rad/hr to 1.1×10^{-4} (deg/hr)^2 per rad/hr.

Both of these phenomena have been traced to the rotor spin bearings and are discussed below.

1. Periodic Drift Component

A periodic drift component has been observed on all Nutatron buildups with a variety of spin bearings. The one sigma amplitude of this periodic function had narrow spread of between 0.1 and 0.25 deg/hr and the frequency in general ranged between 0.5 to 0.1 rpm. As a result of investigative tests the following characteristics of the periodic drift were uncovered:

(a) The drift periodicity of about 0.01 Hz exists with the housing rotation disabled. (Periodic 2ν noise level change at 0.01 Hz.) Its frequency is directly proportional to the spin speed.

(b) Using an asynchronous reference for the Nutatron signal detection demodulators, rather than 2ν, revealed many noise peaks at discrete frequencies between 18 and 20 Hz.

(c) The periodic drift pattern repeats approximately for every 0.5 rpm increment in housing rotation speed. Figure 65 is the plot of the period of the longer of the two beat periods as the housing frequency is varied from 0.5 rpm to 1.5 rpm. Periods exceeding 1/2 hour can be observed at approximately 0.87 and 1.37 rpm.

(d) The drift periodicity is slightly changed by the axial preload of the bearing. It is also modified by the axial g loading.

From the investigative tests it is possible to construct a mathematical model of the disturbing nutatron torques which could cause the periodic drift and which fits the observed data well.

A short 2ν noise pulse occurring approximately every 300 revolutions of the spin bearing (0.5 rpm), superimposed on the standing level of 2ν bearing noise could explain the periodicity. The observed instability of the ball bearing retainer, the measured 2ν noise about the spin axis, and the increased Nutatron rotor torque at a frequency of about 0.5 rpm confirm this possibility.

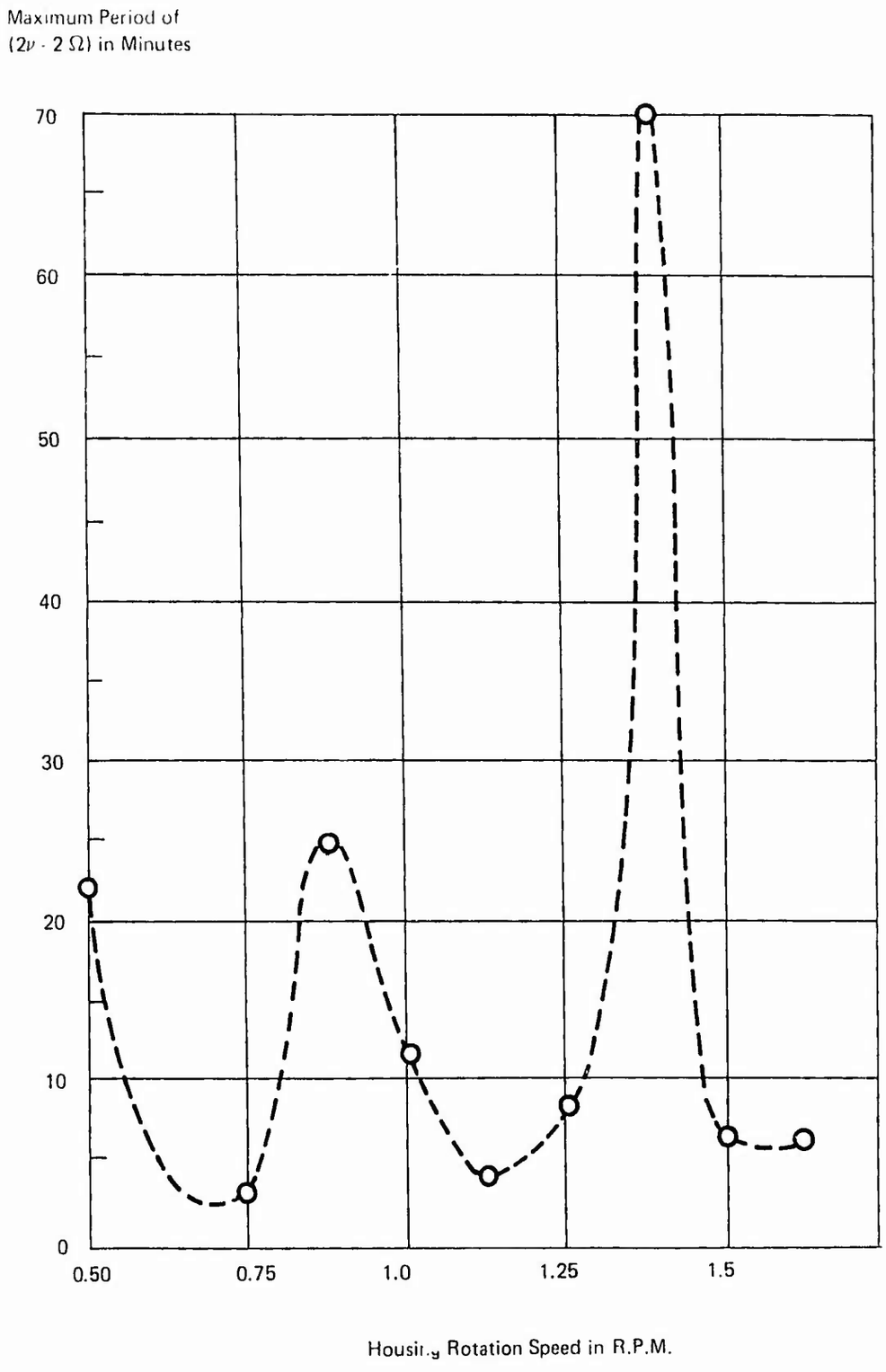

Figure 65. Period of $2\nu - 2\Omega$ versus Housing Rotation Speed (Experimental Data)

The 2ν bearing noise of the rotor may therefore have the approximate form as given in Figure 66.

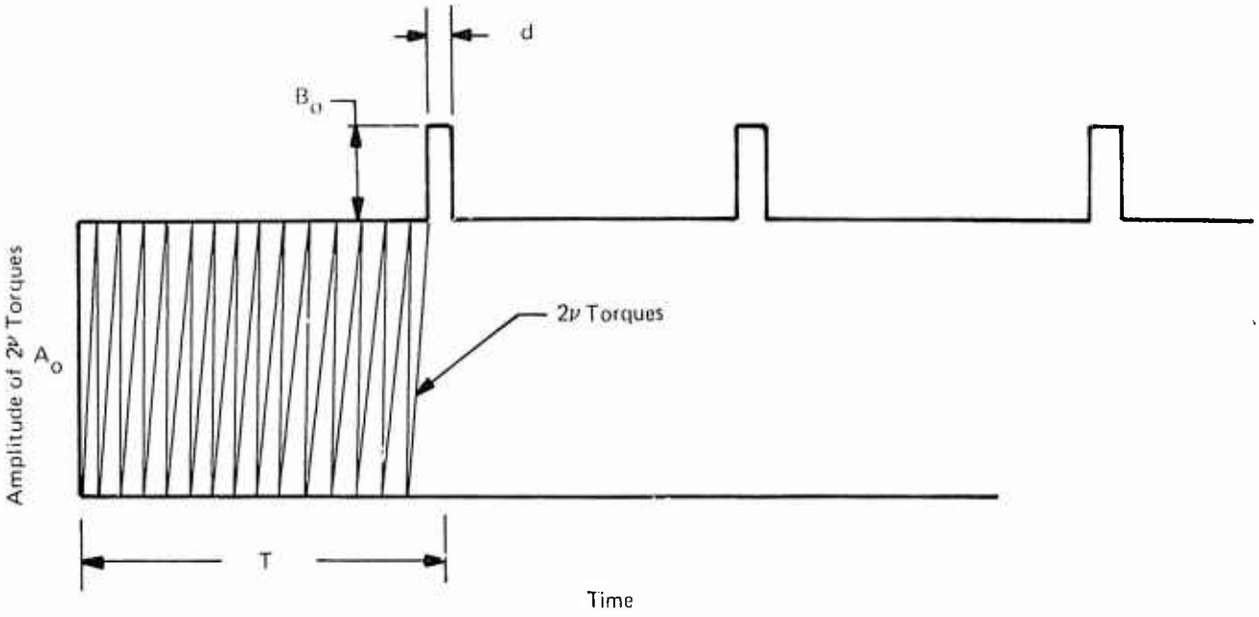

Figure 66. Bearing Torques as a Function of Time

This form of 2ν torque can be expressed as follows:

$$T'_{2\nu B} = A_O \sin(2\nu t + \phi_1) + B_O \sin(2\nu t + \phi_2) \sum_{o}^{n} \frac{\sin n\pi \frac{d}{T}}{n\pi \frac{d}{T}} \sin n \frac{1}{T} t$$

where

$T'_{2\nu B}$	is the 2ν bearing noise in case rotation reference system
A_O	is the standing level of 2ν bearing noise
B_O	is the amplitude of the periodic 2ν bearing noise pulse
ν	is the rotor frequency
n	is the harmonic
d	is the width of the pulse in seconds
ϕ_1, ϕ_2	are phase angles

T is the period between pulses in seconds

T has been observed to be about 30 seconds

d has not been accurately measured but appears to be in the order of a few tenths of a second from retainer instability observations.

For the first ten harmonics, the coefficient $\frac{\sin n\pi \frac{d}{T}}{n\pi \frac{d}{T}}$ is essentially unity with a ratio of 0.01 for $\frac{d}{T}$. Torques at or near the Nutatron frequency cause coning motion as discussed in Appendix (I) equation (I-7). The bearing noise torque in the rotating system is therefore expressed.

$$T'_{2\nu Bx} = A_o \cos(2\nu t + \phi_1) + B_o \cos(2\nu t + \phi_2) \sum_{o}^{n} \sin n \frac{1}{T} t$$

$$T'_{2\nu By} = A_o \sin(2\nu t + \phi_1) + B_o \sin(2\nu t + \phi_2) \sum_{o}^{n} \sin n \frac{1}{T} t$$

where $T'_{2\nu Bx}$, $T'_{2\nu By}$ are the bearing noise torques at 2ν in the case rotation system and all other terms have been previously defined.

Resolving these noise torques into the fixed system with the standard matrix,

$$\begin{bmatrix} T_{2\nu Bx} \\ T_{2\nu By} \end{bmatrix} = \begin{bmatrix} \cos \Omega t & - & \sin \Omega t \\ \sin \Omega t & + & \cos \Omega t \end{bmatrix} \begin{bmatrix} T'_{2\nu Bx} \\ T'_{2\nu By} \end{bmatrix},$$

where $T_{2\nu Bx}$, $T_{2\nu By}$ are the bearing noise torques at 2ν in fixed system,

Ω is the case rotation matrix, the noise as it affects Nutatron operation is obtained. The standing level bearing noise component represented by the amplitude A_o is modulated at Ω and becomes

$$T_{2\nu Bx1} = A_o \cos(2\nu t + \Omega t + \phi_1)$$

$$T_{2\nu By1} = A_o \sin(2\nu t + \Omega t + \phi_1)$$

Since the Nutatron precession signal occurs at a frequency of $2\nu + 2\Omega$, the standing level of 2ν bearing noise is separated in the frequency domain by Ω and can be effectively eliminated by filtering.

The pulsed 2ν noise (B_o) resolved into the fixed system

$$T_{2\nu Bx2} = \frac{B_0}{2} \sum_{0}^{n} \sin\left(2\nu + \Omega + n\frac{1}{T} + \phi_2\right)t + \sin\left(2\nu + \Omega - n\frac{1}{T} + \phi_2\right)t$$

$$T_{2\nu By2} = \frac{B}{2} \sum_{0}^{n} \cos\left(2\nu + \Omega + n\frac{1}{T} + \phi_2\right)t + \cos\left(2\nu + \Omega - n\frac{1}{T} + \phi_2\right)t \ ,$$

where all terms have been defined previously.

1/T is in the order of 0.5 rpm and its harmonics are 1, 1.5, 2, 2.5, . . . rpm. Any housing rotation frequency from 0-10 rpm will generate at least two low frequency beats against two harmonics of the series. The highest possible frequency beat results from adjusting the case rotation equally distant between two harmonics, and this still has a relatively low frequency of 0.25 rpm.

It appears that the beat phenomena can be eliminated by shifting the fundamental frequency (1/T) above the case rotation frequency. One obvious and simple approach would be to increase the rotor frequency and decrease the case rotation frequency. Bearing geometry changes may also accomplish this. It is recommended that techniques be investigated and implemented to eliminate this undesirable low frequency periodicity which prevents quick gyrocompassing.

2. White Noise

The true random noise of Nutatrons assembled with various bearing configurations has varied by a factor of about 3, with one sigma values between 0.01 to 0.03 deg/hr. The white noise randomness has not been of high priority concern during the development effort because of the urgent need to eliminate larger error sources.

The ball bearings used with the Nutatron have been of commercial quality and did not feature the latest techniques developed by MIT and the Air Force for ultra smooth surface finishes of the races and balls. An effort was made in that direction. A set of bearings incorporating the latest techniques of glow discharge cleaning, ball lapping and surface phosphate treatment were prepared by the DELCO laboratory. When they were available the decision had been made to change to larger outer race curvature bearings and these bearings with a curvature of 0.55 were not installed. However, torque tests conducted on the Delco treated bearings indicated a substantial noise improvement.

It is recommended that bearings used in future Nutatrons be properly treated with these latest techniques. A 1 sigma randomness of under 0.005 deg/hr should be achievable.

C. G-SENSITIVE NUTATRON NOISE

G-sensitive Nutatron noise was uncovered early in the development program and two of the basic error mechanisms identified. The bearings represent a stiff spring along the two radial bearing axes. If these spring constants are not quite equal, a radial motion at the Nutatron frequency (2ν) develops in response to a radial load. This is illustrated by Figure 67.

A bearing is a rather complex mechanical structure and the radial stiffness is a function of many bearing parameters, including preload, ball compliment, outer race curvature, contact angle, etc. A computer program has been developed from bearing literature* to solve for the behavior of bearings particularly at the Nutatron frequency 2ν.

*Rolling Bearing Analysis, Tedrick Harris, 1966.

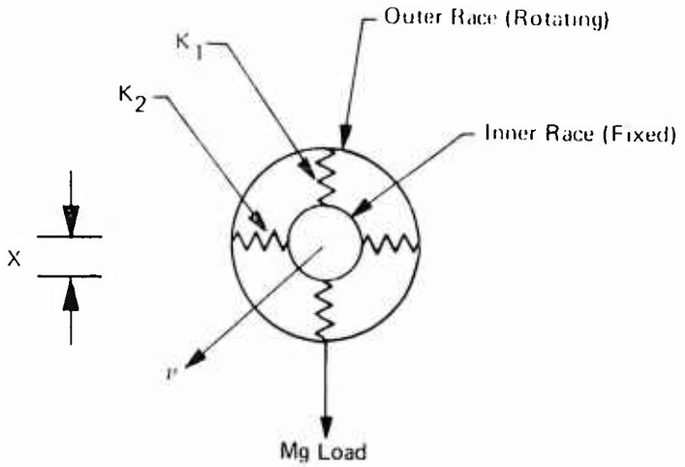

K_1, K_2 two radial bearing stiffness

$K_1 = K_B + \Delta K$

$K_2 = K_B - \Delta K$

$X = \frac{Mg}{K_B} (1 + 2\Delta K \sin 2Pt)$

K_1 and K_2 are the radial stiffnesses

M is mass of rotor

g is gravity vector

K_B is average radial bearing stiffness

ΔK is the difference between the orthogonal radial stiffnesses

X is the radial deflection

Figure 67. Deflection of the Nutatron Rotor as a Function of Unequal Radial Stiffnesses

The parameters of four bearings which have been tested with the Nutatron are listed in Table XV. The average displacement as a function of radial load for these bearings is illustrated in Figure 68. The displacement is small, in the order of a few micro-inches, and is of no consequence to Nutatron performance.

Of vital importance are the factors which make the orthogonal radial stiffnesses somewhat unequal. Two mechsnisms have been found, elliptic run-out of the outer race and tilt of the outer race about a radial axis.

TABLE XV. BEARING PARAMETERS

Vendor	New Hampshire	Fafnir	Fafnir	Barden
Pitch Dia.	0.3750	0.4375	0.4375	0.3750
Free Contact Angle	15°	5°	10°	15°
No.of Balls	8	7	7	11
Ball Dia.	0.0781	0.125	0.125	0.0675
Inner Race Curvature	0.555	0.570	0.570	0.550
Outer Race Curvature	0.555	2.0	2.0	2.0
Retainer Speed Ratio	0.6006	0.6423	0.6406	0.5804
Load Deflection Coefficient	3.038×10^6	2.723×10^6	2.723×10^6	2.019×10^6

1. Elliptic Run-out of Outer Race

The displacement and equivalent Nutatron noise at twice rotor frequency 2ν as a function of elliptic run-out was computed and the results are shown for bearing configuration in Figure 69. Since even moderately precise bearings have an outer race elliptic run-out of under 3 micro-inches this is only a minor contributor to the g-sensitive drift.

2. Tilted Installation of Nutatron Bearings

The sensitivity to angular tilt about a radial axis manifested itself some time ago in the Nutatron program. Shimming of the New Hampshire bearing was found to be critical and posed just the kind of adjustment which we were trying to eliminate with the Nutatron approach. Using the previously mentioned computer program, the sensitivity was found to be proportional to the square of the tilt angle with a sensitivity of about 1.3 deg/hr per milliradian^2. To confirm this a fixture which permitted controlled changes of bearing tilt was designed and attached to the end cap of the Nutatron rotor. Curve A, Figure 70, shows the result of the controlled tilt test and indicates an even higher sensitivity than the theoretical data.

By changing various bearing parameters in the computer analysis the outer race curvature was found to have the major effect on the tilt sensitivity.

Figure 71 plots the theoretical tilt sensitivity for curvature ratios from 0.55 (normal) to 3.6 (almost self-aligning). In order to confirm the tilt sensitivity on outer race curvature and to possibly use it to compensate for residual g-sensitive noise, bearings with outer race curvature of 2.0

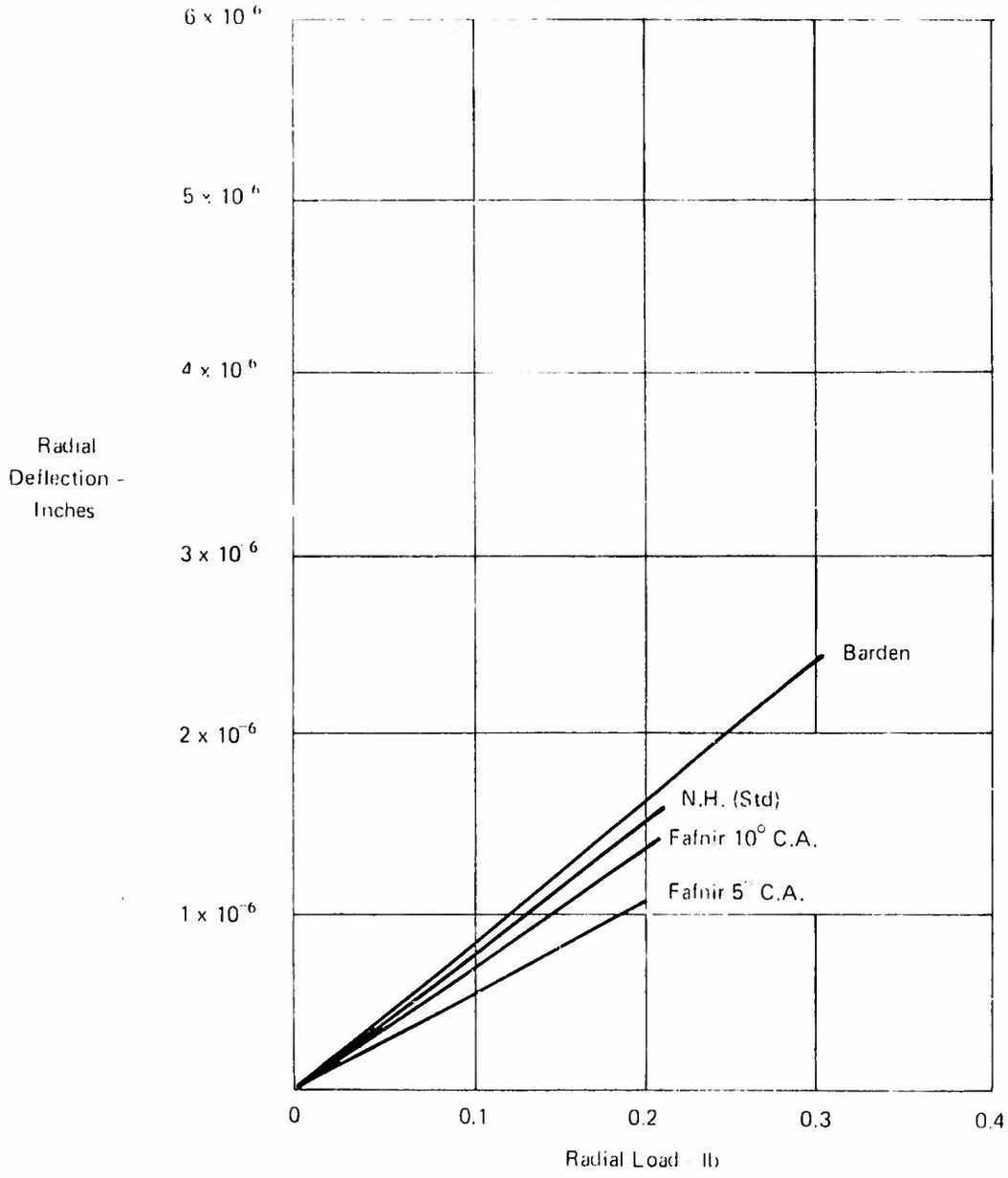

Figure 68. Radial Displacement versus Radial Load

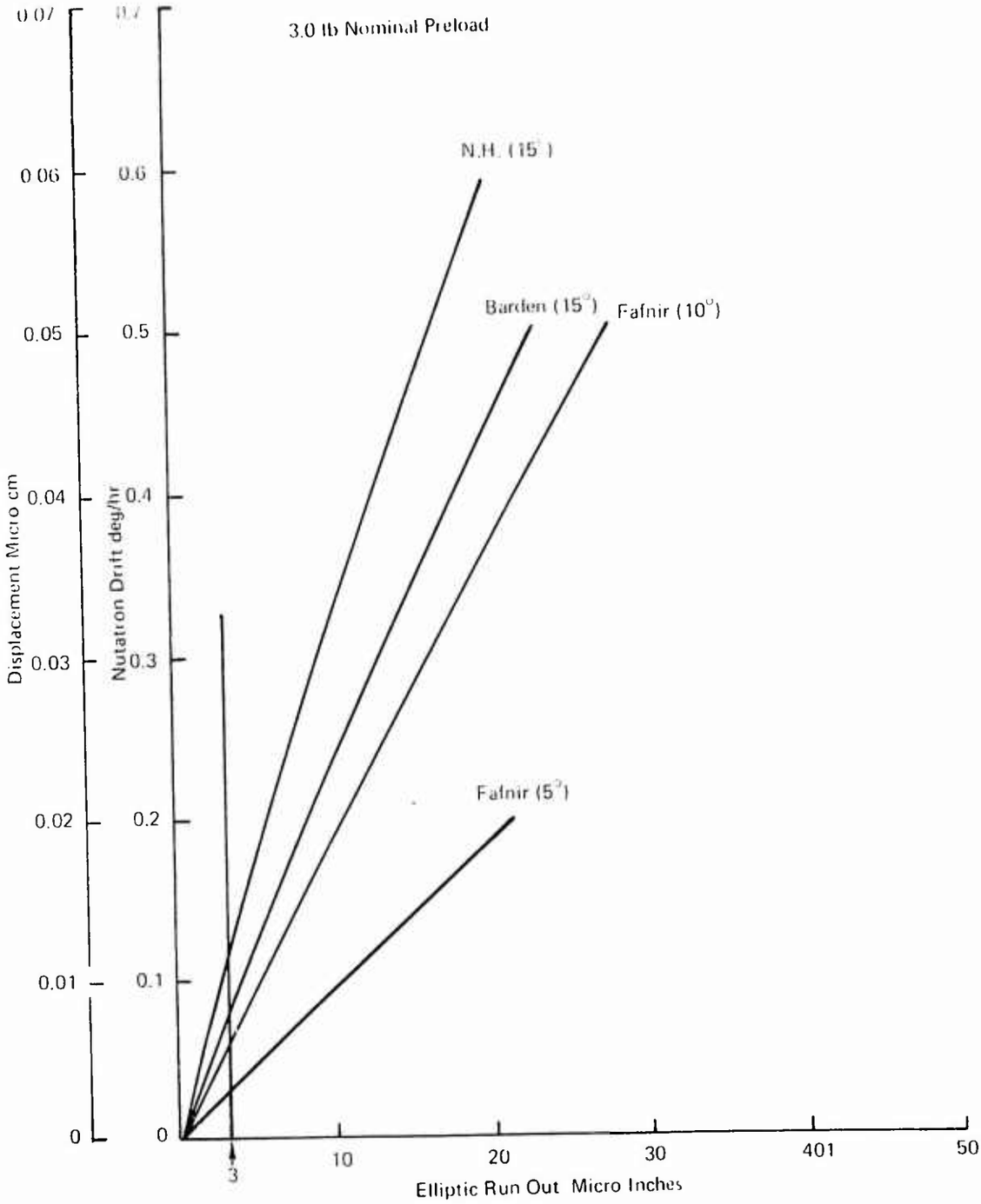

Figure 69. G-Sensitive Motion versus Ellipticity Error

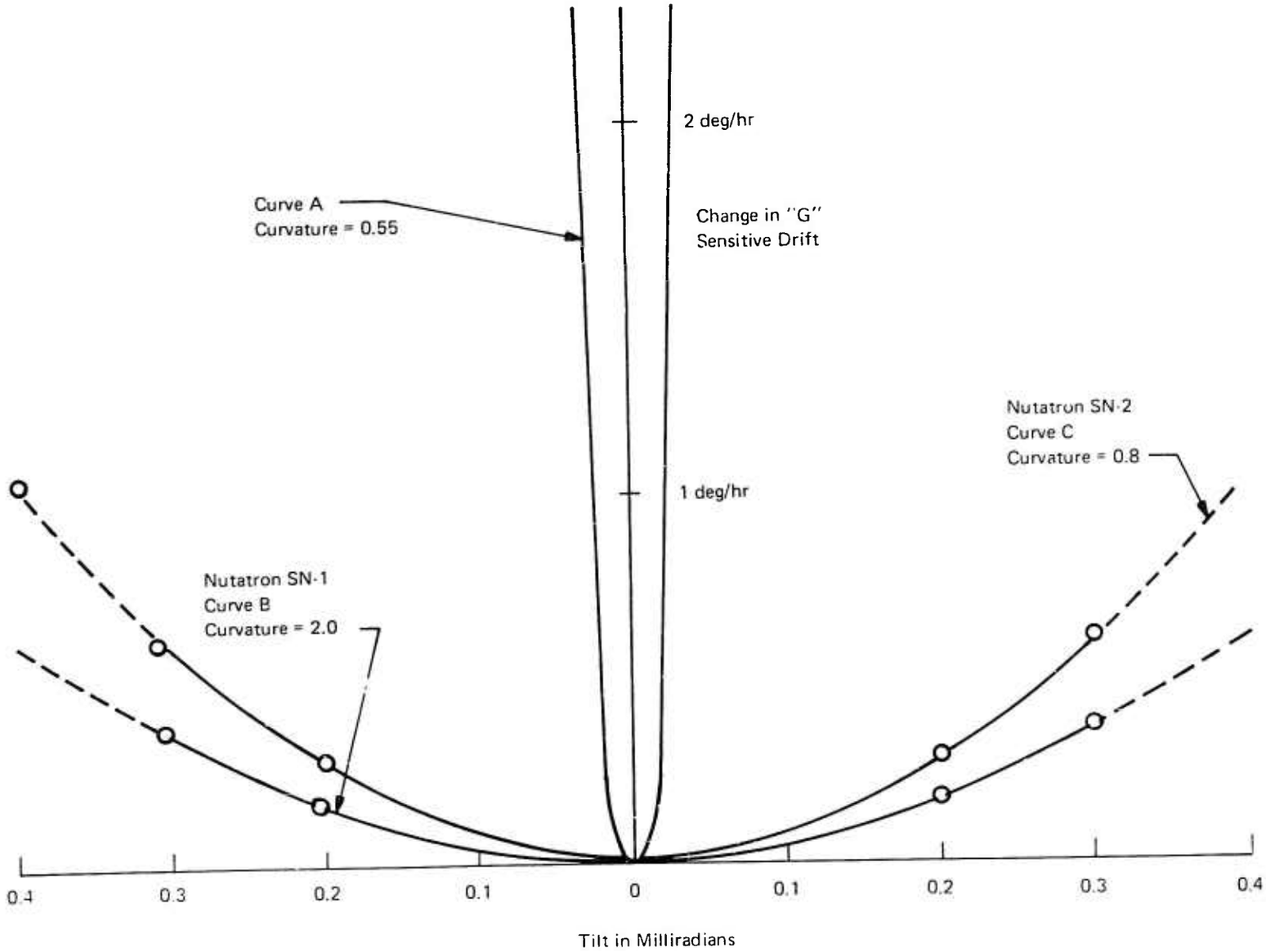

Figure 70. Comparison of Tilt Sensitivity for Various Curvatures

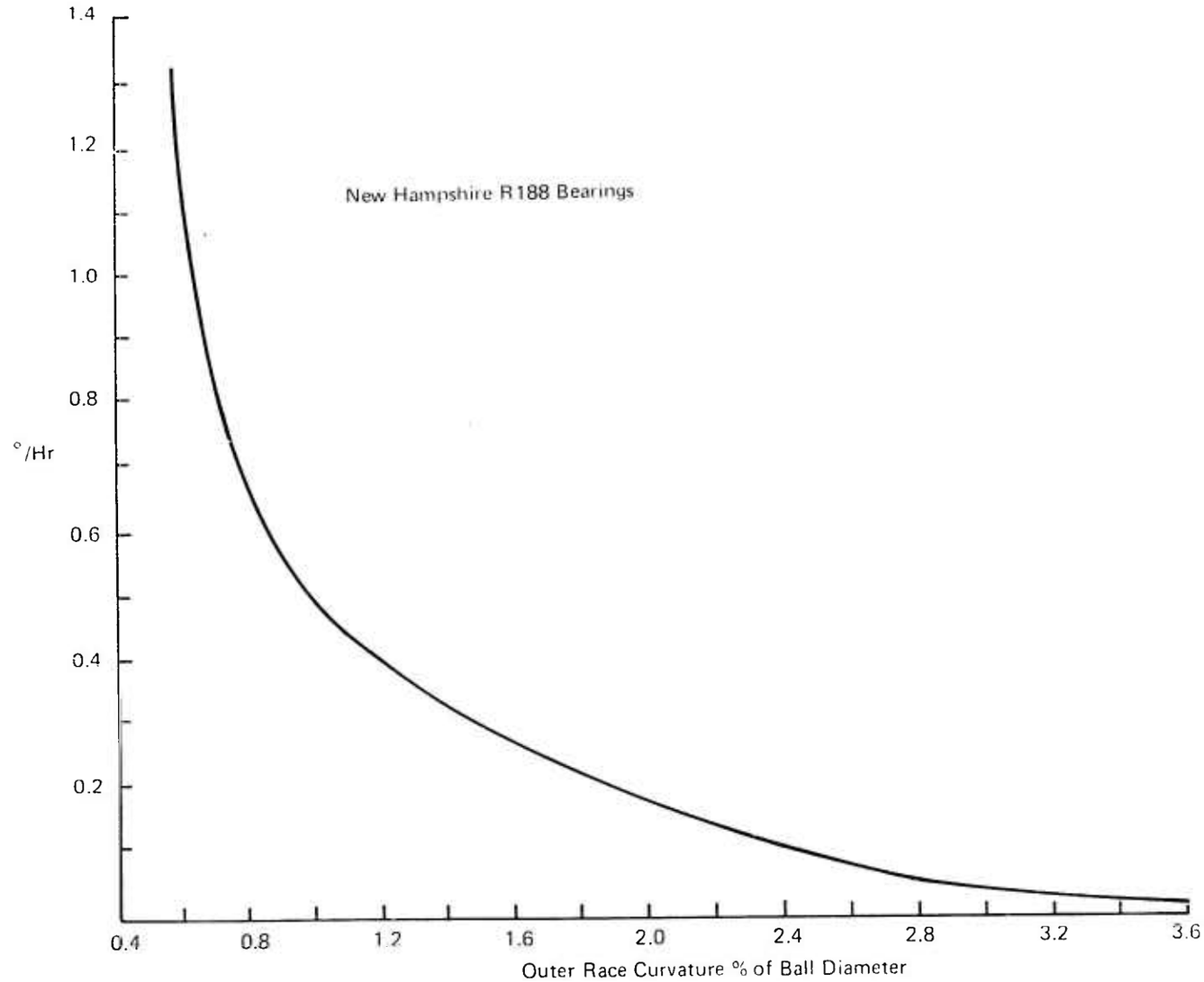

Figure 71. G-Sensitive Drift per One Millirad Squared Tilt

were installed in Nutatron SN-1, and bearings with curvature of 0.8 were installed in Nutatron SN-2. Investigative tests were run with each of these units to experimentally determine the effects of axial preload and outer race tilt on g-sensitive noise.

The bearings are preloaded with a washer type shim placed between the outer race and a shim retainer on the rotor end cap. The thickness of this shim establishes the average axial preload. The bearing outer race can be tilted by slightly wedge shaped shims. Shims with wedge angles from 0.1 to 0.3 milliradian were installed, and the resultant changes in g-sensitive noise were measured. Curves B and C, Figure 70, show the results of these tests. The curves confirm that the sensitivity is proprtional to the square of the tilt angle and is dependent on the outer race curvature. The experimental sensitivity is higher than the theoretical data, which may be due to a somewhat less compliant rotor structure than assumed in the calculations.

Tilt angles greater than 0.3 milliradian were not attainable because of lack of clearance between the bearing O.D. and the bearing bore in the rotor end cap. As a result, it was not possible to use controlled outer race tilt to completely compensate for g-sensitive noise from other sources.

The axial preloads were varied from 2.5 to 4.0 pounds with no observable change in the g-sensitive noise. However, with the lower initial preload, the bearings became unloaded when the operating temperature was increased 20°C. This caused a shift in the g-sensitive noise of up to 1.0 deg/hr/g, which remained after the temperature was lowered to the normal operating level. With the higher initial preloads this shift (hysteresis) was significantly lower (see test Data Section V, Table XI).

D. MAGNETIC SENSITIVITY (TEST NO. 9 - TABLE XIV)

The Nutatron drift and torquing scale factor magnetic sensitivities were measured with and without a magnetic shield. The results for Nutatron SN-1 and SN-2 were similar, with very low sensitivities as recorded on Table 12.

1. Magnetic Drift Sensitivity

Considerable care had been exercised to eliminating magnetic materials from the rotating element of the Nutatron which might cause 2ν torques from being generated when spinning in a magnetic field. The degree of success achieved is demonstrated by the low magnetic sensitivities, 0.006 deg/hr and under 0.003 deg/hr per gauss with and without a magnetic shield respectively. The magnetic sensitivity with the magnetic shield was within the drift randomness and larger magnetic field tests will be required to determine its existence. No modifications are required to improve this characteristic.

2. Torquing Scale Factor Magnetic Sensitivity

The Nutatron is torqued at the Nutatron frequency by the interaction of flux generated by current through the torquing coil and a constant reluctance dc magnetic field produced by a permanent magnet. External magnetic fields parallel to that produced by the permanent torquing magnet (parallel to spin axis) either strengthen or weaken the torquer flux density and hence the torquing scale factor by about 0.15% per gauss. This is reduced by more than an order of magnitude with magnetic shielding to an insignificant level. Radial magnetic fields have a much lower effect.

In the original configuration (Figure 9) with torquing magnets symmetrically mounted on either end of the Nutatron, the scale factor magnetic sensitivity would have been lower because of common mode rejection. As one magnetic torquing field is strengthened the other is weakened. The effectiveness of magnetic shielding however does make single-ended operation possible with the attendant simplification and increased M factor.

E. SCALE FACTOR TEMPERATURE SENSITIVITY (TEST NO. 3, TABLE VII)

The scale factor temperature sensitivity is almost identical for both instruments and in the order of 0.18% per °C. It is entirely attributable to the temperature coefficient of the Alnico V permanent torquing magnet. For platform operation where the command precession rate will be limited to 20 deg/hr, temperature compensation using the Nutatron thermistors will be more than adequate.

For the large torquing rates associated with strap down operation, better stability of the torquing scale factor is required. The following options are possible to achieve this.

(1) Explore the possibility of lower temperature coefficient permanent magnet materials. The rare earth magnet materials hold promise in that direction.

(2) Resort to a combination of temperature compensation and a crude (±5°C) temperature control.

(3) Substitute permanent magnets with electromagnets driven from a well controlled current source. The Brig II gyros effectively used this technique, but it required a precision current supply.

F. VIBRATION SENSITIVITY

No vibration tests were conducted nor was the rotor statically balanced to minimize drift induced by vibration at or near the Nutatron frequency. A short analysis is presented here to indicate what can be expected with reasonable mass balance requirements and vibration environments.

The relation of the performance of an undamped inertial navigation system to random drift noise as expressed by its white noise drift power spectral density can be approximated

$$\sigma_p^{\,2} = 9.2 \times 10^{12} P_\omega \left[\frac{1}{3} t^3 - \frac{1}{2\omega_e^{\,2}} \left(t - \frac{\sin 2\omega_e t}{2\omega_e} \right) \right]$$

where

σ_p is the rms error in ft

P_ω is the drift power spectral density $(\text{deg/hr})^2$ per rad/hr

t is time in hours

ω_e is the Shuler frequency (approximately 4.2 rad/hr)

This equation can be reduced for periods over one hour to

$$\sigma_p^2 = 3.07 \times 10^{12} P_\omega t^3 \quad \text{and}$$

$$\sigma_p = 1.75 \times 10^6 \sqrt{P_\omega}\ t^{3/2}$$

For a navigation error of 4 nautical miles after 4 hours of flight the permissible white power spectral density is approximately 3×10^{-6} $(\text{deg/hr})^2$ per rad/hour.

The relationship between torques at the Nutatron frequency and drift is derived in Appendix I and is

$$\omega = \frac{T_{2\nu}}{\nu (A - B)} 2 \times 10^5$$

where

ω is the resultant drift in deg/hr

$T_{2\nu}$ is the torque at or near the Nutatron frequency in dyne-cm

ν is the rotor speed

A, B are the radial moments of inertia

2×10^5 is the approximate conversion factor from rad/sec to deg/hr

The torque power spectrum induced by a vibration power spectrum is

$$P_t = P_g \times (M_{ub})^2 \times 4.4 \times 10^{-5}$$

where

P_t is torque power spectral density in dyn^2 per rad/hr

P_g is vibration power spectral density in g^2/Hertz

M_{ub} is the rotor mass unbalance in dyn cm/g

Combining the two equations the relationship between the vibration power spectrum, the mass unbalance and the drift power spectrum is

$$P_\omega = \frac{P_g (M_{ub})^2 \quad 1.76 \times 10^6}{[\nu (A - B)]^2}$$

Assuming a vibration power spectrum of 0.01 g^2/Hz (4.5 g, 0 to 2000 Hz), a mass unbalance of 0.5 dyn cm, the drift power spectrum with the present parameters of the Nutatron will be 1.2×10^{-5} $(deg/hr)^2$ per rad/hr. Even a modest increase in rotor speed, which is being recommended to reduce drift periodicity discussed in Section VI, will minimize the vibration induced drift errors to an insignificant level. If in addition, vibration isolation is used, high vibration inputs can be tolerated and the mass balance requirement further reduced.

VII. SUMMARY OF CONCLUSIONS AND RECOMMENDATIONS

The test results of the two prototype Nutatrons and a discussion of the data given in this report indicate the outstanding characteristics as well as areas that require further improvements. The following conclusions can be drawn from this information.

A. CONCLUSIONS

(1) The long term stability, the low temperature coefficients, the repeatability from turn on to turn on, subsequent to wide temperature exposures substantiates the performance independence from changes in dimensions and material characteristics. The potential of the Nutatron concept to lead to a low cost, reliable angular rate sensor with few precision parts and delicate assembly processes is verified.

(2) The predominant portion of the drift randomness is in fact a periodicity resulting from a beat between bearing noise spikes at the Nutatron frequency and the case rotation frequency. This low frequency drift periodicity can theoretically be eliminated by wider separation between rotor and housing frequency.

(3) The remaining Nutatron drift noise appears to be white and to stem from the surface finish imperfection of the commercial ball bearings used.

(4) Case rotation is effective in eliminating standing level of 2ν bearing noise.

(5) The use of large outer race curvature bearings has greatly reduced the effect of tilted installation of the bearing on acceleration sensitive drift.

(6) The Nutatron with the 0.8 outer race curvature bearing demonstrated considerably better repeatability and lower acceleration squared sensitive drift. The optimum ratio of outer race curvature may be between 0.55 and 0.8 but requires verification.

(7) The compound circular flexure provides the required stiffness about the spin axis in combination with the desired compliance about the two input axes. Large oscillations about the spin axis have been eliminated.

(8) A minute axial displacement of the two orthogonal centers of suspension of the compound circular flexure results in a 2Ω signal proportional to cross axis accelerations. This signal is effectively used to trim standing level of acceleration sensitive drift.

(9) The resonant control loop effectively adjusted the flexure spring constant for resonant operation at the Nutatron frequency. It appears that most drift producing noise at the Nutatron frequency also resonates and it may be possible to eliminate this loop in the future.

(10) The automatic alignment loop effectively aligns the case rotation and spin axes. The errors produced by small misalignments are negligible and it may be possible to eliminate this loop in the future.

(11) Nutatron drift introduced by torque noise at $2\nu + 2\Omega$ decreases with higher rotor speed, while that caused by displacement noise at the Nutatron frequency increases with it. Investigation of the nature of the noise indicates that it may be possible to increase the rotor speed of the Nutatron. This will benefit the periodic drift, decrease the sensitivity to external vibration, and make it easier to stabilize a platform system. Further investigation will be required to determine how fast the rotor can be run.

B. RECOMMENDATIONS

The demonstrated data of the Nutatron concept so far, the understanding of the remaining error mechanisms and the simplicity of the postulated techniques to improve performance, warrant the further development of this unconventional angular rate sensor. It is recommended that a program be initiated to implement the modifications discussed in this report for performance improvements and for low cost producibility. These are briefly summarized in Table XVI.

TABLE XVI. RECOMMENDATIONS

Modification	Why	Potential Problems	Recommended Action
Increase rotor speed	Eliminate low frequency drift periodicity. Reduce sensitivity to vibration	Displacement noise at Nutatron frequency will increase	Conduct tests at various rotor speeds to establish feasibility
Full ball complement bearings, solid film lubricant bearings	Reduce retainer instability which is cause of low frequency drift periodicity	Effect on other bearing parameters is unknown	Analyze and conduct tests with bearings in new configurations on Nutatron
Give bearings latest surface finish treatments (ion discharge cleaning ball lapping, phosphating)	Reduce white noise drift level	None	Give all bearings latest surface finish treatment in future
Move spin motor stator from suspended element to case	Increase modulation factor by 2 or 3, reduce g and g^2 sensitive drift, simplification and cost reduction	Additional motor noise at Nutatron frequency (should be small)	Analysis, design motor, modify Nutatron and conduct tests
Reduce outer race curvature but above 0.6	Reduce g^2 sensitive drift	None	Analysis, install bearings and conduct tests
Eliminate resonant operation	Simplification/ cost reduction	Increase in non-resonant noise (should be small)	Conduct tests to establish feasibility
Eliminate Alignment Loops	Simplification/ cost reduction	Additional drift noise (should be small)	Conduct tests to establish feasibility
Improved pickoff preamp. using latest IC_s	Reduce white noise drift level	None	Design, fabricate and install improved preamp.

APPENDIX A

DERIVATION OF THE STEADY-STATE NUTATRON EQUATION

DERIVATION OF THE STEADY STATE NUTATRON EQUATION

In this appendix the solutions for the pickoff angles in the steady state are derived. Included in the analysis are:

Constant torque inputs,
Input torques at twice the rotor speed (2ν),
Constant base rate inputs,
Bearing angle noise at 2ν,
Suspension spring constant.

Beginning with Euler's equations in the rotating coordinate system

$$\left[\underline{T}_o'\right] = [G]\left[\underline{\omega}_s' + \underline{\omega}'_o\right] + \left[K_1\right]\left[\underline{\theta}_s'\right] \quad *$$

where

$$\left[\underline{T}_o'\right] = \begin{bmatrix} T_{xo}' \\ T_{yo}' \end{bmatrix} = \text{input torques}$$

$$\left[\underline{\omega}_o'\right] = \begin{bmatrix} \omega_{ox}' \\ \omega_{oy}' \end{bmatrix} = \text{input or base rates (earth rates)}$$

$$\left[\underline{\omega}_s'\right] = \begin{bmatrix} \omega_{sx}' \\ \omega_{xy}' \end{bmatrix} = \text{Angular velocity of float relative to case which is the pivot spring deflection rate of change.}$$

$$\left[\underline{\theta}_s'\right] = \begin{bmatrix} \theta_{sx}' \\ \theta_{xy}' \end{bmatrix} = \text{angle between float and case which is the pivot spring deflection}$$

$$[G] = \begin{bmatrix} pA & \nu(C-B) \\ -\nu(C-A) & pB \end{bmatrix} = \text{Euler's gyro matrix}$$

$$\left[K_1\right] = \begin{bmatrix} K_1 & 0 \\ 0 & K_1 \end{bmatrix} = \text{Pivot-spring-constant matrix}$$

A, B, C = principal moments of inertia of rotor about the x, y, and z axes respectively including non-rotating inertias.

ν = rotor speed

p = $\frac{d}{dt}$ = derivative operator

*Primed variables are rotating coordinate system variables.

In stationary coordinates, $\underline{\omega}_s = p\,\underline{\theta}_s$. However, in rotating coordinates this simple relation does not hold. Since $\underline{\theta}_s$ is small (the pivot spring deflection) it may be considered a vector; then

$$\underline{\theta}_s' = [\nu t]\,\underline{\theta}_s$$

where

$$\underline{\theta}_s = \begin{bmatrix} \theta_{sx} \\ \theta_{sy} \end{bmatrix} = \text{spring deflection in stationary coordinates.}$$

$$[\nu t] = \begin{bmatrix} \cos \nu t & \sin \nu t \\ -\sin \nu t & \cos \nu t \end{bmatrix} = \text{coordinate transformation matrix from stationary to rotating coordinate vectors.}$$

Similarly,

$$\underline{\omega}_s' = [\nu t]\,\underline{\omega}_s$$

$$\underline{T}_o' = [\nu t]\,\underline{T}_o$$

$$\underline{\omega}_o' = [\nu t]\,\underline{\omega}_o$$

where

$$\underline{\omega}_s = \begin{bmatrix} \omega_{sx} \\ \omega_{sy} \end{bmatrix} = \text{spring deflection rate in stationary coordinates}$$

$$\underline{T}_o = \begin{bmatrix} T_{xo} \\ T_{yo} \end{bmatrix} = \text{torques in stationary coordinates}$$

$$\underline{\omega}_o = \begin{bmatrix} \omega_{ox} \\ \omega_{oy} \end{bmatrix} = \text{base rates in stationary coordinates}$$

Since,

$$\underline{\theta}_s' = [\nu t]\,\underline{\theta}_s,$$

$$\underline{\omega}_s' = [\nu t]\,\underline{\omega}_s = [\nu t]\,p\,\underline{\theta}_s = [\nu t]\,p\,[\nu t]^{-1}\,\underline{\theta}_s'$$

$$= \begin{bmatrix} p & -\nu \\ \nu & p \end{bmatrix} \underline{\theta}_s' = [M]\,\underline{\theta}_s', \text{ then}$$

$$\underline{T}_o' = [G]\,\underline{\omega}_o' + \left\{ [G]\,[M] + \left[K_1\right] \right\} \underline{\theta}_s'$$

A solution for $\underline{\theta}_S'$ gives spring deflection angles in the rotating system in terms of base rates and input torques. The pick-off signals are then

$$\underline{\theta}_S \quad - \quad [\nu t]^{-1} \quad \underline{\theta}_S'$$

$\underline{T}_O'$ may consist of the following:

(1) Constant gyro error torques
(2) Torques introduced from the torquers
(3) Torques at twice rotor frequency.

In the present Nutatron, which is electrically caged, the d.c. torquer signals are proportional to the base rates and gyro error torques. The constrainment loop electronics filters out the d.c. torquer signal at twice rotor frequency (2ν) resulting from base rate torques. Torques at twice rotor frequency appear from 2ν signals applied to the a.c. feedback torquer and from error sources.

The pick-off angles in rotating coordinates are

$$\underline{\theta}_S' \quad = \quad + \left\{ [G]\ [M] \ + \ [K_1] \right\}^{-1} \left\{ \underline{T}_O' - [G]\ \underline{\omega}_O' \right\}$$

$$\underline{\theta}_S' \quad = \quad \begin{bmatrix} p^2A+\nu^2\,(C-B)+K_1 & -\nu p\Delta \\ \nu p\Delta & p^2B+\nu^2(C-A)+K_1 \end{bmatrix}^{-1} \left\{ \begin{bmatrix} T_{xo}' \\ T_{yo}' \end{bmatrix} - \begin{bmatrix} pA & \nu\,C-B) \\ -\nu\,(C-A) & pB \end{bmatrix} \begin{bmatrix} \omega_{ox}' \\ \omega_{oy}' \end{bmatrix} \right\}$$

where $\Delta \quad = A+B-C.$

1. CONSTANT INPUT TORQUES AND PRECESSION RATES

Excluding torques at twice rotor frequency for the moment, T_{xo} and T_{yo} are constant torques. Also ω_{ox} and ω_{oy} are constant earth rates sensed by the Nutatron. The T_{xo}', T_{yo}', ω_{ox}', ω_{oy}' are seen in rotating coordinates as oscillating torques at ν ; that is,

$$\underline{T}_O' \quad = [\nu\, t]\ \underline{T}_O \text{ and } \underline{\omega}_O' \ = [\nu\, t]\ \underline{\omega}_O$$

Therefore, steady-state ac circuit techniques may be used to determine $\underline{\theta}_S'$. Letting $p = j\nu$, $\sin \nu t = +1$. and $\cos \nu t = j$ denoting a 90 deg phase lead of the cosine signal,

$$\underline{\theta}_S (j\nu \ = \begin{bmatrix} K_1 - \nu^2\Delta & -j\,\nu^2\,\Delta \\ j\,\nu^2\,\Delta & K_1 - \nu^2\,\Delta \end{bmatrix}^{-1} \left\{ \begin{bmatrix} j & +1 \\ -1 & j \end{bmatrix} \begin{bmatrix} T_{xo} \\ T_{yo} \end{bmatrix} - \begin{bmatrix} j\,\nu\,A & \nu\,(C-B) \\ -\nu\,(C-A)\,j\,\nu\,B \end{bmatrix} \begin{bmatrix} i & 1 \\ -1 & j \end{bmatrix} \begin{bmatrix} \omega_{xo} \\ \omega_{yo} \end{bmatrix} \right\}$$

$$= \frac{1}{K_1\,(K_1 - 2\,\nu^2\Delta)} \begin{bmatrix} j(K_1 - 2\nu^2\Delta) & K_1 - 2\nu^2\,\Delta \\ -(K_1 - 2\nu^2\,\Delta)\, & j(K_1 - 2\nu^2\,\Delta\,) \end{bmatrix} \begin{bmatrix} T_{xo} \\ T_{yo} \end{bmatrix}$$

$$- \frac{\nu}{K_1(K_1-2\nu^2\Delta)} \begin{bmatrix} j(K_1A-\nu^2\Delta C) & K_1(C-B)-\nu^2\Delta C \\ -K_1(C-A)+\nu^2\Delta C & j(K_1-\nu^2\Delta C) \end{bmatrix} \begin{bmatrix} j & 1 \\ -1 & j \end{bmatrix} \begin{bmatrix} \omega_{xo} \\ \omega_{yo} \end{bmatrix}$$

$$= \frac{1}{K_1} \begin{bmatrix} j & 1 \\ -1 & j \end{bmatrix} \begin{bmatrix} T_{xo} \\ T_{yo} \end{bmatrix} - \frac{\nu}{K_1(K_1-2\nu^2\Delta)}$$

$$\begin{bmatrix} [+2\nu^2\Delta C-K_1(A-B+C)] & -j[+2\nu^2\Delta C-K_1(A-B+C)] \\ j[2\nu^2\Delta C-K_1(-A+B+C)] & [2\nu^2\Delta C-K_1(-A+B+C)] \end{bmatrix} \begin{bmatrix} \omega_{xo} \\ \omega_{yo} \end{bmatrix}$$

In stationary coordinates

$$\underline{\theta}_S = [\nu t]^{-1} \underline{\theta}_S' = \begin{bmatrix} \cos\nu t & -\sin\nu t \\ \sin\nu t & \cos\nu t \end{bmatrix} \begin{bmatrix} \theta_{sx}'(t) \\ \theta_{sy}'(t) \end{bmatrix}$$

and after converting $\underline{\theta}_S'(j\nu)$ back to the time domain by letting $j = \cos\nu t$, $1 = \sin\nu t$, we may write the pick-off angles, $\underline{\theta}_S$ as

$$\begin{bmatrix} \theta_{sx} \\ \theta_{sy} \end{bmatrix} = \frac{1}{K_1} \left\{ \begin{bmatrix} T_{xo} \\ T_{yo} \end{bmatrix} + \nu C \begin{bmatrix} 0 & -1 \\ 1 & 0 \end{bmatrix} \begin{bmatrix} \omega_{xo} \\ \omega_{yo} \end{bmatrix} \right\} - \frac{\nu(A-B)}{K_1-2\nu^2\Delta} \begin{bmatrix} -\sin 2\nu t & \cos 2\nu t \\ \cos 2\nu t & \sin 2\nu t \end{bmatrix} \begin{bmatrix} \omega_{xo} \\ \omega_{yo} \end{bmatrix} \quad \text{(I-1)}$$

The dc component of the pick-off angles is the first term and in the steady state

$\begin{bmatrix} \theta_{sx} \\ \theta_{sy} \end{bmatrix} = \frac{1}{K_1} \begin{bmatrix} T_x \\ T_y \end{bmatrix}$ where $\begin{bmatrix} T_x \\ T_y \end{bmatrix}$ consists of gyro error torques plus torques proportional to base rates; that is,

$$T_x = T_{xo} - \nu C\ \omega_{yo} \cong -H\ \omega_{yo}$$

$$T_y = T_{yo} + \nu C\ \omega_{xo} \cong H\ \omega_{xo}$$ where H is angular momentum.

The ac pick-off signal is proportional to base rates only as expected.

$$\begin{bmatrix} \theta_{sx} \\ \theta_{sy} \end{bmatrix}_{ac} = \frac{-\nu(A-B)}{K_1-2\nu\Delta^2} \begin{bmatrix} -\sin 2\nu t & \cos 2\nu t \\ \cos 2\nu t & \sin 2\nu t \end{bmatrix} \begin{bmatrix} \omega_{xo} \\ \omega_{yo} \end{bmatrix} \quad \text{(I-2)}$$

$$\text{If } K_1 \ll 2\nu^2\Delta, \frac{-\nu(A-B)}{K_1-2\nu^2\Delta} \cong \frac{A-B}{2\nu(A+B-C)} = \frac{M}{2\nu}$$

2. GENERAL 2ν TORQUE INPUTS

Consider input torques which occur at the 2ν frequency only. Then for a general 2ν torque defined as

$$\begin{bmatrix} T_{x2\nu} \\ T_{y2\nu} \end{bmatrix} = \begin{bmatrix} m\cos(2\nu t + \phi) \\ n\sin(2\nu t + \theta) \end{bmatrix}$$

where m and n are the respective amplitudes of the torque signals in the two axes and ϕ and θ are the arbitrary phase angles. In rotating coordinates

$$\begin{bmatrix} T_{x2\nu'} \\ T_{y2\nu'} \end{bmatrix} = [\nu t] \begin{bmatrix} T_{x2\nu} \\ T_{y2\nu} \end{bmatrix}$$

$$= \frac{1}{2} \begin{bmatrix} m\cos(3\nu t+\phi) & -n\cos(3\nu t + \theta) + m\cos(\nu t+\phi) & +n\cos(\nu t+\theta) \\ -m\sin(3\nu t+\phi) & +n\sin(3\nu t + \theta) + m\sin(\nu t+\phi) & +n\sin(\nu t+\theta) \end{bmatrix}$$

In rotating coordinates there is a torque at ν and a torque at 3ν. Again, using steady-state ac techniques, we may let $p = j\nu$, $\cos\nu t = j$, $\sin\nu t = 1$ for the ν component and $p = j3\nu$, $\cos 3\nu t = j$, $\sin 3\nu t = 1$ for the 3ν component; then after expanding $\cos(3\nu t + \phi)$, $\cos(3\nu t + \theta)$, $\sin(3\nu t + \phi)$, $\sin(3\nu t + \theta)$ etc. into $(\cos 3\nu t \cos\phi - \sin 3\nu t \sin\phi)$, etc. we have

$$\begin{bmatrix} T_{x\nu'} \\ T_{y\nu'} \end{bmatrix} = \frac{1}{2} \begin{bmatrix} j & -1 \\ 1 & j \end{bmatrix} \begin{bmatrix} m\cos\phi + n\cos\theta \\ m\sin\phi + n\sin\theta \end{bmatrix} = \frac{1}{2} \begin{bmatrix} j & -1 \\ 1 & j \end{bmatrix} \begin{bmatrix} a \\ b \end{bmatrix}$$

$$\begin{bmatrix} T_{x3'\nu} \\ T_{y3'_\nu} \end{bmatrix} = \frac{1}{2} \begin{bmatrix} j & 1 \\ -1 & j \end{bmatrix} \begin{bmatrix} m\cos\phi & -n\cos\theta \\ n\sin\theta & -m\sin\phi \end{bmatrix} = \frac{1}{2} \begin{bmatrix} j & 1 \\ -1 & j \end{bmatrix} \begin{bmatrix} c \\ d \end{bmatrix}$$

At ν

$$\begin{bmatrix} \theta_{sx\nu'} \\ \theta_{sy\nu'} \end{bmatrix} = \frac{1}{2} \begin{bmatrix} K_1 - \nu^2\Delta & -j\nu^2\Delta \\ j\nu^2\Delta & K_1 - \nu^2\Delta \end{bmatrix}^{-1} \begin{bmatrix} j & -1 \\ 1 & j \end{bmatrix} \begin{bmatrix} a \\ b \end{bmatrix}$$

$$= \frac{1/2}{K_1(K_1 - 2\nu^2\Delta)} \begin{bmatrix} K_1 - \nu^2\Delta & +j\nu^2\Delta \\ -j\nu^2\Delta & K_1 - \nu^2\Delta \end{bmatrix} \begin{bmatrix} j & -1 \\ 1 & j \end{bmatrix} \begin{bmatrix} a \\ b \end{bmatrix}$$

$$= \frac{1/2}{K_1 - 2\nu^2\Delta} \begin{bmatrix} j & -1 \\ 1 & j \end{bmatrix} \begin{bmatrix} a \\ b \end{bmatrix} .$$

Since

$$\begin{bmatrix}\theta_{sx}\\ \theta_{sy}\end{bmatrix} = [\nu t]^{-1} \begin{bmatrix}\theta'_{sx}\\ \theta'_{sy}\end{bmatrix} .$$

$$\begin{bmatrix}\theta_{sx}\\ \theta_{sy}\end{bmatrix} = \frac{1/2}{K_1 - 2\nu^2\Delta} \begin{bmatrix}\cos\nu t & -\sin\nu t\\ \sin\nu t & \cos\nu t\end{bmatrix} \begin{bmatrix}\cos\nu t & -\sin\nu t\\ \sin\nu t & \cos\nu t\end{bmatrix} \begin{bmatrix}a\\ b\end{bmatrix}$$

$$= \frac{1/2}{K_1 - 2\nu^2\Delta} \begin{bmatrix}\cos 2\nu t & -\sin 2\nu t\\ \sin 2\nu t & \cos 2\nu t\end{bmatrix} \begin{bmatrix}a\\ b\end{bmatrix}$$

where

$$a = m\cos\phi + n\cos\theta$$
$$b = m\sin\phi + n\sin\theta$$

The ν component of the torque in the rotating system results in a pick-off signal at 2ν in the stationary system which resonates whenever $K_1 = 2\nu^2\Delta$. If m = -n and $\phi = \theta$, this component disappears.

At 3ν,

$$\begin{bmatrix}\theta'_{sx3\nu}\\ \theta'_{sy3\nu}\end{bmatrix} = \begin{bmatrix}K_1 - 9\nu^2 A + \nu^2 (C-B) & -j3\nu^2\Delta\\ j3\nu^2\Delta & K_1 - 9\nu^2 B + \nu^2 (C-A)\end{bmatrix}^{-1} \begin{bmatrix}T'_{x3\nu}\\ T'_{y3\nu}\end{bmatrix}$$

$$= \frac{1}{2D} \begin{bmatrix}K_1 - 9\nu^2 B + \nu^2 (C-A) & j3\nu^2\Delta\\ -j3\nu^2\Delta & K_1 - 9\nu^2 A + \nu^2 (C-B)\end{bmatrix} \begin{bmatrix}j & 1\\ -1 & j\end{bmatrix} \begin{bmatrix}c\\ d\end{bmatrix}$$

where

D = the determinant of the matrix.

$$= [K - 4\nu^2 (C - 2\Delta)] [K - 2\nu^2 (2C + \Delta)] - 16\nu^4 (A - B)^2 .$$

$$\begin{bmatrix}\theta'_{sx3\nu}\\ \theta'_{sy3\nu}\end{bmatrix} = \frac{1}{2D} \begin{bmatrix}j(K_1 - 4\nu^2\Delta - 8\nu^2 B) & K_1 - 4\nu^2\Delta - 8\nu^2 B)\\ -(K_1 - 4\nu^2\Delta - 8\nu^2 A) & j(K_1 - 4\nu^2\Delta - 8\nu^2 A)\end{bmatrix} \begin{bmatrix}c\\ d\end{bmatrix}$$

Since

$$\begin{bmatrix}\theta_{sx}\\ \theta_{sy}\end{bmatrix} = [\nu t]^{-1} \begin{bmatrix}\theta'_{sx3\nu}\\ \theta'_{sy3\nu}\end{bmatrix}, \text{ letting } j = \cos 3\nu t,\ l = \sin 3\nu t$$

$$\begin{bmatrix}\theta_{sx}\\ \theta_{sy}\end{bmatrix} = \frac{1}{2D}\begin{bmatrix}(M-N)\cos 4\nu t + (M+N)\cos 2\nu t & (M-N)\sin 4\nu t + (M+N)\sin 2\nu t\\ (M-N)\sin 4\nu t - (M+N)\sin 2\nu t & -(M-N)\cos 4\nu t + (M+N)\cos 2\nu t\end{bmatrix}\begin{bmatrix}c\\ d\end{bmatrix}$$

where

$M = K_1 - 4\nu^2\Delta - 8\nu^2 B$ $\qquad c = m\cos\phi - n\cos\theta$

$N = K_1 - 4\nu^2\Delta - 8\nu^2 A$ $\qquad d = n\sin\theta - m\sin\phi$

The pickoff signal contains frequencies at 2ν and 4ν. Because we are only interested in the 2ν component, $\frac{M+N}{2} = K_1 - 4\nu^2 (C + 2\Delta)$. Then the total 2ν pickoff motion from the general 2ν torque input is

$$\begin{bmatrix}\theta_{x2\nu}\\ \theta_{y2\nu}\end{bmatrix} = \frac{1/2}{K_1 - 2\nu^2\Delta}\begin{bmatrix}\cos 2\nu t & -\sin 2\nu t\\ \sin 2\nu t & \cos 2\nu t\end{bmatrix}\begin{bmatrix}a\\ b\end{bmatrix}$$

$$+\frac{K_1 - 4\nu^2 (C + 2\Delta)}{D}\begin{bmatrix}\cos 2\nu t & \sin 2\nu t\\ -\sin 2\nu t & \cos 2\nu t\end{bmatrix}\begin{bmatrix}c\\ d\end{bmatrix} \qquad (I\text{-}3)$$

If $m = n$, $\phi = \theta$, the latter term disappears, and the latter term does not resonate when $K_1 = 2\nu^2 \Delta$.

C. PLANAR 2ν TORQUE INPUTS

Assume a planar 2ν torque input of the general form:

$T_{X2\nu} = T_N \cos(2\nu t + \zeta)\cos\eta$

$T_{Y2\nu} = T_N \cos(2\nu t + \zeta)\sin\eta$,

where

ζ = arbitrary phase angle of planar torque

η = angle of planar torque with respect to the X axis

We may make the identifications between: m, n, T_N, ϕ, θ, ζ and η.

$m\cos\phi = T_N\cos\zeta\cos\eta$

$m\sin\phi = T_N\sin\zeta\cos\eta$

$n\cos\theta = -T_N\sin\zeta\sin\eta$

$n\sin\theta = T_N\cos\zeta\sin\eta$

Then

$a = T_N\cos(\eta + \zeta)$

$b = T_N\sin(\eta + \zeta)$

$c = T_N\cos(\eta - \zeta)$

$d = T_N\sin(\eta - \zeta)$

Finally,

$$\begin{bmatrix}\theta_x\\ \theta_y\end{bmatrix}_{2\nu} = \frac{T_N}{2}\left\{\frac{1}{K_1 - 2\nu^2\Delta}\begin{bmatrix}\cos(2\nu t+\zeta+\eta)\\ \sin(2\nu t+\zeta+\eta)\end{bmatrix} + \frac{1}{K_1 - 2\nu^2(C+2\Delta)(1+P)}\begin{bmatrix}\cos(2\nu t+\zeta-\eta)\\ -\sin(2\nu t+\zeta-\eta)\end{bmatrix}\right\}, \tag{I-4}$$

where $P = \dfrac{8\nu^2(A-B)^2}{(2C+\Delta)(K_1 - 4\nu^2(C+2\Delta)}$.

4. BEARING ANGLE NOISE AT 2ν

The pickoff response to bearing noise requires a new analysis. The procedure is the same as used for torques; basically, the bearing noise at 2ν is decomposed into two counter rotating coning signals. The "plus" coning term appears at ν in the rotating coordinate system and the "minus" coning term appears at 3ν in the rotating system. The response to each is derived and the result is resolved back into the stationary system.

Disregarding input torques and input rates, the matrix equation to be solved in the rotating coordinate system is

$$\begin{bmatrix}(p^2(A'+I)+\nu^2(C-B'-I)+K_1 & -\nu p(A'+B'-C+2I)\\ \nu p(A'+B'-C+2I) & p^2(B'+I)+\nu^2(C-A'-I)+K_1\end{bmatrix}\begin{bmatrix}\theta^1_x\\ \theta^1_y\end{bmatrix}$$

$$= \begin{bmatrix}p^2A'+\nu^2(C-B) & -\nu p(A'+B'-C)\\ \nu p(A'+B'-C) & p^2B'+\nu^2(C-A')\end{bmatrix}\begin{bmatrix}\theta^1_{XN}\\ \theta^1_{YN}\end{bmatrix} \tag{I-5}$$

where

I = the symmetric nonrotating inertia of the gyroscopic element,

$A' = A - I$ = the principal moment of inertia of the rotor about the X Axis

$B' = B - I$ = the principal moment of inertia of the rotor about the Y Axis

θ^1_X, θ^1_Y are pickoff signals in rotating coordinates

θ^1_{XN}, θ^1_{YN} are X and Y components of bearing noise in rotating coordinates.

Equation (I-5) is derived as follows: Recognizing that the relationship between angles and rates in rotating coordinates is

$$\begin{bmatrix}\omega^1_X\\ \omega^1_Y\end{bmatrix}\begin{bmatrix}p & -\nu\\ \nu & p\end{bmatrix}\begin{bmatrix}\theta^1_X\\ \theta^1_Y\end{bmatrix}$$

let the subscript 1 represent rotor angle variables and subscript 2 represent non-rotating angle variables then Euler's gyro equations are written as

$$\begin{bmatrix} T_X^1 \\ T_Y^1 \end{bmatrix} = 0 = \begin{bmatrix} pA' & \nu(C - B') \\ -\nu(C - A') & pB' \end{bmatrix} \begin{bmatrix} p - \nu \\ \nu \quad p \end{bmatrix} \begin{bmatrix} \theta_{1X}^1 \\ \theta_{1Y}^1 \end{bmatrix} + I \begin{bmatrix} p & -\nu \\ \nu & p \end{bmatrix}^2 \begin{bmatrix} \theta_{2X}^1 \\ \theta_{2Y}^1 \end{bmatrix}$$

$$+ \begin{bmatrix} K_1 & 0 \\ 0 & K_1 \end{bmatrix} \begin{bmatrix} \theta_{2X}^1 \\ \theta_{2Y}^1 \end{bmatrix}$$

The first term on the right is the torque from rotor motions, the second term is the torque from the non-rotating inertia, (referred to the rotating system) and the third term is the torque from the pivot spring.

The angles θ_{1X}^1, θ_{1Y}^1 differ from θ_{2X}^1, θ_{2Y}^1, respectively, by the bearing motion such that

$$\theta_{1X}^1 = \theta_{2X}^1 - \theta_{NX}^1$$

$$\theta_{1Y}^1 = \theta_{2Y}^1 - \theta_{NY}^1$$

where θ_{NX}^1 and θ_{NY}^1 are bearing angular displacements. Combining terms we have equation (I-5) where θ_X^1, θ_Y^1 are pickoff signals of the non-rotating inertia referred to the rotating system.

For a planar bearing noise in the stationary system,

$$\begin{bmatrix} \theta_{XN} \\ \theta_{YN} \end{bmatrix} = \theta_N \cos(2\nu t + \zeta) \begin{bmatrix} \cos\eta \\ \sin\eta \end{bmatrix}$$

where ζ = arbitrary phase of planar noise, η = angle of planar noise with respect to the X axis, the equivalent signal in rotating coordinates is

$$\begin{bmatrix} \theta_{XN}^1 \\ \theta_{YN}^1 \end{bmatrix} = \frac{\theta_N}{2} \begin{bmatrix} \cos\nu t & -\sin\nu t \\ \sin\nu t & \cos\nu t \end{bmatrix} \begin{bmatrix} \cos(\eta + \zeta) \\ \sin(\eta + \zeta) \end{bmatrix}$$

$$+ \frac{\theta_N}{2} \begin{bmatrix} \cos 3\nu t & \sin 3\nu t \\ -\sin 3\nu t & \cos 3\nu t \end{bmatrix} \begin{bmatrix} \cos(\eta - \zeta) \\ \sin(\eta - \zeta) \end{bmatrix}$$

Using steady state ac techniques, we may find the response to the ν and 3ν signals in rotating coordinates. These are

$$\begin{bmatrix} \theta_X^1 \\ \theta_Y^1 \end{bmatrix} = \frac{\theta_N}{2} \frac{\begin{bmatrix} K_1-\nu^2\Delta & j\nu^2\Delta \\ -j\nu^2\Delta & K-\nu^2\Delta \end{bmatrix} \begin{bmatrix} -\nu^2\Delta' & -j\nu^2\Delta' \\ j\nu^2\Delta' & -\nu^2\Delta' \end{bmatrix} \begin{bmatrix} j & -1 \\ 1 & j \end{bmatrix} \begin{bmatrix} \cos(\eta+\zeta) \\ \sin(\eta+\zeta) \end{bmatrix}}{K_1-2\nu^2\Delta}$$

$$+\frac{\theta_N}{2} \frac{\begin{bmatrix} K_1-\nu^2\Delta-8\nu^2B'(j3\nu^2\Delta) \\ -j3\nu^2\Delta \quad (K_1-\nu^2\Delta-8\nu^2A') \end{bmatrix} \begin{bmatrix} -\nu^2\Delta'-8\nu^2A'(-j3\nu^2\Delta') \\ j3\nu^2\Delta' \quad (-\nu^2\Delta'-8\nu^2B') \end{bmatrix} \begin{bmatrix} j & 1 \\ -1 & j \end{bmatrix} \begin{bmatrix} \cos(\eta-\zeta) \\ \sin(\eta-\zeta) \end{bmatrix}}{[K_1-4\nu^2(C+2\Delta)][K_1-2\nu^2(2C+\Delta)(1+P)]}$$

where $\Delta = A'+B'-C+2I$

$\Delta' = A'+B'-C$

Multiplying out, converting to the time domain, and resolving back to stationary coordinate we obtain the 2ν pickoff signals:

$$\begin{bmatrix} \theta_X \\ \theta_Y \end{bmatrix}_{2\nu} = -\theta_N \left\{ \frac{+\nu^2\Delta'}{K_1-2\nu^2\Delta} \begin{bmatrix} \cos(2\nu t+\zeta+\eta) \\ \sin(2\nu t+\zeta+\eta) \end{bmatrix} \frac{\nu^2(2C+\Delta')(1+N)}{K_1-2\nu^2(2C+\Delta)(1+P)} \begin{bmatrix} \cos(2\nu t+\zeta-\eta) \\ -\sin(2\nu t+\zeta-\eta) \end{bmatrix} \right\} \text{(1-o)}$$

where $N = \dfrac{8\nu^2(A-B)^2}{(2C+\Delta')(K_1-4\nu^2(C+2\Delta))}$

P and N are nondimensional correction factors for the anisometric rotor. For symmetrical rotors P = N = 0. In the Nutatron assume

$\nu = 63$
$A = 485$
$B = 185$
$C = 520$
$\Delta = 150$
$\Delta' = 50$

$K_1 \leqslant 2\cdot10^6 < 4\nu^2(C+2\Delta) = 1.58\cdot10^4(820) = 13.0\cdot10^6$

$$P = \frac{8(3960)(300)^2}{1190(-13\cdot10^6)} = -0.227$$

$$N = \frac{8(3960)(300)^2}{1090(-13\cdot10^6)} = -0.248$$

A comparison of these equations shows the correlation between bearing noise and torque noise. The torque equivalent for a given bearing noise amplitude is:

$$T_N = -\nu^2 \Delta' \ \theta_N \quad \text{for the "plus" coning term}$$

$$T_N = -\nu^2 (2C+\Delta') \ (1+N) \ \theta_N \quad \text{for the "minus" coning term}$$

The pickoff sensitivity to bearing noise for the two terms for K = 0 in the Nutation is:

$$\theta_{X2\nu} = \frac{\theta_N}{2} \left[\frac{\Delta'}{\Delta} \cos(2\nu t+\zeta+\eta) + \frac{(2C+\Delta')(1+N)}{(2C+\Delta)(1+P)} \cos(2\nu t+\zeta-\eta) \right]$$

$$= \frac{\theta_N}{2} \left[0.33 \cos(2\nu t+\zeta+\eta) + 0.9 \cos(2\nu t+\zeta-\eta) \right]$$

$$= \theta_N \left[0.615 \cos(2\nu t+\zeta) \cos\eta + 0.285 \sin(2\nu t+\zeta) \sin\eta \right]$$

$$\theta_{y2\nu} = \frac{\theta_N}{2} \left[0.33 \sin(2\nu t+\zeta+\eta) - 0.9 \sin(2\nu t+\zeta-\eta) \right]$$

$$= \theta_N \left[-0.285 \sin(2\nu t+\zeta) \cos\eta + 0.615 \cos(2\nu t+\zeta) \sin\eta \right]$$

Note that the coefficient of the "plus" coning term is about 1/3 the coefficient of the "minus" coning term. Note also that as K is increased, the "plus" coning term comes into resonance long before the "minus" coning term. Therefore, the Nutatron signal resonant rise needs to exceed 3 before bearing noise resonance would be noted experimentally.

5. TOTAL 2ν PICKOFF RESPONSE

Combining Equations 1-2, 1-4, 1-6, we obtain the total pickoff motions at 2ν in response to constant precession rate inputs, planar 2ν torque inputs, and planar 2ν angular bearing noise inputs.

$$\begin{bmatrix} \theta_x \\ \theta_y \end{bmatrix}_{2\nu} = \frac{-\nu(A-B)}{K_1 - 2\nu^2\Delta} \begin{bmatrix} -\sin 2\nu t & \cos 2\nu t \\ \cos 2\nu t & \sin 2\nu t \end{bmatrix} \begin{bmatrix} \omega_{XO} \\ \omega_{YO} \end{bmatrix}$$

$$+ \frac{T_N}{2} \left\{ \frac{1}{K_1 - 2\nu^2\Delta} \begin{bmatrix} \cos(2\nu t+\zeta+\eta) \\ \sin(2\nu t+\zeta+\eta) \end{bmatrix} + \frac{1}{K_1 - 2\nu^2 (C+2\Delta)(1+P)} \begin{bmatrix} \cos(2\nu t+\zeta-\eta) \\ -\sin(2\nu t+\zeta-\eta) \end{bmatrix} \right\}$$

$$+ \theta_N \left\{ \frac{\nu^2\Delta'}{K_1 - 2\nu^2\Delta} \begin{bmatrix} \cos(2\nu t+\zeta+\eta) \\ \sin(2\nu t+\zeta+\eta) \end{bmatrix} + \frac{\nu^2 (2C+\Delta')(1+N)}{K_1 - 2\nu^2(2C+\Delta)(1+P)} \begin{bmatrix} \cos(2\nu t+\zeta-\eta) \\ -\sin(2\nu t+\zeta-\eta) \end{bmatrix} \right\}$$

(1-7)

6. AC TORQUE REBALANCING

In the ac torque rebalance test mode, the X axis 2ν pickoff motion is nulled by the ac feedback torquer, and the suspension spring rate is adjusted so that $K_1 \simeq 2\nu^2\Delta$. Equation I-7 then becomes for the X axis:

$$\theta_{X2\nu} = 0 = -\nu(A-B)(-\Omega_{ex} \sin 2\nu t + \Omega_{ey} \cos 2\nu t) - T_{x\sin}(\sin 2\nu t) - T_{x\cos}(\cos 2\nu t)$$
$$\frac{T_\eta}{2} \cos(2\nu t + \phi) + \theta_N(\nu^2\Delta')\cos(2\nu t + \theta), \qquad \text{(I-8)}$$

where

Ω_{ex}, Ω_{ey} are the components of earth rotation about the input axes.

$T_{x\sin}$, $T_{x\cos}$ are the required X axis torques at $\sin 2\nu t$ and $\cos 2\nu t$ to null the X axis 2ν motion.

T_η is a 2ν noise torque at some arbitrary phase angle, ϕ

θ_N is a 2ν bearing noise angle at some arbitrary phase angle θ.

Equation (I-8) may be re-written:

$$T_{x\sin}(\sin 2\nu t) + T_{x\cos}(\cos 2\nu t) = -\nu(A-B)(-\Omega_{ex}\sin 2\nu t + \Omega_{ey}\cos 2\nu t)$$
$$+ T_{\eta x\cos}(\cos 2\nu t) + T_{\eta x\sin}(\sin 2\nu t)$$

where

$$T_{\eta x\cos} = \left(\frac{T_\eta}{2}\cos\phi + \theta_N\nu^2\Delta'\cos\theta\right)$$
$$T_{\eta x\sin} = -\left(\frac{T_\eta}{2}\sin\phi + \theta_N\nu^2\Delta'\sin\theta\right)$$

Finally, equating like terms, we obtain:

$$T_{x\sin} = \nu(A-B)\Omega_{ex} + T_{\eta x\sin}$$

$$T_{x\cos} = -\nu(A-B)\Omega_{ey} + T_{\eta x\cos}$$

which are the expressions used in the discussion of the test method, Section V.

APPENDIX II

FLEXURE DESIGN
AND
2Ω IN FIXED SYSTEM

A. PIVOT DESIGN

The original Nutatron pivot was a simple necked-down cylindrical pivot. Because of the relatively low torsional stiffness of this type of pivot (1.4×10^6 dyne cm/rad), the suspended element of the Nutatron would occasionally oscillate from stop to stop in response to spurious rotor bearing torques. This pivot was replaced with a compound circular flexure[1], which combines high axial, lateral, and torsional stiffness with relatively low, two-degree-of-freedom bending stiffness. The flexure, seen in Figures II-1 and II-3 consists of a hollow beryllium copper cylinder slotted as shown in the figures. Figure II-2 is an expanded view of one of the flexure sections. The design requirements for the new pivot were:

(a) The same mechanical interfaces to permit direct replacement without modification of other parts.

(b) A sensitive axes bending stiffness between 2×10^6 and 3×10^6 dyne cm/rad so that no modifications to the Spring Rate compensation were required.

(c) A minimum 5 g loading capability in all axes.

(d) A lateral and axial stiffness at least as high as that of the original pivot.

Analysis of the new design configuration indicated that the two most critical parameters with respect to g capability are the shear stress due to lateral load (S_{sl}), and tensile or compressive stress due to lateral load (S_{tl}). The equations for these stresses are

$$S_{sl} = \frac{3}{4}\frac{Ma}{bt_o}, \tag{II-1}$$

$$S_{tl} = \frac{27}{4}\frac{Ma}{b}\sqrt{\frac{R}{3t_o^3}}, \tag{II-2}$$

where

M is the mass of the suspended element

a is the acceleration in equivalent g level

R, b, and t_o are defined in Figure II-2.

From Equation (II-1), a minimum allowable value was calculated for t_o. This was based on the maximum allowable shear stress in the beryllium copper, an assumed acceleration of 5 g, and cylinder wall thickness (b) of 0.025 in. Equation (B.3) was then rewritten:

$$\sigma_{tl} = \frac{27}{4}Ma\sqrt{\frac{R}{3t_o^3}}, \quad \text{which yields}$$

$$R = 3\left(\frac{4b\sigma_{tl}^2}{27M}\right)\frac{t_o^3}{a^2}. \tag{II-3}$$

[1] "Flexures", Victor Billig, Machine Design, February 4, 1960.

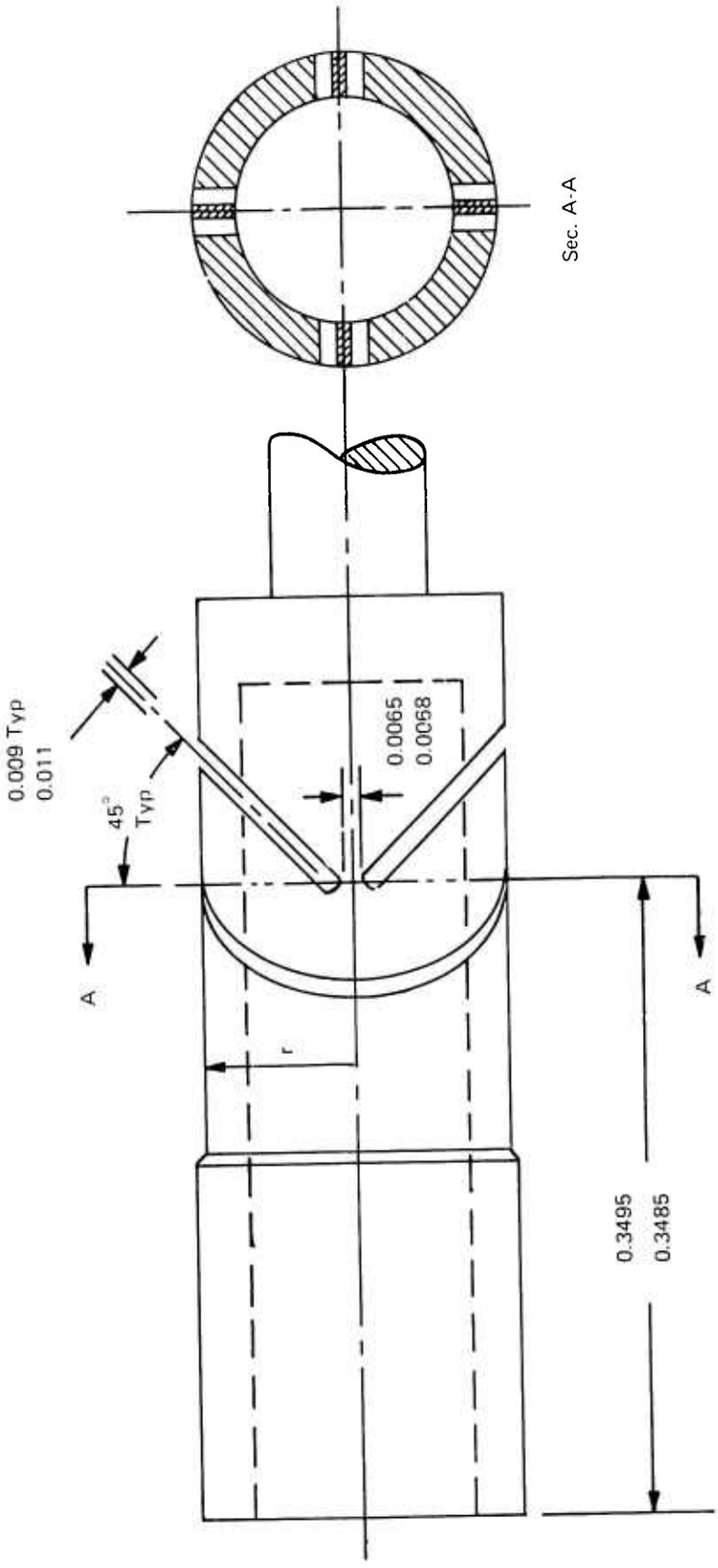

Figure II-1. Compound Circular Flexure

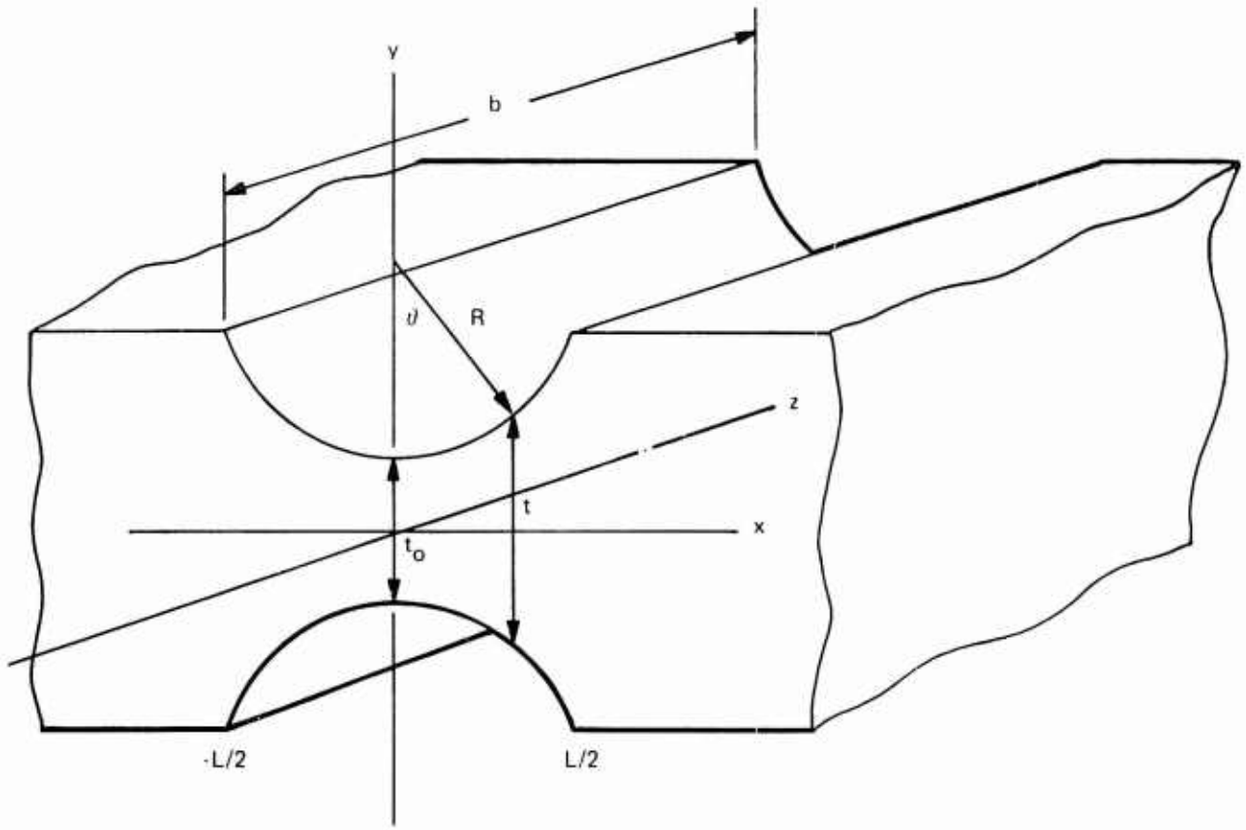

Figure II-2. Geometry of Basic Flexure Section

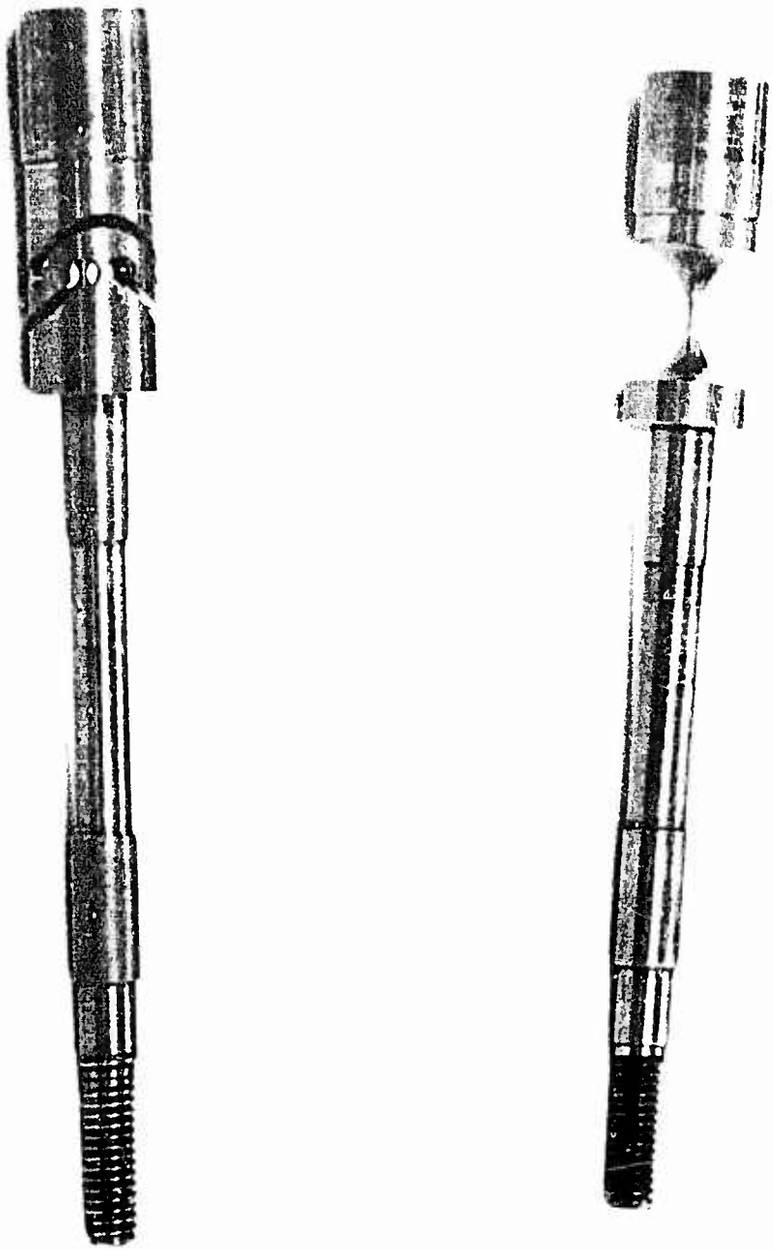

(a) Compound Circular Flexure

(b) Necked Down Flexure

Figure II-3. Compound Circular and Necked Down Cylindrical Flexures

where σ_{11} is the endurance limit of the beryllium copper. Equation (II-3) establishes a relationship between R and t_o for any given g level. Values of R were calculated for permissible values of t_o (above the minimum allowable value) for g levels from 5 to 10 g. The solid line curves in Figure II-4 are a family of constant g curves relating R to t_o. All points (t_o, R) to the right of the 5 g curve and above the shear limit provide at least 5 g capability.

These permissible values were then used in a computer program to calculate values for bending stiffness. The exact equation for the bending stiffness is a rather complicated expression involving the axial stiffness, stiffness about the y-axis, and stiffness about the z-axis, each of which depends on t_o and R. The computer program varies both t_o and R in 0.001-inch increments, and calculates corresponding stiffness values. The results are then plotted as curves of constant bending stiffness versus R and t_o. These are the dashed curves shown in Figure II-4. As is indicated in the figure, the final design point was chosen so that $t_o = R_o = 0.006$ inch. This provides bending stiffness of 2.95 x 10^6 dyne cm/rad and approximately 6 g loading capability. Table II-1 is a comparison of the parameters, for the old and new flexure suspension systems. It is seen that the torsional stiffness has been increased by a factor of approximately 800 with no degradation in the other parameter.

TABLE II-1. COMPARISON OF COMPOUND CIRCULAR PIVOT WITH NECKED-DOWN CYLINDRICAL PIVOT

	Necked-Down Cylindrical 0.017 Dia. Weak Section	Compound Circular r = 0.078 R = 0.006 t_o = 0.006 b = 0.025	Factor of Increase with Compound Circular
Axial Stiffness dyne/cm	1.19 x 10^{10}	5.3 x 10^{10}	4.5
Bending Stiffness dyne cm/rad	2.06 x 10^6	2.95 x 10^6	1.4
Lateral Stiffness dyne/cm	1.02 x 10^9	5.3 x 10^{10}	50.0
Torsional Stiffness dyne cm/rad	1.37 x 10^6	1.13 x 10^9	800.0

B. ACCELERATION SENSITIVE TORQUE AT 2Ω

After the test program was reinitiated with the new pivot, a relatively large pickoff signal at twice housing frequency was noted when the suspension axis was oriented off the vertical. This signal seemed at first disturbing because of its magnitude (between 10^{-3} and 10^{-4} radians) and its cause was investigated. The 2Ω signal was quickly traced to the technique used to manufacture the pivot, and while not planned, it is presently serving the very useful purpose of measuring the cross axis accelerations. The Nutatron is now a multisensor and measures the accelerations along the two input axes with sufficient accuracy to permit compensation of g sensitive Nutatron drift.

The performance of this two axis acceleration measurement capability has not been evaluated, but the growth potential appears excellent indeed. In effect, the Nutatron is also a two axis rotating accelerometer (at Ω) which inherently should have excellent null bias performance as suspension torques occur at dc and the low frequency domain while the acceleration signal takes place at 2Ω frequency.

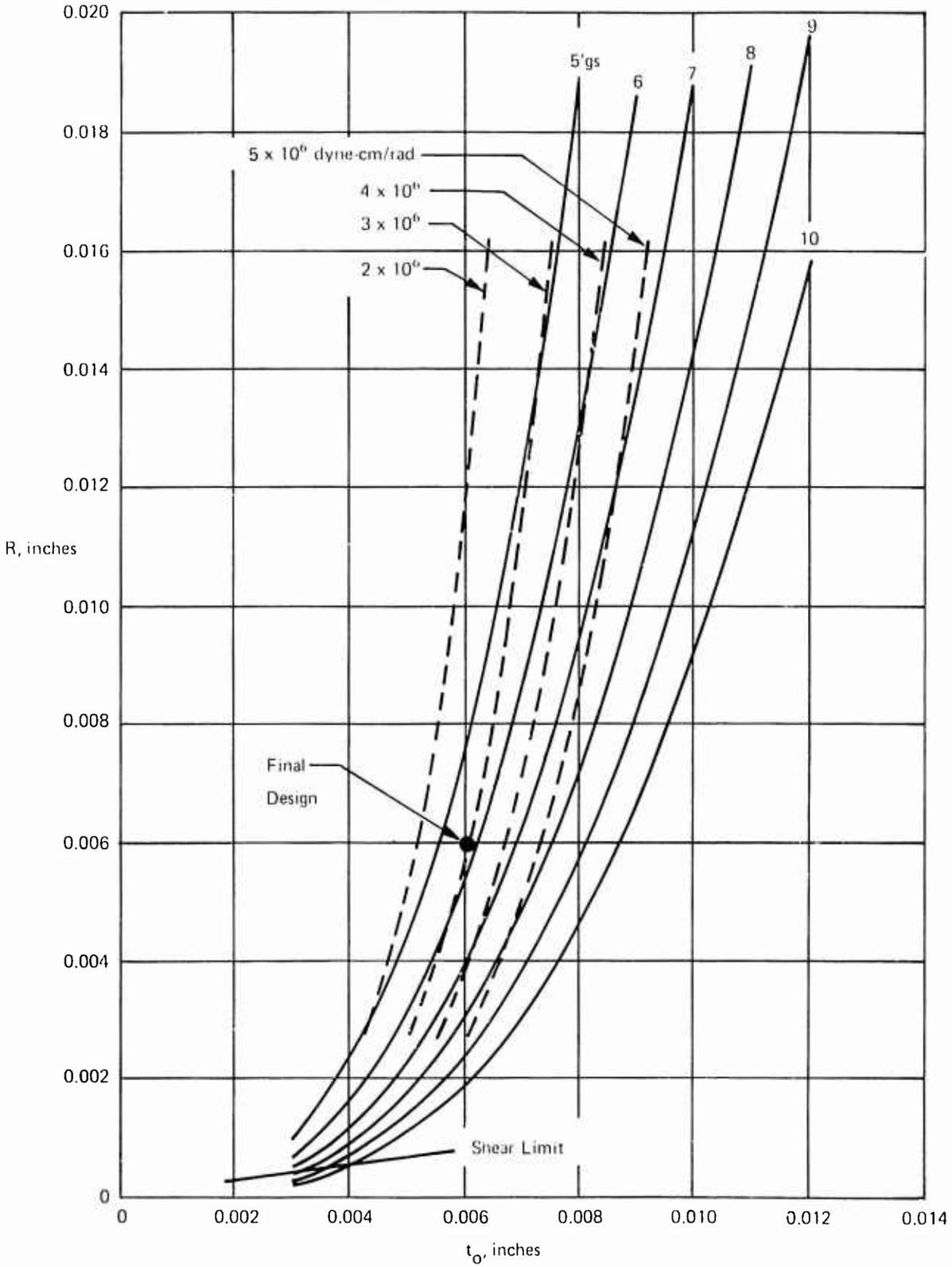

Figure II-4. Design Chart - Compound Circular

The slots are cut in the pivot using an Electrical Discharge Machining (EDM) process. This process removes the metal without applying any force to the part. However, it is difficult to control the process perfectly and some axial displacement of the two orthogonal flexures is unavoidable. This displacement causes a torque at 2Ω (twice the housing rotation frequency) in response to g loading perpendicular to the spin axis as the centers of flexure and mass shift at that frequency.

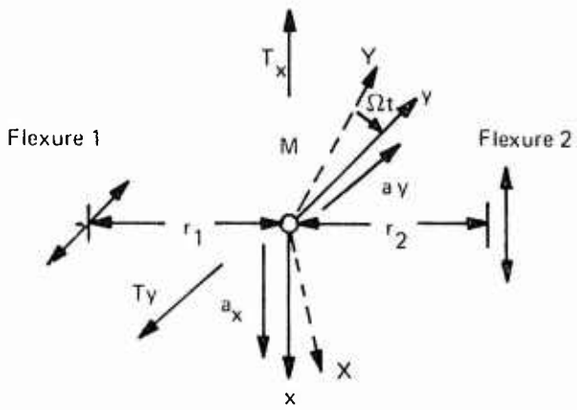

Figure II-5. Free Body Diagram of Compound Flexure

Figure II-5 is a free body diagram of the compound circular flexure with the flexures displaced axially. Flexure 1 permits bending about the x axis. Flexure 2 permits bending about the y axis. In the figure:

r_1 is the distance from flexure 1 to the center of mass of the suspended element.

r_2 is the distance from flexure 2 to the center of mass of the suspended element.

x and y are the rotating system coordinates.

a_X and a_Y are the components of acceleration in the rotating system.

X and Y are the fixed system coordinates.

Ωt is the rotation angle between the fixed and rotating systems.

In the rotating system, the torques required to keep the suspended element at null are:

$$T_X = -r_1 M a_Y \qquad \text{(II-4)}$$

$$T_Y = r_2 M a_X \qquad \text{(II-5)}$$

a_X and a_Y are time varying accelerations resulting from steady-state acceleration in the fixed system. The transformation from fixed to rotating system with the rotation as shown is:

$$\begin{bmatrix} a_x \\ a_y \end{bmatrix} = \begin{bmatrix} \cos\Omega t & -\sin\Omega t \\ \sin\Omega t & \cos\Omega t \end{bmatrix} \begin{bmatrix} a_X \\ a_Y \end{bmatrix},$$

where a_X and a_Y are the steady-state acceleration components in the fixed system. The acceleration components in the rotating system are thus seen to be:

$$a_x = a_X \cos\Omega t - a_Y \sin\Omega t$$

$$a_y = a_Y \cos\Omega t + a_X \sin\Omega t.$$

Using these expressions in Equations (II-4) and (II-5) gives the torque in the rotating system due to steady-state acceleration in the fixed system:

$$T_x = -r_1 M(a_Y \cos\Omega t + a_X \sin\Omega t) \qquad \text{(II-6)}$$

$$T_y = -r_2 M(a_X \cos\Omega t - a_Y \sin\Omega t). \qquad \text{(II-7)}$$

Transforming these expressions to the fixed system yields:

$$\begin{bmatrix} T_X \\ T_Y \end{bmatrix} = \begin{bmatrix} \cos\Omega t & \sin\Omega t \\ -\sin\Omega t & \cos\Omega t \end{bmatrix} \begin{bmatrix} T_x \\ T_y \end{bmatrix}, \text{ or}$$

$$T_X = T_x \cos\Omega t + T_y \sin\Omega t$$

$$T_Y = -T_x \sin\Omega t + T_y \cos\Omega t.$$

Substituting the values of T_x and T_y from Equations (II-6) and (II-7),

$$T_X = -r_1 M (a_Y \cos\Omega t + a_X \sin\Omega t) \cos\Omega t$$
$$-r_2 M (a_X \cos\Omega t - a_Y \sin\Omega t) \sin\Omega t, \qquad \text{(II-8)}$$

$$T_Y = r_1 M (a_Y \cos\Omega t + a_X \sin\Omega t) \sin\Omega t$$
$$-r_2 M (a_X \cos\Omega t - a_Y \sin\Omega t) \cos\Omega t \qquad \text{(II-9)}$$

Rewriting Equation (II-8),

$$T_X = -r_1 Ma_Y \cos\Omega t \cos\Omega t - r_1 Ma_X \sin\Omega t \cos\Omega t$$
$$-r_2 Ma_X \cos\Omega t \sin\Omega t + r_2 Ma_Y \sin\Omega t \sin\Omega t.$$

Let $r_1 = r_2 + \Delta$. Then,

$$T_X = -Ma_Y r_2 (\cos^2\Omega t - \sin^2\Omega t) - Ma_Y \Delta \cos^2\Omega t$$
$$-Ma_X r_2 (\sin\Omega t \cos\Omega t + \cos\Omega t \sin\Omega t)$$
$$-Ma_X \Delta \sin\Omega t \cos\Omega t$$

$$= -Ma_Y r_2 \cos 2\Omega t - Ma_Y \Delta \frac{1}{2} (1 + \cos 2\Omega t)$$

$$-Ma_X r_2 \sin 2\Omega t - Ma_X \Delta \frac{1}{2} \sin 2\Omega t$$

$$T_X = -Ma_Y \left\{ (r_2 + \frac{\Delta}{2}) \cos 2\Omega t + \frac{1}{2}\Delta \right\} - Ma_X (r_2 + \frac{\Delta}{2}) \sin 2\Omega t.$$

In a similar manner T_Y can be shown to be:

$$T_Y = Ma_Y (r_2 + \frac{\Delta}{2}) \sin 2\Omega t$$
$$-Ma_X \frac{l}{l} (r_2 + \frac{\Delta}{2}) \cos 2\Omega t + \frac{1}{2}\Delta \frac{l}{l}.$$

It is thus seen that the axial displacement of the two orthogonal flexures causes 2Ω signals in the fixed system in response to acceleration (or g-loading) perpendicular to the axis of the suspension. The dc terms are analogous to axial mass unbalance with a conventional pivot. If the center of mass is located midway between the two flexures ($r_1 = r_2 = r$, and $\Delta = 0$), the equations become:

$$T_X = -Mr (a_Y \cos 2\Omega t + a_X \sin 2\Omega t) \quad \text{(II-10)}$$

$$T_Y = -Mr (a_Y \sin 2\Omega t - a_X \cos 2\Omega t) \quad \text{(II-11)}$$

Equations (II-10) and (II-11) show that either of the fixed axis torque feedback signals can be used to determine the acceleration components in both axes. In actual operation the acceleration signals are derived in the torque feedback mode. The X-axis signal is demodulated with $\sin 2\Omega t$ and $\cos 2\Omega t$ reference phases. The outputs of these demodulators are dc signals proportional to a_X and a_Y. These signals are appropriately scaled to provide signals that are used to compensate the g-sensitive Nutatron noise. This is discussed in Section IV.C.2.h.

APPENDIX III
NUTATRON ELECTRONICS
SCHEMATICS AND LAYOUTS

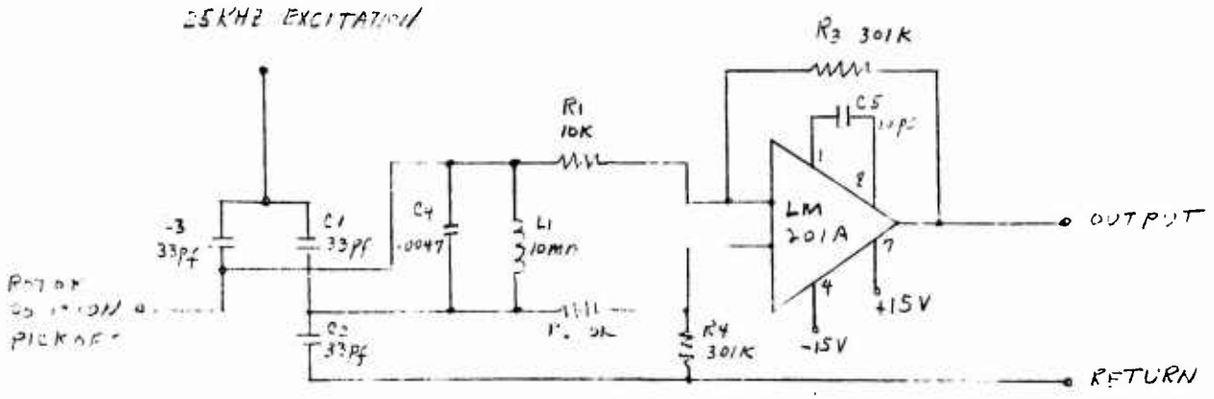

Figure III-1a. Rotor Position Pickoff Preamp

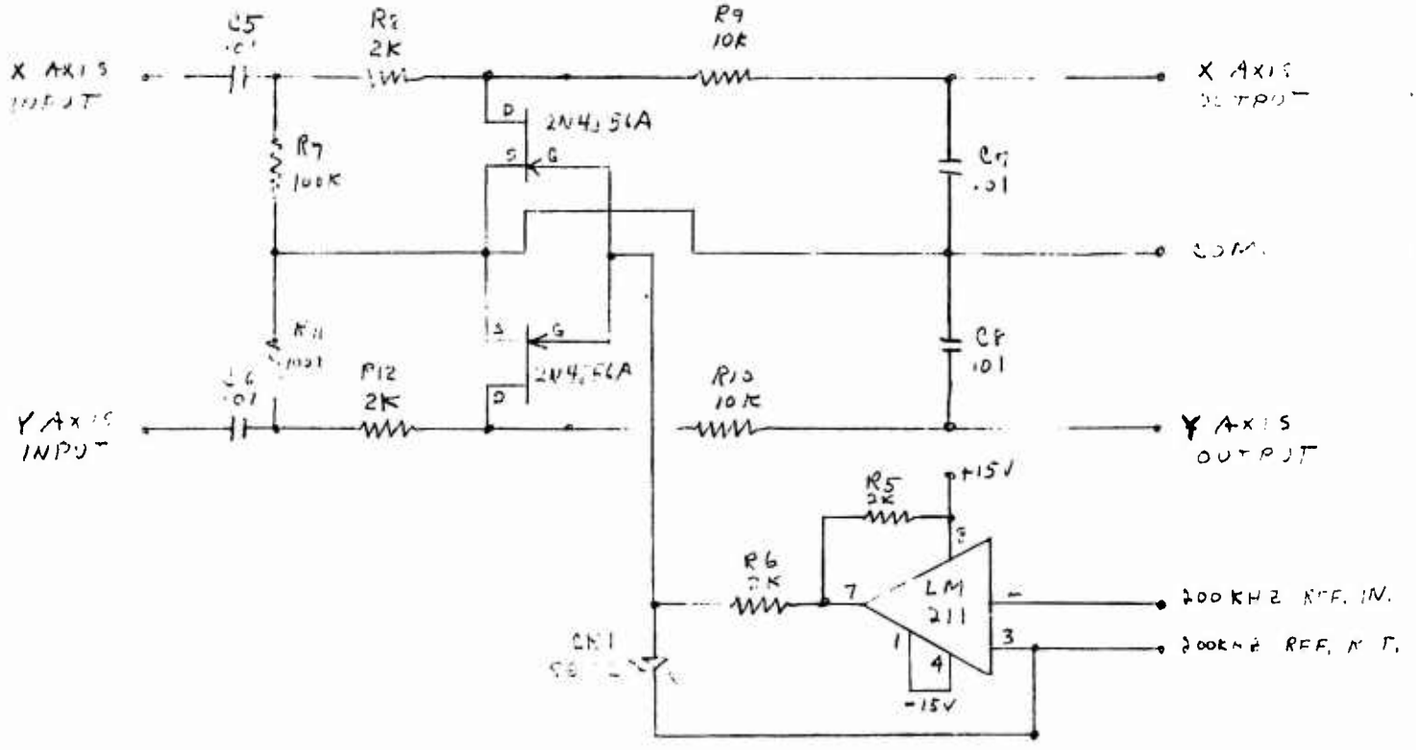

Figure III-1b. 200 kHz Ref Driver and Demodulators

Figure III-1. Nutatron Holding Fixture Electronics

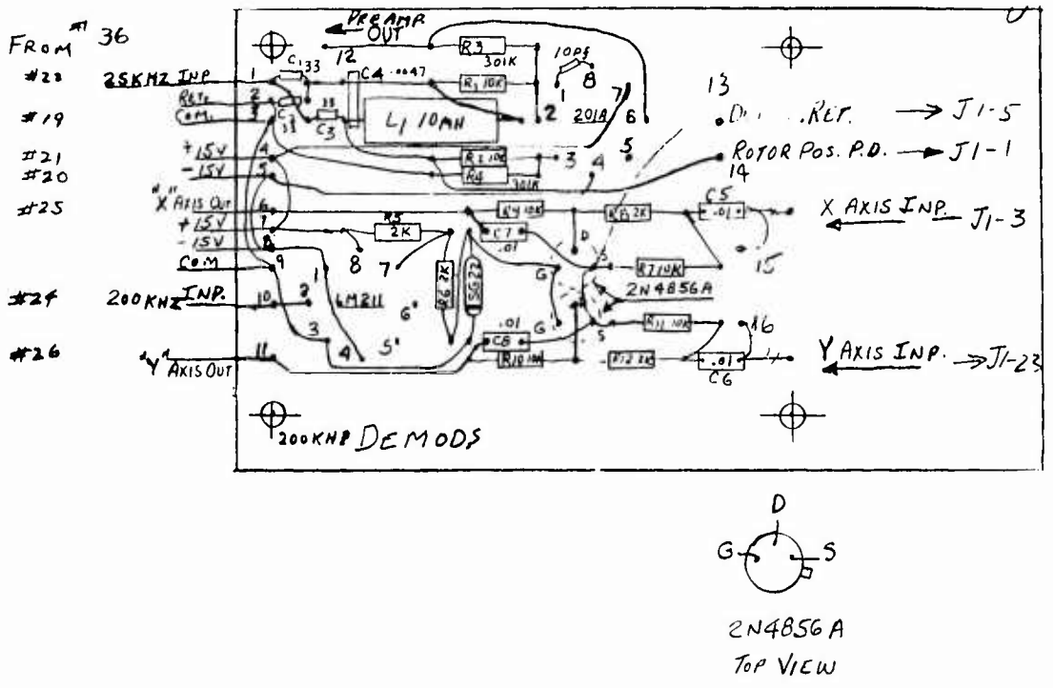

Figure III-2. 25 kHz Rotor Pickoff Preamp

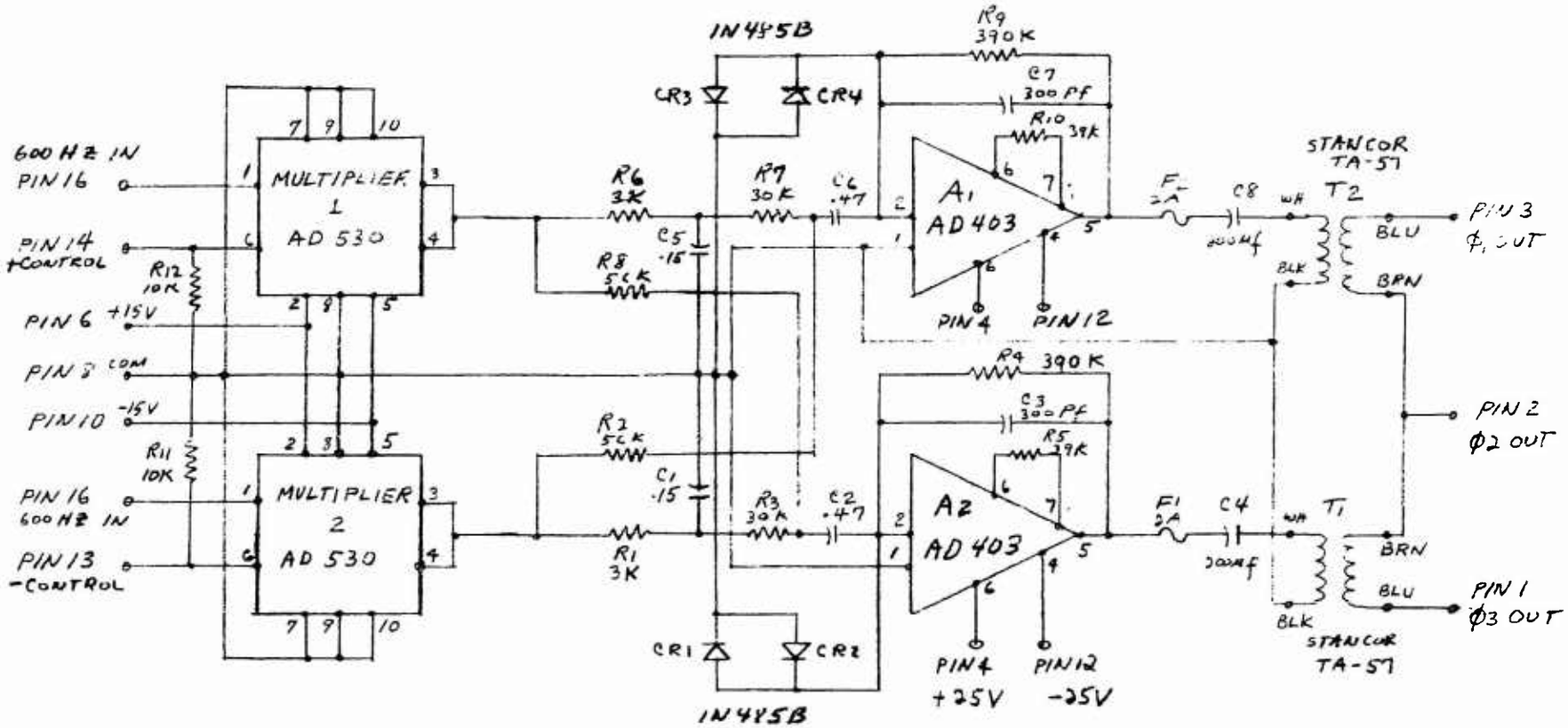

Figure III-3. Spin Motor Power Supply (Board No. 1)

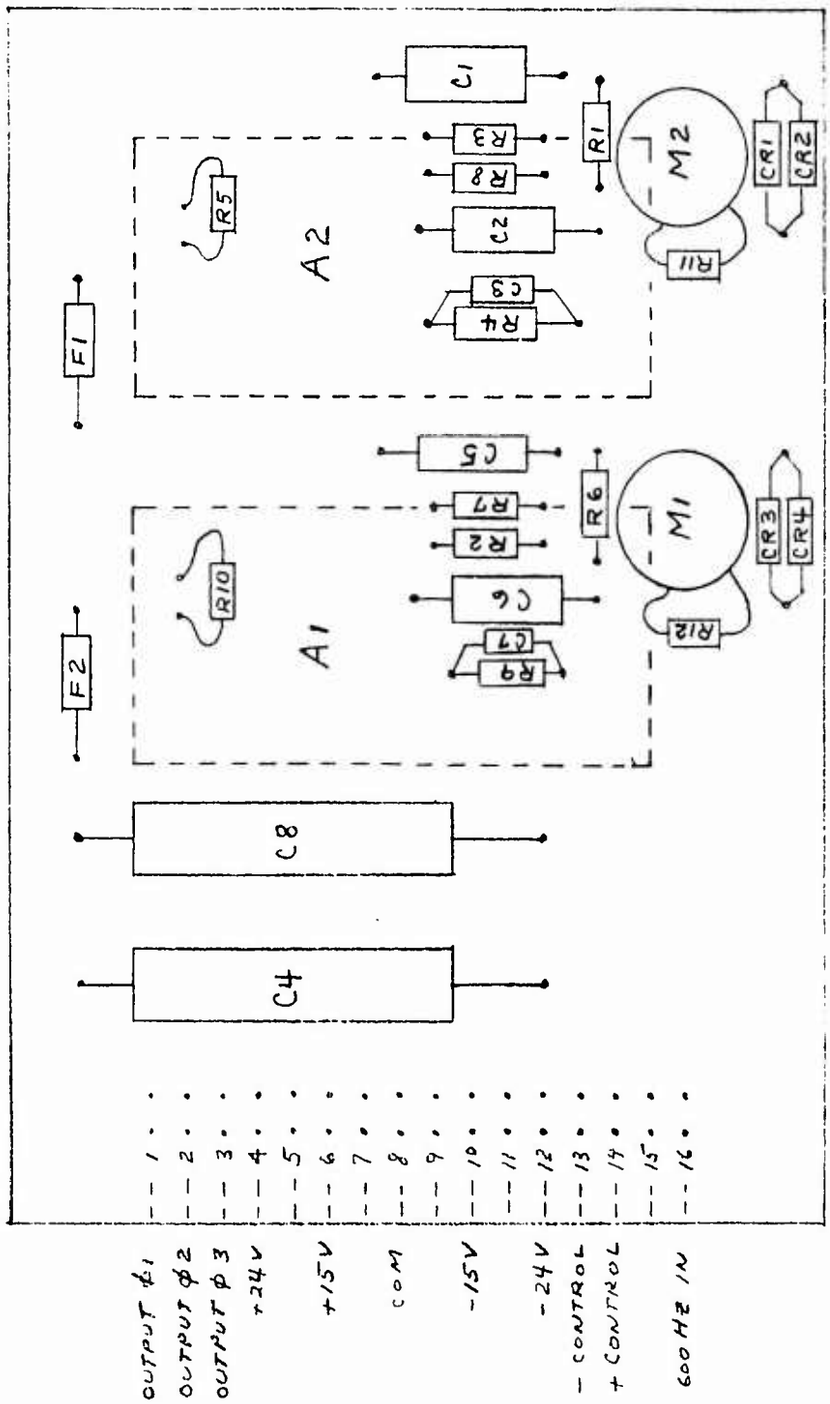

Figure III-4. Board No. 1 Layout

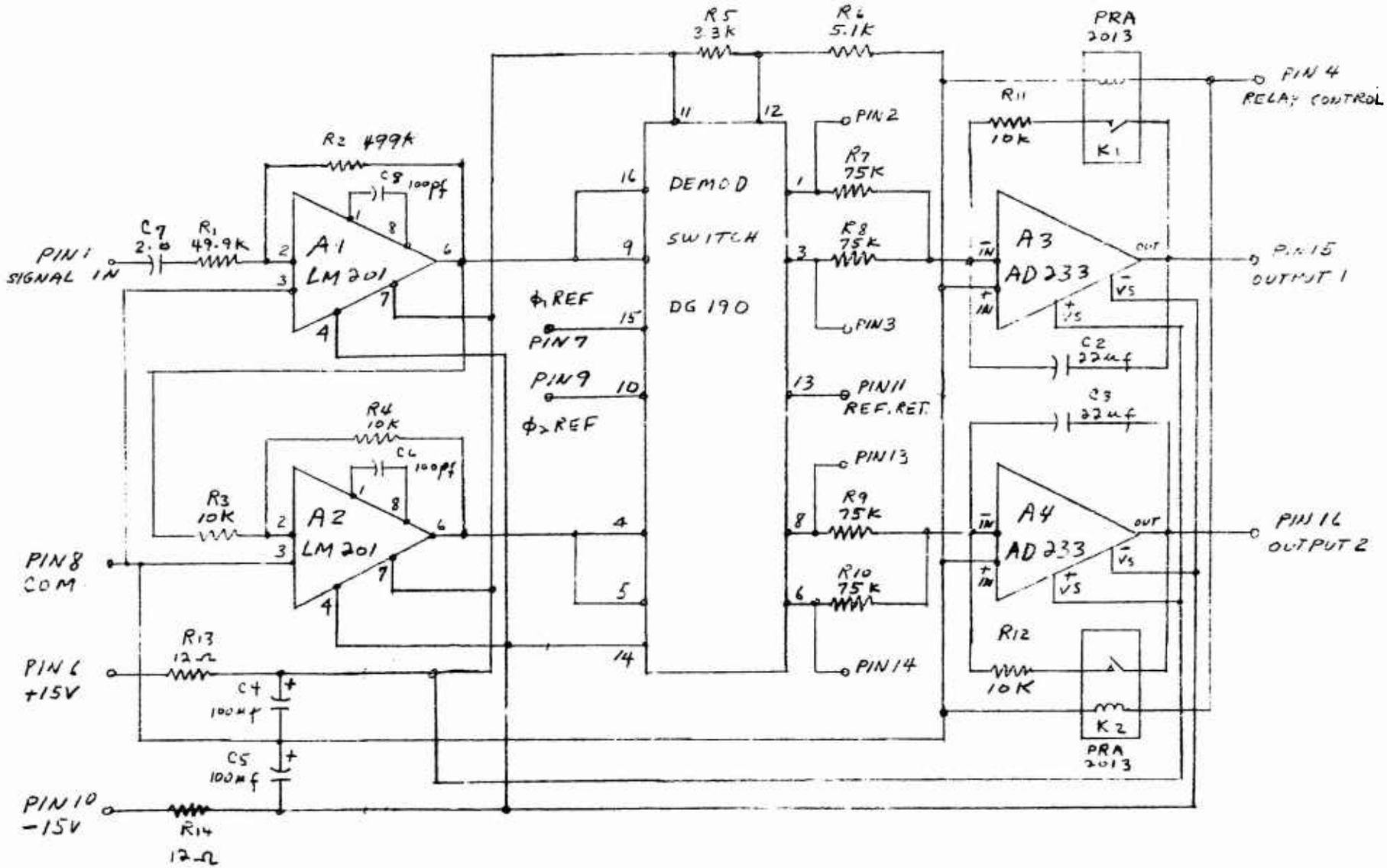

Figure III-5. Axis Alignment Amp Demod Integ (Board No. 2)

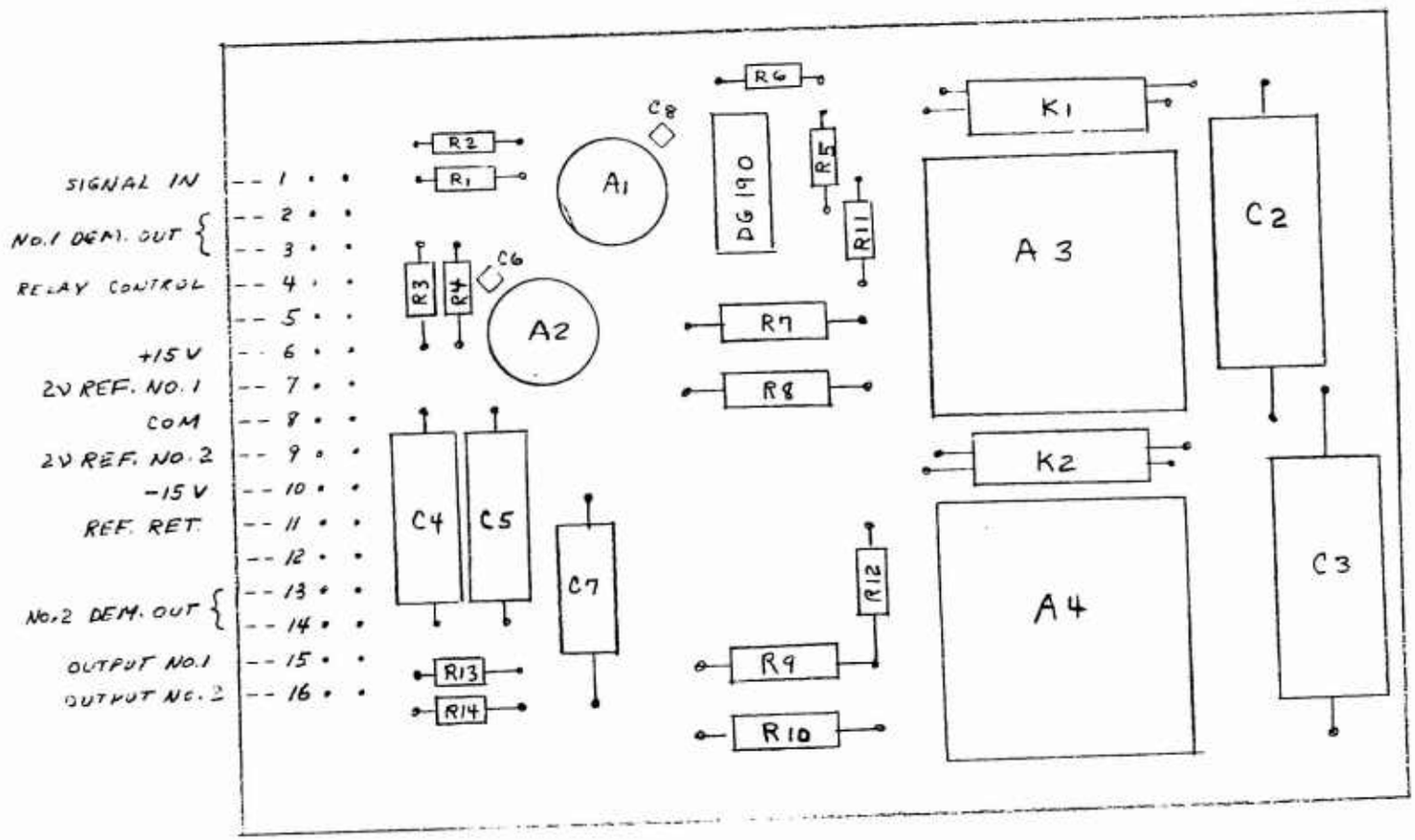

Figure III-6. Board No. 2 Layout

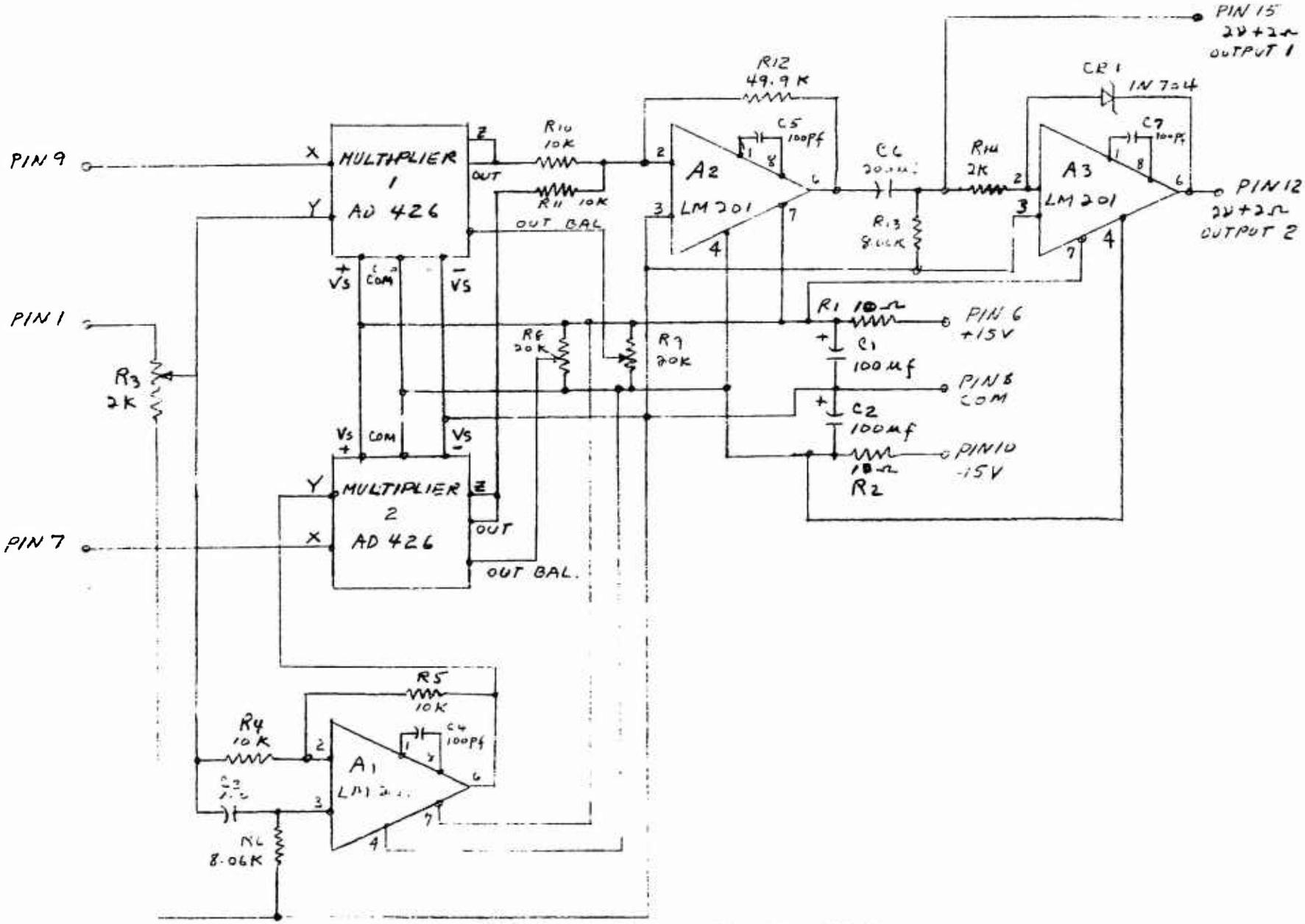

Figure III-7. $\partial v + 2\Omega$ Generator (Mult. Board No. 3)

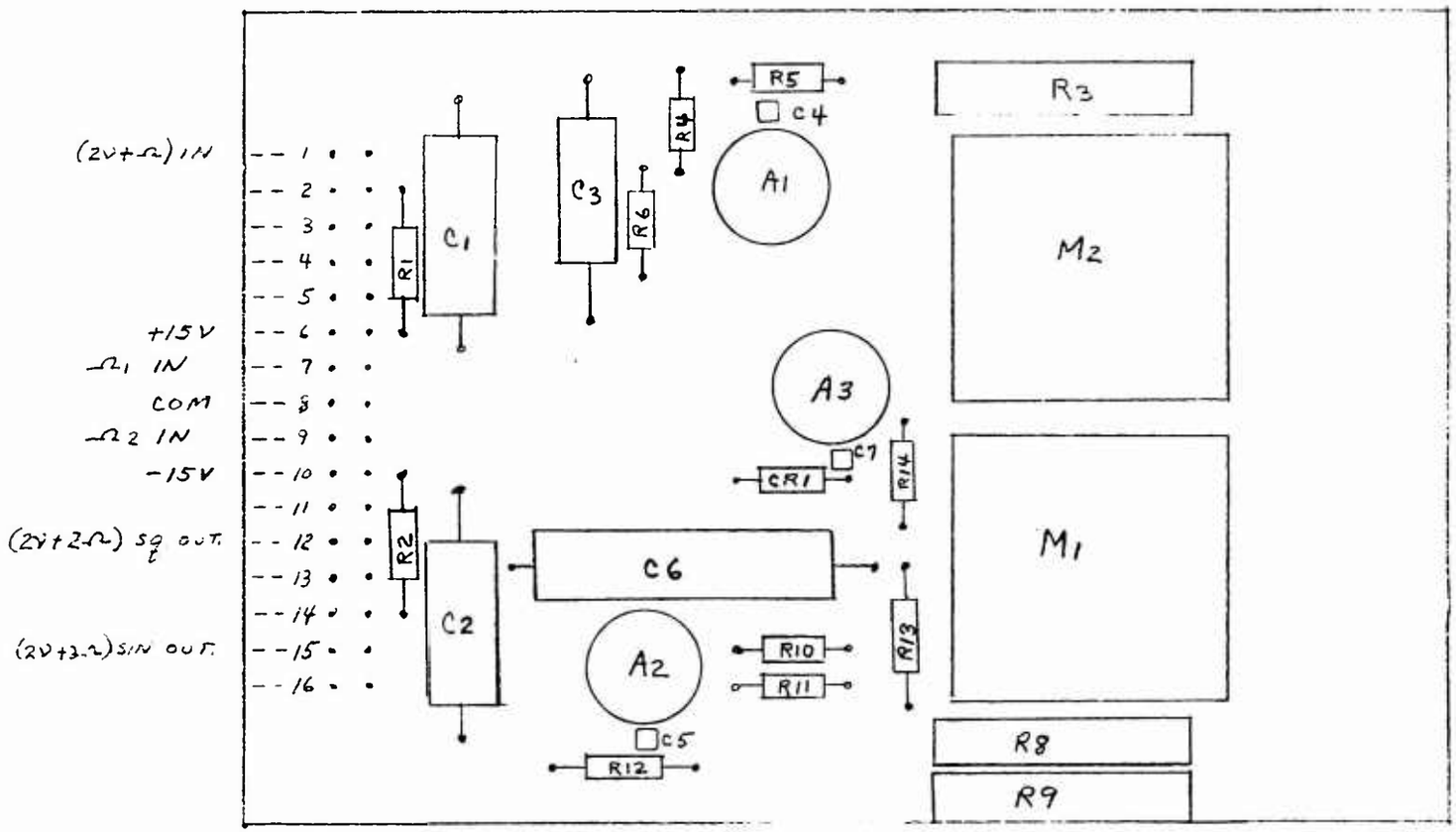

Figure III-8. Board No. 3 Layout

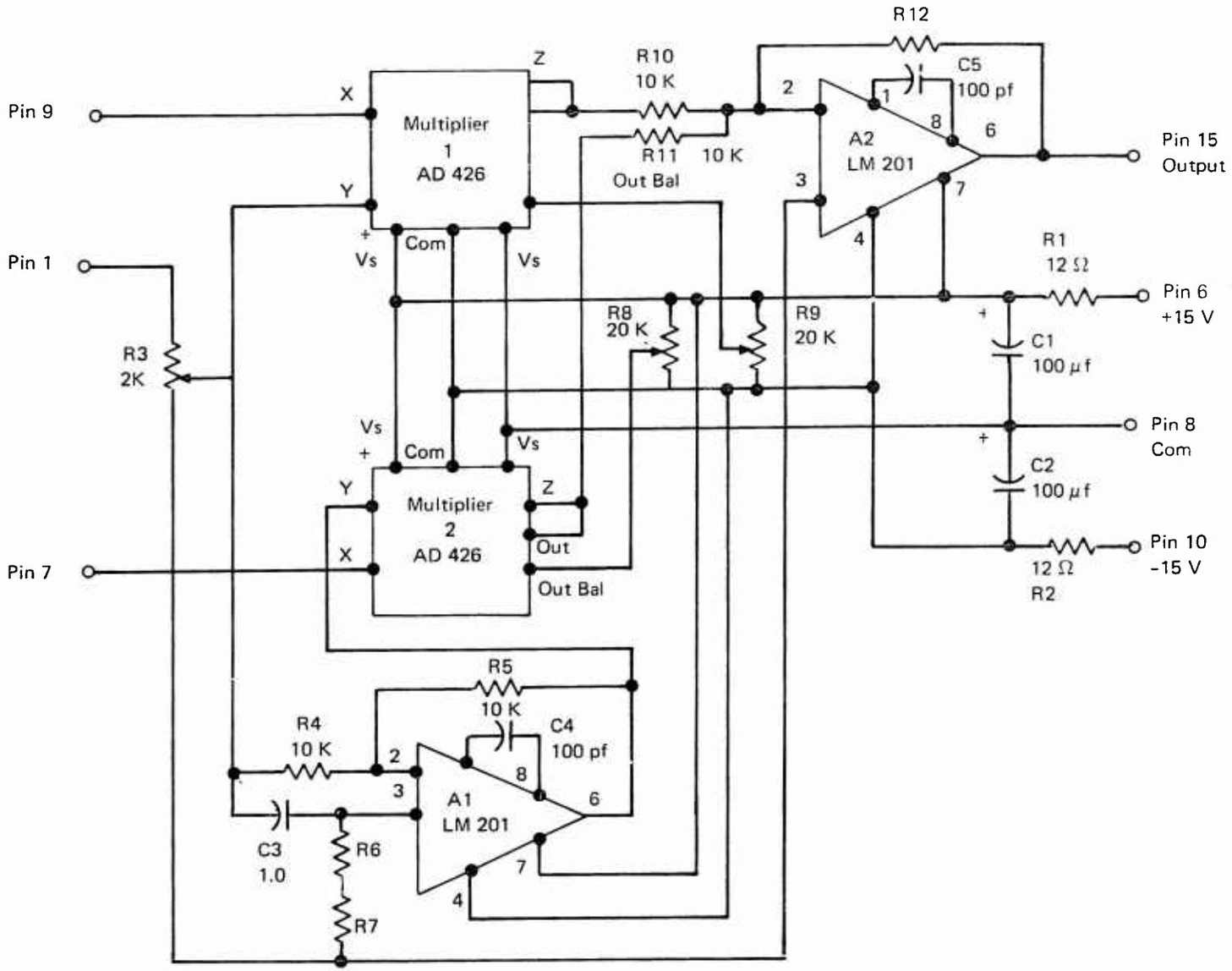

Figure III-9. $2\nu + \Omega$ Generator (Mult Board No. 4)

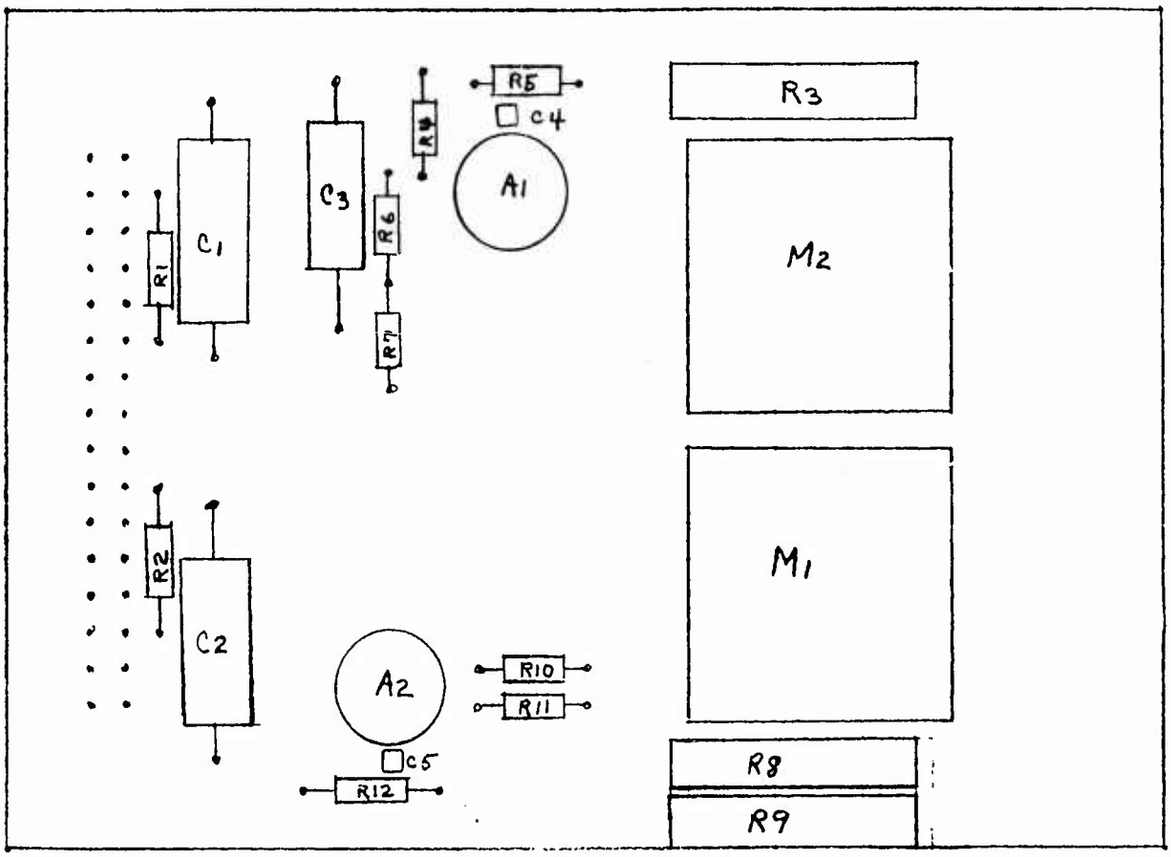

Figure III-10. Board No. 4 Layout

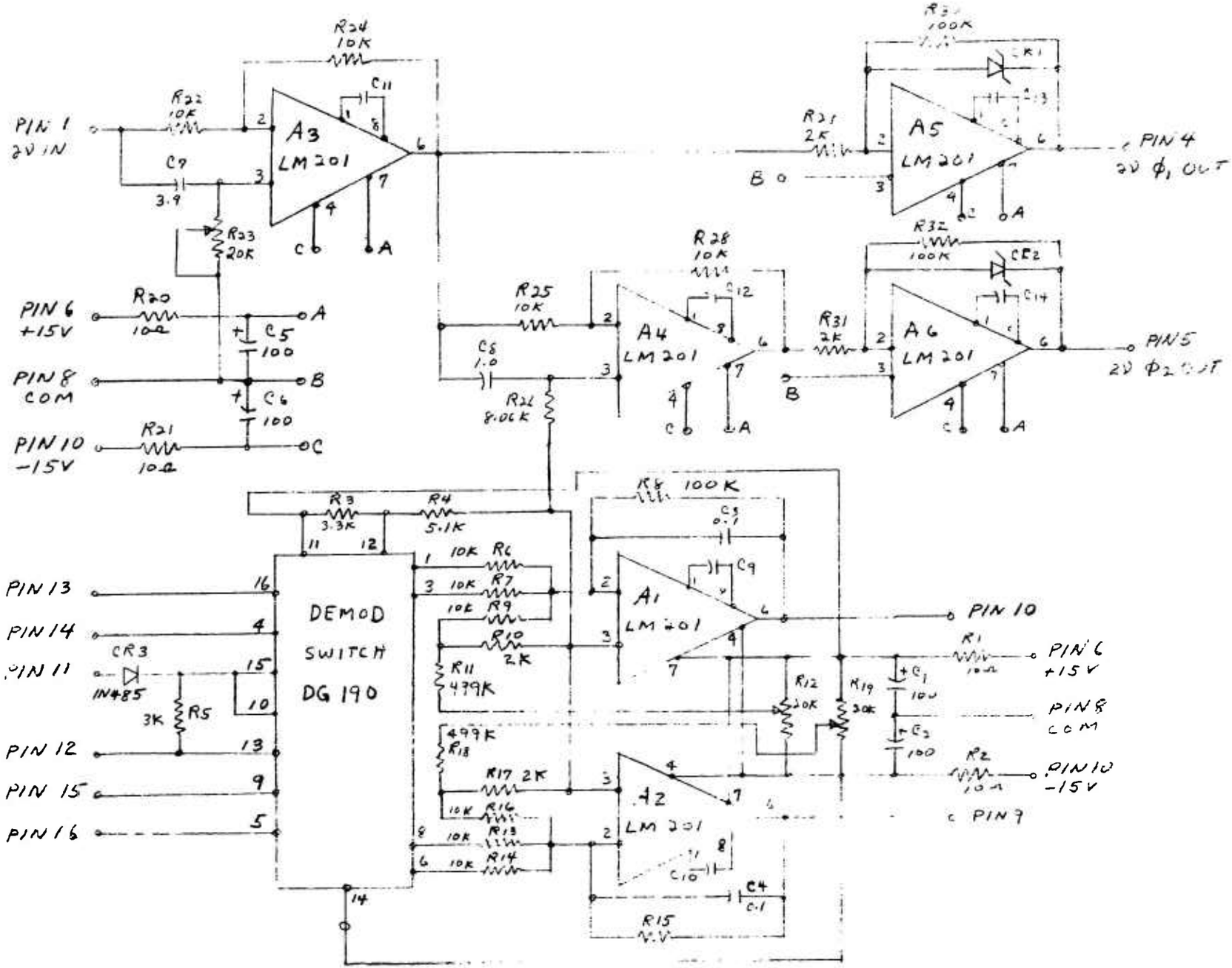

Figure III-11. Board No. 5 2v Ref Gen and Ω Gen

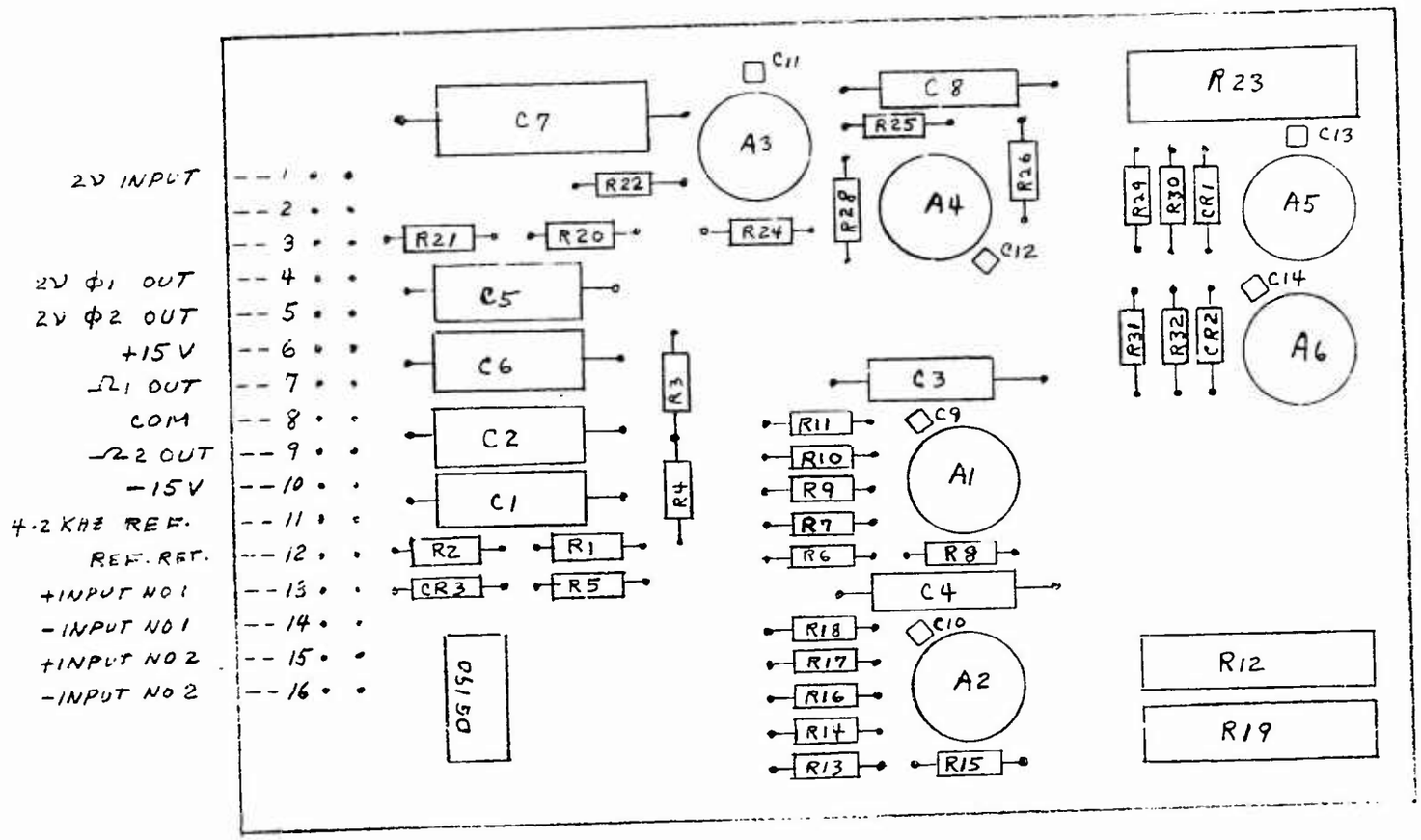

Figure III-12. Board No. 5 Layout

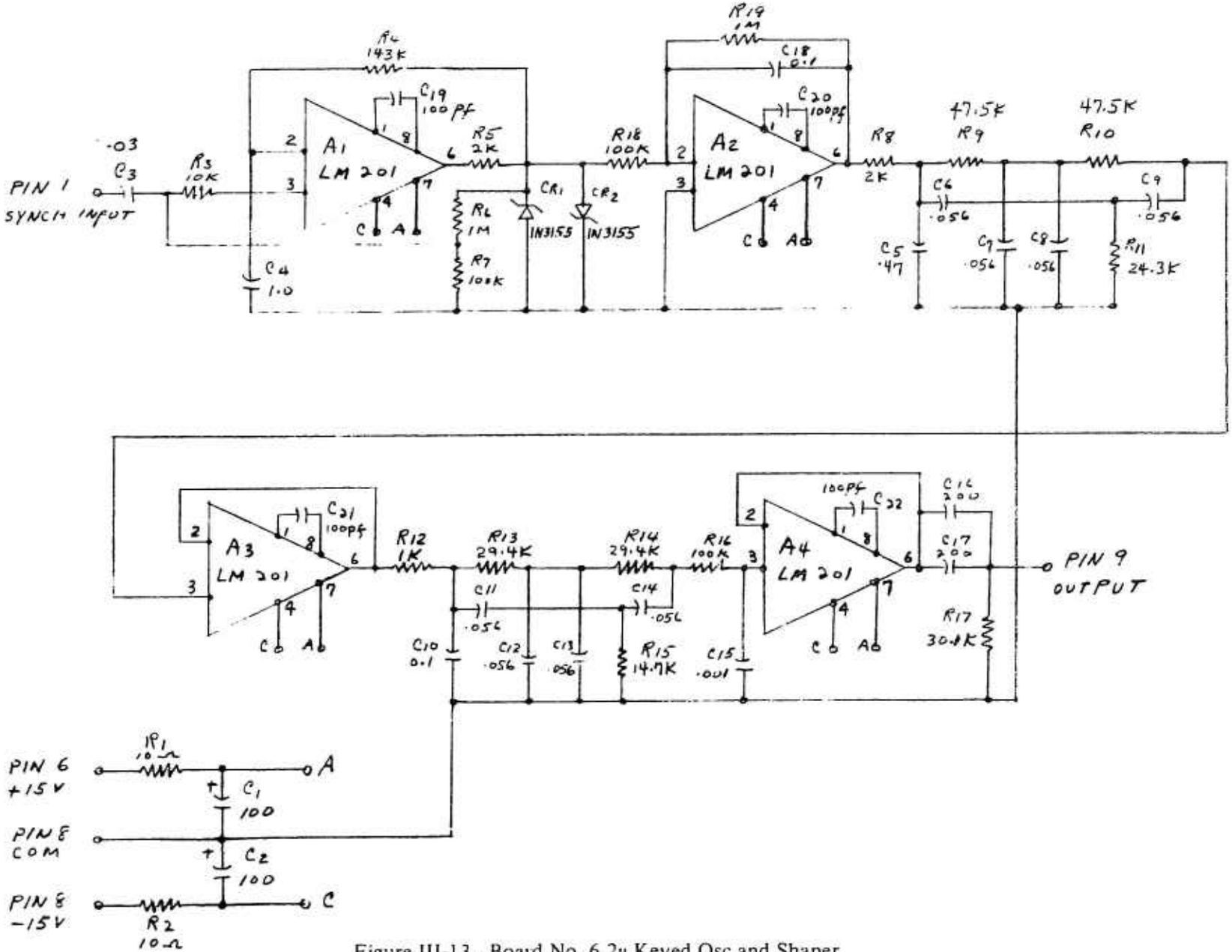

Figure III-13. Board No. 6 2ν Keyed Osc and Shaper

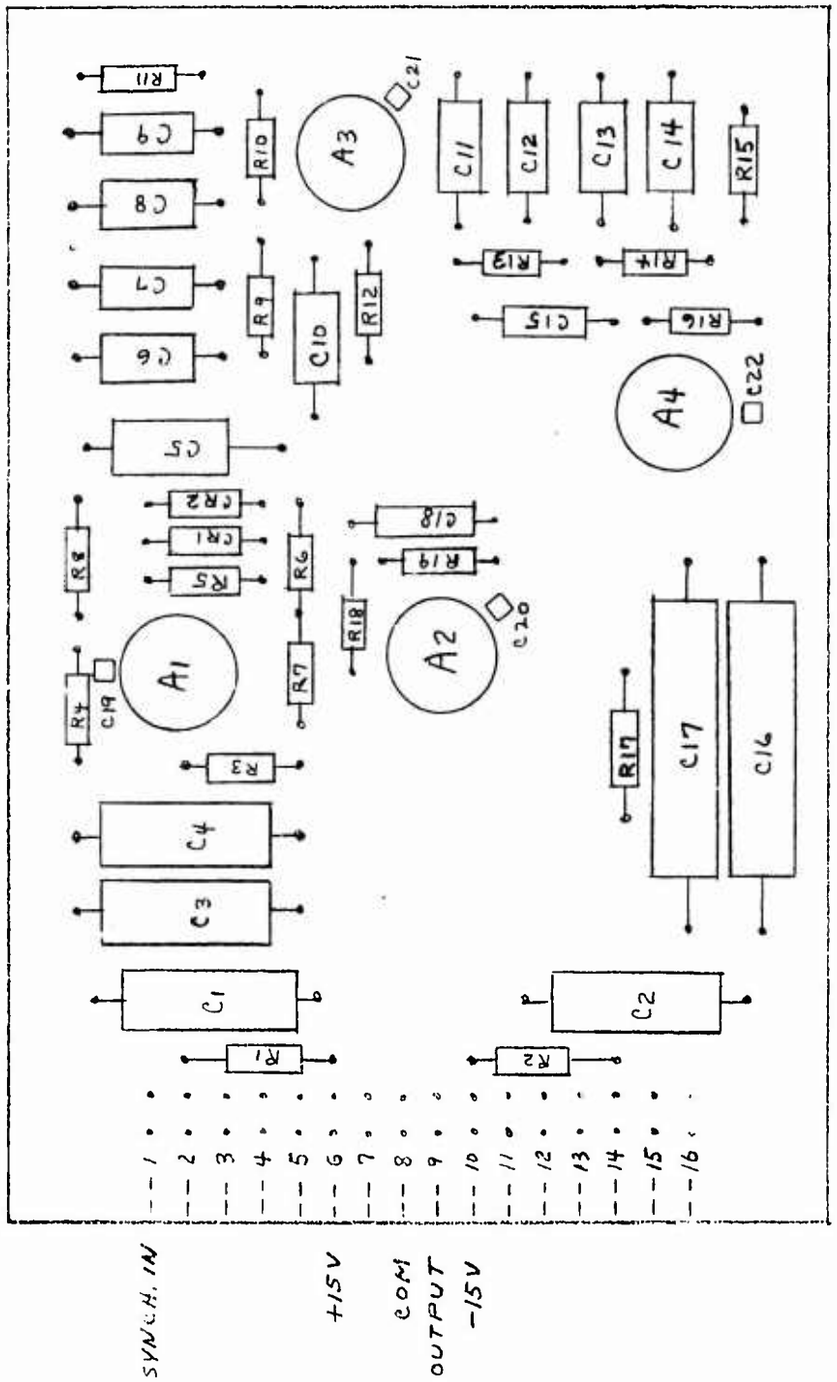

Figure III-14. Board No. 6 Layout

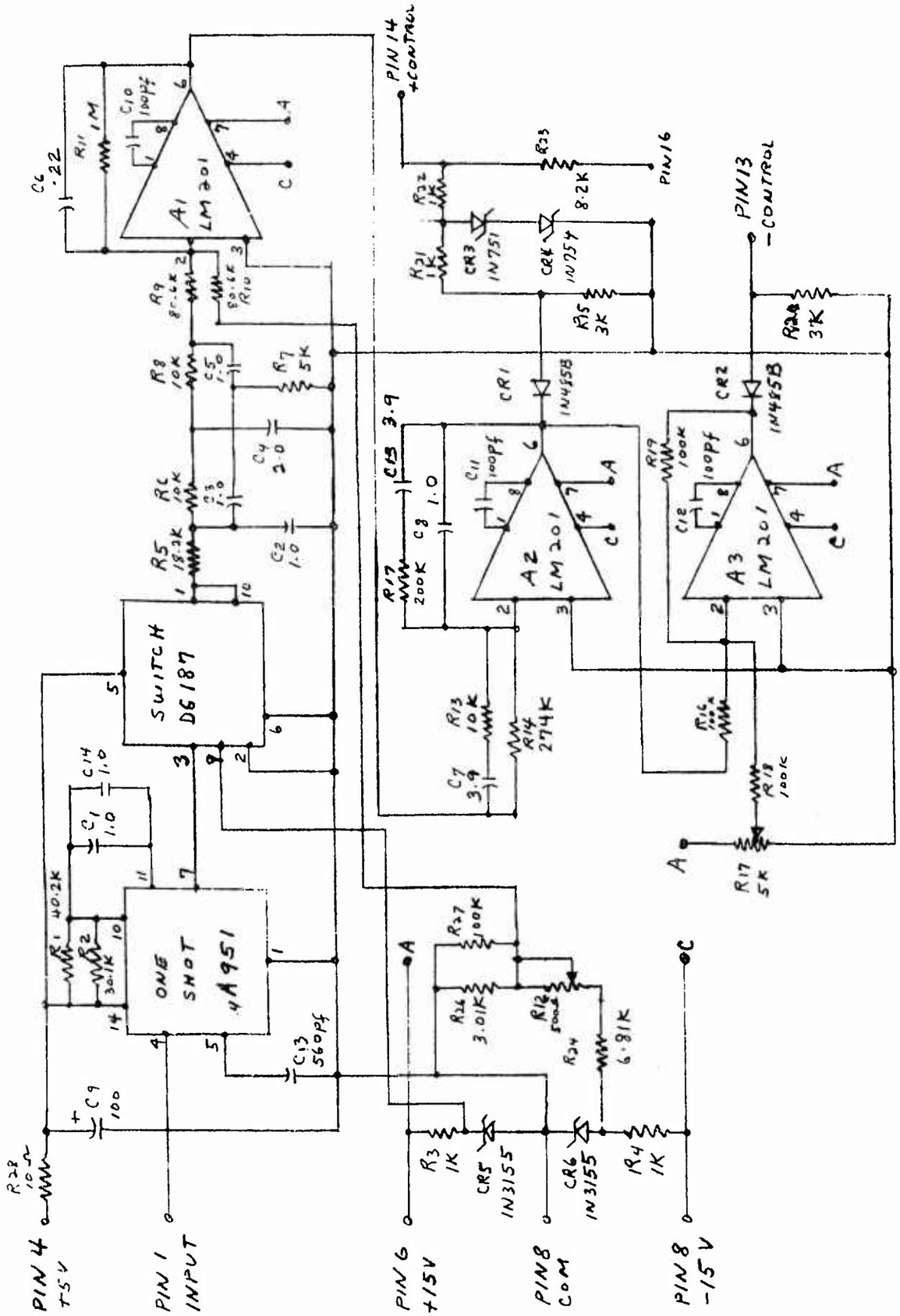

Figure III-15. Board No. 7 Speed Control

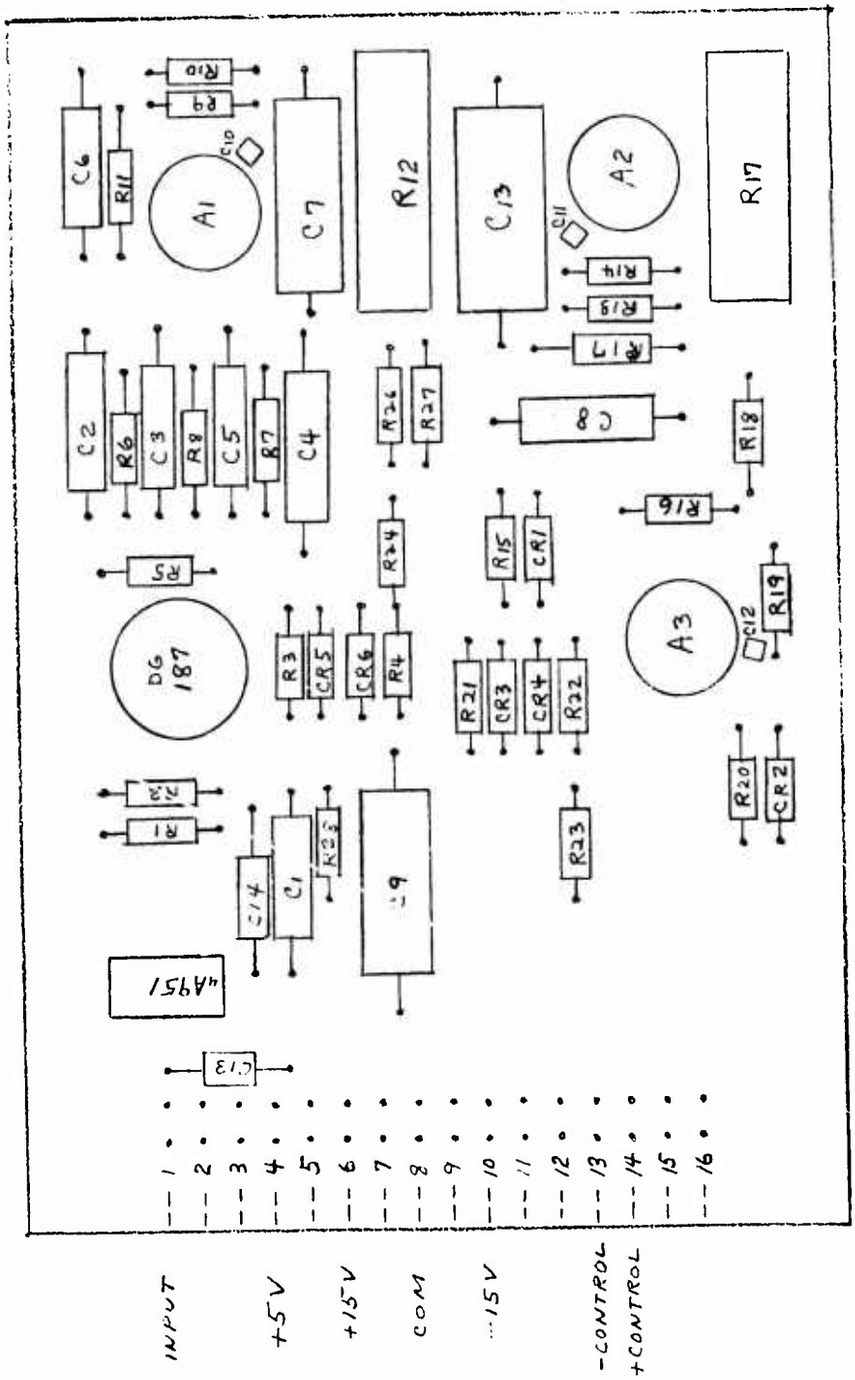

Figure III-16. Board No. 7 Layout

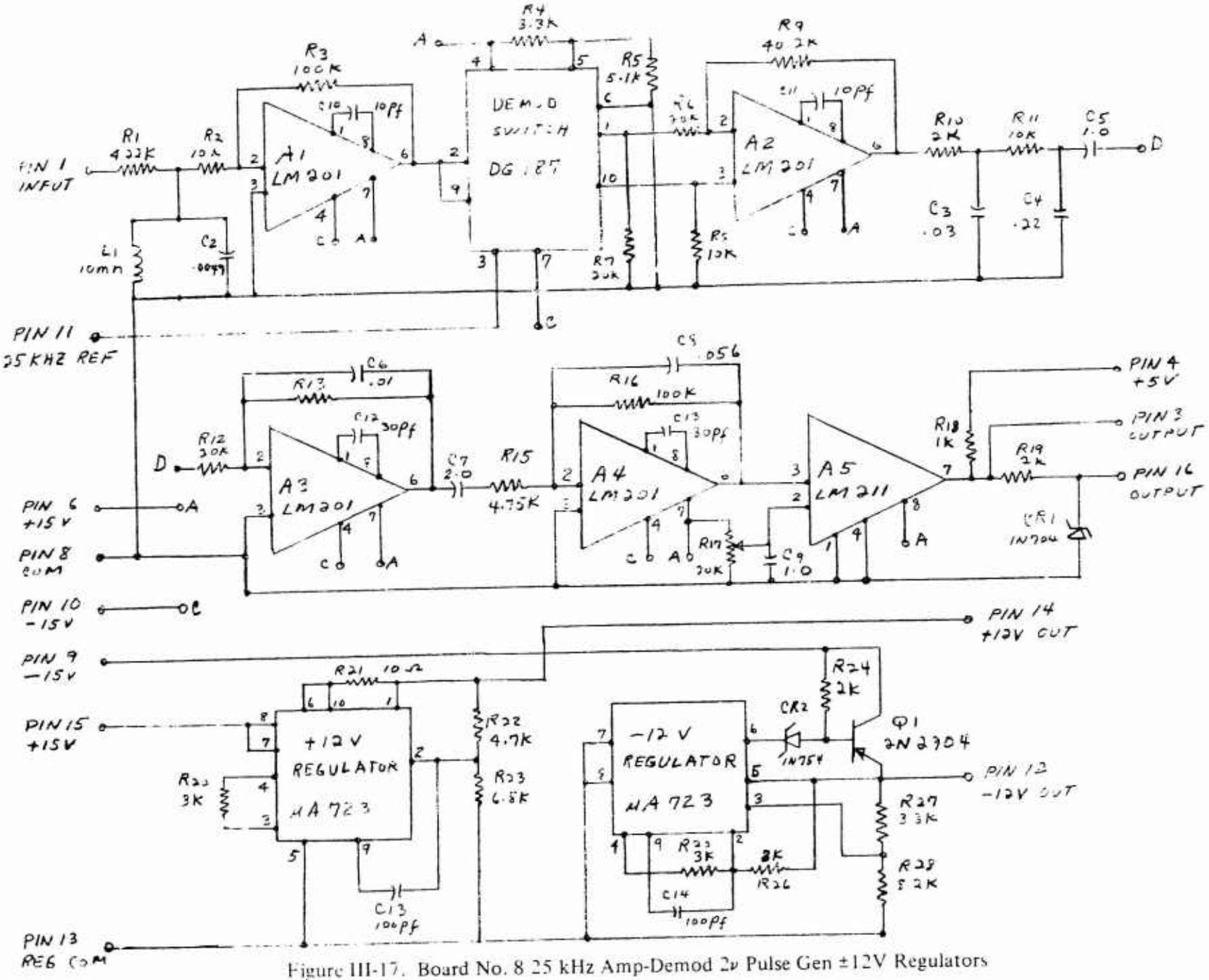

Figure III-17. Board No. 8 25 kHz Amp-Demod 2v Pulse Gen ±12V Regulators

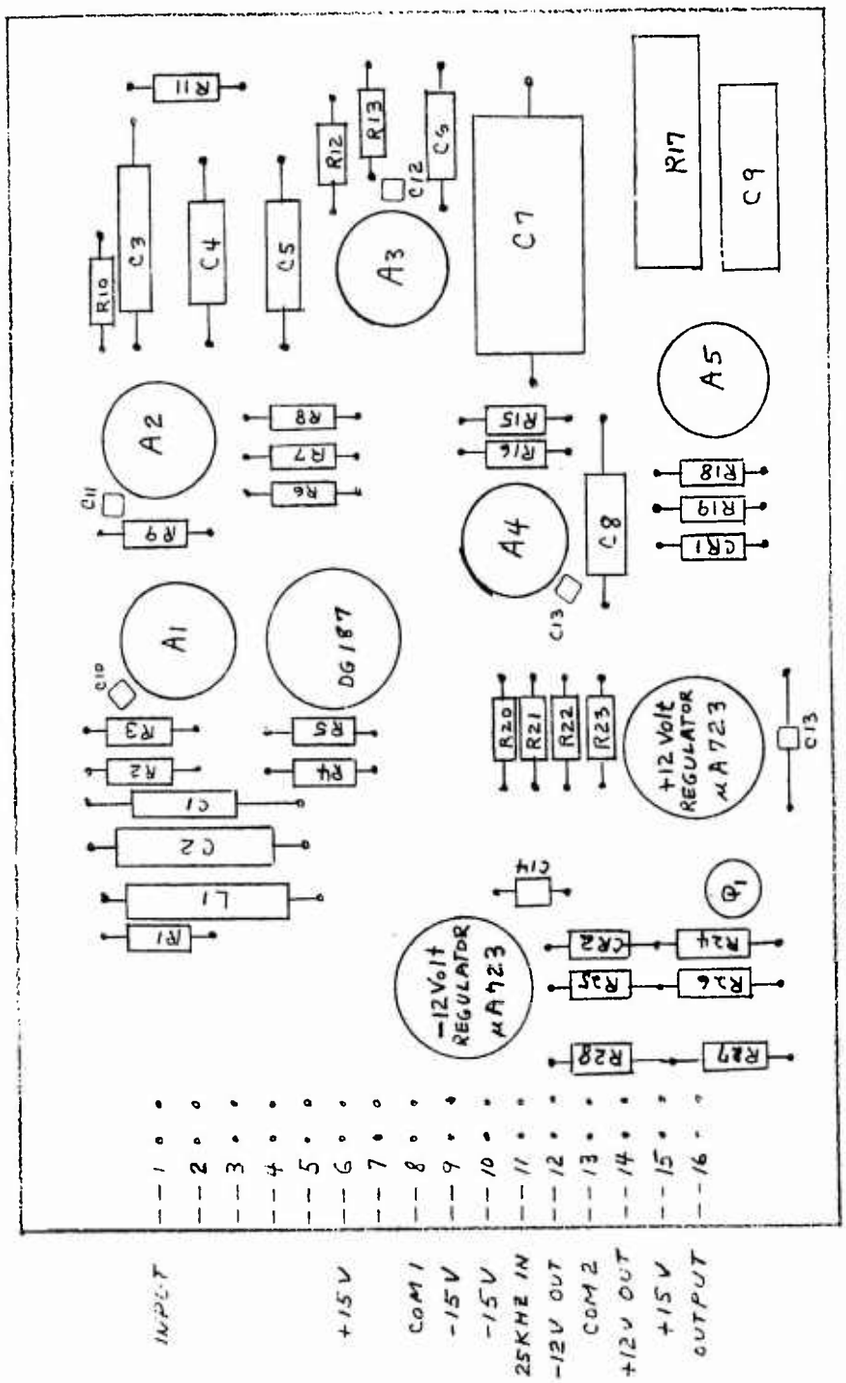

Figure III-18. Board No. 8 Layout

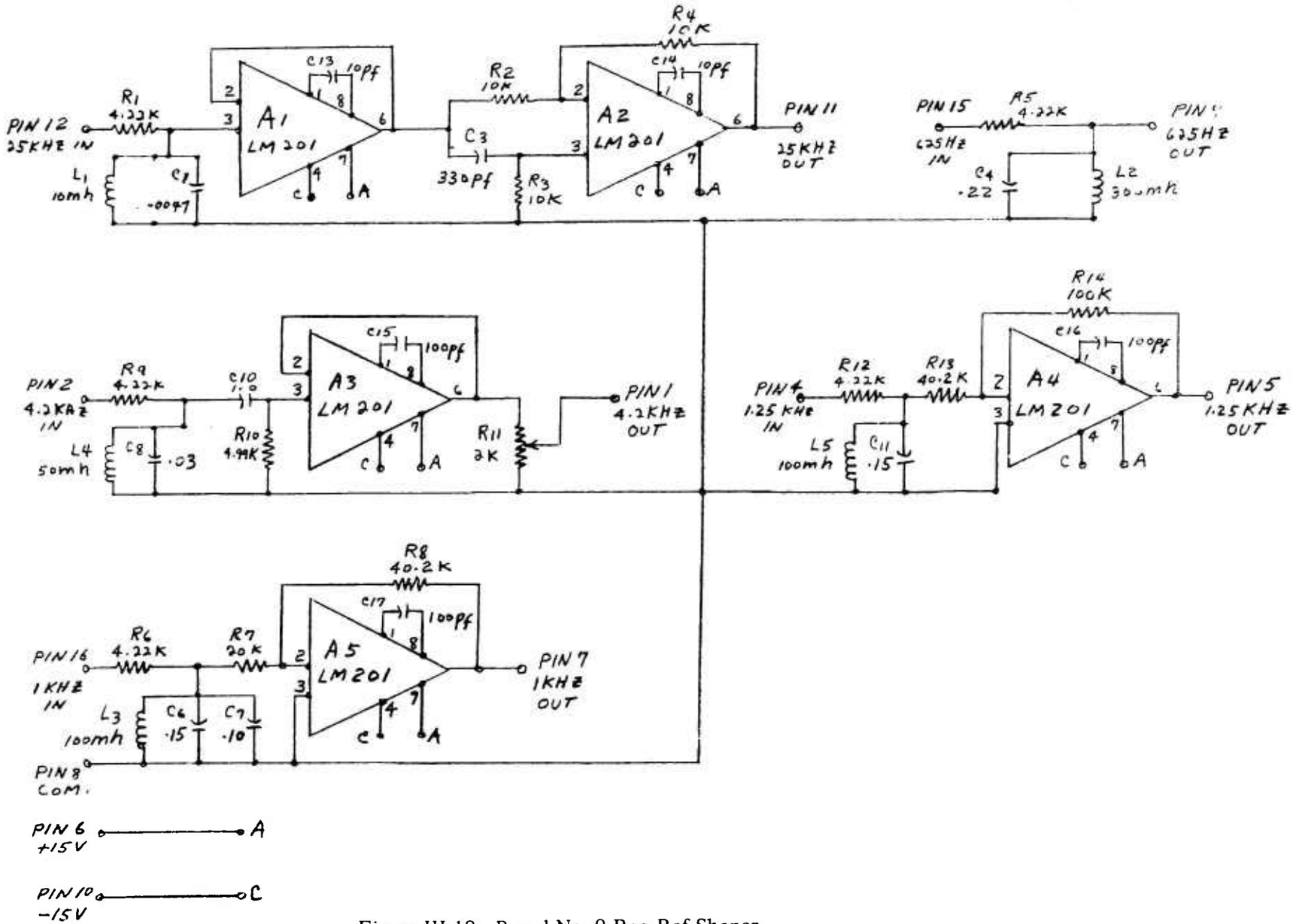

Figure III-19. Board No. 9 Req Ref Shaper

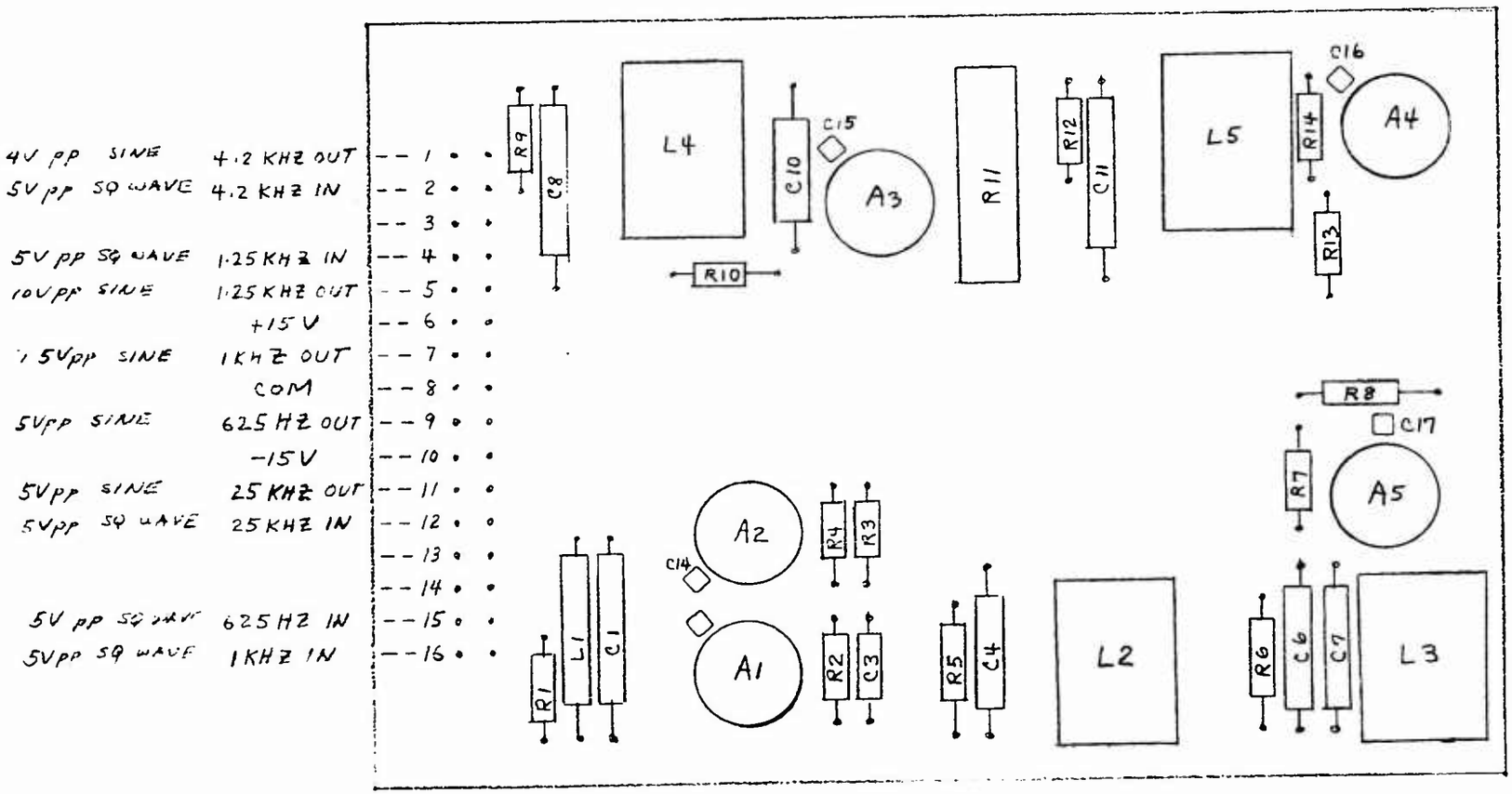

Figure III-20. Board No. 9 Layout

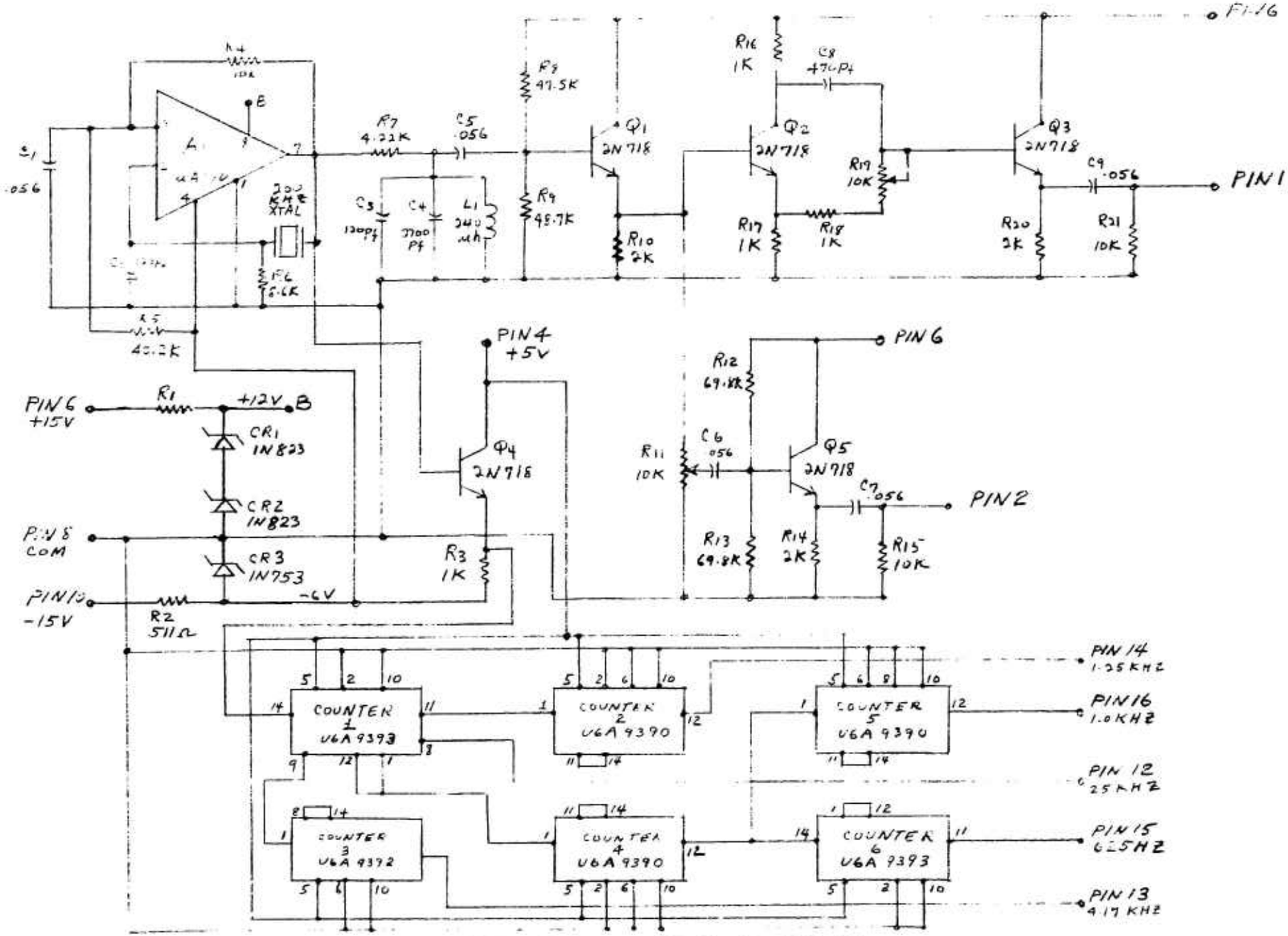

Figure III-21. 200 kHz Oscillator and Divider (Board No. 10)

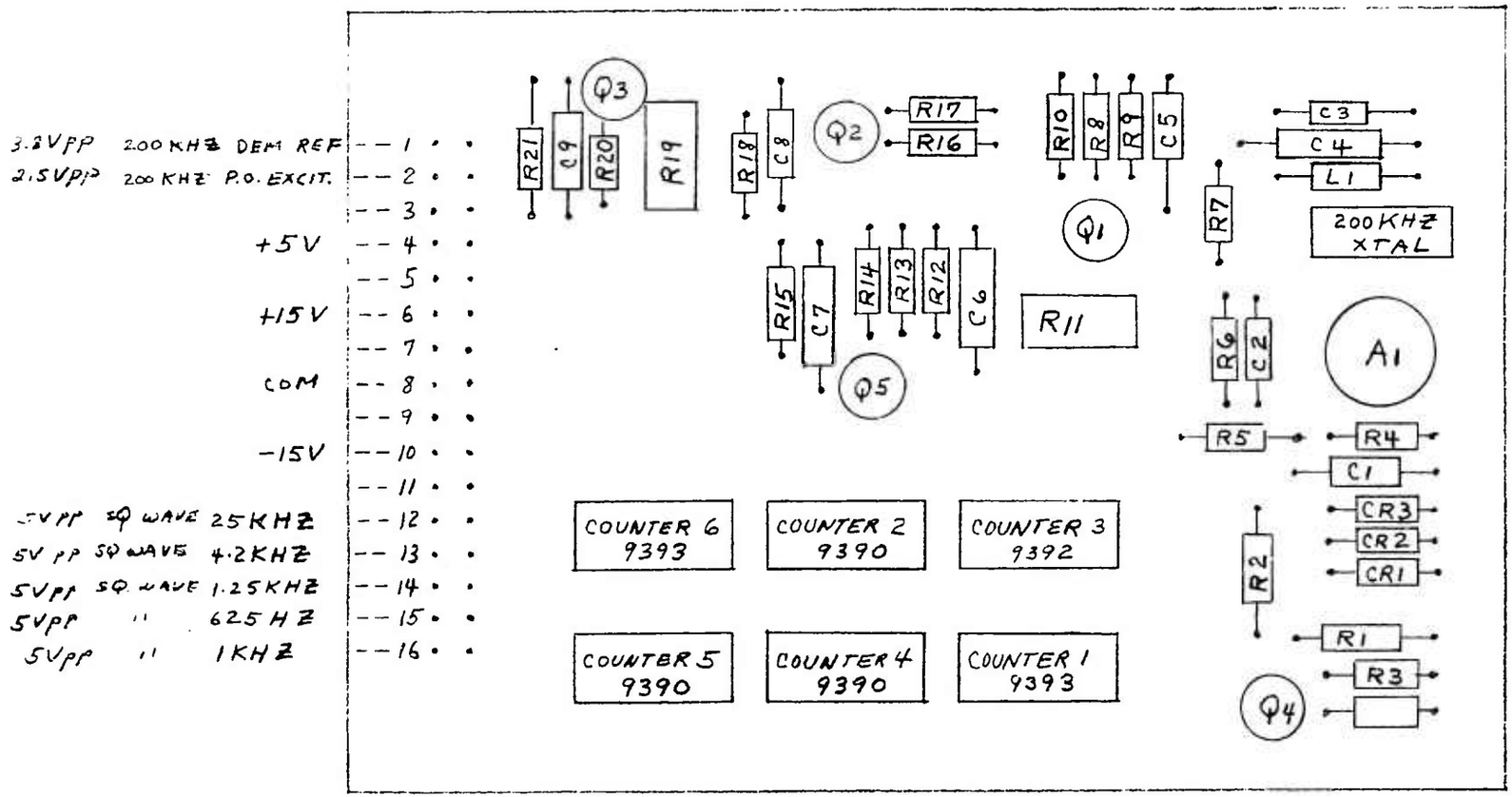

Figure III-22. Board No. 10 Layout

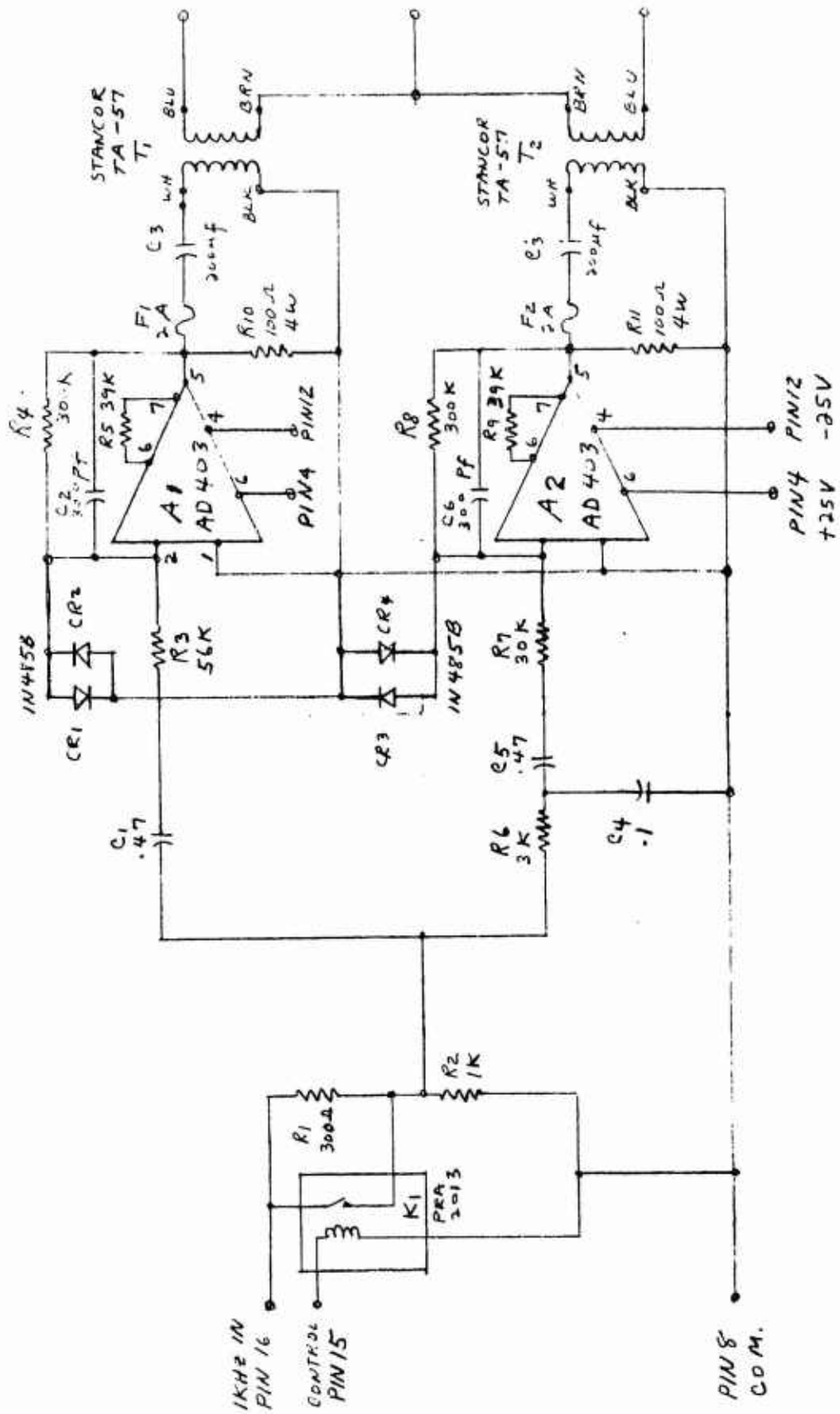

Figure III-23. Housing Drive Power Supply Model No. 1 (Board No. 11)

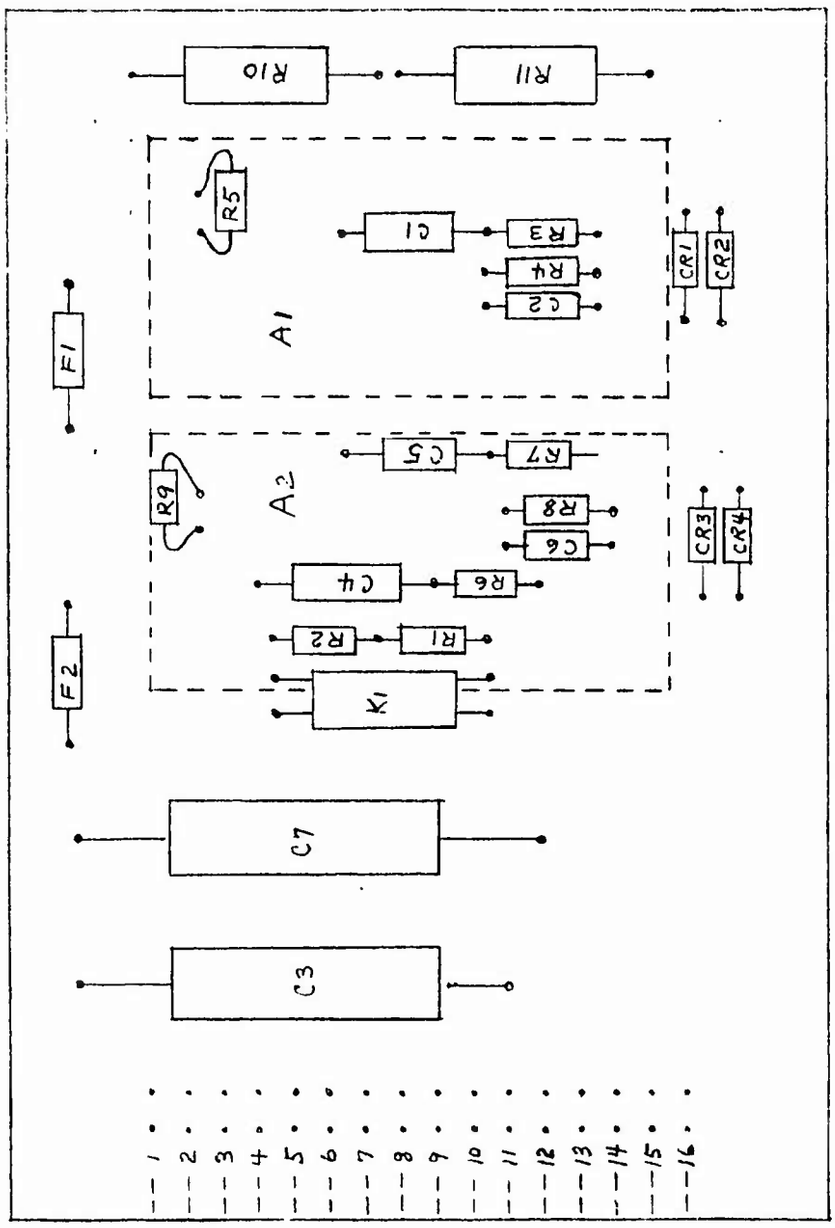

Figure III-24. Board No. 11 Layout

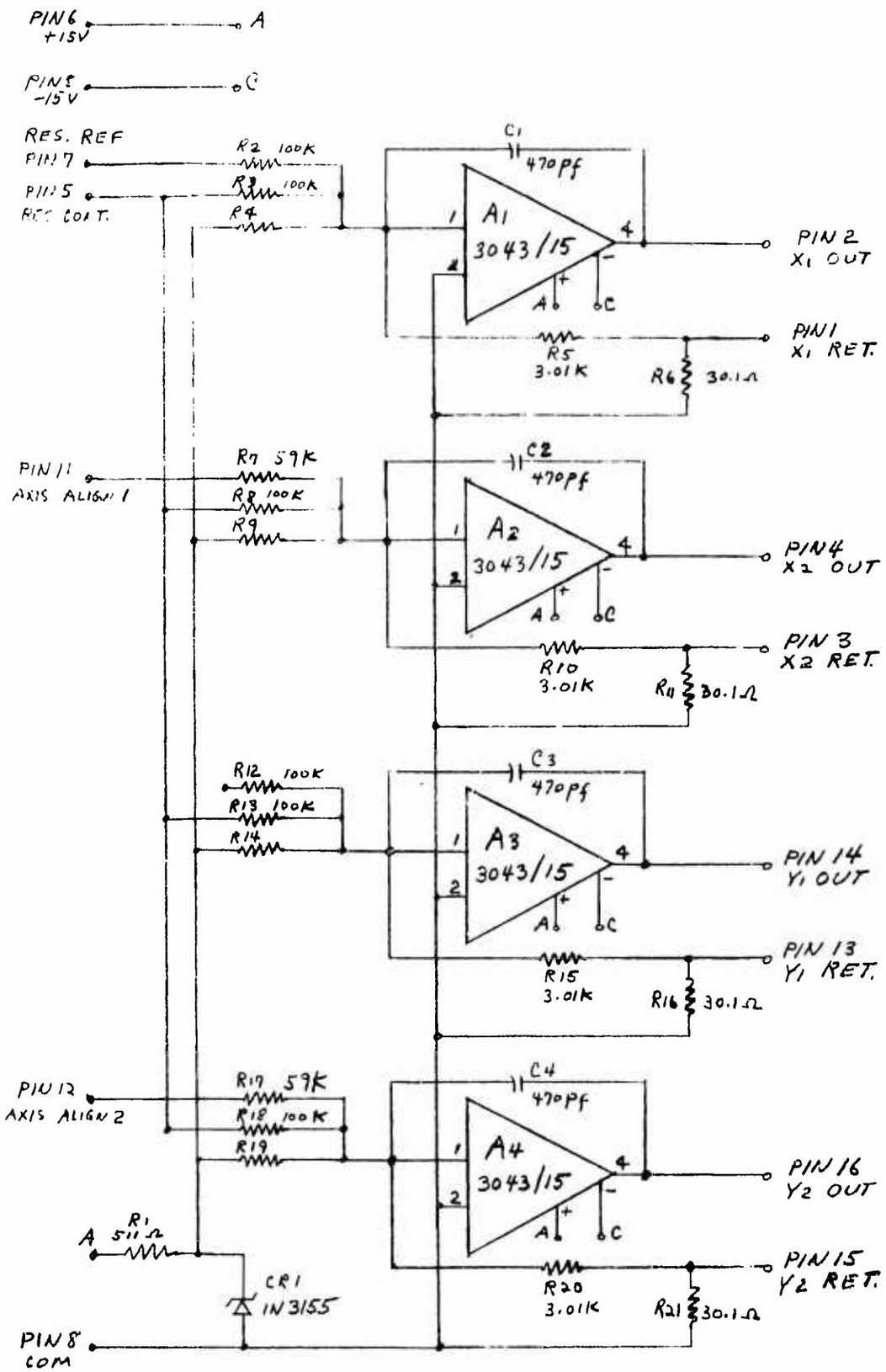

Figure III-25. Board No. 12 Comp Driver Amps

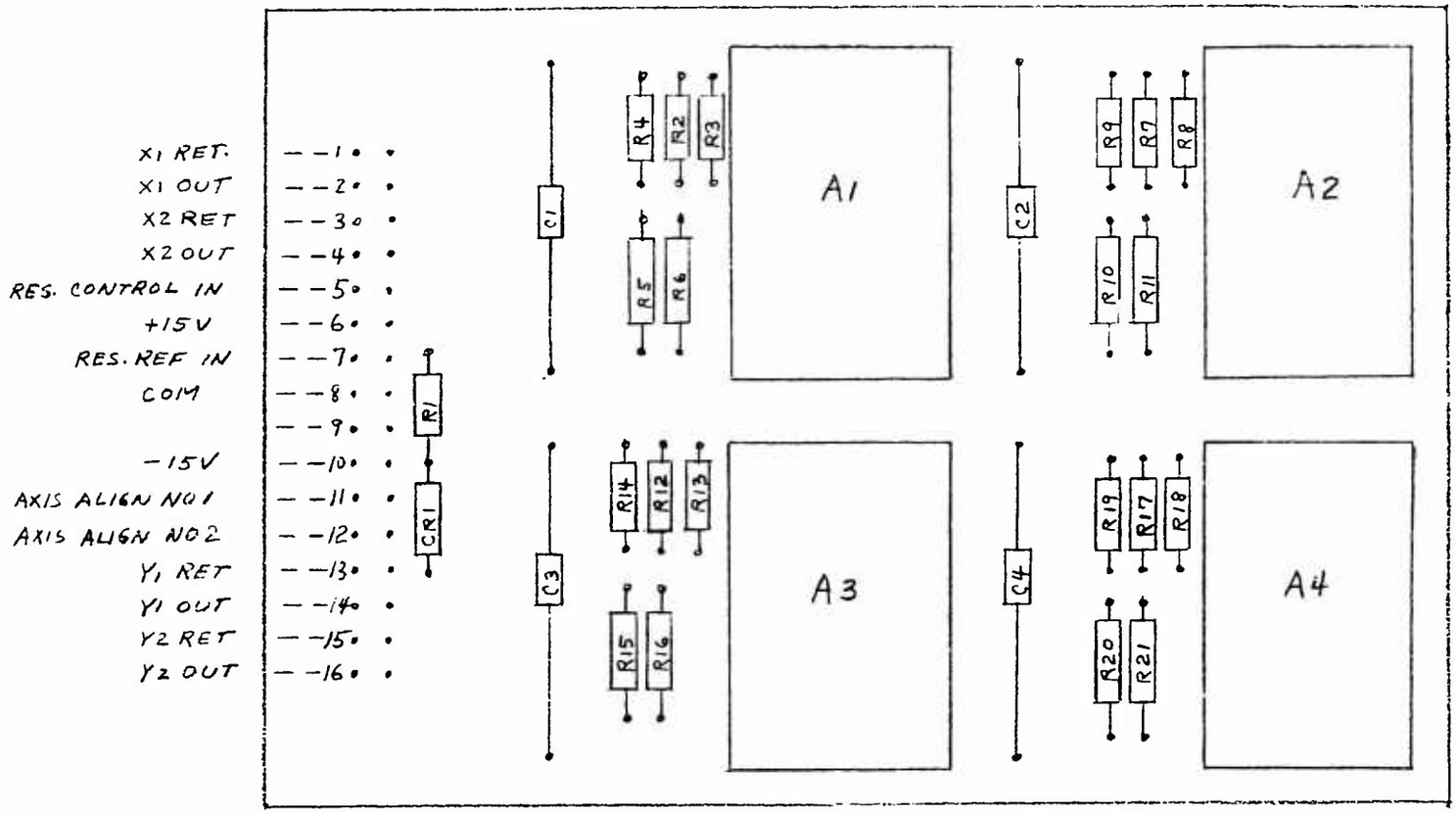

Figure III-26. Board No. 12 Layout

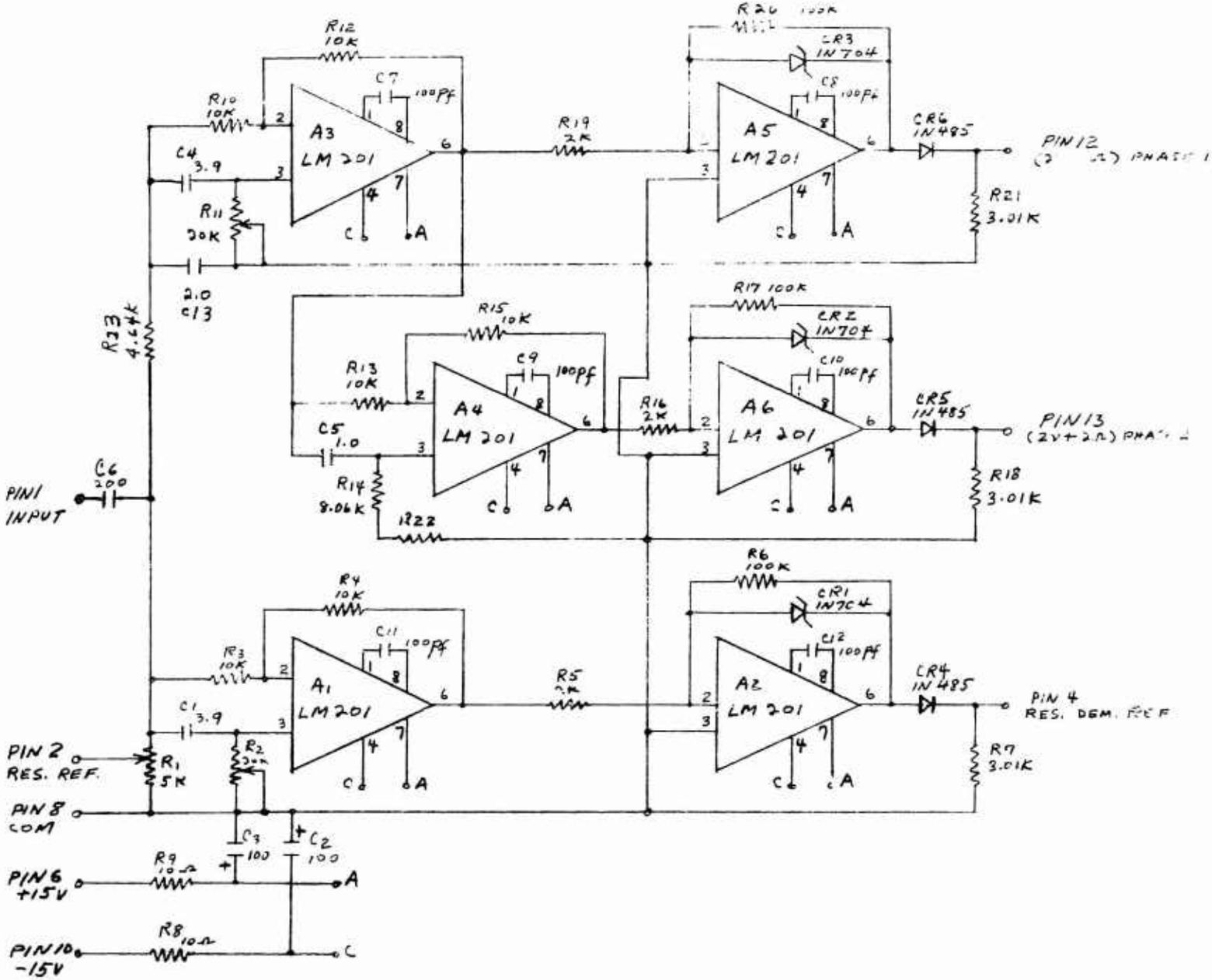

Figure III-27. Board No. 13 (2v + 2Ω) Ref Driver

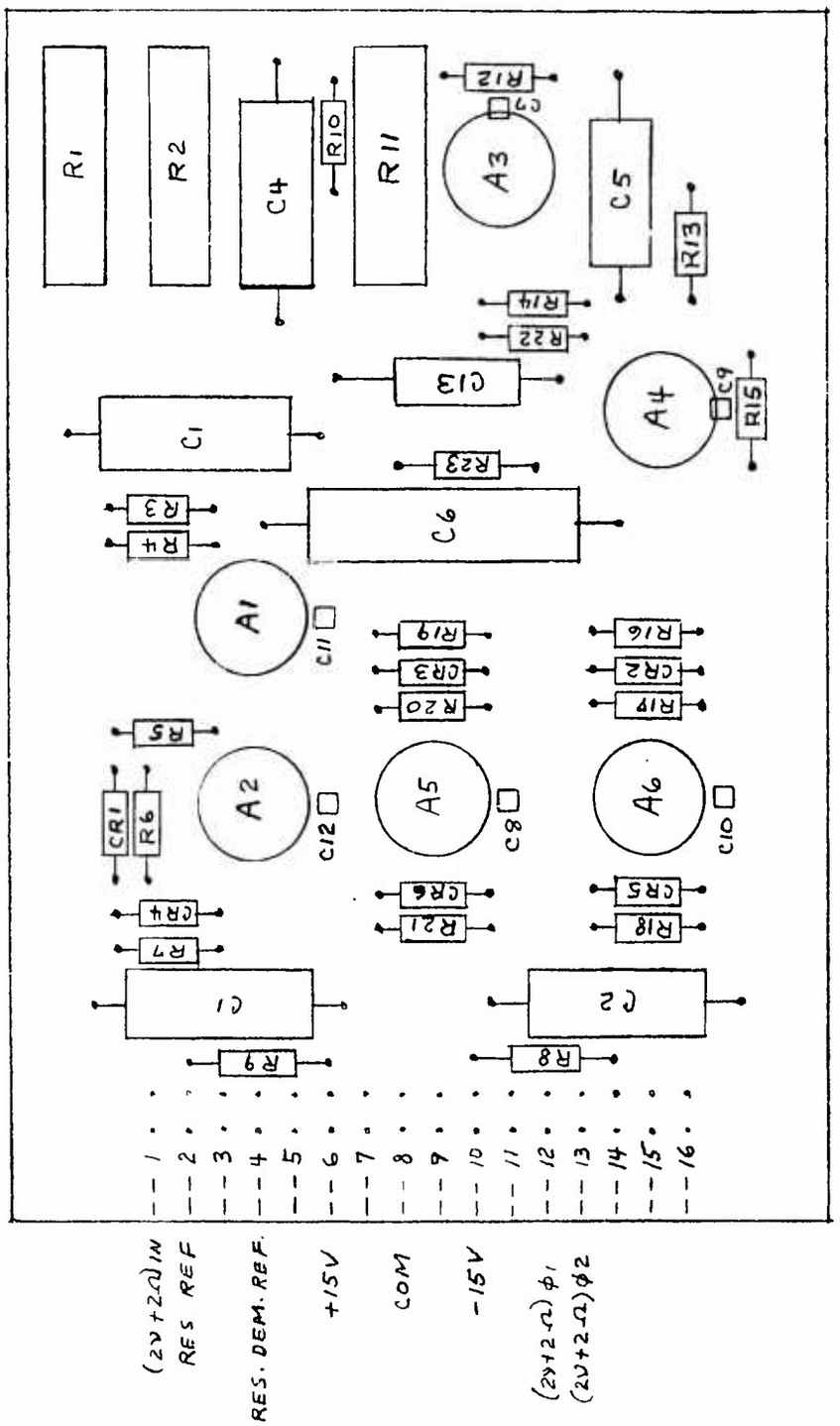

Figure III-28. Board No. 13 Layout

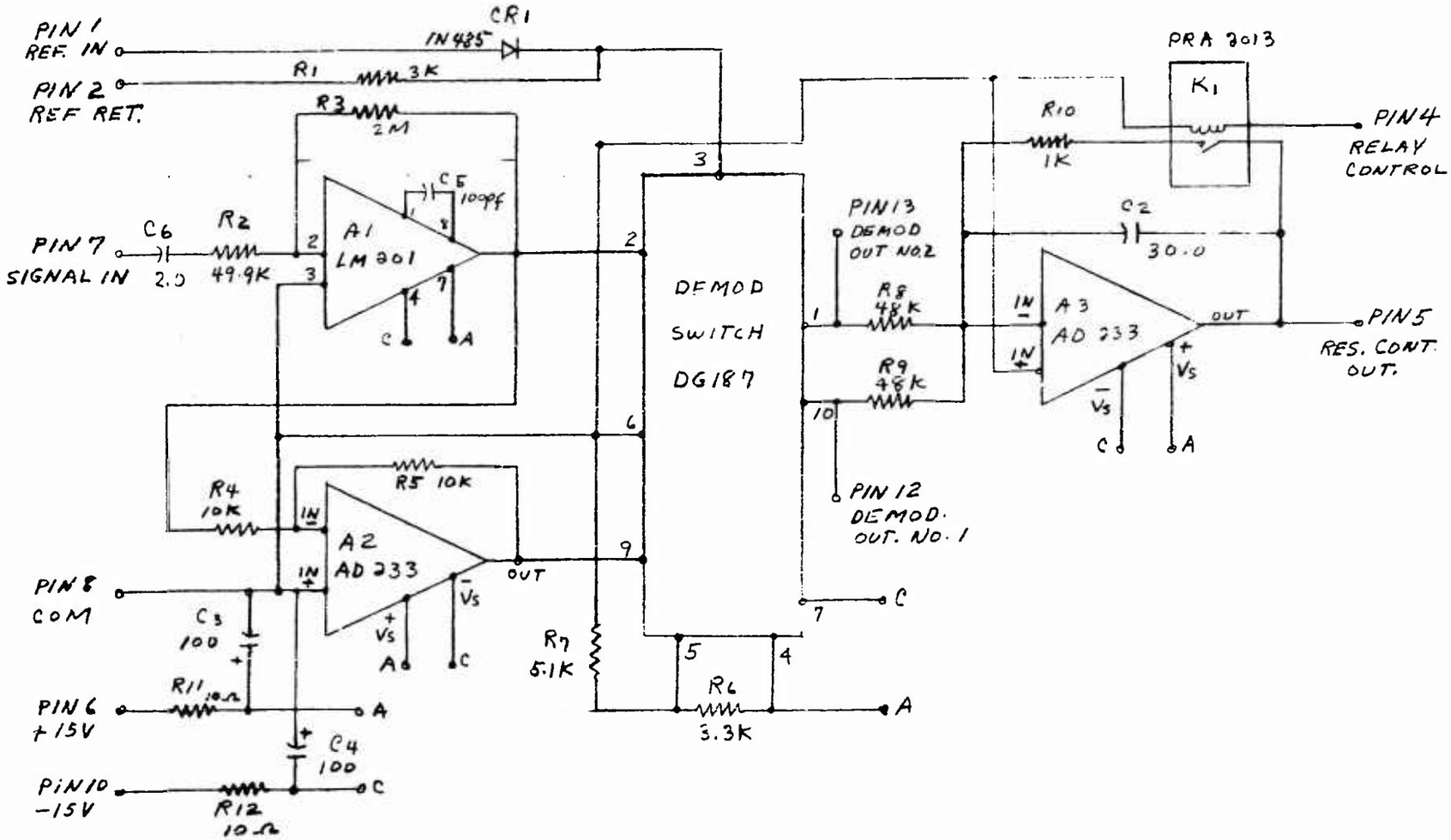

Figure III-29. Board No. 14 Resonance Loop Amp-Dem Integ

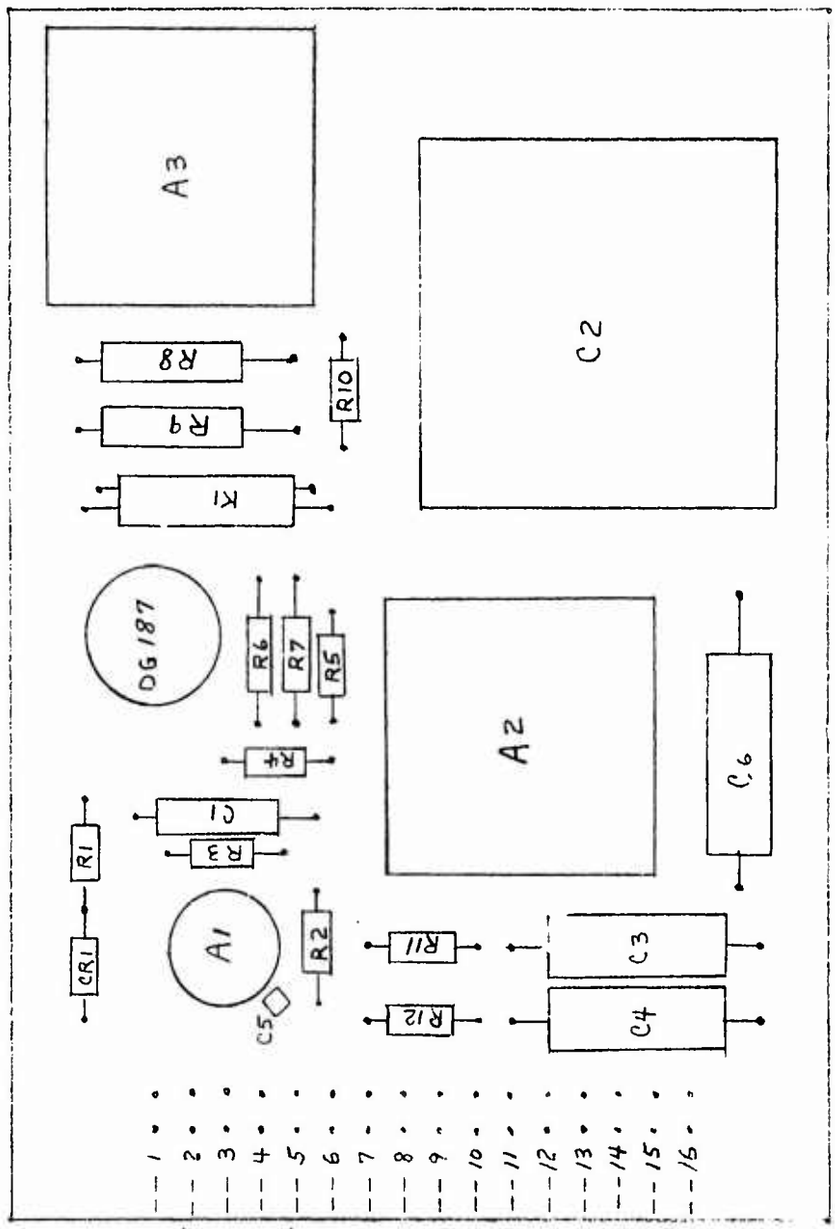

Figure III-30. Board No. 14 Layout

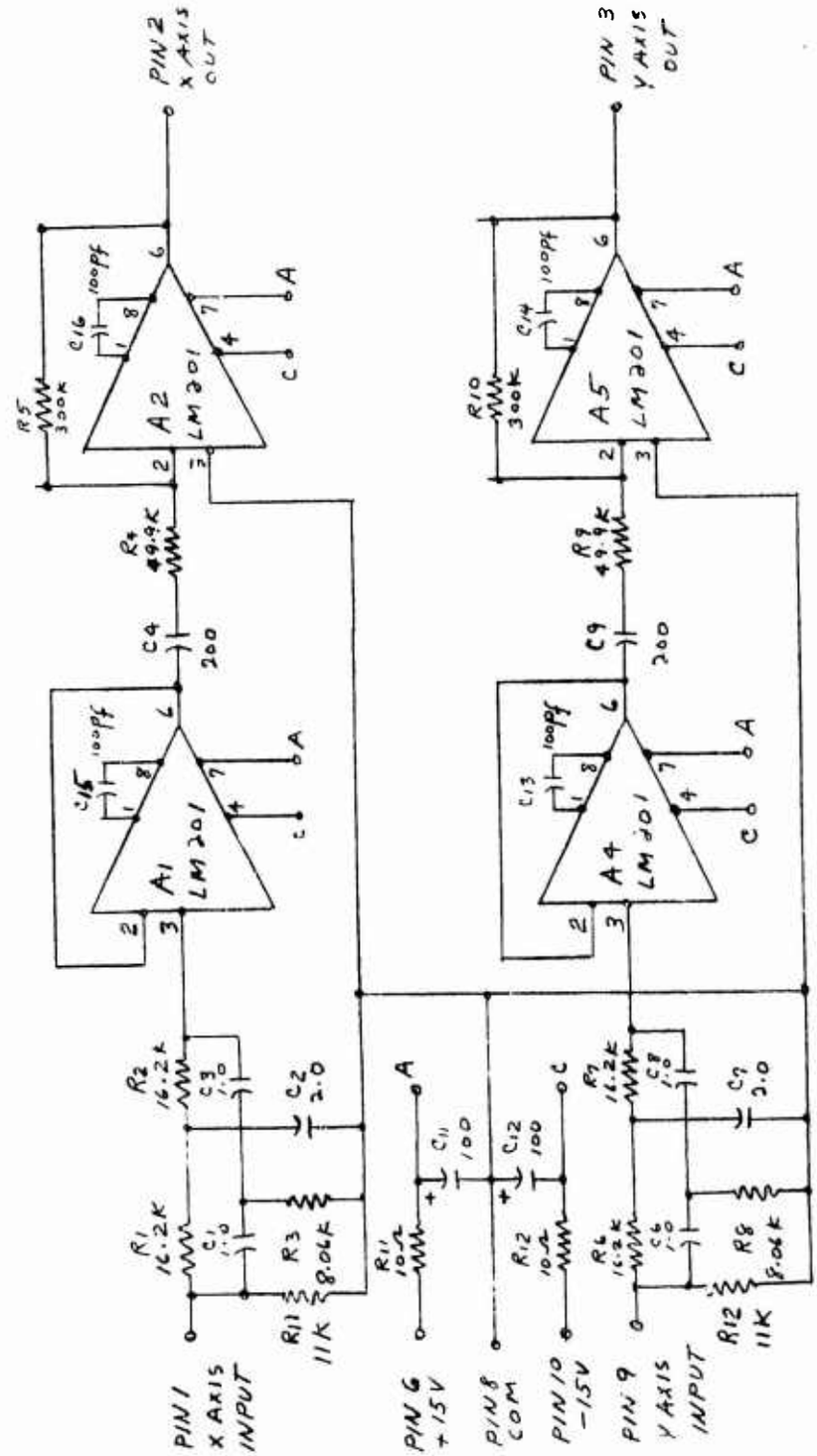

Figure III-31. Board No. 15 Rot Syst DC Amp (Pickoff Amp)

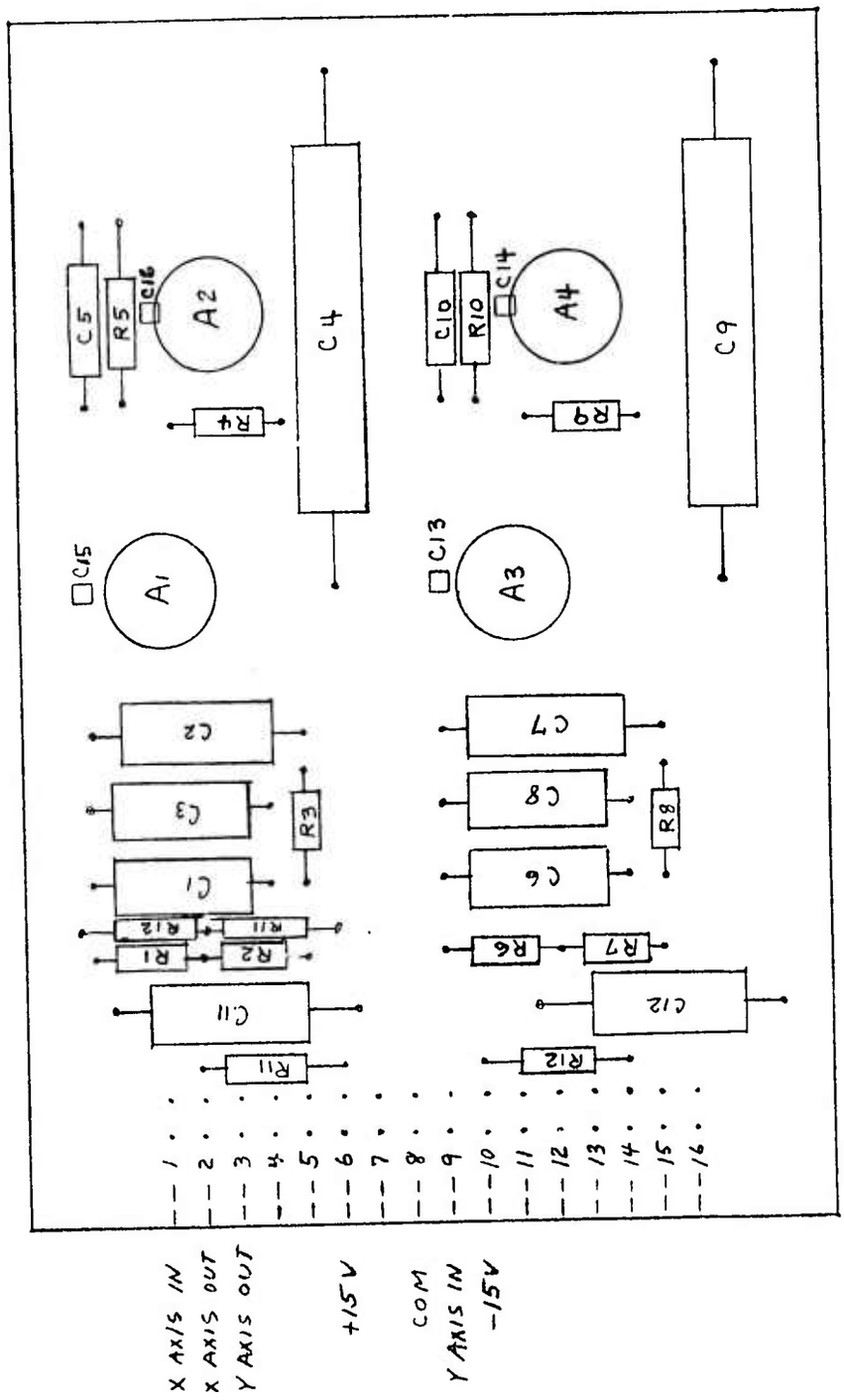

Figure III-32. Board No. 15 Layout

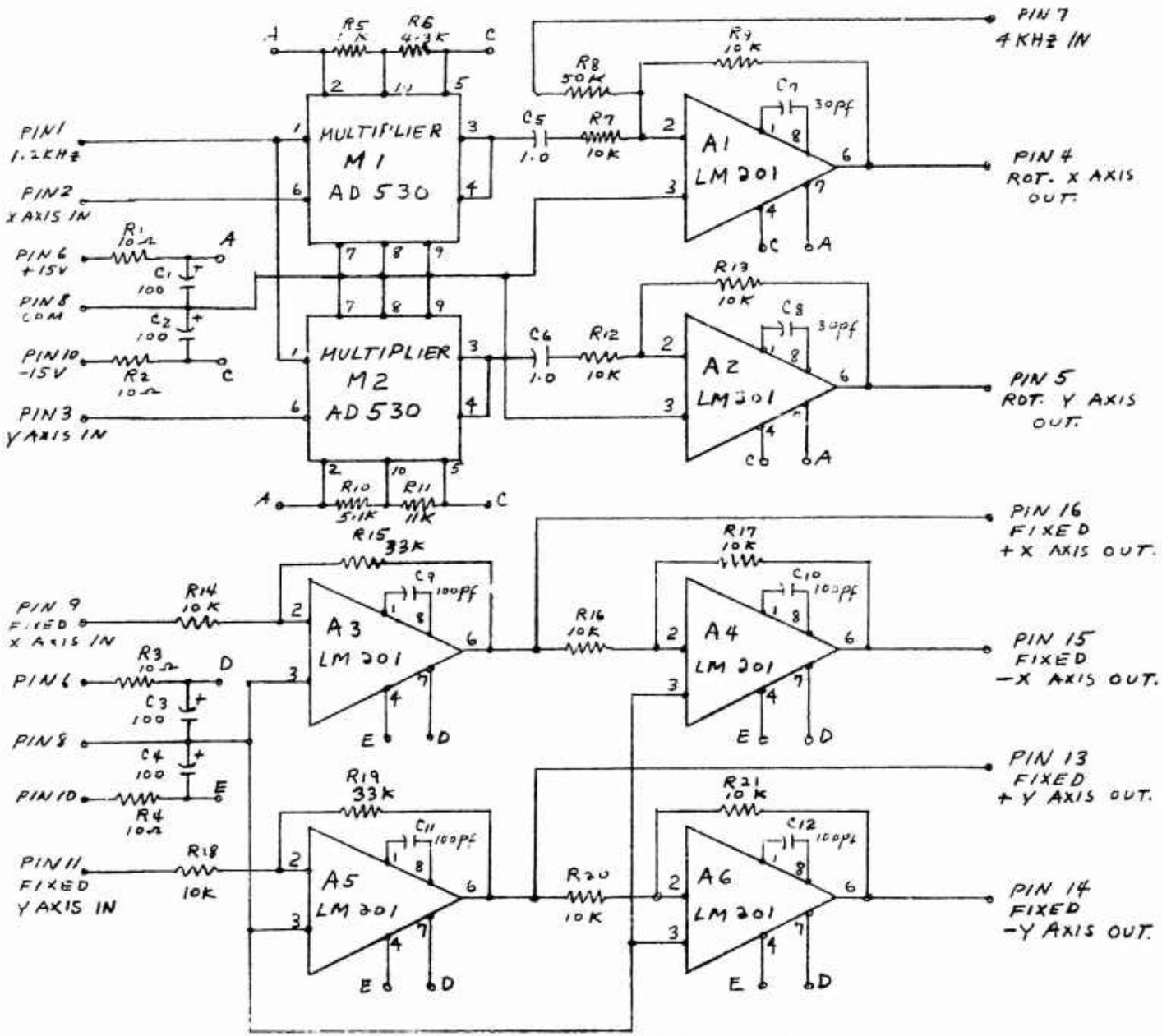

Figure III-33. Board No. 16 Mod Res Driver, Fixed Axes Amps

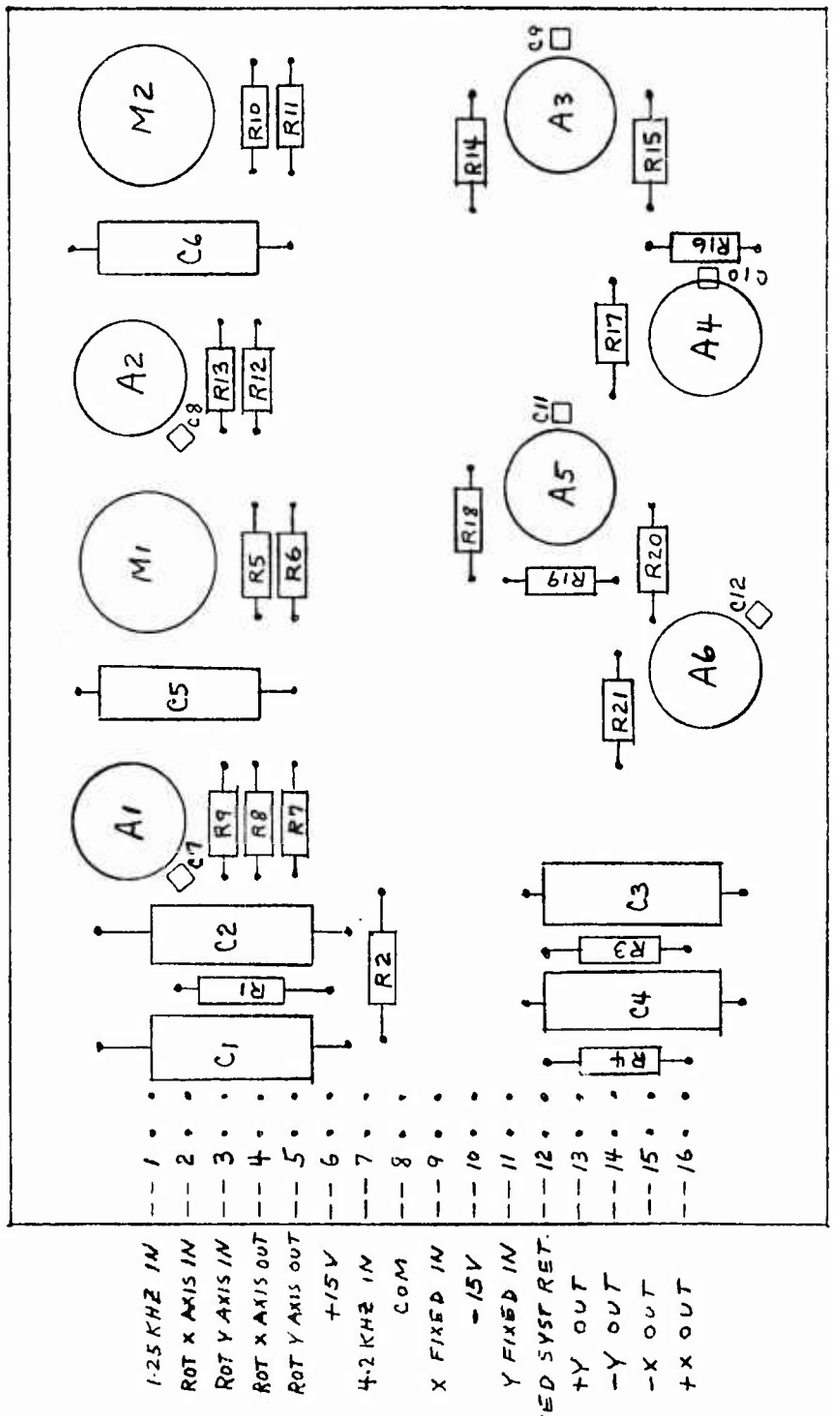

Figure III-34. Board No. 16 Layout

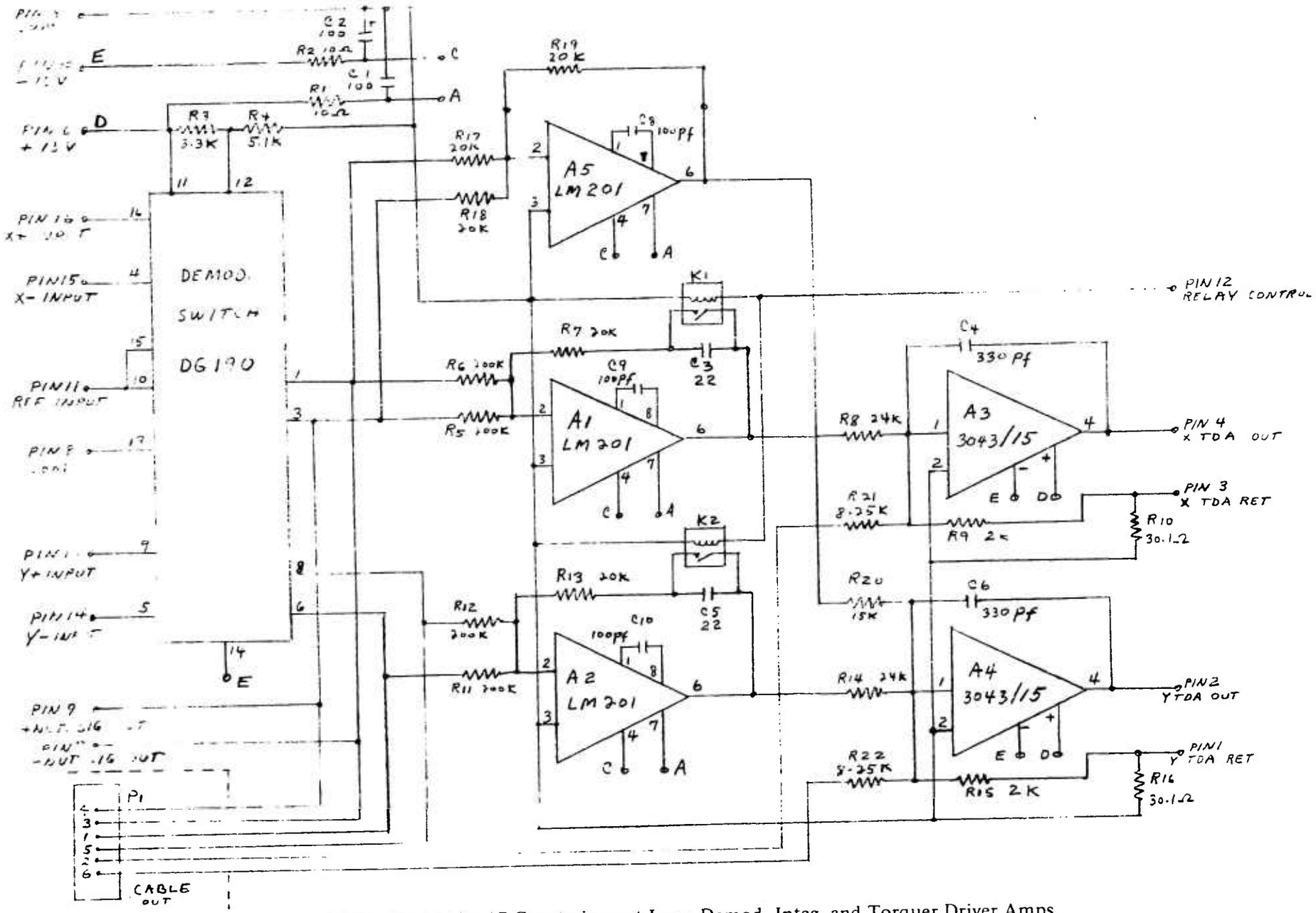

Figure III-35. Board No. 17 Constrainment Loop Demod, Integ, and Torquer Driver Amps

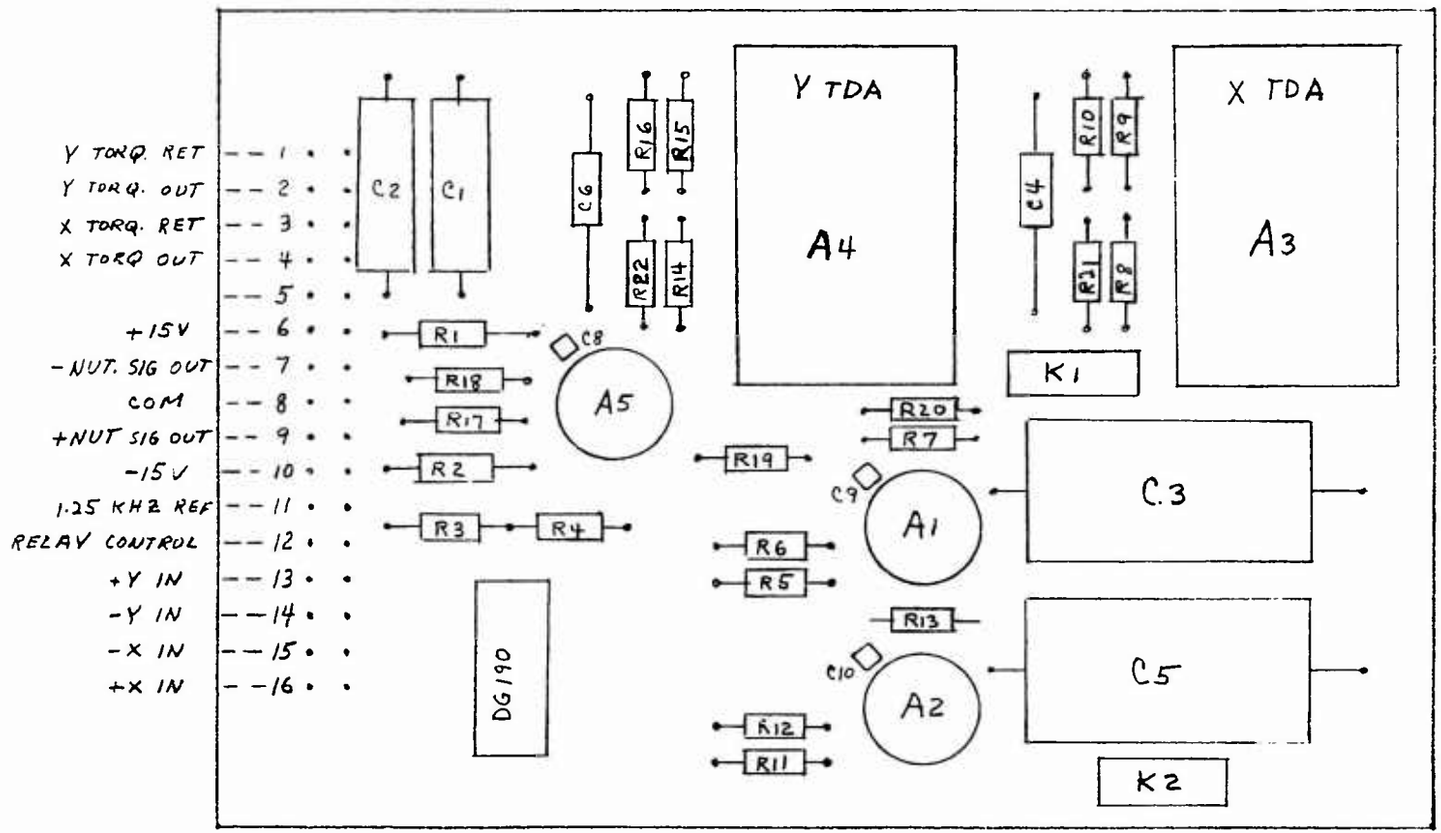

Figure III-36. Board No. 17 Layout

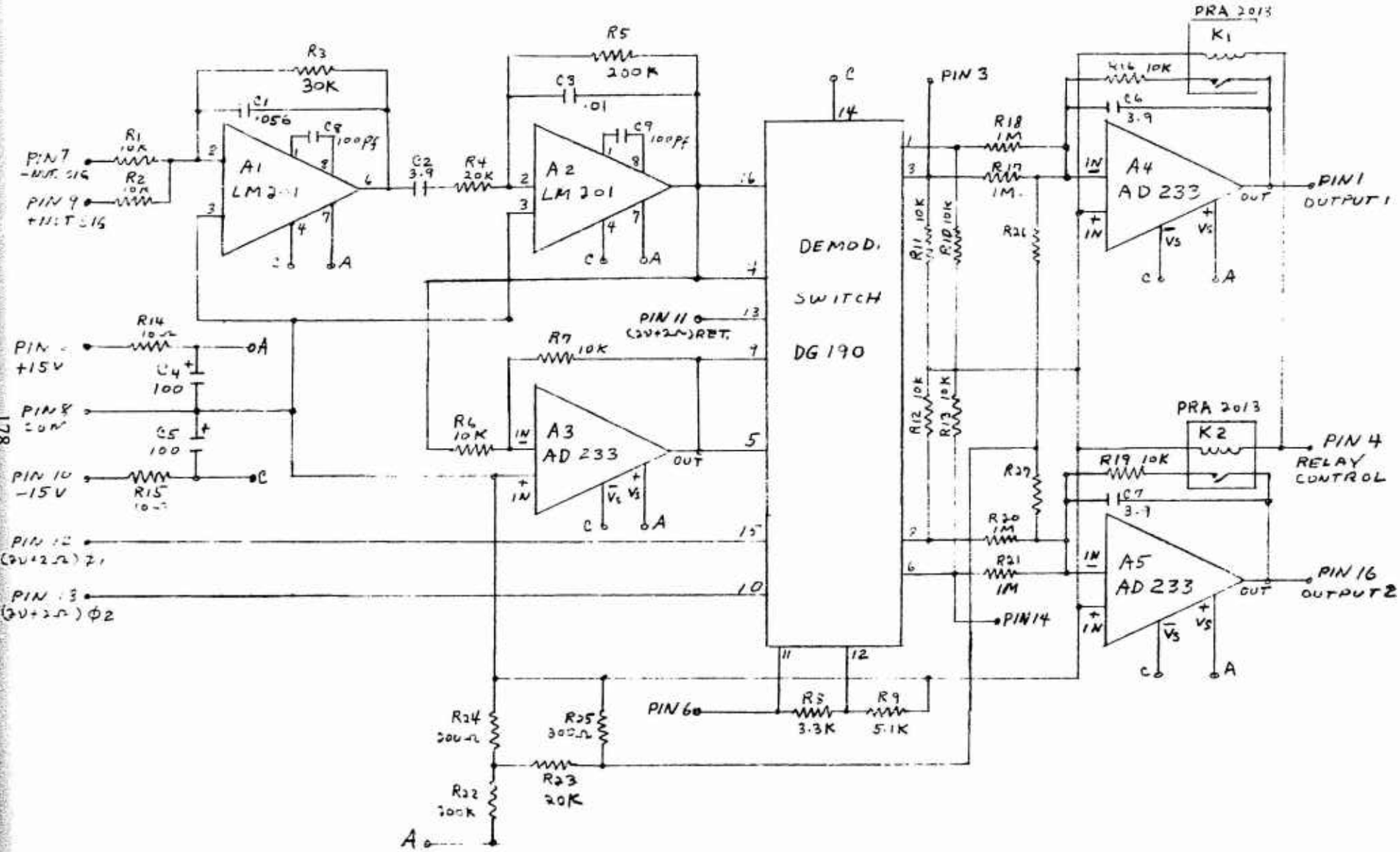

Figure III-37. Nutatron Signal Amplifier and Demod (Board No. 18)

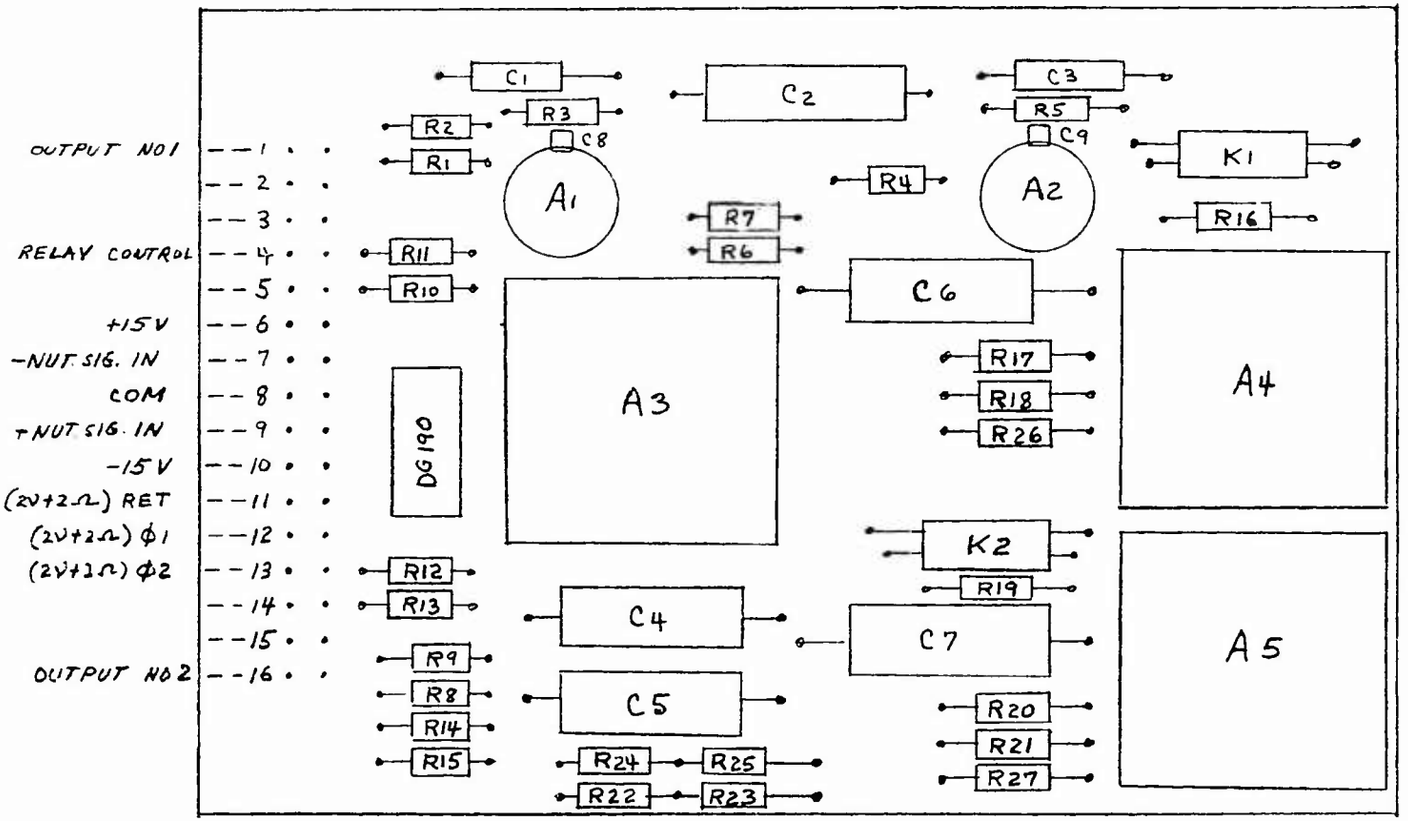

Figure III-38. Board No. 18 Layout

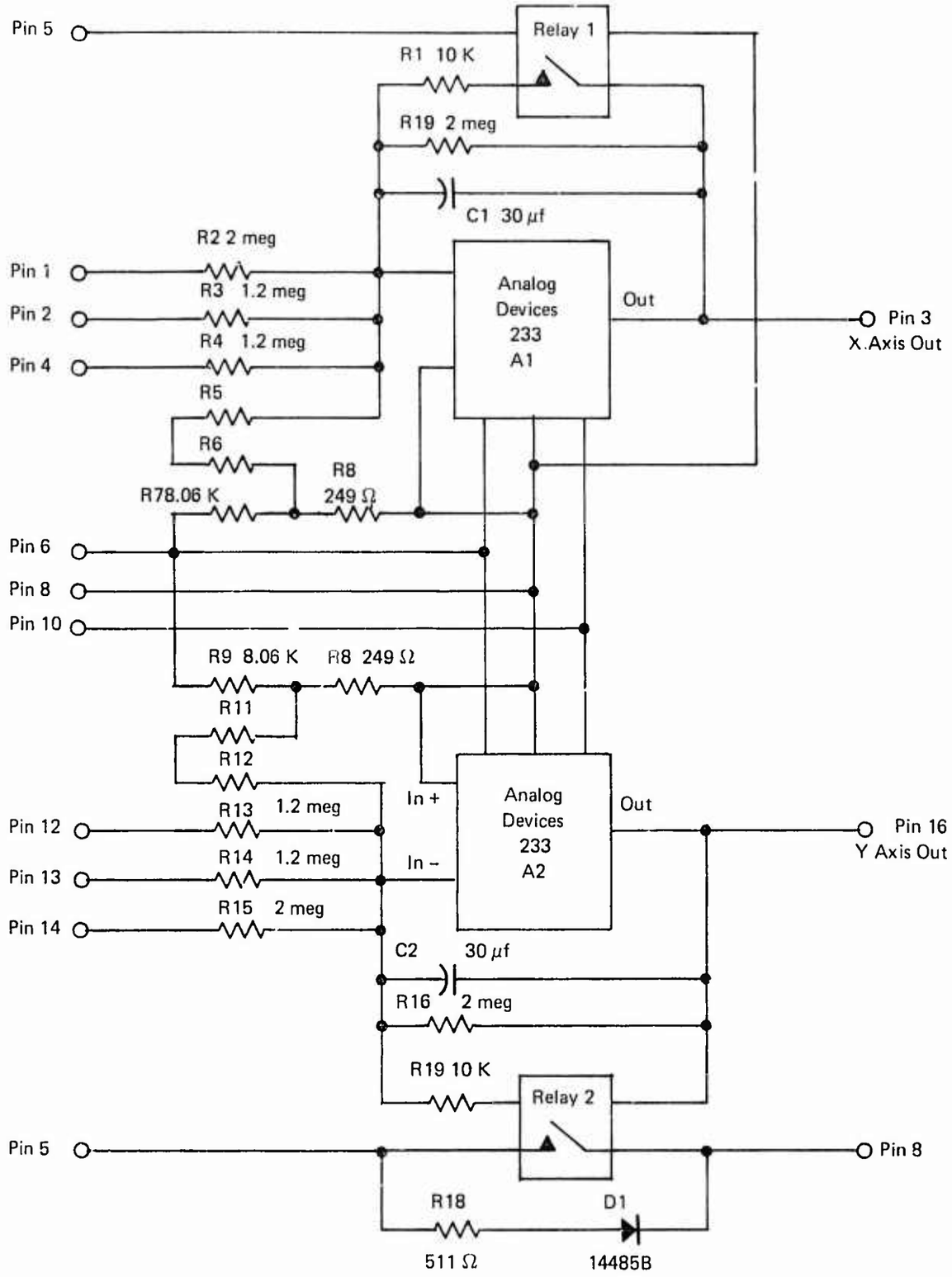

Figure III-39. Nutatron Signal Filter Schematic (Board No. 19)

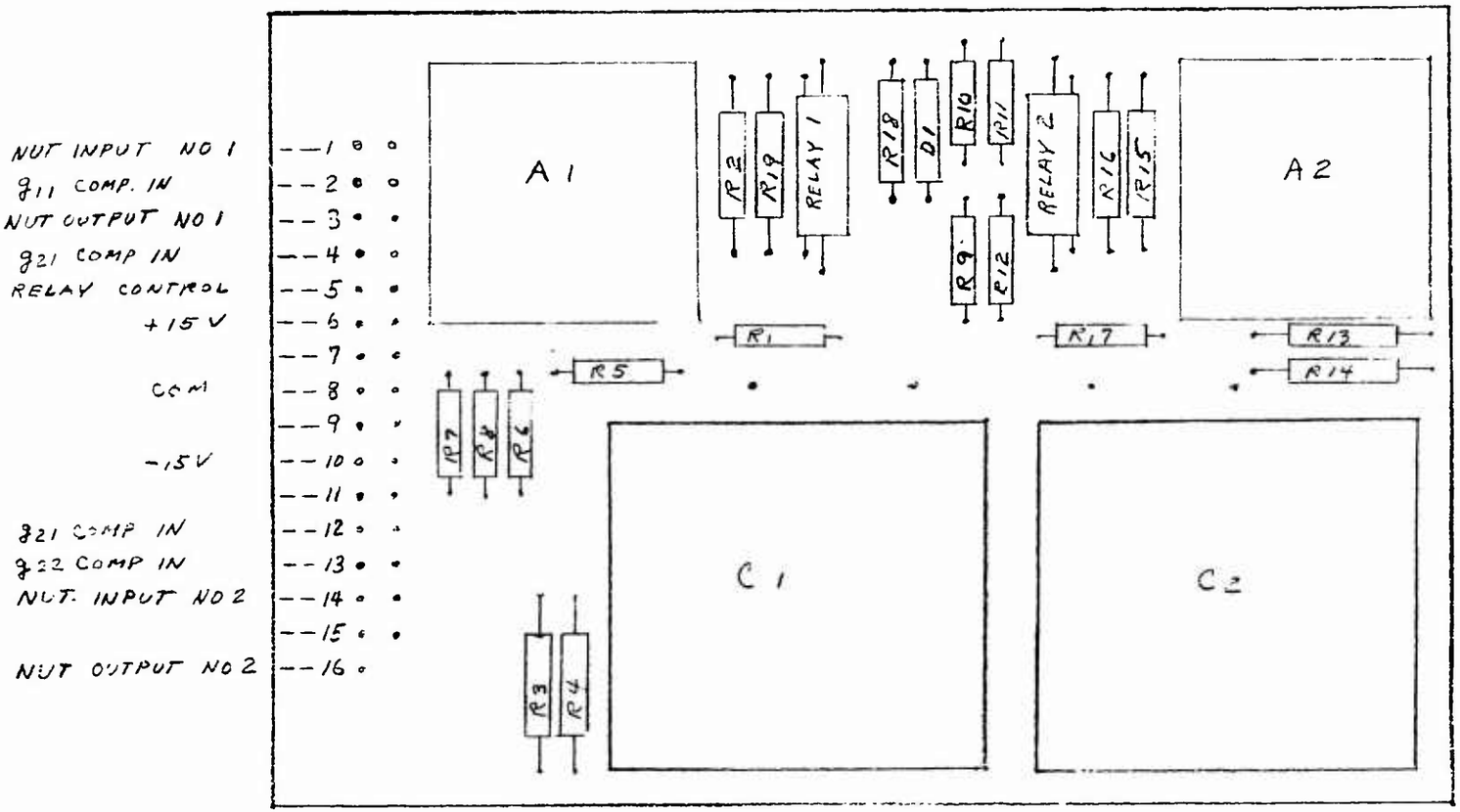

Figure III-40. Board No. 19 Layout

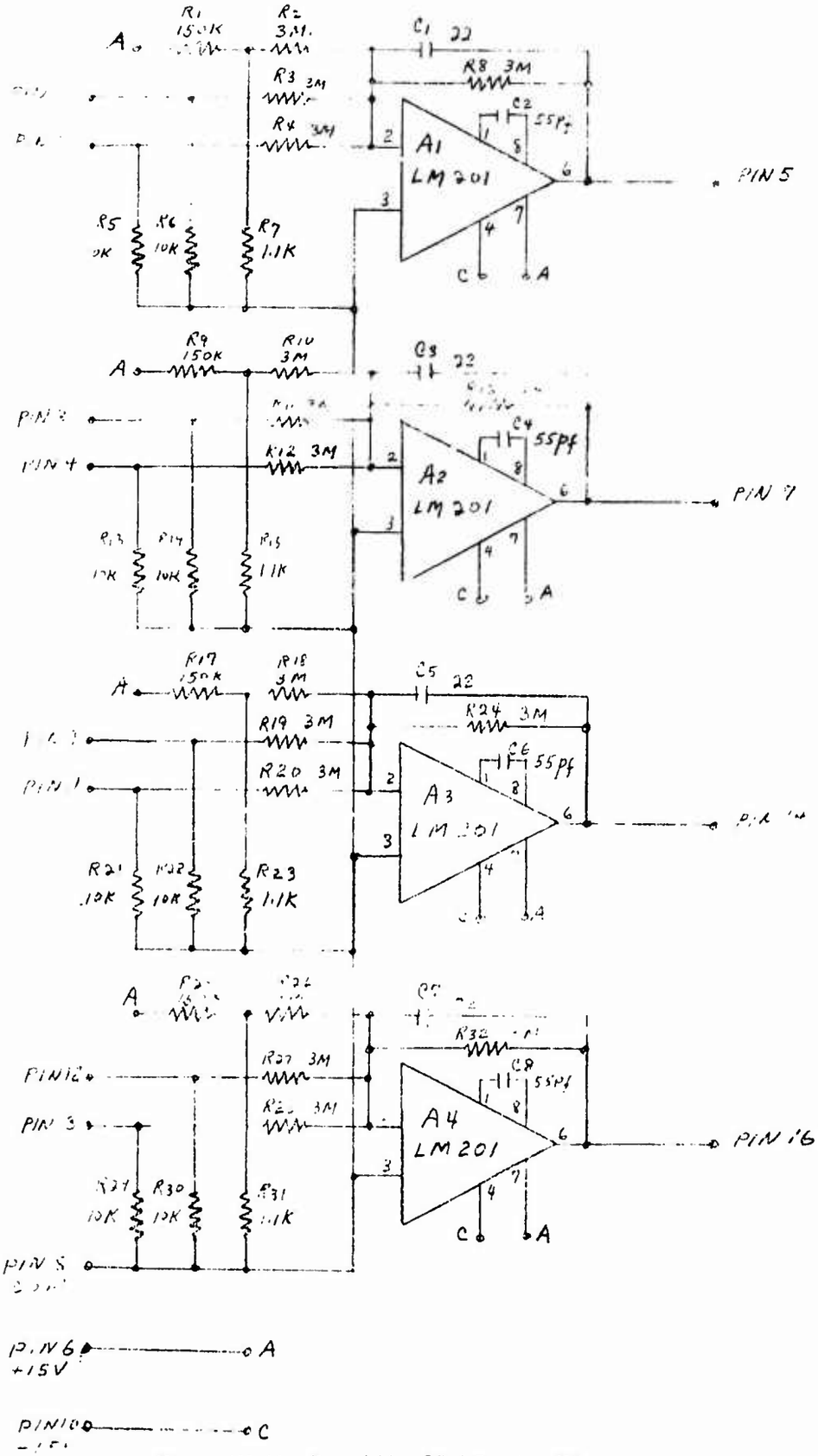

Figure III-41. Board No. 20 4-Section Filter

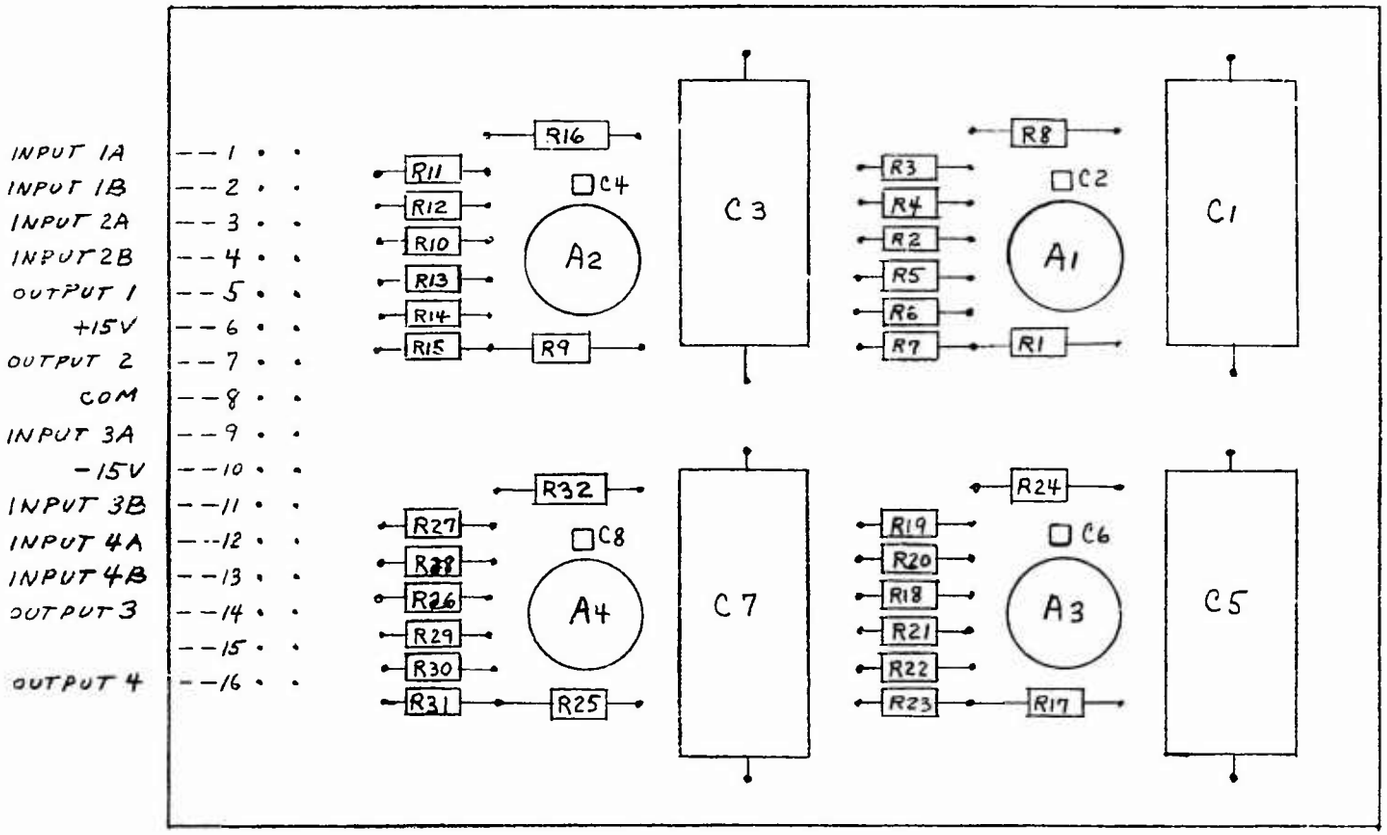

Figure III-42. Board No. 20 Layout

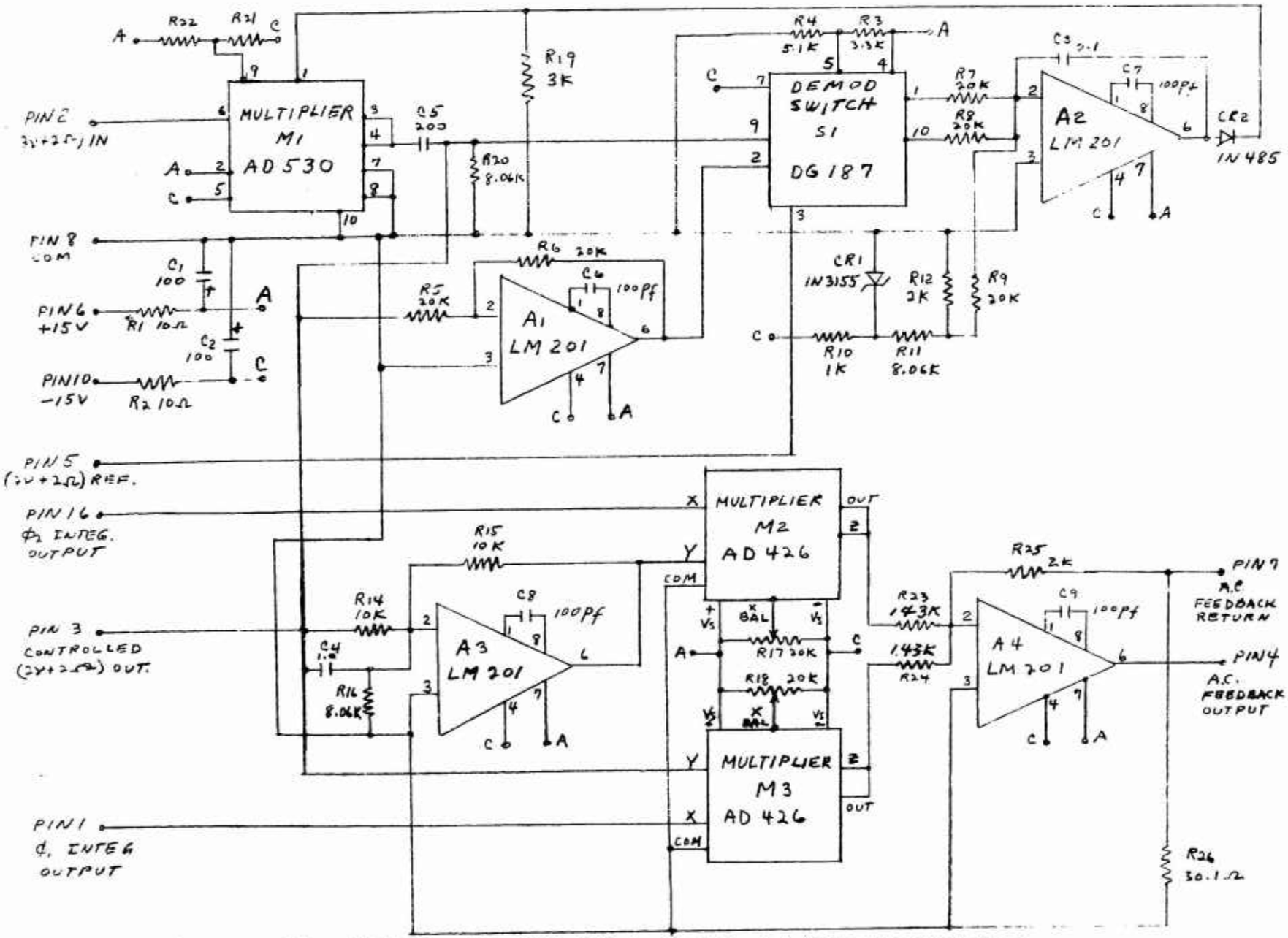

Figure III-43. Board No. 21 2v + 2Ω Amplitude Control AC Feedback Modulators and Summing Amp

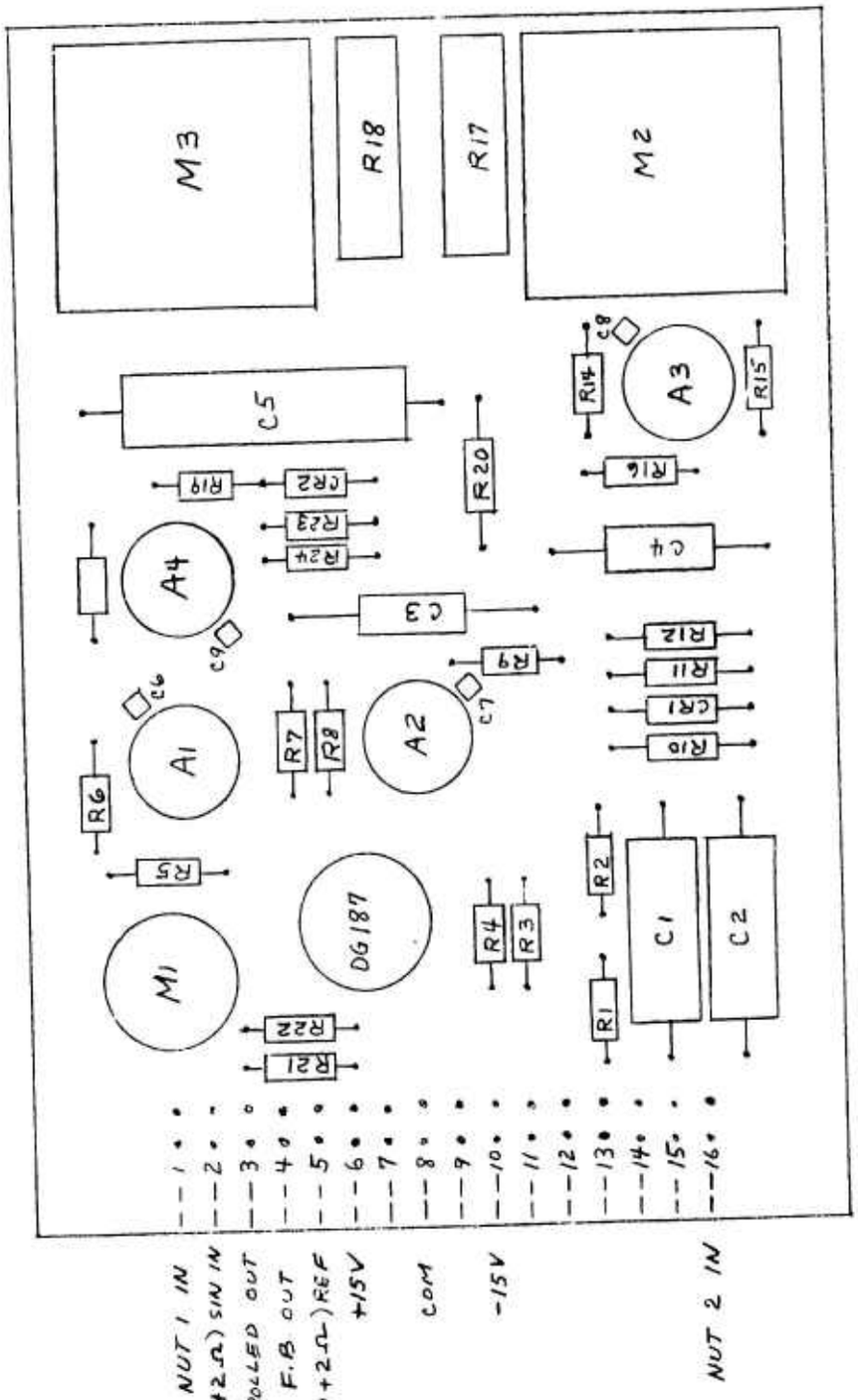

Figure III-44. Board No. 21 Layout

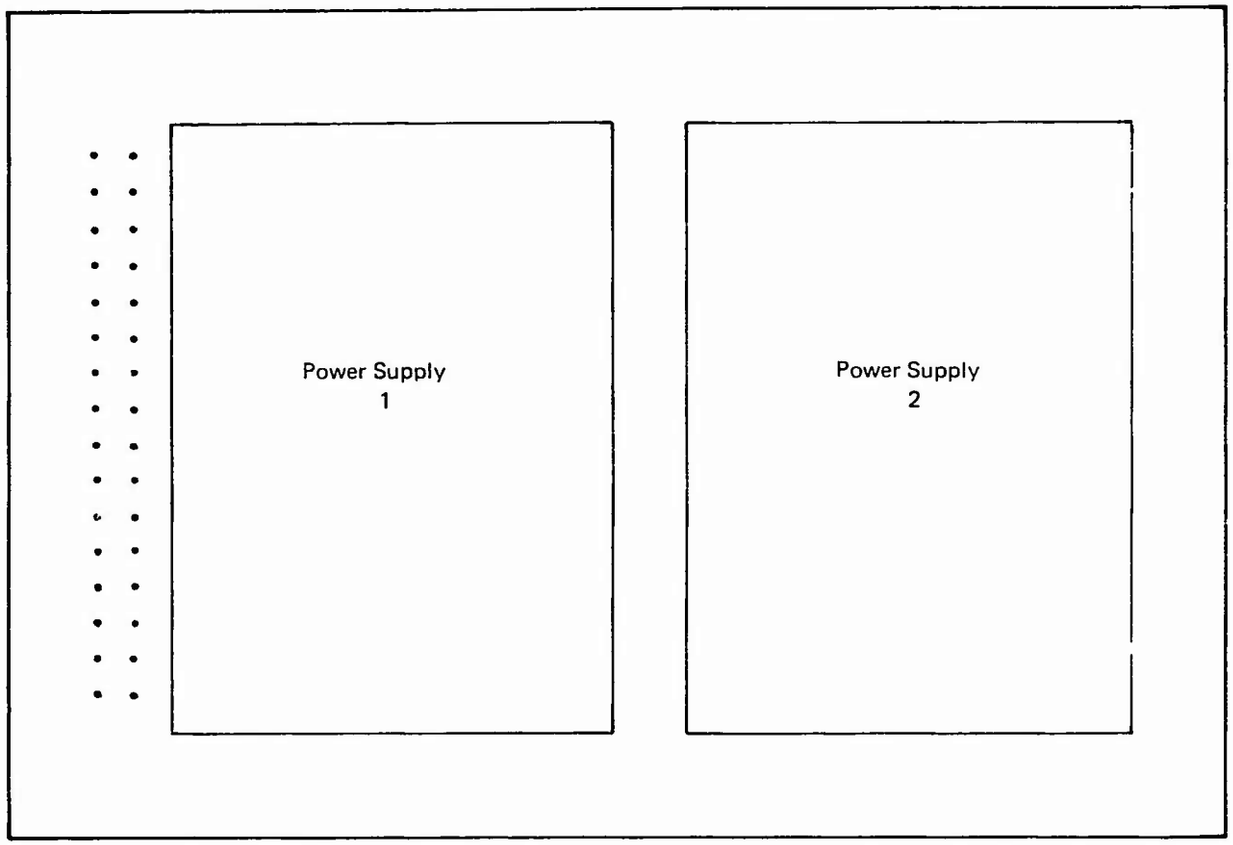

Figure III-45. 2Ω Power Supply (Board No. 22)

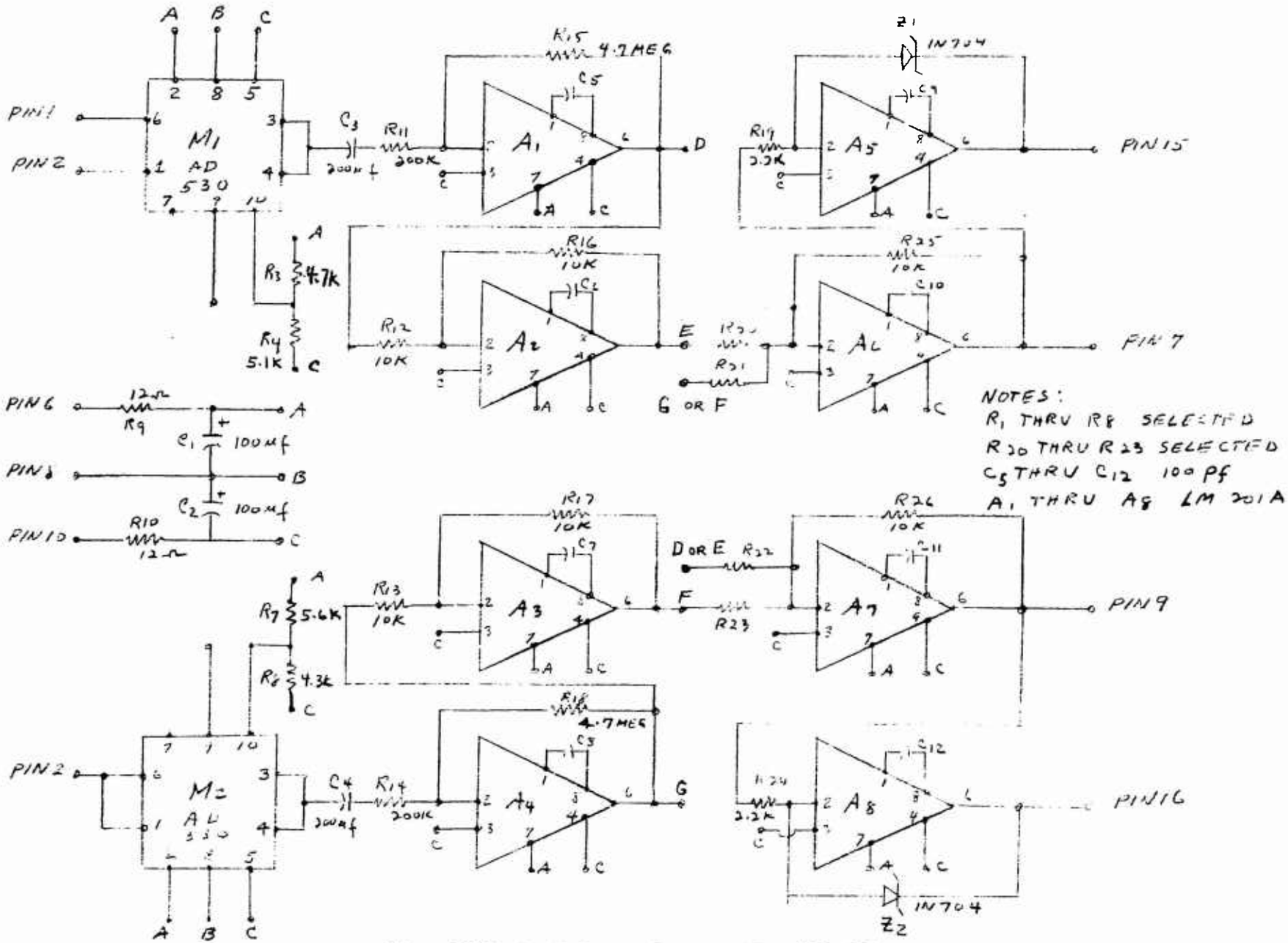

Figure III-46. 2Ω Reference Generator (Board No. 23)

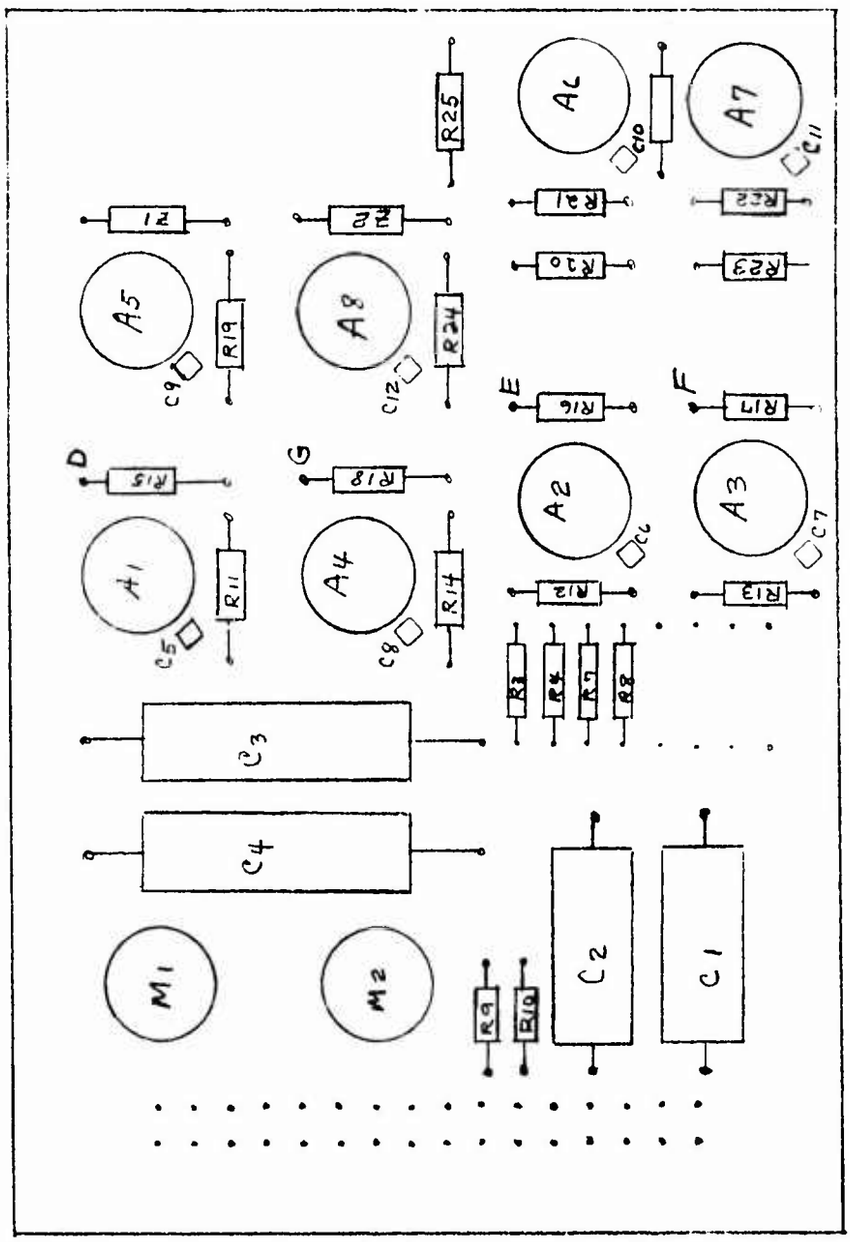

Figure III-47. Board No. 23 Layout 2Ω Ref Gen

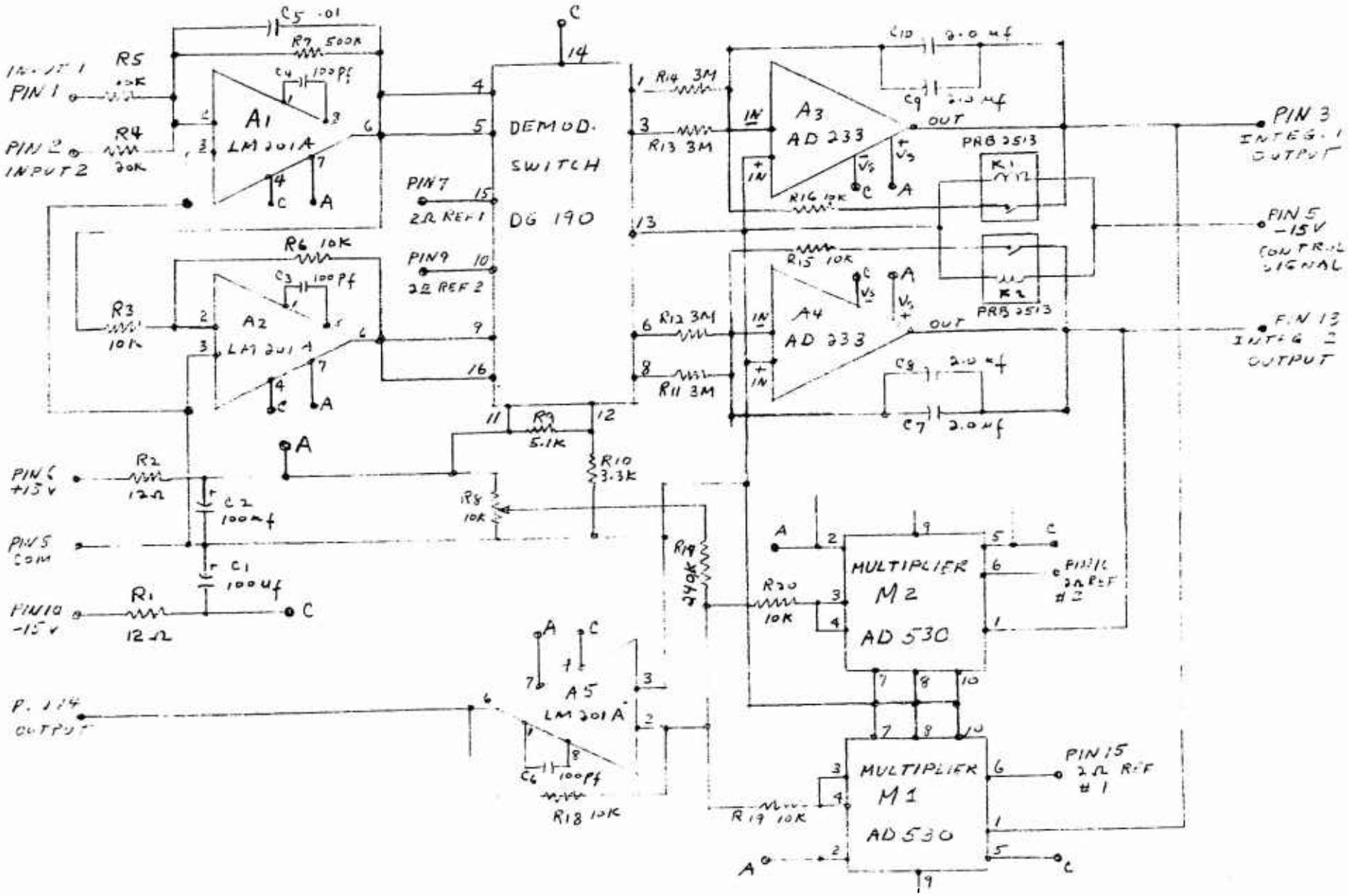

Figure III-48. 2Ω Loop Electronics One Axis (Boards No. 24 and 25)

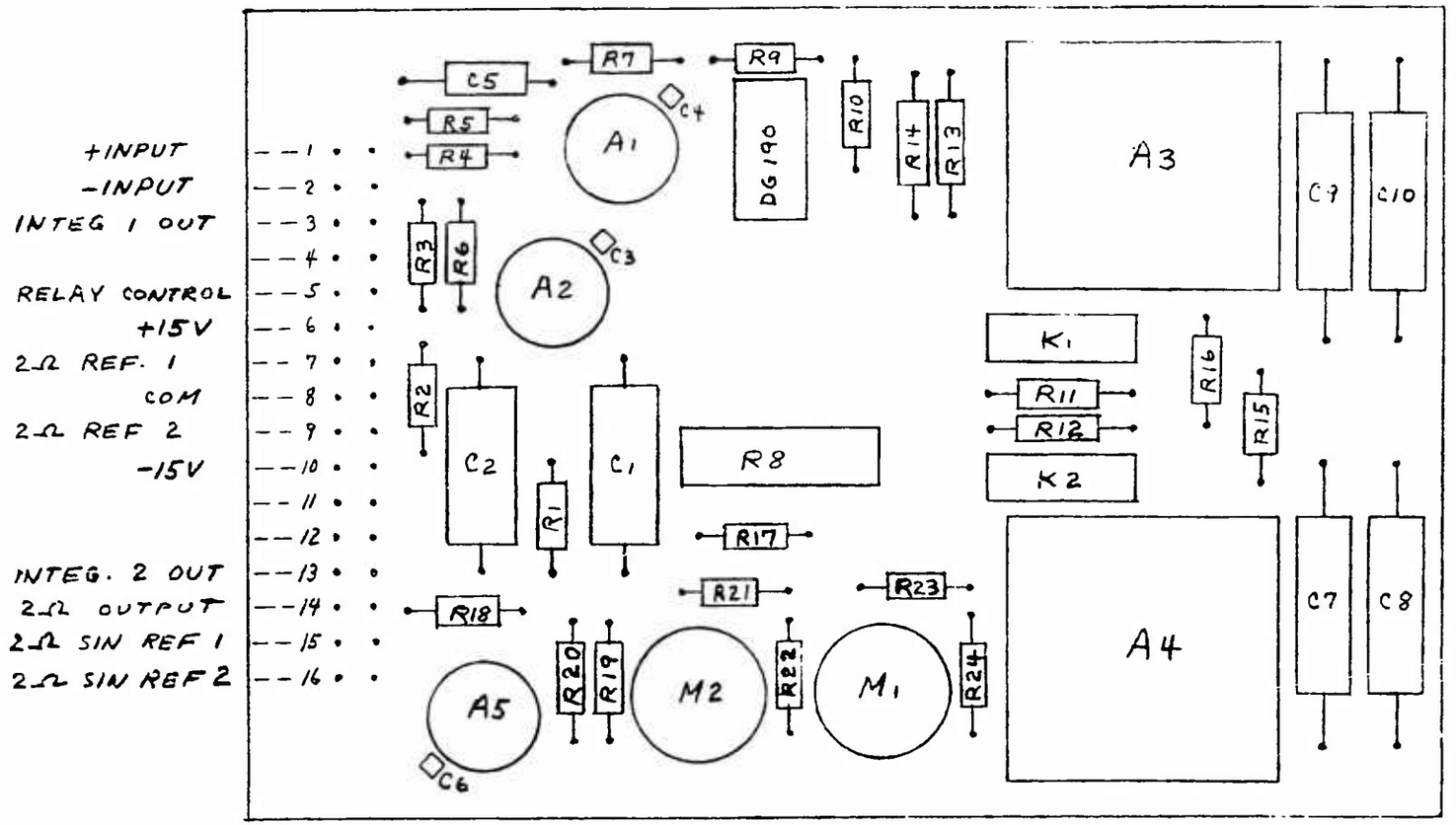

Figure III-49. Boards No. 24 and 25 Layout

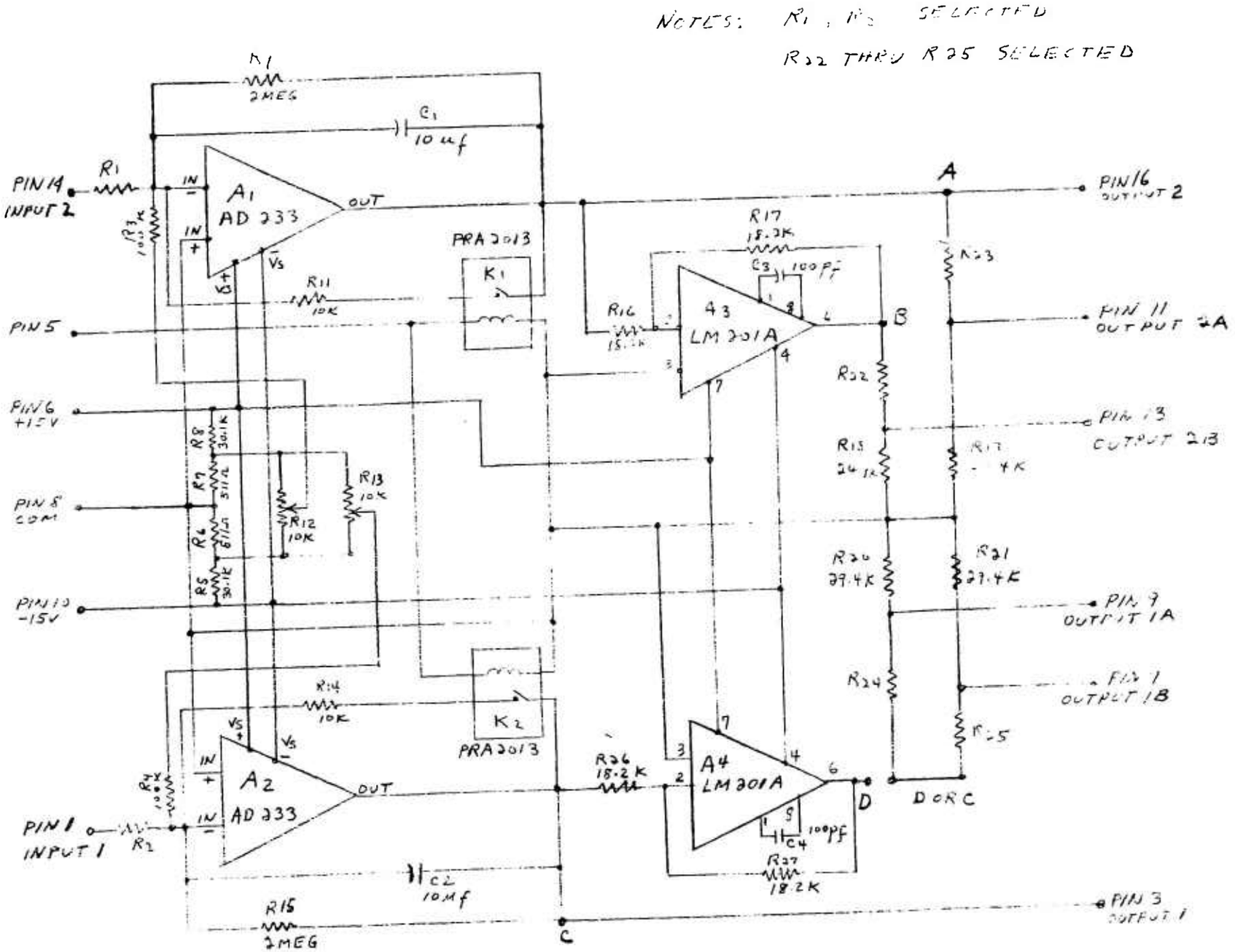

Figure III-50. G-Sensitivity Correction Filter (Board No. 26)

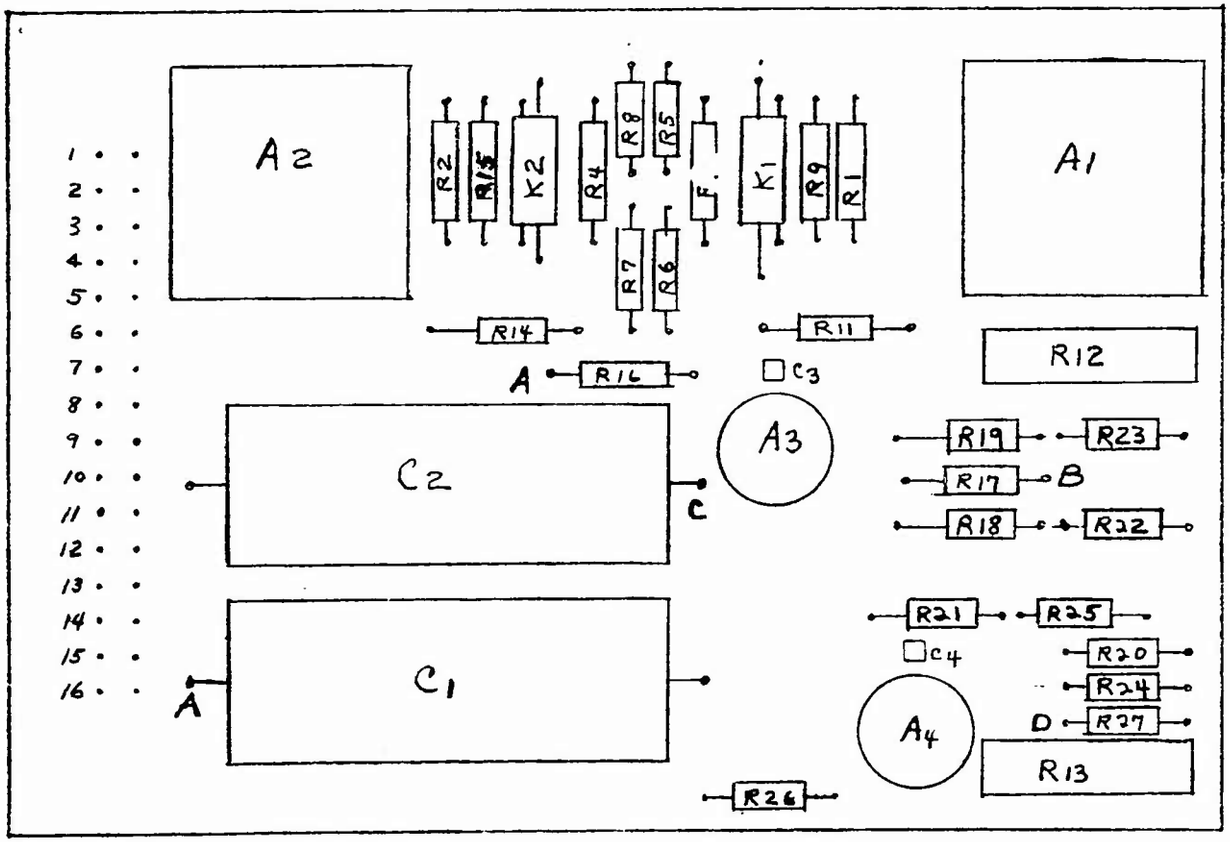

Figure III-51. Board No. 26 Layout g-Sensitivity Correction Filter

APPENDIX IV

NUTATRON WIRING DIAGRAM

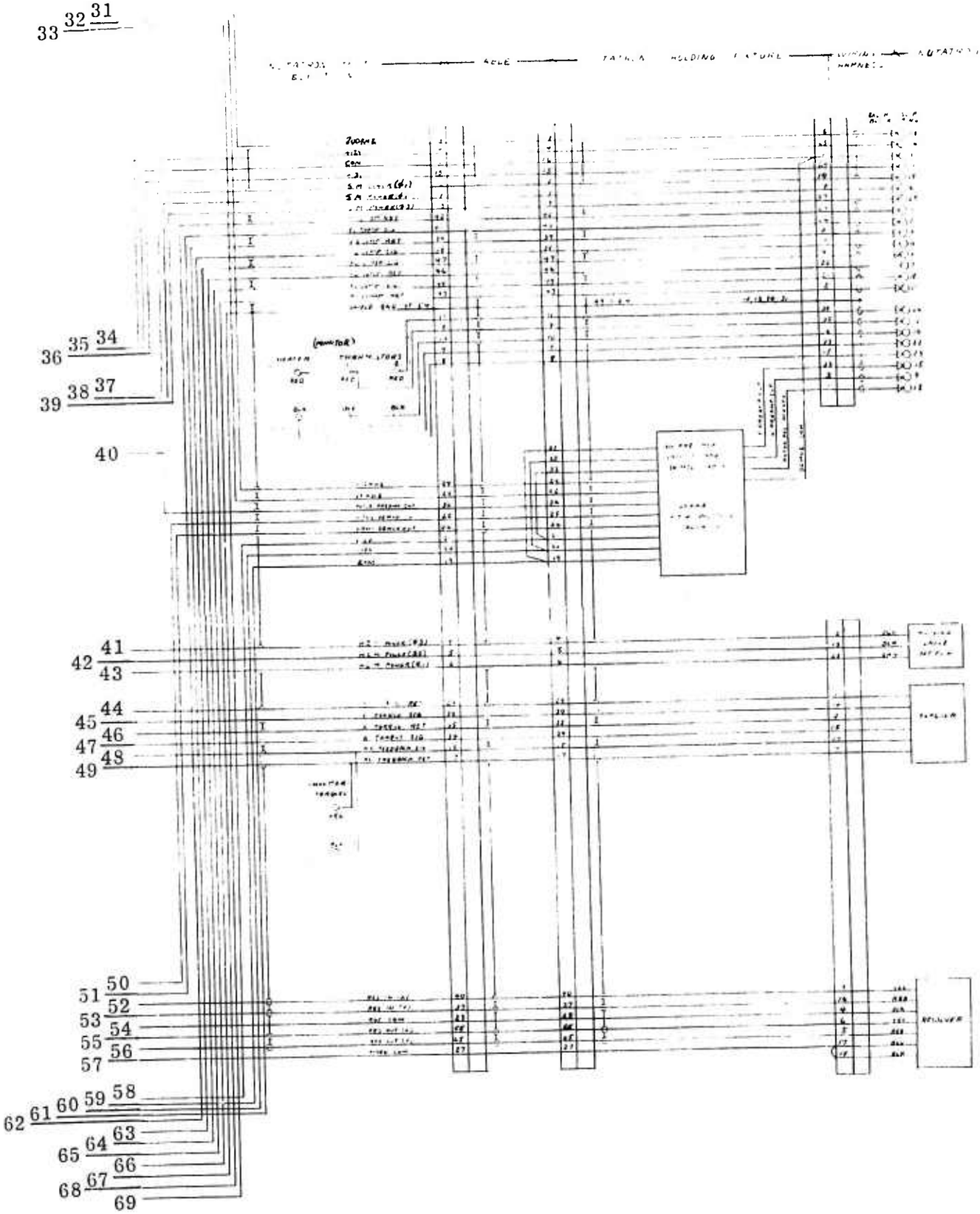
33 32 31
36 35 34
39 38 37
40
42 41
43
45 44
47 46
49 48
51 50
53 52
55 54
57 56
62 61 60 59 58
65 64 63
68 67 66
69

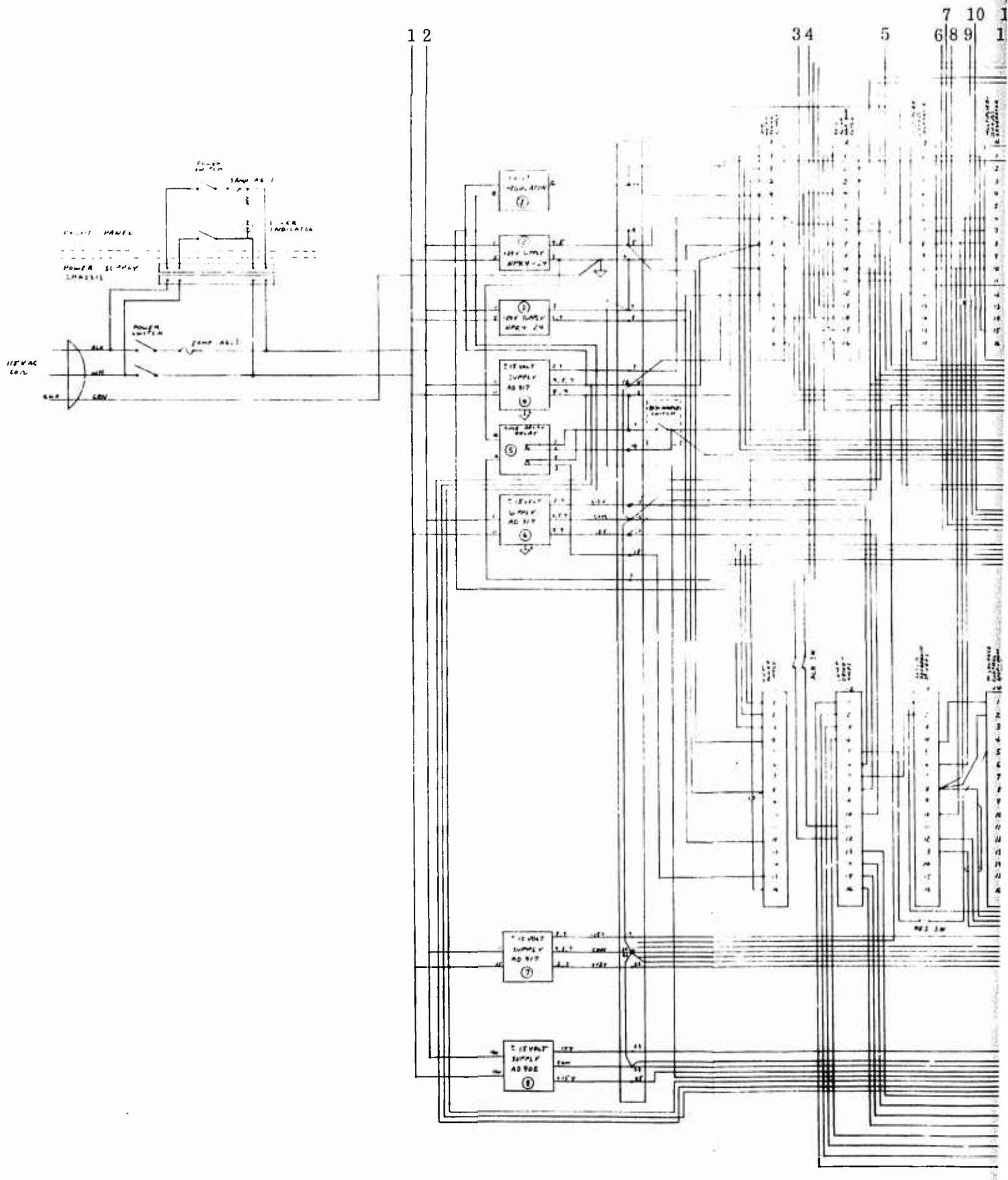
1 2
3 4
5
6 7 8 9 10 1
FRONT PANEL
POWER SUPPLY CHASSIS
POWER SWITCH
LAMP ADJ.
115 VAC COM

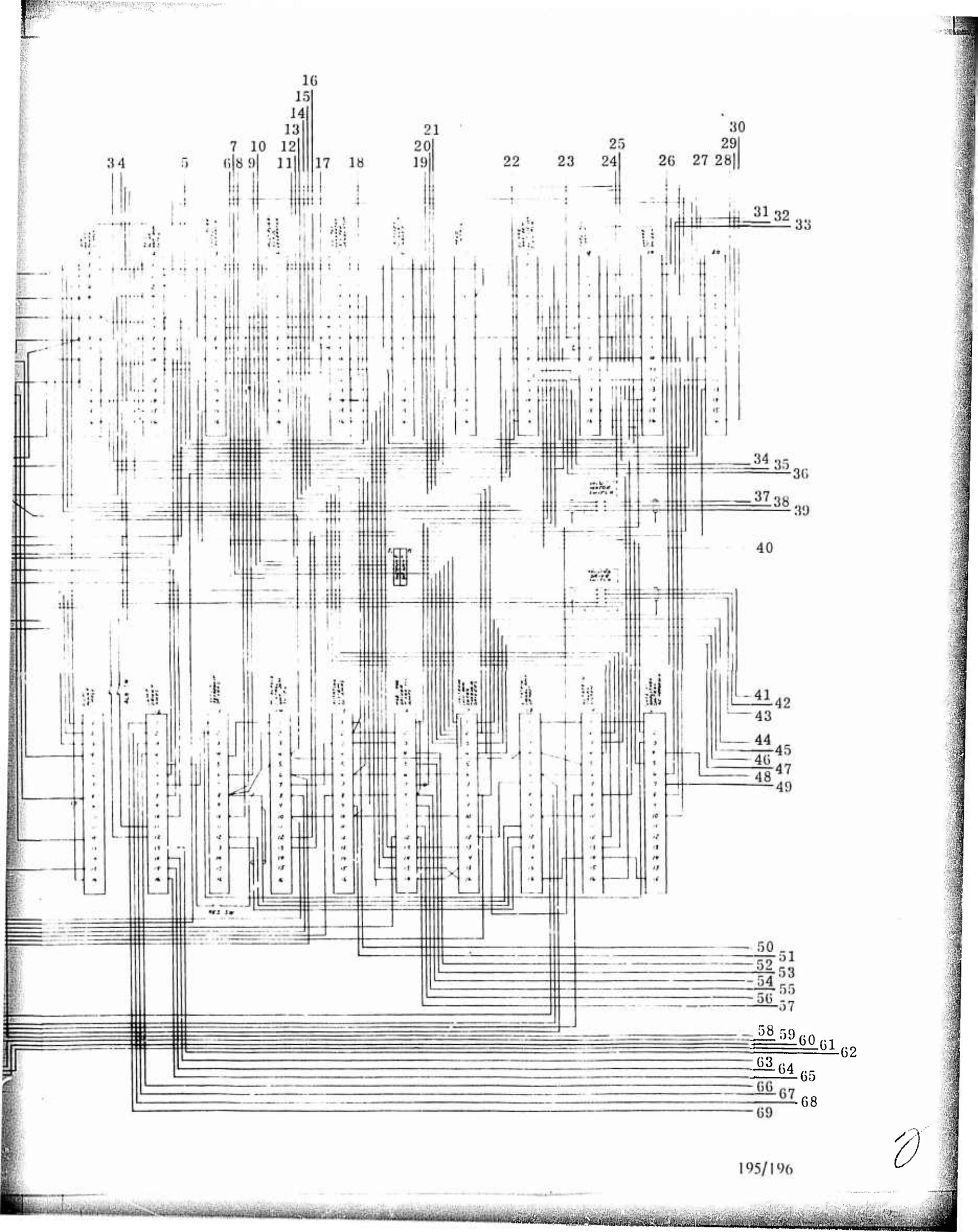
16
15
14
13
21
7
10
12
20
25
30
29
3 4
5
6 8 9
11
17
18
19
22
23
24
26
27 28
31 32 33
34 35 36
37 38 39
40
41 42
43
44 45
46 47
48 49
50 51
52 53
54 55
56 57
58 59 60 61 62
63 64 65
66 67 68
69

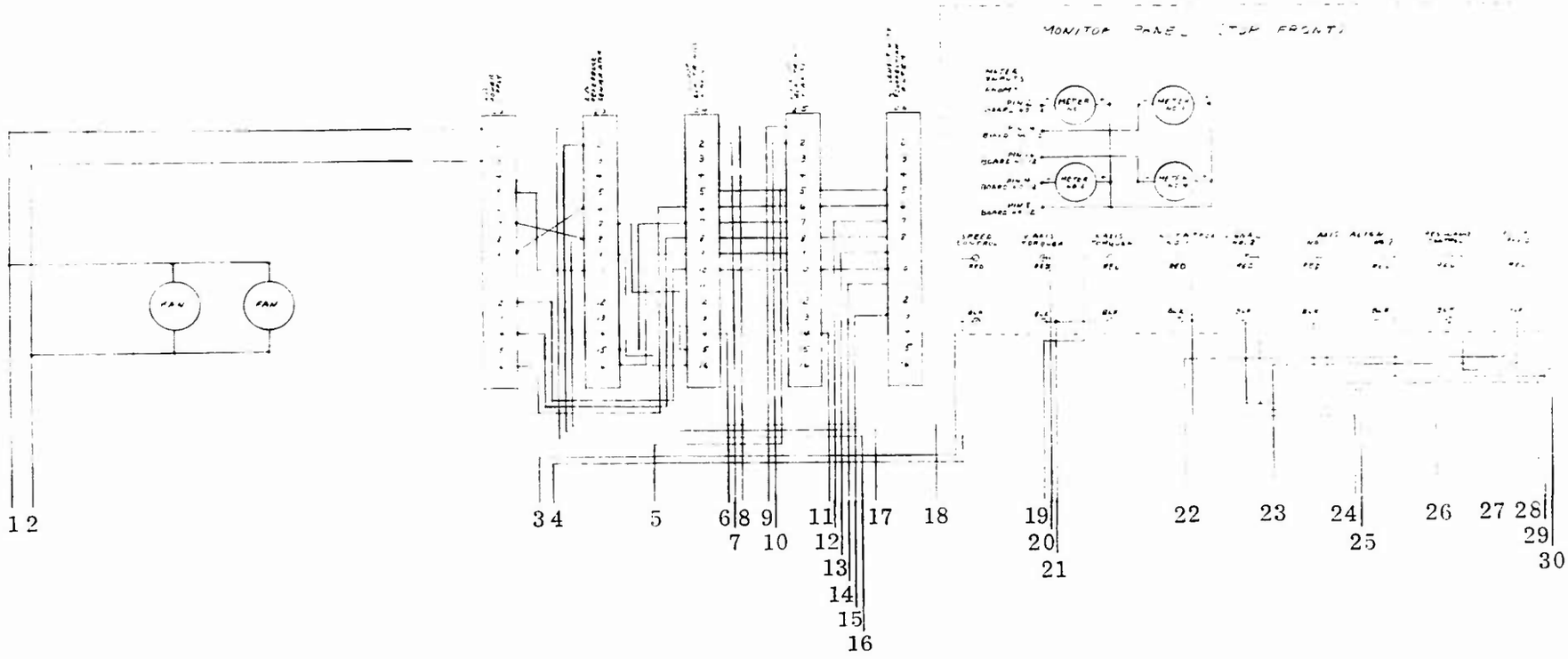
MONITOR PANEL (TOP FRONT)
METER
FAN
FAN
1 2
3 4
5
6 8
7
9
10
11
12
13
14
15
16
17
18
19
20
21
22
23
24
25
26
27
28
29
30

Unclassified

Security Classification

DOCUMENT CONTROL DATA - R & D

(Security classification of title, body of abstract and indexing annotation must be entered when the overall report is classified)

1. ORIGINATING ACTIVITY (Corporate author)	2a. REPORT SECURITY CLASSIFICATION
Bell Aerospace Company Division of Textron, P.O. Box One Buffalo, New York 14240	Unclassified 2b. GROUP

3. REPORT TITLE

DEVELOPMENT OF UNCONVENTIONAL GYRO (NUTATRON TECHNIQUE) FOR TACTICAL AIRCRAFT INERTIAL NAVIGATION SYSTEMS

4. DESCRIPTIVE NOTES (Type of report and inclusive dates)

Technical Report (Final) October, 1970 to June, 1973

5. AUTHOR(S) (First name, middle initial, last name)

Giles M. Hofmeyer
Ernest H. Metzger

6. REPORT DATE	7a. TOTAL NO. OF PAGES	7b. NO. OF REFS
September, 1973	197	

8a. CONTRACT OR GRANT NO.	9a. ORIGINATOR'S REPORT NUMBER(S)
F33615-71-1092 F33615-72-1137 b. PROJECT NO. 6095 c. Task No. 01 d.	6006-950005 9b. OTHER REPORT NO(S) (Any other numbers that may be assigned this report)

10. DISTRIBUTION STATEMENT

Distribution limited to U.S. Government Agencies only; Test and Evaluation; June 1973. Other Requests for this Document must be referred to Air Force Avionics Laboratory (NVN), WPAFB, Ohio

11. SUPPLEMENTARY NOTES	12. SPONSORING MILITARY ACTIVITY
	(NVN) Ohio, 45433

13 ABSTRACT

This report covers the latest phase of the Nutatron angular rate sensor development effort, culminating in the delivery of two prototype sensor and an electronic test set to the U.S. Air Force Central Inertial Guidance Test Facility (CIGTF) at Holloman AFB. The objectives of the Nutatron Program is to lead to angular rate sensor for tactical fighter navigation systems, offering fast reaction from a cold start, low temperature coefficients and good long term stability. The Nutatron concept features an automatic drift compensation technique, eliminating the requirement for high tolerance, highly stable parts and materials. The report tabulates the attained performance parameters, discusses the results and underlying remaining error mechanisms and concludes in recommendations to further improve performance. The electromechanical and electronic modifications made under this phase are discussed and their impact on performance described.

Reports AFAL-TR-65-170, AFAL-TR-67-54, and AFAL-TR-69-76, give the results of the previous efforts of this unconventional angular rate sensor development program.

DD FORM 1 NOV 65 1473

Unclassified

Security Classification

14 KEY WORDS	LINK A		LINK B		LINK C	
	ROLE	WT	ROLE	WT	ROLE	WT
Angular Rate Sensor						
Gyro						
Nutatron Technique						
Unconventional						
Dual Axis						
Automatic Drift Correction						